Eye Alignment: A Novel Approach

Joseph Edward Davies
Doctor of Philosophy
Aston University

March 2012

Aston University

Eye Alignment: A Novel Approach

Joseph Edward Davies

Doctor of Philosophy

2012

This thesis describes the design and development of an eye alignment/tracking system which allows self alignment of the eye's optical axis with a measurement axis.

Eye alignment is an area of research largely over-looked, yet it is a fundamental requirement in the acquisition of clinical data from the eye. New trends in the ophthalmic market, desiring portable hand-held apparatus, and the application of ophthalmic measurements in areas other than vision care have brought eye alignment under new scrutiny. Ophthalmic measurements taken in hand-held devices with out an clinician present requires alignment in an entirely new set of circumstances, requiring a novel solution.

In order to solve this problem, the research has drawn upon eye tracking technology to monitor the eye, and a principle of self alignment to perform alignment correction. A hand-held device naturally lends itself to the patient performing alignment, thus a technique has been designed to communicate raw eye tracking data to the user in a manner which allows the user to make the necessary corrections.

The proposed technique is a novel methodology in which misalignment to the eye's optical axis can be quantified, corrected and evaluated. The technique uses Purkinje Image tracking to monitor the eye's movement as well as the orientation of the optical axis. The use of two sets of Purkinje Images allows quantification of the eye's physical parameters needed for accurate Purkinje Image tracking, negating the need for prior anatomical data. An instrument employing the methodology was subsequently prototyped and validated, allowing a sample group to achieve self alignment of their optical axis with an imaging axis within 16.5-40.8 s, and with a rotational precision of 0.03-0.043°(95% confidence intervals).

By encompassing all these factors the technique facilitates self alignment from an unaligned position on the visual axis to an aligned position on the optical axis. The consequence of this is that ophthalmic measurements, specifically pachymetric measurements, can be made in the absence of an optician, allowing the use of ophthalmic instrumentation and measurements in health professions other than vision care.

Keywords: Alignment, Purkinje Images, Self Alignment and Optical Axis

Dedicated to Sarah and my family

Acknowledgments

This research has been fascinating; however the experience has been made more enjoyable by the support of family, friends and colleagues whom I would like to thank now.

I would firstly like to thank my supervisors Mark and James. Mark's confidence and enthusiasm has been infectious, his continual support and faith in me has been a great source of encouragement, while his good humour has always made his supervision enjoyable. I would also like to thank James, he has always managed to make time for me in a busy schedule, no matter how mundane the question. I have also found him to be a true gentleman, in all aspects of his work, and a real inspiration.

My thanks also go to my sponsor company Lein Applied Diagnostics, and all their employees, both past and present. I would particularly like to thank Robin for his continual support for the project and for maintaining strong links between Aston and my sponsor company. He has always offered advice in a manner which is beneficial to my research, demonstrating concern for me personally, for this I thank him wholeheartedly.

In addition to my principal supervisors I would like to thank the technical staff at Aston, specifically Graham, James and Mike who have always offered valuable advice with any obscure component I required. Their support and good humour has made Aston a great place to work.

I would also like to thank my colleagues in the Bio-Medical Research Group, particularly Tom, Ben, Jon and Alec who have made going to work thoroughly enjoyable and have been a great source of advice (and welcome distraction) throughout my studies.

Lastly I would like to thank my family, Sarah's family and Sarah for their love and support. In the absence of a witty comment which meets Sarah's approval - Sarah, I love ya!

Contents

List of Figures

List of Tables

Glossary

Cardinal Points - The points in an arrangement of lenses used to describe the optical system.

Emmetropic - The condition of the eye in which vision correction with either glasses or contact lenses is not required.

Eye Rotations - rotations of the eyeball within the eye socket.

Fixation - when the eye regards an image or object using fixational movements: ocular tremor, ocular drift and microsaccades.

Keratoconus - Keratoconus is the deformation of the cornea to a more conical shape. It is caused by structural changes within the cornea.

Keratography - Keratography is the analysis of the cornea.

Limbus - The limbus is the point at which the iris and sclera join.

Nodal Points - Within a lens, light rays directed at one nodal point will appear from the corresponding nodal point due to the refraction of the lens. Lenses are thus said to contain an entrance and exit nodal point.

Ophthalmophakometer - An instrument desgined by Tscherning similar to phakometer.

Pachymeter - An ophthalmic measurement device for measuring corneal thickness.

Sclera - The white of the eye.

Stigmatic - Stigmatism dictates the ability of lens to focus a single point source in the object plane to a point in the image plane. A stigmatic lens is thus a lens which can achieve this.

Toric - Toric refers to lenses with different refractive powers in planes perpendicular to each other.

Translation - the movement of the eyes with the head along the axes of rotation.

Chapter 1

Introduction

1.1 Eye Alignment

In the context of this research, eye alignment is a generic term referring to the alignment of an ophthalmic instrument's measurement axis with a reference axis in the eye. Eye alignment plays a pivotal role in allowing repeatable measurements to be taken; yet, it is an area of research largely overlooked.

Technological advances in the field of ophthalmic instrumentation have resulted in an improvement of measurement accuracy; however, to benefit from higher accuracy measurement precision must also improve. The validity of accurate measurements depend on a greater certainty of the position/angle/location at which the measurements are taken. Attempts to solve this problem have led to a wide range of alignment techniques, each owing their differences to the method of measurement used.

Although this diversity is intriguing, there are inevitable inconsistencies, particularly between comparable measurements taken with competing devices. When differences in measurement are found, very rarely is the difference attributed to the initial alignment between the eye and the instrument. Logically, this should be the first area of investigation, as measurements will differ if they are taken from different locations on or within the eye.

The potential for inconsistency is increased by the non-standard identification of the eye's axes. The axes of the eye have been defined to aid in the modelling of the eye's geometric and optical properties, as well as for eye alignment. There are a multitude of axes contained within the eye, each having the potential to be aligned to. The choice of axis is largely up to the instrument designer, although there are some general conventions. There is, however, confusion regarding the definition of these axes, primarily because of the difficulties in defining a biological system which is naturally variable.

1.2 Self Alignment

Even though there are subtle differences present in all alignment techniques, there are constants which remain. The blue print for the majority of ophthalmic equipment is the bench-top chin-rest design which requires the optometrist to perform alignment. This type of instrument requires patients to visit the optician. While this is not unreasonable, it limits the use of optometric equipment in other health care areas and to the clinical practice in which the instrument resides. To counter this, manufacturers must adapt to produce ophthalmic devices which are portable; consequently, the alignment procedure would have to be performed in an entirely new set of circumstances requiring a novel solution.

Several manufacturers have already developed hand-held devices such as the portable tonometer - Bicom.inc (New York, USA); however, these devices still require the presence of an optician to perform the measurement. The natural progression for this type of hand-held instrument is to have the patient perform the measurement and alignment, requiring the alignment system to either: compensate for misalignment in the measurement or communicate alignment correction to the user, facilitating self alignment. In addition to this, depending on the type of measurement, a self aligning hand-held device would enable self diagnosis, or at least alert the patient to seek advice from a clinician.

1.3 Eye Tracking

To allow self alignment, the instrument must monitor the position of the eye for two purposes: firstly, to evaluate the amount of misalignment, secondly, to identify alignment once alignment has been corrected. One way this can be achieved is by the tracking of the eye. Eye tracking is generally performed irrespective of alignment; however, tracking data can be related to misalignment providing the aligned position is known. For this reason eye tracking forms a significant part of this thesis as both a tool for investigation and implementation in the final alignment technique.

Eye tracking has seen a resurgence recently for a variety of reasons. The improvement in image capture and processing techniques has stimulated the use of eye tracking in research. There has also been a drive to use eye tracking for computer interfaces, both for the disabled and the general computing market. Yet, while some ophthalmic instruments use basic pupil tracking for measurement purposes, eye tracking is sparingly used in eye alignment (Reichert 7 Auto Tonometer - Reichert (Buffalo, New York, USA), uses a method of automatic alignment). Eye tracking would be a powerful tool in alignment and ophthalmic instrumentation as it would enable a device to take better informed measurements. The benefits lie both before measurements, to help in the movement of the device/eye to the correct position and after measurements, to validate.

1.4 v360 Pachymeter

The v360 pachymeter - Lein Applied Diagnostics (Reading, United Kingdom), can measure corneal thickness accurately (+/- 1.65 µm, see Chapter 4 for instrument evaluation); however, due to the measurement principle it is prone to misalignment. The measurement is a reflection based technique and thus receives the maximum amplitude in return signal when the measurement is on the corneal apex; a point which is located on the eye's optical axis. The amplitude in return signal quickly deteriorates with movement off the corneal apex, prompting the requirement for an accurate alignment system.

Due to its compact size, the device lends itself to being hand-held, thus requiring alignment in an unusual set of circumstances. These circumstances encourage self alignment, rather than alignment by a clinician or third party, requiring a novel alignment methodology.

The measurement has also been shown to correlate with glucose concentrations in the blood, highlighting its potential as a non-invasive form of glucose monitoring. It is important to mention that this type of measurement is not an evaluation of the patients visual system but rather, it uses the anatomy of the eye to determine other properties of the patient's health. In this case, it can be assumed that both the patient and the clinician are not vision care specialists, thus an accurate self alignment strategy is required.

The absence of an optician also means that the alignment technique must be self validating, as the patient would be unable to make an informed decision on the success of the measurement.

1.5 Aims and Objectives

The aim of this research is to develop an alignment technique capable of self alignment to the eye's optical axis with the view to integration within the v360 pachymeter. The desired outcome of the research would be a technique, validated by a prototype, capable of allowing a patient to align their optical axis with the prototype's measurement or imaging axis. The self alignment aspect of the technique is an important point; integrating a self alignment technique with a hand held measurement devices allows the measurement to be taken without the presence of a clinician. This then allows a certain degree of self diagnosis by the end user while also allowing eye diagnostic measurements to be used in areas other than vision care. Alignment also raises a wider-reaching issue. There are a number of ophthalmic devices available to the clinician, each having a unique alignment requirement, dependent on the measurement technique; however, their effect on measurement precision is unquantified. The wider scope of this research is then to identify and quantify the impact misalignment has on measurement precision, making a valid contribution to the research in this area.

To achieve the aims of the research and to investigate the alignment issue as a whole, the research was performed in 8 steps:

1. Investigate the causes of misalignment by reviewing the literature on eye movements and determine the probability of their presence in typical alignment procedures.

2. Review current eye tracking techniques to assess their potential for alignment based on their accuracy, identification of alignment and ease of integration into the v360 pachymeter.

3. Determine device specific specifications from the v360 pachymeter for the alignment system.

4. Construct a geometric mathematical model cornea to relate pachymetric measurement characteristics to alignment tolerances for the alignment technique.

5. Design and develop a novel eye alignment/tracking system for both the tracking of the eye and identification of alignment to the optical axis.

6. Determine the actual magnitude of misalignment and its causes by tracking the eye during fixation with the newly developed alignment/tracking technique.

7. Devise a self alignment strategy to be used in the newly developed eye alignment/tracking system.

8. Evaluate the self alignment technique, and quantify its potential impact on the v360 pachymeter.

1.6 Thesis Outline

The thesis is presented in 8 chapters:

Chapter 1, the reader is introduced to eye alignment and the current challenges within this area of research. The requirement for greater precision is described as a result of increased measurement accuracy and resolution. The requirement of alignment in new circumstances, encouraging self alignment, is also discussed.

Chapter 2 discusses anatomy, mechanics and physical dynamics of the eye. The axes of the eye are also discussed with reference to their natural variation. A large range of eye movements are described in order to evaluate their presence in typical alignment circumstances. The stimulus and mechanics of eye movement are also discussed.

Chapter 3, a range of eye tracking techniques are analysed with reference to their accuracy and potential for use in eye alignment. Specifically, tracking techniques are assessed on accuracy, alignment identification and potential ease of integration into the v360 pachymeter.

Chapter 4 describes the identification of specifications for the alignment system. As the alignment system has an intended instrument for integration (v360 pachymeter), the accuracy and the precision in the measurement of this instrument is analysed. The chapter also describes the construction of a mathematical model cornea to convert the precision and range in the pachymetric measurement to an alignment tolerance for the alignment system.

Chapter 5 charts the design and development of a combination eye alignment/tracking system, built to the specifications outlined in the previous chapter and based on the most appropriate form of tracking technique determined from Chapter 3. The chapter also discusses its evaluation in terms of accuracy, safety and in comparison to other tracking techniques.

Chapter 6, investigations into the eye's movement during fixation are discussed. Fixation is a typical tool used in alignment to maintain the eye in a fixed location allowing repeatable measurements. The validity of this method of alignment is investigated. Chapter 2 highlights the importance of the visual scene in the magnitude of eye movement, thus, alluding to the potential for an optimum alignment target for the minimisation of eye movement. Chapter 6 then describes the investigations in to the identification of this target.

Chapter 7 describes the devised alignment strategy for alignment of the eye to the v360 pachymeter. The method is evaluated by a comparison of the newly developed alignment technique with the previously defined specifications. The chapter also describes potential benefits in the application of this technique in the v360 pachymeter.

Chapter 8 concludes the work described in the thesis and discusses the potential for future development and investigations.

Chapter 2

Anatomy, Mechanics and Physical Dynamics of the Eye

2.1 Chapter Overview

To evaluate the potential implications of both the eye's structure and movement on misalignment each factor is analysed separately.

In order to determine the variation in alignment position as a result of the definition of the eye's axes, each axis is discussed separately with reference to its positional variation. The positional variation is attributed to the biological nature of the points used to define these axes.

To determine eye movements which contribute most misalignment during alignment procedures, the entire range of eye movement is analysed. Typical ophthalmic instruments facilitate alignment by providing the patient with a small target to fixate on, thus reducing the range of eye movements performed. Each eye movement is then evaluated by determining its stimulus and the presence of this stimulus in typical alignment procedures.

The chapter concludes by suggesting the alignment axis with the least biological deviation in its reference points and the eye movements most likely to occur in alignment procedures.

2.2 Introduction

Eye diagnostic measurements requiring alignment find immediate obstacles in the eye's structure and movement.

The eye is famously described as the "world's worst camera" [6] and there is valid reason for this. As with any biological system, there is inherent natural variation making structural definition difficult. This is apparent in the definition of the eye's axes, axes which are relied upon for alignment. For example, the LenStar (Haag-Streit AG, Koeniz, Switzerland), Pentacam (Oculus, Germany) and IOL Master (Carl Zeiss, Jena, Germany) are all ophthalmic instruments capable of measuring comparable biometric properties. Each system, however, uses a different alignment method. Although the LenStar and IOL Master both align to the visual axis, the Pentacam aligns to the corneal apex[1] which lies on the optical axis (the difference is illustrated in figures 2.2 and 2.3).

The implication of this is that axes defined in one device may differ from axes defined in others; in the event that instruments use similar definitions there is still variation due to the way the reference points are detected. This leads to inconsistent measurements between devices.

The eye's movement is another source of variation in eye alignment. The eye performs a range of movements to both keep the cells of the retina stimulated and manoeuvre a subject's visual attention to the desired location.

[1] The corneal apex is often referred to as the corneal vertex.

2.3 Anatomy of the Eye

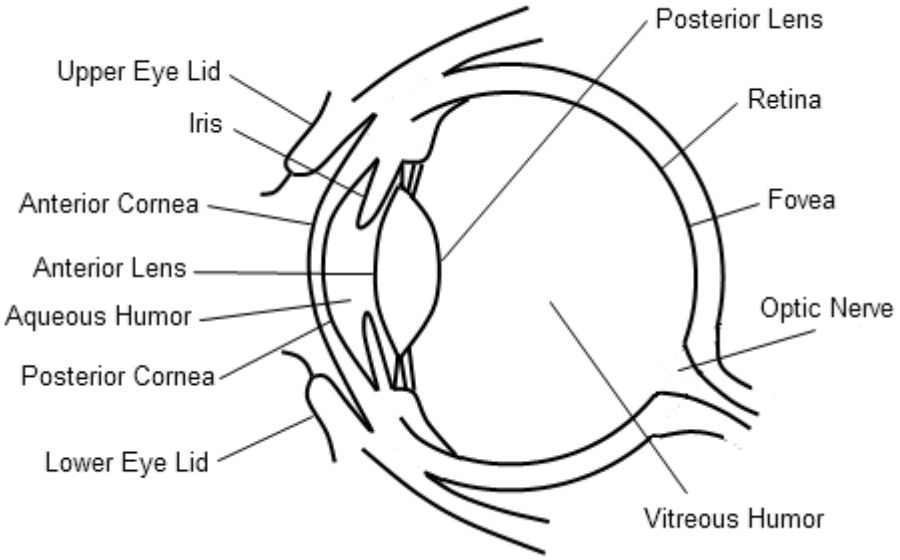

Figure 2.1: Anatomy of the eye.

Figure 2.1 describes the anatomy of the human eye. The optics of the human eye include 2 refracting elements: the cornea is responsible for 2/3 of the eye's overall refraction [7], while the lens performs finer focal adjustments to ensure clarity of image. The pupil acts as the aperture of the eye and is formed by the iris; the iris causes pupil dilation in low light conditions and constriction in bright light.

2.4 Axes of the Eye

The properties of an optical system can be determined by the location of its cardinal points. These cardinal points consist of the nodal points and pupil points, each having entrance and exit locations; and the centres of curvature for each refracting element. Approximations for the positions of these points have been determined for the eye and are used to construct the relevant axes. In total there are 4 axes which are predominately used for alignment in ophthalmic instrumentation [8].

2.4.1 Optical Axis

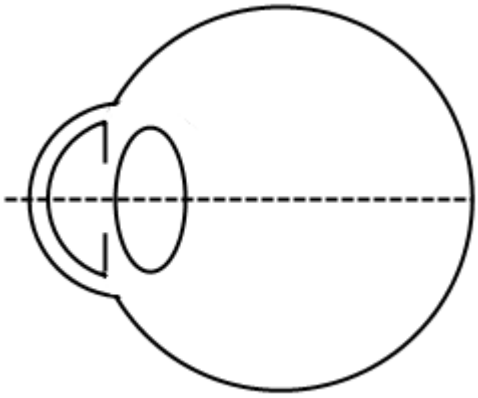

Figure 2.2: Optical axis of the eye.

The traditional optical axis of any optical system is an axis which passes through the centre of curvature of each refracting element in the arrangement [8, 7]. The eye is comprised of two toric lenses which are tilted with respect to one another; therefore an optical axis as defined above is not possible. This classical definition was used to describe the optical axis in early centred schematic eyes in which the ocular misalignments were not incorporated.

If an axis such as this was present in an eye, then light entering the eye along this axis would also emerge on the same axis, this reasoning has been used to suggest that the eye may contain a unique optical axis, although not necessarily passing through the centres of curvature [9].

Tscherning estimated the position of the optical axis in relation to the visual axis (Section 2.4.2) with his ophthalmophakometer and thus an estimated position of the optical axis is also said to be the closest alignment of the Purkinje Images [10]. The Purkinje images are reflections from each of the refractive components in the eye and allow investigation of the eye's optical alignment. In total there are four Purkinje reflections, normally denoted in Roman numerals. The reflections from the anterior and posterior corneal surfaces are termed Purkinje Image I and Purkinje Image II respectively, while reflections from the anterior and posterior lens surfaces are termed Purkinje Image III and Purkinje Image IV (these images can be seen in figure 3.3). In a human eye, which has the cornea and

the lens centred round the optical axis, these reflections will appear aligned. Typically, alignment of these images is rare and thus the optical axis is approximated by their closest alignment [8, 10].

Misalignment of the Purkinje images can be attributed to three factors, global rotation of the eyeball, lens tilt and lens decentration. A number of instruments have been designed to evaluate these quantities [11, 12, 13, 14, 15, 3] due to the repercussions in intraocular lens (IOL) implantation. Lens decentration measurements in normal eyes have been recorded at 0.09 - 0.45 mm horizontally and 0.09 - -0.22 mm vertically, lens tilts measurements have been recorded in the region of 2.8- -2.87°horizontally and 2.58 - -1°vertically [13].

While a true optical axis is not considered present in the eye, its approximated position can be imaged by use of the Purkinje Images and therefore allows direct assessment of the position of the optical axis when defined by the Purkinje Images.

2.4.2 Visual Axis

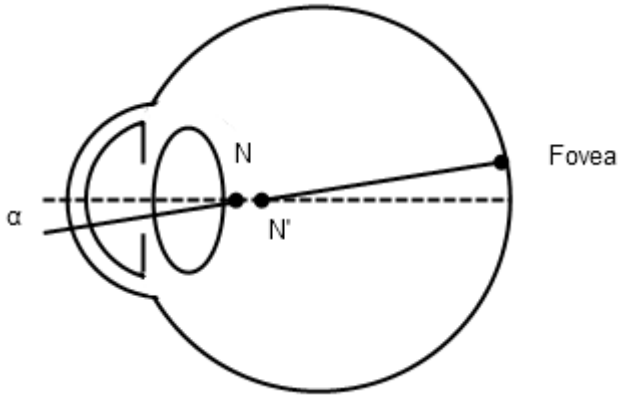

Figure 2.3: Visual axis of the eye in respect to the optical axis.

The visual axis is constructed by two lines, the first line joins the object and the entrance nodal point (denoted as N in figure 2.3), the second line is constructed between the exit nodal point (denoted as N' in figure 2.3) and the fovea [8]. The nodal points of an optical system contain the property that light rays intersecting the entrance nodal point will emerge from the exit nodal point. The light ray will intersect the nodal points at the same angle, relative to the optical axis, both on entrance and exit. With respect to the visual axis, this angle is termed angle α [8, 16, 10, 7].

The visual axis and the line of sight are similar in definition and are only distinguishable by the cardinal points which they subtend. To add confusion, the visual axis is occasionally defined as the line of sight with the latter being termed the nodal axis [10].

The relaxed Gullstrand –Emsley schematic eye places the entrance and exit nodal points at 7.06 mm and 7.36 mm respectively behind the corneal vertex leading to a small separation of 0.3 mm, this separation increases to 0.35 mm during accommodation [2][10]. The difference between the two nodal points are declared negligible and thus the visual axis becomes a line between the object and the fovea [17].

Although alignment to this axis is logical, it is not without errors. Traditional nodal points as described in early model eyes [18] are only present in stigmatic and centred optical systems [7]. The eye is not a centred optical system and contains significant asphericity, thus the presence of a visual axis as defined in the classical sense is improbable. There have been redefinitions of the eye's nodal points by the introduction of expanded nodes. Nodes provide an area in which light rays pass through rather than specific points, it has also been suggested that the centre of these nodes can act as approximations for nodal points [19]. Other definitions have introduced object-space and image-space visual axes. These suggestions also contain a visuo-optical angle composing of 5°horizontally and 2°vertically [19] designed to replace angle α.

[2] Accommodation is the process in which the lens deforms to increase its refractive power.

The angle α raises another factor of variability in the visual axis as the angle is said to vary. This variation is typically between 4 - 8°[8].

The absence of clearly definable nodal points in the eye's optical system demonstrates the theoretical nature of this axis, while the population variation in the angle α highlights the vulnerabilities in alignment to this axis. However, the anterior cornea's centre of curvature lies close to the nodal points (approximately 0.34 mm) [3]. The implication for visual axis alignment is that the anterior cornea's centre of curvature can be identified via Purkinje Image I. Purkinje Image I is formed between the illumination source and the anterior cornea's centre of curvature thus highlighting an imageable reference for visual axis.

[3] Assuming a corneal radius of 7.7 mm and the exit nodal point placed 7.36 mm behind the corneal apex.

2.4.3 Pupillary Axis

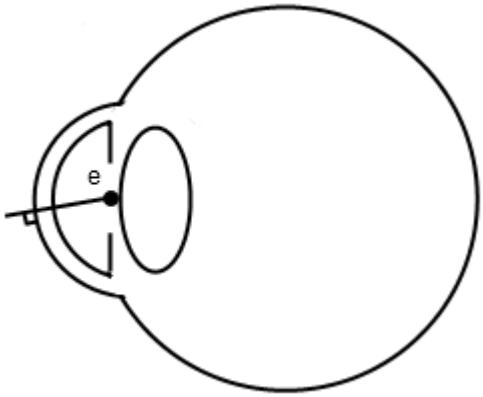

Figure 2.4: Pupillary axis.

The pupillary axis intersects the geometric centre of the pupil (denoted as e in figure 2.4) while passing through the cornea normally. The angle between the pupillary axis and the line of sight is called angle $\varkappa$ [8, 10, 16, 7]. As the pupillary axis lies nasally in relation to the optical axis, angle $\varkappa$ is slightly smaller than angle α [8].

The pupillary axis is not extensively used in areas such as instrument alignment because of the associated problems with the use of the pupil centre as a reference point. The main application of the pupillary axis is in eye tracking because of the ease with which the pupil can be extracted from images of the eye.

2.4.4 Line of Sight

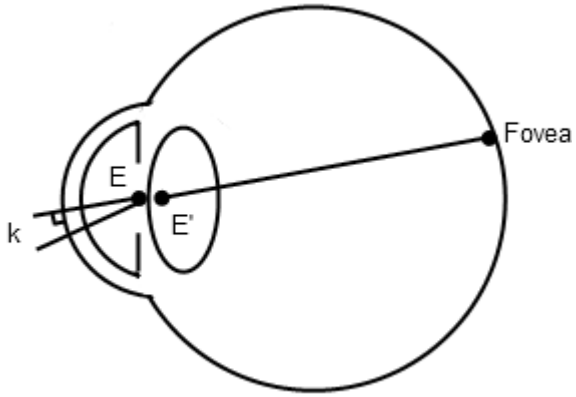

Figure 2.5: The line of sight with respect to the pupillary axis.

The line of sight is similar to the visual axis but rather than the axis intersecting the nodal points it subtends the eye's entrance and exit pupils, shown as E and E' in figure 2.5. In general, optical systems define the entrance and exit pupil points as the position of the images of the aperture as seen through each end of the optical arrangement. In the case of the eye, the entrance pupil point is the image plane of the iris as seen through the cornea. The exit pupil point is the image of the iris as seen through the lens. Thus there is slight positional difference in the pupil point as formed by the iris and the entrance and exit pupil points. The ray travelling through these points emanating from the object is also considered to represent the chief ray travelling from the object to the fovea.

The line of sight intersects the entrance and exit pupil points at 3.05 mm and 3.67 mm respectively behind the corneal apex, this leads to a larger separation than the nodal points of 0.61 mm [16]. Between these points, at 3.60 mm behind the corneal apex, lies the image plane containing the pupil, because of this, the line of sight is often approximated by the line connecting the object and the pupil's geometric centre (as formed by the iris), and the line connecting the pupil centre with the fovea.

Using the pupil centre as a reference point induces instability due to its position and the way it is imaged [20], it has also been suggested that it lies close to the visual axis [17]. The pupil is of non-uniform shape, meaning that any shape fitted to it is a best fit approximation, the pupil centre is then also an approximation. The centre has been reported to lie nasally from the optical axis by 0.25 mm [10], a distance which can increase temporally and nasally [21] by 0.6 mm [22] with constriction. Other reference points have been investigated to evaluate the possibilities of replacement for the pupil centre. The principal alternative reference point is the limbal centre [23], though this has not been used for line of sight alignment.

The line of sight uses a detectable and thus quantifiable reference point, but the stability of this reference point has been shown to affect measurements [24], thus, demonstrating the potential errors in aligning to this axis.

2.4.5 Alternative Alignment Axes

Alternative measurement techniques align to a particular reference point rather than an axis. Keratography is one such technique. Alignment is attempted on the corneal vertex which is defined as the point of the cornea with the smallest radius of curvature [25]. This is particularly important for keratography as accurate alignment is needed for contact lens fitting, implanted intraocular lens power determination and early diagnosis of keratoconus. In practice keratographers and video-keratographers align to an axis called the keratometric axis [7]. This axis is described as the line emanating from the object intersecting the cornea normally, the point of this intersection is termed the vertex normal [26] and lies at an angle of approximately twice angle $\varkappa$ from the pupillary axis [27]. The principle assumes very little displacement of the corneal vertex from the vertex normal; contrary to this, the displacement of the keratometric axis from the corneal apex has been recorded as 0.62 +/- 0.23 mm [28].

Alignment to a specific reference point only provides half of the alignment criteria; in cases such as keratography this principle is adequate due to the relatively high amount of lateral data recorded. In measurements requiring scans through the eye, alignment with a single reference point highlights intersection with the alignment axis rather than a co-linear alignment.

2.5 Stimulus for Eye Movement

Humans possess foveated vision, the consequence of this is that a small proportion of the retina (the fovea) is responsible for observing high detail colour images. A repercussion of this is that all the visual information present in the scene cannot be processed at once. To analyse an image, the important points must be positioned on the fovea. This is achieved through the positioning of both eyes using the relevant combination of eye movements. The decision on which points to analyse is a question of visual attention.

Visual attention is the driving force behind the majority of eye movements. When considering a scene the eyes will be drawn to particular points because they demand more attention. Wolfe et al [29] describes the process of attention in two ways: top down attention, which directs attention based on the observer's knowledge; and bottom-up attention, which is stimulus driven.

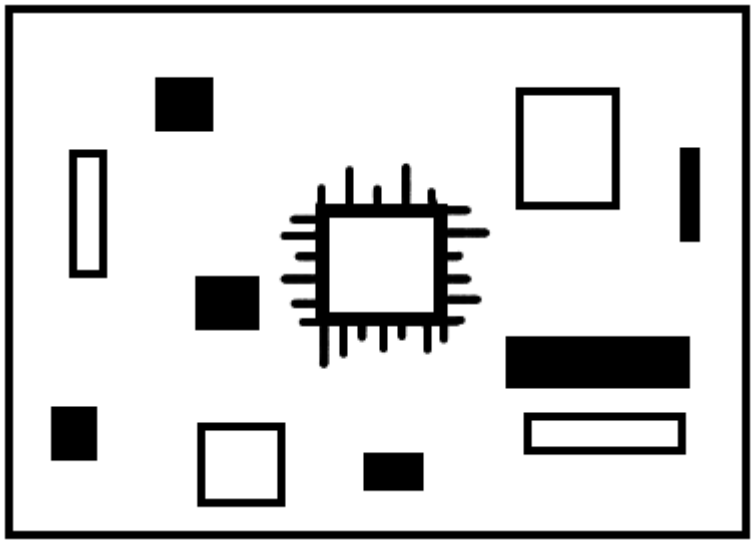

Figure 2.6: Visual attention.

Figure 2.6 demonstrates how difference from the surroundings draws visual attention, in this case, the central spiked rectangle is sufficiently different from the surrounding shapes to attract initial attention. Fundamentally, visual attention is caused by the difference between a point and its background [30]. Studies suggest that colour can be a major component in distinguishing a target [31, 30]. Difference from the background could also occur due to movement, a moving object in an otherwise stationary scene will cause the repositioning of the eye.

2.6 Mechanics of Eye Movement

The positioning of the eye is achieved through the actions of the extraocular muscles which penetrate the sclera in six locations. Four of the six muscles are collectively termed the rectus muscles while the remaining two are termed the oblique muscles. To co-ordinate eye movement the muscles work in pairs (Sherrington's Law), the contraction of one muscle simultaneously relaxes the opposing muscle resulting in the rotation of the eyeball.

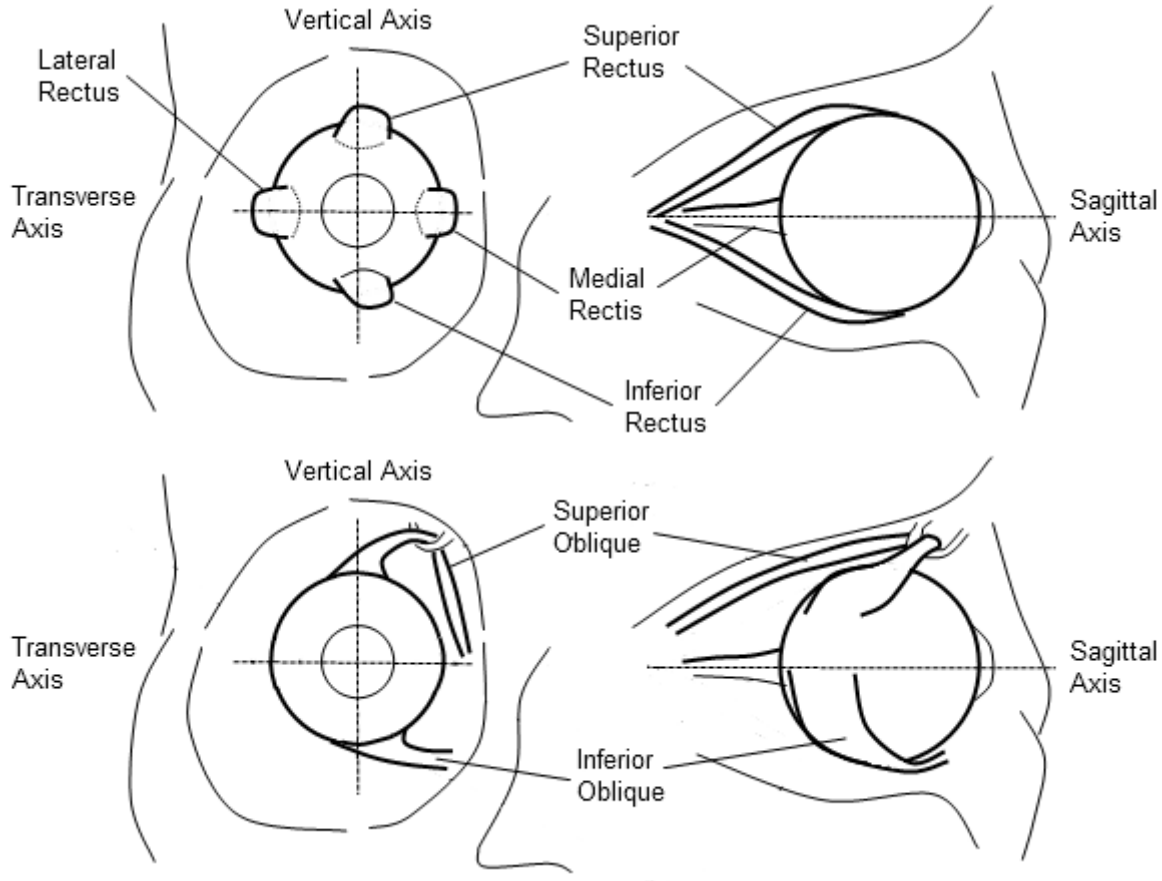

Figure 2.7: Eye muscles.

The eye muscles rotate the eye around 3 axes, the vertical axis, the sagittal axis and the horizontal or transverse axis. Rotations about the vertical axis caused by the medial and lateral rectus muscles are named adductions (rotations towards the nose) and abductions (rotations towards the temple). Rotations around the transverse axis caused by the superior and inferior rectus muscles are named elevations (rotations towards the eyebrows) and depressions (rotations towards the feet). There are also smaller torsional movements which are conducted by the superior and inferior oblique muscles around the sagittal axis. Rotations about this axis are termed intorsion (contraction of the superior oblique) and extorsion (contraction of the inferior oblique).

These movements can be defined in reference to Listing's law.

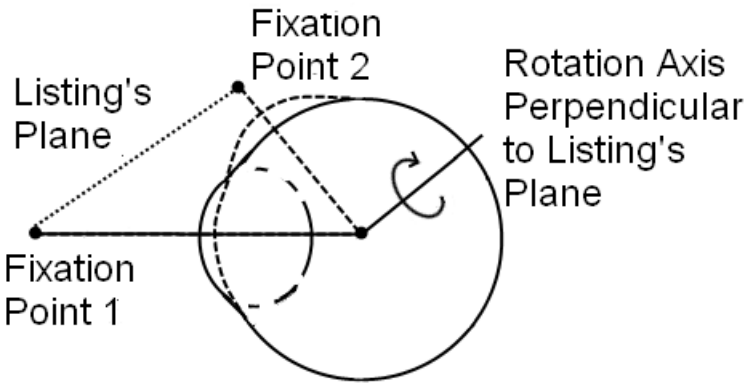

Figure 2.8: Rotational eye movement as described with Listing's law. Rotation is performed round an axis which is perpendicular to Listing's plane. Listing's plane is constructed between the first and second fixation points and the eye's centre of rotation.

Listing's law Listing's law forms a fundamental rule in the explanation of eye movements. Listing states rotations of the eye are completed about an axis which is perpendicular to a plane formed by the original fixation point and the following fixation point. This plane is referred to as Listing's plane [18].

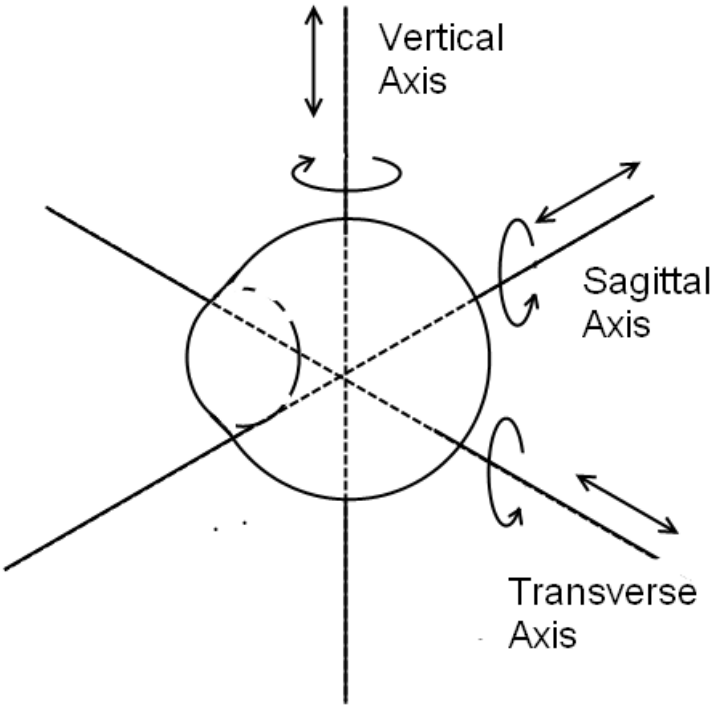

Figure 2.9: The 6 degrees of freedom for eye movement. All rotations are performed by the eye within the socket, all translational movements along the axes are performed by the head.

It is important to note that Listing's law assumes the eye to have 3 degrees of freedom. To assume the eye as having 3 degrees of freedom is assuming the head remains in a fixed position; however, due to the inherent difficulty in keeping the head fixed the eyes have 6 degrees of freedom (fig 2.9). As the head is free to move the eyes then are able to translate along each of the rotation axes. This law also assumes a centre of rotation which is not obvious.

2.7 Movements of the Eye

2.7.1 Saccades

The primary purpose of a saccade is to quickly change the eye's point of regard, directing the most sensitive part of the retina, the fovea, to the intended target [32, 33, 34, 35]. The quick movement, and the corresponding short duration, allow the eye to fixate for approximately 95% of the time [32]. Specifically, saccades are binocular movements performed voluntarily ranging from 0.05-60°[34]; however, involuntary correctional saccades are also performed. These correctional saccades are required due to the overshoot component of the primary saccade. Large saccades over 20°preced a correctional saccade of approximately 10% of the initial saccade [33]. The relatively high correctional aspect of these large saccades can be attributed to their minimal occurrence in normal viewing conditions. In more typical conditions, saccades larger than 20°are rare [32, 36]. This is confirmed by studies which report low and infrequent correctional saccades in typical environments [37, 38].

The requirement for correctional saccades stems from the ballistic nature of saccadic eye movement [33]. The brain employs a method of saccadic masking during saccades to hide the blurred image formed on the retina. This is not to say that images are not processed; in fact, if a stimulus is presented in the latency period of a saccade the eye will perform one of two responses: 'step by step' or 'skip over' [39]. In other words, the subject will either perform saccades to both targets with the second saccade occurring at a reduced reaction time; or, the subject will skip over the first target and saccade straight to the second target.

The latency time for saccades are subject to variation, but the typical range is 120 - 350 ms [33, 40, 21, 34], due to this, the frequency of this eye movement reaches a maximum of 4 Hz. Saccades have a mean velocity of 350 - 500°/s [34] and a peak velocity of 400 - 600°/s [34, 38, 41].

For the majority of circumstances saccades are voluntary and can be readily suppressed during fixation. Involuntary saccades are more of a concern, their connection to larger saccades means that suppression of voluntary saccades will also suppress involuntary saccades. If this is not the case, then the 'skip over' response can still be employed to prevent saccades [39]. It is questionable however, whether suppression would be required, as typically alignment procedures would not present stimulus for saccades.

2.7.2 Eye Fixation and Fixational Movements

Eye fixation is not a natural instinct, the eye constantly moves to stimulate the photosensitive cells of the retina. After images, caused by bleaching of the retinal cells, can last from seconds [42] to several minutes [43] before deterioration. The requisite for fixation is a small but constant movement of the eye to keep the fovea stimulated. An alternative

way of describing this is to imagine placing your hand on a rough surface, if your hand has been placed on there for long enough then the sensation of the rough surface will disappear, if your hand constantly moves over the surface then the sensation of the rough material will never leave. The term fixation is misleading, the actual action of the eye is to use tiny rotations and movements, these movements are categorised in three ways: tremors, drifts and microsaccades, although there is speculation over the importance of the third category in relation to fixation [41]. Fixation is the collective term for all these movements when regarding a portion of an image or object. Due to the small magnitude of these movements the actual area of the image inspected is small, giving the impression of a stationary eye and thus fixation.

2.7.2.1 Ocular Tremors

The ocular tremor is the smallest eye movement out of all three fixation movements. The frequency of this movement has been recorded in a broad range between 40 - 100 Hz [44, 45, 46, 47] with an approximate peak frequency of 80 Hz [45, 48]. The tremor causes a 150 - 200 nm [49, 46] vibration of the eye.

The tremor is an inescapable aspect of eye movement and will always be present; but the importance of this movement in relation to alignment may be considered small due to its low amplitude.

2.7.2.2 Ocular Drift

The maintaining of visual stimulation on the fovea is governed by small ocular drifts which occur in the eye when asked to fixate on an object. These drifts occur at a frequency of 2 - 5 Hz [47, 50] and at amplitudes less than 0.083°[50, 47, 51]. The maximum velocity of ocular drift occurs at 0.5°/s [52] with a mean velocity of 0.083°/s [53]. An ocular drift is typically followed by a saccade or a microsaccade; this is due to the corrective role of a saccade. The deviation of the line of sight from the target acts as a stimulus for corrective saccades. More specifically, it is the movement of the point of interest off the fovea, caused by drifts, which stimulates these corrective saccades [32].

Though the amplitude of these movements would cause minimal misalignment they are still an important aspect of fixation as they give clues to the initiation of saccades, in practical terms, the monitoring of these movements is difficult as they are relatively small.

2.7.2.3 Microsaccades

Of the three fixational movements microsaccades are the largest, although some doubt has been cast over their importance for fixation [41]. Recently there have been a number of investigations [54, 55] which link the propagation of microsaccades to visual fading in the subject's peripheral field of view, a consequence of the Troxler effect [56]. However, there

have been a number of investigations which suggest that microsaccades are negated or suppressed in tasks which require high concentration, such as threading a needle [57, 51, 58, 59, 60]. In addition, there have been studies which show a decrease in microsaccade frequency when subjects are presented with auditory cues [61, 62], or even simply told to keep their eye still rather than fixate [57, 58]. There are also arguments which suggest that microsaccades are a by-product of laboratory testing, and that in natural circumstances the head performs their function [63, 51]. Ambiguity in microsaccades is increased by the variety of ways in which they are defined. There is no clear magnitude boundary at which microsaccades become saccades (Section 2.7.1). Current investigations are concerned with analysing microsaccadic stimulus to see if they share the same shift of attention provocation [61, 62, 64] exhibited in saccades.

Depending on which definition is used, microsaccades are saccadic movements under 0.25°[65], it is also argued that an upper boundary of either 0.42°[35] or 0.5°[52] would encompass the majority of microsaccades. The frequency of microsaccades are typically in the region of 1-3 Hz [51, 52, 65] and are said to interrupt ocular drift [32]. Dynamically, microsaccades are similar to saccades and have a distinct relationship between amplitude and velocity.

Whether or not microsaccades are a result of fixation, they have been recorded during fixation tasks. This then makes them highly likely to occur during alignment procedures. As they perform the highest magnitude of movement out of all three fixation movements they warrant the most consideration. Interestingly, the ability to suppress microsaccades also makes them avoidable, thus, opening opportunity for alignment techniques with the ability to inhibit microsaccades.

2.7.3 Vestibulo-Ocular Movements

The contribution of the vestibulo-ocular movement is to stabilise an image on the fovea while moving, specifically during head rotation.

The inner ear holds three semi-circular canals. One canal holds an almost horizontal position, the other two canals form perpendicular planes to each other. The displacement of fluid in these canals is proportional to head velocity, thus the eye uses this information to compensate for rotational misalignments caused by the head [35]. The response time for this reaction is approximately 34 ms [66]. The gain for vestibulo-ocular movements, defined as the ratio of eye rotation amplitude over head rotation amplitude, approaches unity for frequencies between 0.5 - 5 Hz [67]. Head rotation frequencies in typical tasks such as walking or running fall into a 8 - 20 Hz range, in such activities, the vestibulo-ocular reflex is imperfect [68, 69]; however it does largely allow clear vision [70]. Only when image motion over the retina exceeds 2 - 4°/s does vision become impaired [71].

The vestibulo-ocular reflex may aid in alignment processes as, providing the fixation target moves with the head, the reflex will always compensate for head movement quickly and with high accuracy. Small inaccuracies are only present during activities such as walking and running, none of which would be present during alignment procedures.

2.7.4 Vergence

Vergence differs from other eye movements as it involves the rotation of the eyes in different directions, predominantly, this action is performed horizontally as the range of movement is smaller in the vertical and torsional directions. Vergence causes eye rotations from objects placed at infinity down to distances of 25 cm, a total rotation of approximately 14°; however, 70% of a normal subject's vergence movement will be performed to objects within 1 m [72].

These movements are stimulated by 4 factors, because of this vergence is split into sub categories: disparity, accommodative, tonic and proximal [73], though they are often referred to by other names.

2.7.4.1 Disparity Vergence

The rotational movement of both eyes in opposing directions to allow the line of sight for both eyes to converge on an arbitrary point in 3D space.

2.7.4.2 Accommodative Vergence

Accommodation is generally accompanied by vergence movements. Accommodation involves the deforming of the lens to change the eye's refractive power, during this change, images on the retina appeared blurred stimulating vergence.

2.7.4.3 Tonic Vergence

Under low light conditions the eyes will revert back to the baseline vergence position, this position ranges between 0.62-5 m with an average of 1.2 m [74, 75, 76].

2.7.4.4 Proximal Vergence

Vergence can be stimulated by a knowledge of nearness, investigations have induced vergence movements by changing the size of objects without changing the object's depth [77].

The latency of vergence movement lies between 130 - 250 ms [78], though this can be dependent on stimulus. Dynamically, vergence can mimic stimulus shifts of 40°/s to a 98% accuracy, additionally, stimulus shifts of up 100°/s have been copied with less than 10% error. Peak velocity ranges from 50°/s for 5°cues to 200°/s for vergence changes of 34°[79].

While vergence movements are induced by a wide range of stimuli, their main instigator is disparity. In typical alignment conditions where the depth of the fixation target is constant

there should be little disparity stimuli. Another important aspect of vergence in regards to alignment is monocular viewing, typically alignment is performed with one eye. In this case, it could be argued that vergence is not needed but in fact, the need for the brain to fuse images from both eyes into one image still drives vergence during monocular viewing, however for the reasons stated the impact would be minimal.

2.7.5 Smooth Pursuits

The smooth pursuit actions of the eye facilitate tracking of moving targets in order to stabilise the target on the fovea. They differ from better known saccades as they are not ballistic movements. Smooth pursuits are frequently used in daily activities, they allow slow constant movement of the eye to keep images on the fovea. In their simplest description, smooth pursuit eye movements attempt to match eye velocity to target velocity.

Their relatively short latencies of approximately 100 ms [80, 81, 82, 83, 84] suggest a reflexive response [85, 84] to target velocity, highlighting the involuntary nature of the movement. Their sensitivity to target velocity is detrimental to their positional accuracy, thus in order to compensate for these inaccuracies the eye performs catch-up saccades [81, 86]. Within a specified target velocity range, the eye is able to mimic target velocity accurately with reports of 7 - 8% error [87]. The gain, which is defined as the ratio of eye velocity and target velocity, has been suggested to approach unity up to target velocities of 60°/s [88, 89], although gains of 0.9 have been recorded for velocities up to 100°/s [90].

Smooth pursuits offer an interesting alternative to fixation as the they are free from the associated problems of restricting the eye's movements. These movements, in a specific range, can mimic target velocities very accurately, thus allowing knowledge of the position of the eye relative to the target. However, during smooth pursuits which require catch-up saccades, the eye can deviate from the intended location quickly.

2.8 Discussion

The assessment of axial and eye movement factors affecting alignment in diagnostic measurements has highlighted several areas of discussion.

In regards to the axes of the eye, none of the axes are able to avoid the natural variation in the eye's structure. The use of reference points within the eye mean that definition of any axis is subject to biological changes, especially the pupil. The pupil centre is used to define two of the eye's axes, the pupillary axis and the line of sight. The problems associated with the use of the pupil centre stem from its non-uniform shape and constriction. The pupil does not form a perfect circle so the location of the centre point is dependent on the pupil tracking algorithm used to detect it. The problem is amplified by the asymmetric constriction of the pupil which translates the centre point nasally. There is a certain amount of control over the constriction response, such as maintaining constant illumination levels; however, the response is not solely dependent on illumination and as such the central pupil location still presents a source of error. Interestingly, KAMRA inlays (personalEYES, Sydney, Australia) are fixed diameter aperatures implanted into the eye to improve near vision based on a pin hole effect. Investigations into visual performance with these implants in presbyotic patients suggest improved vision quality[91] and thus indicate that the movement of the pupil centre during dilation or constriction has little effect on the performance of the eye.

One advantage the pupil does have over other reference points is that it can be readily identified and imaged. The visual axis is constructed through theoretical nodal points, these points are only present in non-toric centred optical systems. In addition to this, the nodal points can not be imaged, making them difficult to use for alignment. To negate this issue, Purkinje Image I is used as an approximation. The theoretical position of the nodal points lie very close to the centre of curvature for the anterior cornea. Purkinje Image I is produced between the illumination source and the anterior cornea's centre of curvature making it an imageable attribute of the visual axis; however, it is still an approximation of a theoretical point. The cornea is also susceptible to changes in radius of curvature brought about by corneal diseases such as keratoconus [4] The position of Purkinje Image I is thus directly affected by this parameter providing another benefit to the pupil as a reference point.

The Purkinje Images are valuable tools in the determination of alignment axes, their use can also be found in the quantification of the optical axis. The optical axis, again theoretical in nature, is made tangible by the imaging of the Purkinje Images. In fact, some define the eye's optical axis as the closest alignment of the Purkinje Images. The use of Purkinje Images to define an axis in this way is beneficial because these images are invoked by external light sources negating the natural variation associated with biological reference points.

[4] Keratoconus is a decrease in the cornea's radius of curvature such that the cornea becomes more cone shaped.

In regards to the movements of the eye and their potential contribution to misalignment, the type and magnitude of movement are entirely dependent on the stimulus. During typical alignment procedures, large attentional and disparity stimuli are not generated so movements such as saccades and vergence will be minimal. If saccades are found then there are methods by which they can be suppressed by invoking the skip over response.

Smooth pursuit eye movements allow an interesting alternative to the stereotypical static images used in alignment. As smooth pursuit eye movements accurately mimic target velocities within a certain range, it allows the use of a moving image for alignment. The smooth pursuit movement however, can comprise of catch-up saccades which correct for positional error. Thus the introduction of a moving target would provide stimulus for the eye's larger movements. This approach potentially causes more problems than solutions.

A more beneficial eye movement for alignment is the vestibulo-ocular reflex which compensates for head rotation. This contribution, especially in any alignment process which is hand-held or head mounted, would prevent rotational misalignment caused by the instrument moving relative to the head.

The eye movements most likely to cause misalignment during alignment procedures are the fixational movements, particularly microsaccades. The ocular tremor is the smallest eye movement and is a constant presence; however, its impact on misalignment is minimal as the amplitude of its movement is small. Ocular drift presents a greater magnitude of movement having the potential to cause variation in measurement, warranting identification during alignment. Ocular drifts also have strong links with the initiation of microsaccades, reiterating the benefit in their detection. Out of the three fixational movements, microsaccades have the largest amplitude making them the greatest potential contributor to misalignment. Similarly to their saccadic counterparts, they are also susceptible to suppression during high concentration tasks. Microsaccades then, while potentially being the most prominent in misalignment, are avoidable.

2.9 Conclusions

All of the alignment axes discussed in the review are subject to natural variation and theoretical reference points, this is particularly the case when the pupil is used, as the centre can move up to 0.6 mm on constriction. The visual axis and the optical axis offer more stable reference axes when identified with the Purkinje Images, thus potential alignment/tracking techniques would benefit by detection of either of these axes.

Eye movement contributors to misalignment are predominantly the fixational movements. It is reasonable to consider that the stimulus for larger movements, such as saccades and vergence movements, would be absent in typical alignment procedures. This would not be the case if smooth pursuit movements were employed to control eye movement. Although smooth pursuit eye movements have less than 10% error over specified target velocity ranges, their ability to stimulate saccades mean they would cause more problems than they would potentially solve.

Out of the three fixational movements, microsaccades would cause the most error; potential alignment/tracking techniques would benefit from the detection of these movements. The technique would then need to resolve microsaccadic eye movements between 0.167 - 0.5°occurring at a frequency of 1 - 3 Hz. The technique would also benefit from, though not require, the detection of ocular drift, in which case movements of up to 0.083°would need to be resolved occurring at a frequency of 2 - 5 Hz. Differentiation of the two movements would be achieved on the basis of velocity, as drift (0.083°/s) is slower than microsaccadic velocity, requiring a sampling frequency high enough to analyse this.

Chapter 3

Contact and Non-Contact Eye Tracking Techniques

3.1 Chapter Overview

To critically assess eye tracking technology with reference to its potential application in eye alignment, a literature review was performed on both contact and non-contact forms of eye tracking.

In order to evaluate each tracking technique, the methodologies were analysed against three criteria: accuracy, identification of alignment and ease of integration. Accuracy was evaluated on the technique's ability to resolve eye movements outlined in the Chapter 2, namely microsaccades and, potentially ocular drift. The ability of the technique to identify alignment was also investigated. Ideally the alignment technique would be able to identify alignment, and the magnitude of misalignment, without consulting the measurement taken with the instrument. The final factor, integration, refers to the ease in which the tracking technique can be incorporated into ophthalmic devices, particularly the v360 pachymeter. It is important that the tracking system does not intrude into the instrument's designated function, as this would discourage its use in new devices.

The chapter concludes by suggesting eye tracking techniques most suitable for eye alignment applications.

3.2 Introduction

Eye tracking, although specific in its function, is used in a wide variety of applications which can generally be categorised as either diagnostic or interactive [6]. The distinction originates from whether the eye is tracked for quantitative assessment, as in diagnostic applications or for input into external devices, as in interactive applications. Areas such as neuroscience, psychology and market research are predominately interested in objective accounts of eye movement and gaze direction. However, applications in computer science and engineering require gaze direction, to allow its use as an interactive tool to communicate to other devices.

Interestingly, one of the areas in which eye tracking is under used is in ophthalmic instrumentation, specifically in the form of eye alignment. Eye alignment and eye tracking contain subtle differences in approach, brought about by their purpose. Eye tracking is concerned with measuring the magnitude and direction of eye movement; eye alignment does not require this information, all it is required to distinguish is whether the eye is in the aligned position or not. There are several reasons why eye tracking has advantages over eye alignment, particularly in the context of this research. The main advantage is that tracking allows the quantification of misalignment providing the alignment position is known. This means that tracking systems have the potential to correct misalignment independently. Tracking also allows the position of any diagnostic measurement to be validated at the time of measurement to ensure it was performed on the correct location. Both of these concepts are a goal of the final alignment system and thus, highlight the need for a review of eye tracking technologies.

3.3 Scleral Search Coils

The recording technique thought of as the gold standard in eye tracking is the scleral search coil method, first employed by Robinson [1] and then later refined by Collewijn [92]. It has been used to investigate a host of eye movements from the vestibulo-ocular reflex to saccades [93, 83, 94]. There have also been a number of alternative methods [95, 96, 97] but all still follow the same principle. A copper wire embedded in a contact lens is placed on the eye. The contact lens is typically bigger than a standard contact lens to allow extension onto the limbus. The contact lens adheres to the eye by way of a suction ring on the back, this ensures no slippage during the procedure. The subject is then placed in a set of orthogonal magnetic fields, the current induced in the coils is then proportional to their orientation, the mathematical calculations behind this are explained in Schor and Furman's paper [98].

Figure 3.1: Scleral search coil on the eye. (Copyright © 1963, IEEE [1])

The accuracy of the search coil technique allows tracking within 0.041-0.083°[99], current systems can sample up to 1000 Hz and within a range of +/-20°horizontally and +/-15°vertically [100]. The technique also has the ability to track the eye when it is closed [101]; however, even with this advantage and the high tracking precision, the technique is subject to associated problems. The first and most obvious problem is the contact nature of the technique, for this reason it is recommended by the suppliers that the contact lens is worn for up to 30 mins at a time, although work has been done to extend this to 120

min [102]. More seriously, the contact lenses carry a small risk of corneal ablation[1] [103], as well as directly affecting the dynamics of eye movement, particularly saccades which are reported to take 8% longer and are 5% slower [103].

Although the technique has the ability to track the eye with great accuracy its application in eye alignment would not be advantageous. The covering of the eye with a contact lens would prevent diagnostic measurements in the majority of cases. The application of the contact lens would also be an unwanted addition to any alignment process as well as the additional equipment (magnetic field generators, bite-bar, chin-rest, induction coils, amplification equipment, signal conditioning equipment) which comes with the technique. The technique is sensitive to head movement thus requiring the head to be restrained, something which would not be possible in devices which require hand-held alignment. More importantly, the method does not directly identify an alignment axis, thus the aligned position would have to be inferred from the measurement data.

[1] Corneal ablation is the removal of material from the surface of the cornea.

3.4 Electro-Oculogram

It has long been realised that eye movements can be measured with the corneo-retinal standing potential which is present between the cornea and the retina [104]. The cornea is positively charged with respect to the retina, with a voltage difference of 15 - 200 μV [6, 99]. Electrodes placed at either side of the eye can detect changes in this potential. When the eye rotates the measured reading changes with 20 μV/°typical [6]. The potential is attributed to the higher metabolic rate of the retina when compared to the cornea. The potential also changes depending on illumination [2].

Figure 3.2: Electro-oculography and the corneo-retina standing potential [2].(Reproduced with permission form Elsevier)

Although the technique has the advantage of detecting eye movements when the eye is closed, the signal is very weak and the changes in the potential due to illumination levels affect the stability of the readings. For these reasons, accuracy for this technique is between +/-1.2 - 1.8°[105, 106], much lower than that of scleral search coils. The simplicity in the signal however does allow for high data acquisition frequencies, current systems record at up to 10 kHz (BluGain - Cambrige University, Cambridge, United Kingdom).

Compared with the scleral search coils technique the electro-oculogram is far less intrusive and does not obscure the eye. However, for the purposes of alignment the poor accuracy of approximately 1°mean that it would be unable to detect microsaccades, a strong potential candidate for errors in alignment.

3.5 Purkinje Images

Purkinje Images, shown in figure 3.3, are reflections from each of the refracting components in the eye. The anterior and posterior cornea give rise to Purkinje Image I and II respectively, while Purkinje Images III and IV are formed by the anterior and posterior lens surfaces. They are used in applications such as measuring accommodation; however, their main applications are in the assessment of ocular misalignment [11, 12, 13, 14, 15, 3] and eye tracking [107, 108, 109]. As the Purkinje Images are reflections from the cornea and lens they give valuable insight into the alignment of the eye's optics. This is important in intraocular lenses (IOL), which are implanted after cataract surgery to replace the optical power of the opaque lens, as it is important to know the orientation of the inserted artificial lens to gauge the success of the procedure. They have also been used to assess the accommodative properties of these lenses [110].

Figure 3.3: The Purkinje Images formed by a semi-circular LED array [3].

Their use in eye tracking equipment was first implemented by Cornsweet and Crane [109] and then later improved on by Crane and Steele [107, 108]. The technique uses Purkinje Image I and Purkinje IV to calculate both the translational and rotational movements of the eye. It can do this by the manner these reflections move in reference to each other. During rotation Purkinje Image I and Purkinje Image IV will move towards or away from each other; however, during translation Purkinje Image I and Purkinje Image IV will move through the same distance in the same direction.

Current Purkinje tracking systems reflect the Purkinje Images onto photo-diodes by the use of mirror mounted servo motors. The movement in these servo motors is then proportional to the movement of the eye. Tracking of the eye in this way allows 0.017°accuracy in ranges up to 10 - 20°[109, 108]. The tracking frequency is restricted by the frequency response of the motors, though this is still a considerable 500 Hz [108].

The alignment of the Purkinje Images in the eye suggests the alignment of the optical axis and the illumination source; however, due to the misalignment of the lens with respect to the cornea the alignment of the Purkinje Images is rare. Thus the closest alignment of the Purkinje Images is said to be an approximation of the eye's optical axis. This relationship

between the eye's optical axis and the Purkinje Images has been used for alignment in laser eye surgery with an Optical Coherence Tomography (OCT) device [111]. When this device is used to monitor the eye, the OCT sensor becomes saturated on alignment of the corneal apex with the measurement axis (figure 3.4).

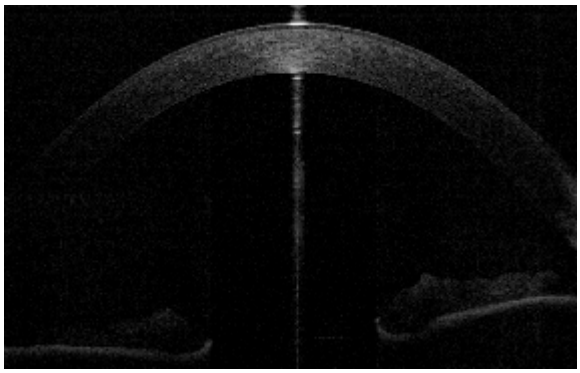

Figure 3.4: OCT alignment with corneal apex. Bright central line through image indicates intersection with the cornea and corneal apex.

Eye tracking with Purkinje Images is performed to a high accuracy as well as being non-invasive. Due to the accuracy of the technique, it is able to detect eye movements such as microsaccades. It also has several other attributes which lend itself to eye alignment. Firstly, by using the Purkinje Images, a direct assessment of the orientation of the eye's optical axis can be made, this includes the quantification of misalignment to this axis. The different movements of the images during eye rotation and translation mean that the tracking system can resolve translational movements (preformed by the head) and rotational movements (preformed by the eye). This information would be invaluable in any feedback system designed to correct for misalignment. Unlike the scleral search coils and electro-oculogram, Purkinje tracking systems are unable to monitor eye movement when the eye is closed; however, for ophthalmic devices this is not necessarily an issue. The main problems with this technique lie in its integration, current tracking systems are too large to merely add onto a device. Thus, in order to rectify this, changes would have to be made to the tracking system to make it a feasible technique for alignment.

3.6 Video-Oculography

Video-oculography (VOG) is a relatively new technique when compared to other techniques, its emergence is largely down to the improvement and miniaturisation of imaging hardware. The technique is based on high speed image acquisition of the eye which is then processed in real-time, although the image can be stored and post-processed. To deduce the eye's movement, the position of features on the eye are recorded and eye movement inferred; common features include the limbus, pupil and blood vessels.

The most frequent feature used is the pupil, this is due to its ease of detection. Its dark appearance gives sufficient contrast difference from the iris to allow its central position to be found. To improve the contrast between the iris and the pupil the bright pupil response is often invoked. Due to the eye's shape, when an IR(infra-red) light source is collinear with the imaging axis the retina will act as a retro-reflector causing the appearance of a bright pupil. IR light is used as it is invisible to the subject, thus allowing the pupil to dilate.

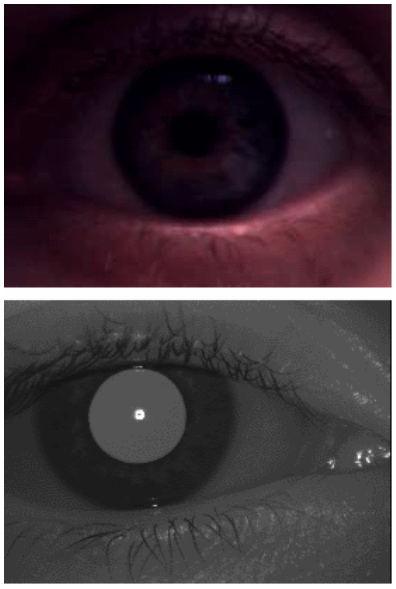

Figure 3.5: Dark and bright pupil comparison.

The bright pupil response is often used in conjunction with Purkinje Image I to form the pupil/corneal reflection[2] technique. In this case, the central pupil position is tracked with respect to Purkinje Image I. The relationship is similar to that of Purkinje Image I and IV. Imaging is made easier in both cases with the presence of the reference points in the same focal plane.

The limbus is another feature often used in tracking as there is a high contrast between it and the sclera. The limbus, unlike the pupil, does not change size leading to a more

[2] In the context of pupil/corneal reflection eye tracking the corneal reflection is the name given to Purkinje Image I

stable reference point; however, it is largely occluded by the upper and lower eye lids. The limbal boundary is also not as well defined as the pupil boundary.

VOG is a very popular technique, and for this reason there is a diverse range in system performance. The difference in systems employing the technique stem from the sophistication of the hardware used to process images of the eye. Instruments which use either dark pupil, bright pupil or pupil corneal reflection have a range of accuracies from 0.125 - 1°[112, 113, 114, 115, 116, 117] with resolutions ranging from 0.01 - 0.1°[112, 113, 114, 115, 116, 117]. Temporal frequencies can range from 25 - 1250 Hz [112, 113, 114, 115, 116, 117] depending on system and the set up.

The high accuracy in this technique and non-contact nature mean it is a viable tracking technique for alignment. The method also has the added benefit in the ability to directly assess the orientation of two alignment axes, both the visual axis and the line of sight.

3.7 Discussion

The suitability of each tracking technique was assessed on the basis of three criteria: accuracy, alignment identification and integration.

The technique found to be the most accurate is the scleral search coils, this method is also considered to be the gold standard in eye tracking. However, the apparatus required for this technique mean that it is not suitable for alignment. The presence of contact lenses in the eye would inhibit the majority of diagnostic measurements, while the additional equipment required to produce and measure the magnetic fields would not lend itself to portability.

Tracking via the electro-oculogram is a far less intrusive process; however, the poor accuracy of the technique means that it would be unable to detect the type of eye movements required for the alignment system. In addition to this the electro-oculogram offers no way to directly assess alignment, which is also a factor in scleral search coils. This discounts both contact forms of eye tracking for alignment.

In terms of the detection of alignment, both non-contact methods hold greater potential. The features which they use to track the eye are also the features by which the position of the alignment axes can be determined. In regards to VOG, the detection of the pupil indicates a reference point for the line of sight. Pupil corneal reflection tracking uses Purkinje Image I, which is a reference point for the visual axis, allowing both the visual axis and the line of sight to be detected. Purkinje Image tracking with the use of Purkinje Image I and IV allows the detection of the eye's optical axis.

Both Purkinje Image tracking and VOG perform to a high accuracy allowing detection of microsaccadic eye movements. In fact, studies comparing VOG to scleral search coils methods have shown discrepancies of less than 1°[118], while other studies have suggested VOG is a viable alternative in longer studies [119]. Larger differences have been shown in scleral search coil comparisons with Purkinje Image tracking; however, this is attributed to the dynamics of the lens [120].

The last remaining criteria, integration, also lends itself to VOG and Purkinje Image tracking. Many ophthalmic instruments have integrated cameras allowing imaging of the eye. Imaging the eye forms the first step in tracking, all that is then required is improvement of the imaging hardware, tracking algorithms and the appropriate illumination.

Due to the significant improvements in imaging technology, the accuracy and resolution which can be achieved with VOG and Purkinje Image techniques is close to that of scleral search coils, the gold standard in tracking. The additional benefits of direct alignment assessment and ease of integration highlight the potential for these methods in alignment.

3.8 Conclusions

The requirement in this research for the alignment system to align to the optical axis of the eye means that a technique based on Purkinje Image tracking would be the most suitable. Research into VOG suggests it could monitor the line of sight and the visual axis to a high accuracy, but the inability to monitor the optical axis means that Purkinje Image tracking is favoured.

Scleral search coils were deemed the most accurate; however, due to the highly intrusive nature of the method, scleral search coils are not feasible for alignment techniques. Although Electro-oculography is far less intrusive, it does not track the eye with the accuracy required to detect microsaccades and ocular drift. Both contact methods also do not allow direct assessment of alignment making them inappropriate.

Chapter 4

Parameters Identification

4.1 Chapter Overview

The objective of this chapter is to identify parameters for the alignment system. This is to enable the construction of an alignment instrument to apply novel alignment philosophies. As the alignment methodology has an intended target for integration, the v360 pachymeter, the alignment parameters are formed with reference to this device.

To determine any systematic error in the v360 pachymeter and its relation to misalignment, a calibration piece of known thickness and refractive index was measured under different amounts of angular misalignment. This also allowed the identification of measurement properties associated with misalignment.

The systematic error and the pachymeter's measurement properties were then related to misalignment from the corneal apex with the aid of a newly created geometric mathematical model.

The chapter concludes by outlining the alignment tolerances as determined from the experimental results and the model cornea.

4.2 Introduction

As with all ophthalmic instrumentation, the precision of alignment is considered relative to the accuracy of the device, thus there is a fundamental link between the two. In relation to this thesis, to validate any novel alignment technique or philosophy, the technique must eventually be incorporated into an ophthalmic instrument. The v360 pachymeter is the instrument which will eventually use any novel alignment technique; thus the performance of this instrument has to be considered in the design of the alignment technique and the construction of alignment specifications. The important measurement properties for the purposes of alignment are the measurement accuracy and the tolerance for misalignment.

While any systematic error in the device is important, it can not be directly used for the eye alignment specifications. The v360 pachymeter makes a reflection based point measurement, thus is affected by the orientation of the surface which the measurement beam intersects, because of this, rotational misalignments of the device to the eye are amplified by the curved surface of the cornea. The thickness of the cornea is also a source of measurement variation as it is not uniform, this stems from the dissimilar eccentric arcs which form the anterior and posterior surfaces of the cornea. The accuracy of the device also needs to be considered in relation to the range of corneal thickness. The lateral distance from the corneal apex, which the pachymeter would be able to resolve differences in corneal thickness, needs to be quantified. It would also be advantageous for alignment tolerance calculations to determine the potential corneal thickness deviation as a function of the alignment precision.

4.3 Device Specific Parameters

The v360 pachymeter is a non contact pachymetric device for measuring central corneal thickness. The device is important in the context of this research as it is the intended target for the alignment technique. In order to aid construction of specifications for the alignment technique, it is necessary to evaluate the performance of the device in terms of its measurement properties, namely, accuracy, precision and range. The range is particularly important as it indirectly describes the alignmen tolerances. Specifically, the range refers to the maximum and minimum corneal thickness measurements recorded in the measurement procedure. The accuracy and precision over this range are also important in the evaluation of the instrument. The resolution of the thickness measurement can then be used in conjunction with the eye movement data, detailed in the literature review, to form the resolution specifications of the alignment technique.

Figure 4.1: Illustration of v360 measurement technique. The passage of a focused point of light causes a peak in the return signal when intersecting changes in refractive index. (Reproduced with permission from author [4])

The measurement principle of the v360 pachymeter is based on the spatial difference between reflections from the anterior and posterior corneal surfaces. The device translates a focused point of light through the cornea, allowing a non contact pachymetric measurement. The translation of the focused point of light is recorded via an encoder. On intersection with a surface the light is reflected back into the device, through a pin hole, registering a peak in the return signal. The corneal thickness is then determined by the separation between the anterior and posterior peaks as recorded by the encoder. As the technique is reflection based, intersection with a surface which is not perpendicular to the measurement axis results in the reflection of light outside the return path. This results in poor surface detection due to the low amplitude in signal.

In order to assess the accuracy, precision and range of the device, a static object of known thickness is measured in variable rotations. A static object is used as opposed to a human

eye because this method of testing allows the systematic error of the instrument to isolated without the random error associated with the eye. A static object also allows greater manipulation of angular orientation, thus greater control of the rotation variable.

4.3.1 Aim

The purpose of the investigation was to determine the measurement properties of the v360 pachymeter for the formulation of alignment specifications. The measurement properties were evaluated in terms of measurement accuracy, precision and range. Specifically, the experiment aimed to determine the affect of angular misalignment on these properties.

4.3.2 Method

4.3.2.1 Apparatus and Procedure

The v360 pachymeter was fixed to an optical breadboard (Thorlabs, Germany). A dual surface optical flat (SLS Optics, Isle of Man), refractive index 1.45601140 at 670 nm, and thickness 408.75 +/-0.2 µm, was placed in front of the pachymeter. The optical flat was held in position with a 5 axis rotation/translation stage (Thorlabs, Germany) with 0.167 +/-0.083°angular resolution. The stage was factory calibrated prior to purchase. Figure 4.2 shows the experimental set up.

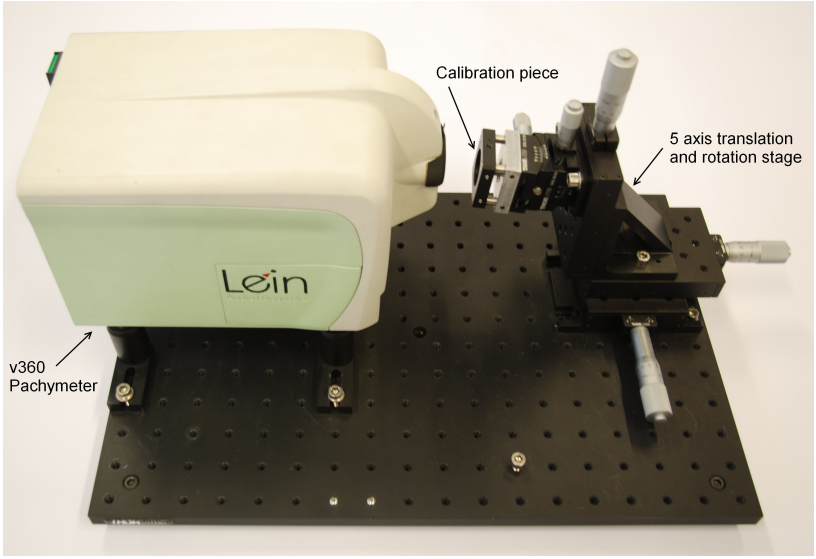

Figure 4.2: Experimental set up. The v360 Pachymeter is positioned infront of a 5 axis translation and rotation stage used for manipulating the calibration piece.

The data was acquired by way of 3 sets of 30 scans (thickness measurements) for each 0.167°increment between 0°and 5°of misalignment. For each set, the incremental order of misalignments between 0°and 5°was randomised.

Initial alignment was achieved by manipulating the rotational axes of the translation rotation stage in order to achieve the maximum peak from the front surface of the optical flat.

Both the optical flat and the protruding optics of the v360 pachymeter were cleaned with optical cleaning fluid and micro-fibre cloth prior to experimentation.

All data was acquired in one session.

4.3.2.2 Processing

All acquired data was processed in Matlab (Mathworks, USA). The raw data takes the form of scan data, the thickness measurement is then inferred from the position of the peaks. A generic find-peaks function was used to determine the location of the peaks.

Thickness measurements used for the accuracy results were obtained by determining the mean thickness value for each set of 30 scans and then calculating the overall mean for the 3 sets. Measurement error was then calculated by determining the magnitude of the difference between the actual thickness of the optical flat and the measured thickness. The actual thickness is defined as the thickness of the calibration piece along the pachymetric measurement axis, this takes into account the increase in measured thickness as a result of the angular displacement.

Measurement precision was calculated by a similar process. The standard deviation was determined for each set of 30 scans, the overall mean was then determined from the 3 sets.

Range was calculated in a similar process to precision, however the standard deviation calculation was replaced with a range calculation.

4.3.2.3 Statistical Analysis

For each set of results, accuracy, precision and range, the coefficient of correlation was determined by applying the relevant regression model.

4.3.3 Results

4.3.3.1 Accuracy

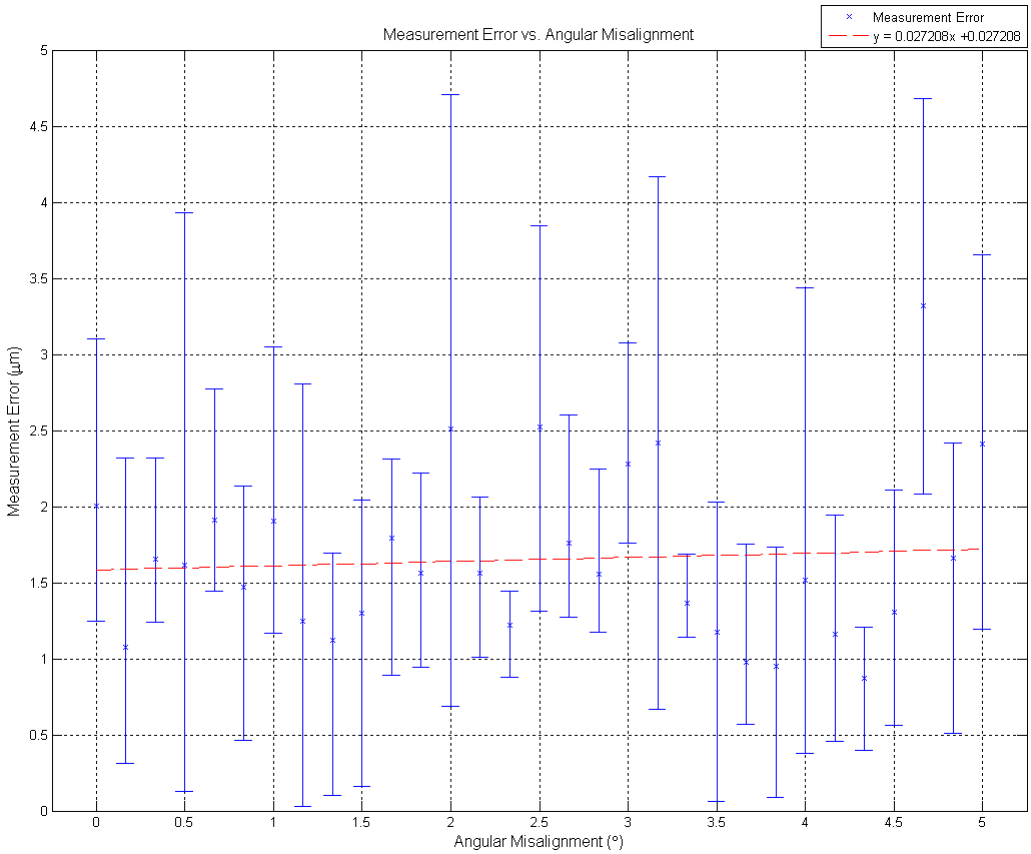

Figure 4.3: Accuracy vs misalignment, the error bars represent the maximum and minimum values when calculating the mean.

Figure 4.3 displays the measurement error in the v360 pachymeter's thickness measurement. The graph also includes a line of best fit highlighting an almost constant value in measurement error under varying amounts of misalignment. The average measurement error was calculated at 1.65+/-0.56 µm (SD), suggesting high accuracy in the thickness measurement.

Statistical Analysis

Inpsection of the graph relating accuracy to misalignment suggests there is no correlation between misalignment and accuracy. To statistically test this assumption, the significance of the Pearson's correlation coefficient is calculated at the 0.05 significance level.

$H_o : r = 0$

$H_a : r \neq 0$

Statistical analysis of the correlation between the instrument's accuracy and angular misalignment suggests that the relationship is not significant. The obtained p-value is 0.345, higher than the predefined confidence level of 0.05. The null hypothesis is then accepted and there is no correlation between accuracy and misalignment in the 0°to 5°misalignment range. The Pearson's correlation coefficient for this data set is 0.0732. The results are shown in table 4.1.

Pearson's Correlation Coefficient (r)	p-value
0.0732	0.345

Table 4.1: Accuracy vs misalignment statistical analysis.

4.3.3.2 Precision

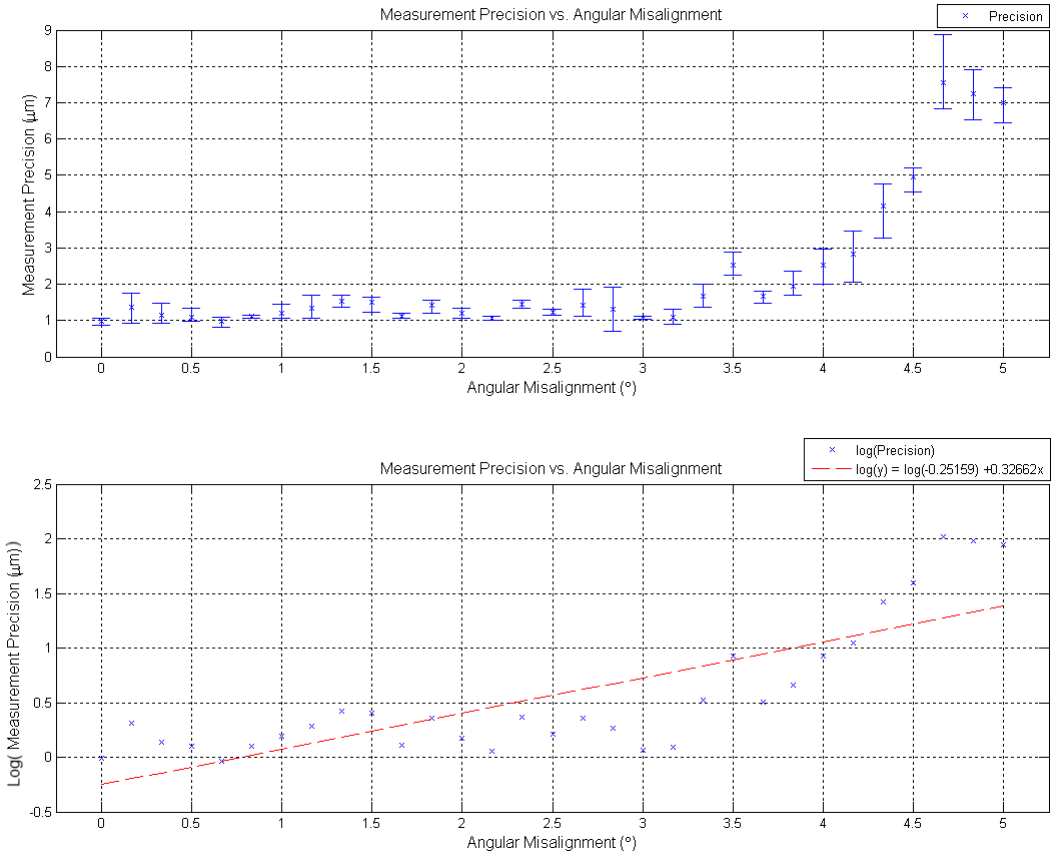

Figure 4.4: Precision vs misalignment, the error bars represent the maximum and minimum values when calculating the mean.

Figure 4.4 shows the relationship between the v360 pachymeter's thickness measurement precision and angular misalignment. In terms of this experiment, precision is defined as the standard deviation in the thickness measurement. Each thickness measurement is an average of 30 repeated measures, the overall mean is calculated by the average of 3 of these thickness measurements. The maximum and minimum values are the maximum and minimum values obtained from all 90 scans. Inspection of the top graph suggests an exponential relationship between measurement precision and misalignment; the bottom graph examines this relationship further by taking the natural logarithms of the precision data points and fitting a line of best fit. The minimum mean precision value was 0.97 µm while the maximum was measured at 7.55 µm. The results suggest that the precision measurement properties remain approximately constant until 3°of misalignment.

Statistical Analysis

To statistically examine this relationship an exponential regression analysis is carried out on the data set to validate the exponential model.

Table 4.2 displays the exponential regression analysis performed on the precision results. The results suggest that the exponential model used to fit the precision data points is a valid fit at the 0.05 confidence level producing a p value of 0. The coefficient of correlation for these statistics was also calculated yielding an R value of 0.8026, suggesting a moderate correlation between measurement precision and angular misalignment in the 0°to 5°range.

Precision Exponential Regression Analysis					
Source	df	SS	MS	F	p value
Regression	1	7.349	7.349	52.508	0.000
Error	29	4.059	0.14		
Total	30	11.408			

Table 4.2: Precision vs misalignment statistical analysis.

4.3.3.3 Range

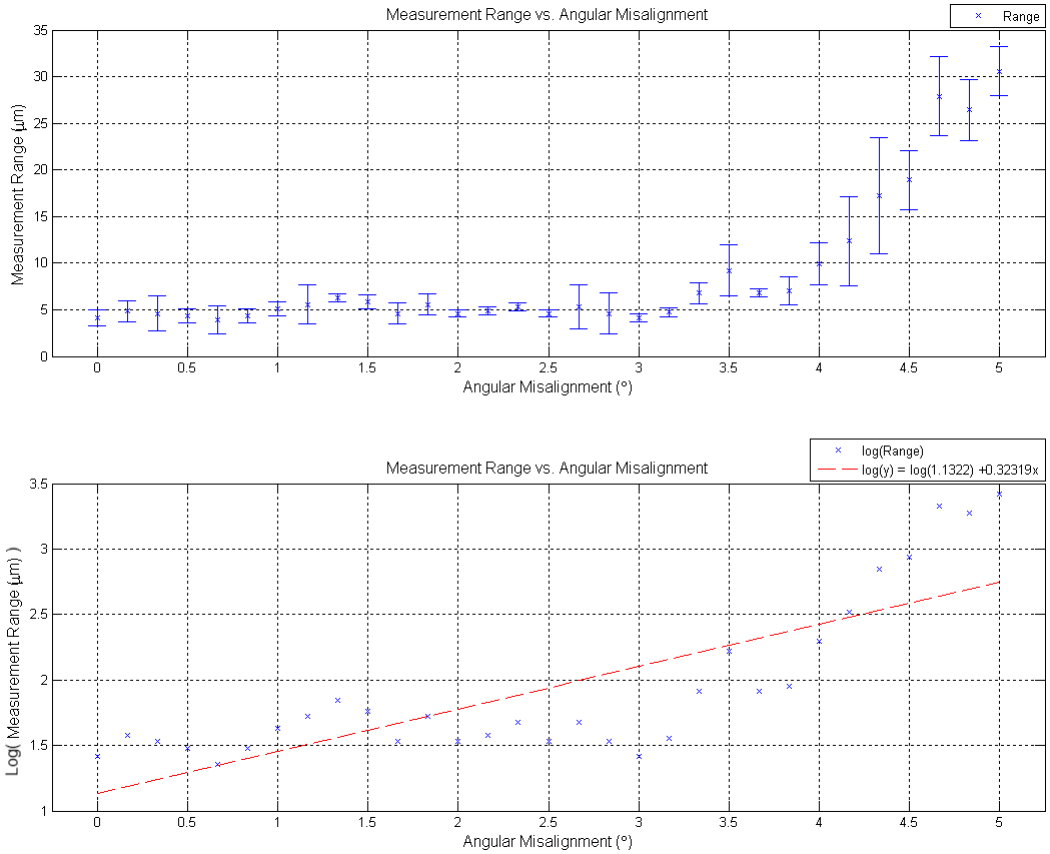

Figure 4.5: Range vs misalignment, the error bars represent the maximum and minimum values when calculating the mean.

Figure 4.5 shows the relationship between the v360 pachymeter's thickness measurement range and angular misalignment. In terms of this experiment, range is defined as the difference in maximum and minimum thickness measurements from the thickness measurement array used to calculate the mean. As in the precision analysis, the results suggest a exponential relationship between misalignment and range. The minimum mean range value was measured at 3.88 µm while the maximum range was measured at 30.58 µm. The results suggest that the precision measurement properties remain relatively constant until 3°of misalignment.

Statistical Analysis

To statistically examine this relationship an exponential regression analysis is carried out on the data set to validate the exponential model.

Table 4.3 displays the exponential regression analysis performed on the range results. The results suggest that the exponential model used to fit the range data points is a valid fit at the 0.05 confidence level producing a p value of 0. The coefficient of correlation for these statistics was also calculated yielding a R value of 0.8009, suggesting a moderate correlation between measurement precision and angular misalignment in the 0°to 5°range.

Range Exponential Regression Analysis					
Source	df	SS	MS	F	p value
Regression	1	7.196	7.196	51.871	0.000
Error	29	4.023	0.139		
Total	30	11.219			

Table 4.3: Range vs misalignment statistical analysis.

4.3.3.4 Peak Amplitude

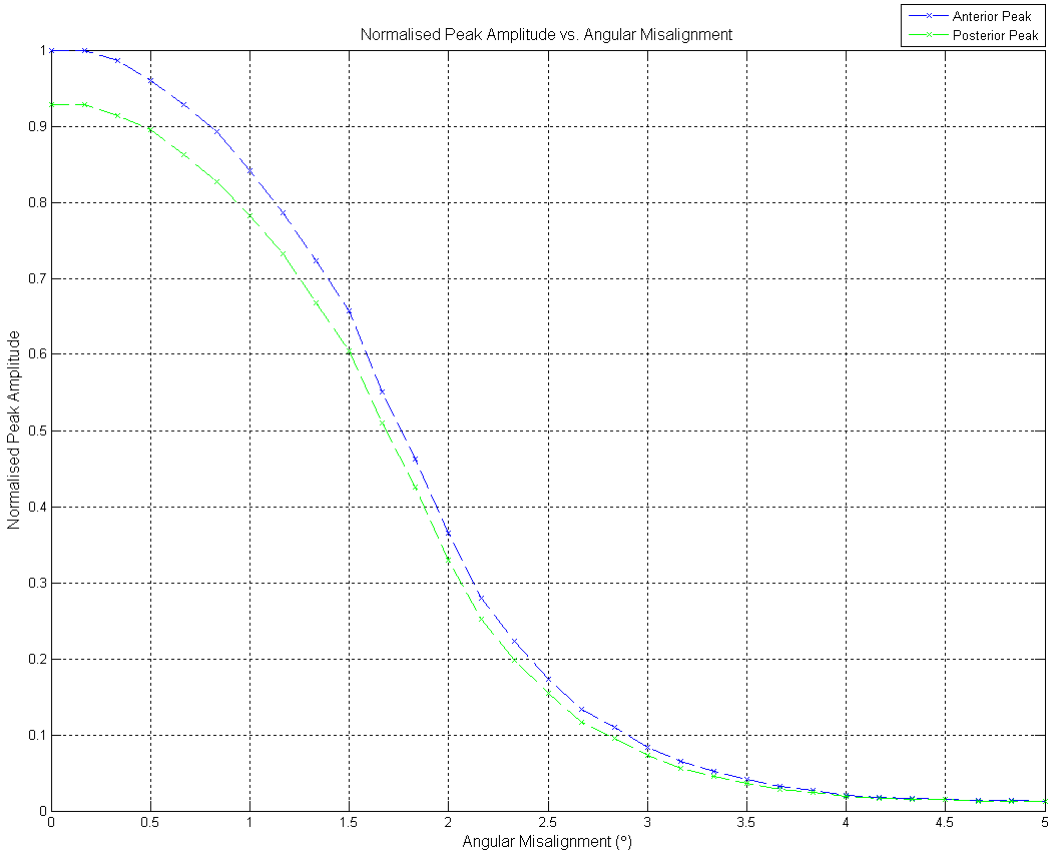

Figure 4.6: Anterior and posterior peak amplitude vs misalignment.

Figure 4.6 describes the normalised average peak amplitudes obtained from the experiment. The anterior peak amplitude refers to the amplitude of the peak obtained from the front surface of the optical flat, the posterior peak amplitude refers to the corresponding amplitude of the peak obtained from the back surface of the optical flat. Both peaks show a rapid decrease in amplitude with increasing misalignment before approaching similar amplitude levels at approximately 4°of angular misalignment.

4.3.4 Discussion

The results suggest measurement error remains constant throughout the investigated range of misalignment. This can be seen in figure 4.3 and the statistics contained in table 4.1. However, the results also suggest measurement precision and range have an exponential relationship with misalignment, whilst demonstrating a moderate correlation with misalignment (table 4.2, table 4.3).

One potential reason for the exponential relationship not being mirrored in the accuracy results is the averaging performed on the thickness measurement to obtain the final thickness value. Even with the decrease in precision and increase in range over 3°of misalignment the 3×30 scans are sufficient to correct the measurement accordingly.

In terms of the quality of measurement, ultimately this is dependent on the appearance of the peaks in the scan data[1]. There are a number of ways in which the peaks could be improved to achieve a more defined peak, however, the raw data is sufficient to gauge the performance of the instrument at its very basic level. It can be inferred from the accuracy evaluation that the peaks are formed in the correct position, as an accurate measurement can still be achieved by averaging repeated measures. It is then the quality of peaks in the raw data which introduce the decrease in measurement precision and increase in measurement range.

Even though there is an obvious deterioration in measurement precision and range, this deterioration does not occur until after 3°of misalignment, meaning that the measurement properties remain constant up until this point. In fact, the most notable change with misalignment is the change in peak amplitude (figure 4.6) which demonstrates a rapid decrease in amplitude with increasing misalignment. However, the affects of this rapid decrease do not propagate through to other measurement properties until after 3°of misalignment.

When relating these findings to the eye there are 2 major points to consider. Firstly, the peak amplitude will greatly diminish when the measurement is performed on the eye, particularly the peak obtained from the posterior cornea. This can be attributed to the lower refractive index change at the posterior corneal - aqueous humor interface, when compared to the fused silica - air interface, found at the back surface of the optical flat. This is an important consideration as the experiment has highlighted the importance of the quality of peaks in the thickness measurement. Secondly, the experiment used an optical flat; in a human eye the instrument will be presented with 2 curved surfaces. The repercussion of this is that the rate at which misalignment will occur due to eye rotation will increase due to the shape of the cornea.

While the results do not directly allude to the alignment tolerance for the intended alignment device, they do dictate the systematic error in the instrument. This then forms the starting point for the generation of alignment tolerance specifications. In this regard, the most notable result is the measurement range, this forms the resolution of the system for one off measurements. Also of note is the constant nature of the measurement properties

[1] Where quality refers to the appearance of the peak at its very tip

up until 3°of angular misalignment. The alignment tolerance for the alignment device can then be based on either: the 3°of angular misalignment in which the measurement accuracy remains constant or, the area round the apex of the anterior cornea corresponding to a corneal thickness of <3.88 µm. The system performs a repeatable measurement up until 3°of angular misalignment, thus the lateral movement over the surface of the cornea and the amount of eye rotation which causes this misalignment must be calculated to obtain the relevant alignment tolerance. As the instrument cannot resolve thickness changes under 3.88 µm, there is no advantage of aligning to an area round the corneal apex which contains thickness changes less than this amount, thus this area must be calculated for the alignment tolerances.

There is then a need to relate the measurement properties to the cornea to determine the final alignment specifications.

4.3.5 Conclusions

Thickness measurement error relating to accuracy in the v360 pachymeter was found to be 1.65+/-0.56 μm, this remained constant throughout the investigated range of 0°to 5°of misalignment. The poor correlation (R = 0.073) between accuracy and misalignment is attributed to the averaging performed on the thickness measurement. This averaging determines the mean thickness from 30 scans and repeats this process a further 2 times. Once 3 means have been collected the mean of these means is determined and displayed as the thickness measurement.

Analysis of the precision and range results suggest an exponential relationship with misalignment. The correlation coefficients for precision (R = 0.8026) and range (R = 0.8006) suggest moderate correlation between each property and misalignment. The consequence of this is that the measurement properties, namely accuracy, precision and range, remain constant up until 3°of angular misalignment.

In relation to the original aim of the experiment, to determine the relationship of the thickness measurement properties with misalignment, the notable results are a 3.88 μm measurement resolution and a 3°angular misalignment tolerance. In order to convert these values to actual alignment specifications the results must be mapped onto the cornea.

4.4 Geometric Mathematical Model Cornea

The construction of a geometric mathematical model cornea forms a significant aspect of the research, it gives the ability to relate the v360 pachymetric measurements to the eye. Ideally, the evaluation of the instrument would be achieved directly as it measures a cornea; however, practically this is difficult due to the inability to manipulate and hold the eye in precise locations, relative to the instrument. The inspection of mathematical geometric model alleviates this difficulty making it a valuable source of information when defining the alignment technique's specification.

The creation of a mathematical model cornea is not a novel task, mathematical model eyes have been defined as early as the beginning of the 20th century in the works of Gullstrand [121]. Many more models have been conceived since then, each varying due to their purpose. Models such as Gullstrand's [121], often termed paraxial models, attach more importance to the optical characteristics of the eye. The paraxial models also tend to model the cornea as spherical, which is a good approximation for the central 4 mm, but not a true representation of the cornea as a whole. Improved proficiency in imaging and measuring the cornea has led to growing interest in cornea's actual shape, thus many models now incorporate the cornea's half elliptical shape [122, 123, 124]. These models are often rotationally symmetric round the optical axis[2]. Amongst other techniques for measuring the cornea, corneal topography has shown meridian changes in the shape of the cornea, generally a slightly larger radius of curvature in the horizontal meridian when compared to the vertical (with-the-rule astigmatism) [7]. Very recent models incorporate this meridian change by including a cosine function to describe the change in radius of curvature relative to meridian [125, 126].

Generally, model corneas are developed to investigate the optical properties of the eye. To aid in these investigations the anterior and posterior surfaces of the cornea are modelled as sharing an optical axis; however, in reality, the apex of the posterior cornea is offset from the anterior apex. The consequence of this is that the thinnest part of the cornea does not lie behind the anterior corneal apex. Thus, in order to accurately interpret the measurement properties of the pachymeter a novel model cornea was constructed which included the offset of the thinnest part of the cornea relative to the anterior apex.

The analysis of the newly constructed geometric model cornea was performed by two methods. Firstly, the model was interrogated to find the corresponding location on the anterior cornea which produced the angular misalignment tolerance found in the device specific to this study. Secondly, the model's thickness was correlated with the distance away from the anterior cornea's apex. This allowed the range in potential thickness measurements to be calculated as a function of the distance away from the apex.

In order to perform this analysis on the model cornea, parameters and geometry for a normal cornea had to be investigated and collected. The following sections, in addition to the model analysis, discuss the design and parameters used to construct a normal geometric mathematical model cornea.

[2]The optical axis refers to the axis perpendicular to the apex of the half ellipse

4.4.1 Tear Film

The tear film is constructed in 3 layers, the oily lipid layer forms the first interface with the air, the aqueous layer forms the second and comprises the majority of the tear film, while the mucus layer forms the last interface with the corneal epithelium.

The tear film is an important aspect of the cornea to model, not only because of the tear films dynamic nature but also due to the air - tear film interface containing the largest change in refractive index in the eye. The refractive index of the lipid layer has been measured at 1.482 [127], while the aqueous layer has been measured at a relatively smaller refractive index of 1.337 [128]. The majority of model corneas assume the cornea to be homogeneous [123, 124, 129, 121], with the exception of Barbero [130], and do not consider the large refractive index change at the air – lipid interface. They therefore underestimate total refraction and reflection. To include the contribution of the tear film to the overall characteristics of the eye, an average is taken between the lipid layer and the aqueous layer, the tear film characteristics are summarized in table 4.4.

Layer	Thickness(μm)	Refractive Index
Superficial Lipid Layer	0.1	1.482
Aqueous Layer	7	1.337
Mucus Layer	0.02-0.05	-

Table 4.4: Tear film parameters for modelling

An important aspect of the tear film to mention is the implications of tear film break up. This causes the first interface to then fall between the air and the corneal epithelium. The tear film generally becomes unstable (breaks up) within 1 min of the last blink [131].

4.4.2 Cornea

The cornea is comprised of 5 layers; at 90% [132] of the overall cornea the stroma makes up the largest layer and is responsible for corneal thickening at the periphery. The corneal epithelium is the second largest layer and has the highest refractive index at 1.408 [133]. The remaining layers are the Bowman's layer, sandwiched between the corneal epithelium and the stroma, the Descemet's membrane which lies posterior to the stroma and the endothelium which is the final layer [132].

The changing thickness of the stroma causes a difference in shape between the anterior and posterior surfaces of the cornea. This suggests that the anterior surfaces, including the tear film, can be modelled as having a constant thickness, it is only the stroma layer which changes. The layers of the cornea are shown in table 4.5.

Layer	Thickness	Refractive Index
Corneal Epithelium	50-52	1.401
Bowman's Layer	8-10	-
Stroma (at apex)	450-500	1.380-1.373
Descement's Membrane	8-12	-
Endothelium	4-6	-

Table 4.5: Corneal parameters for modeling.

4.4.3 Geometry

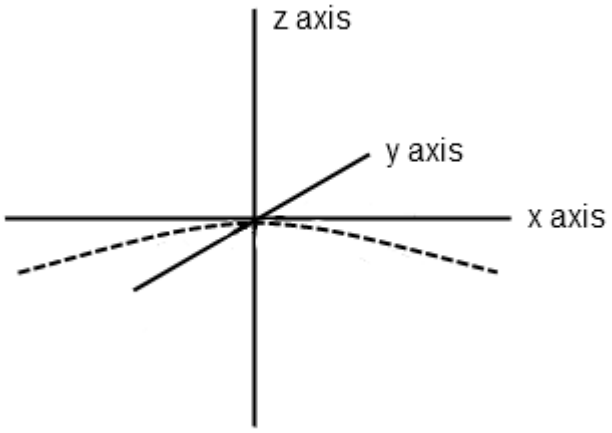

Figure 4.7: Modelling reference geometry.

The elliptical shapes of both the anterior and posterior cornea can be modelled mathematically with a standard conic equation. A conic shape is the most appropriate form to fit to the cornea as it facilitates the flattening of the cornea at the periphery [125].

$$f(z)_a = -p_a z^2 + 2R_a z + x^2 + y^2 \tag{4.1}$$

Where z signifies a point on the anterior cornea with the coordinates x and y and origin at the anterior apex. R_a is the radius of curvature and p_a is an asphericity factor which produces the flattening of the cone at the periphery.

However, due to the cornea's toric shape the radius of curvature changes with respect to meridian. To represent this change in the model cornea the R_a value can be replaced with a cosine function in which the steepest meridian lies orthogonally to the flattest meridian [125, 126].

$$f(x,y)_{R_a} = R_{ao} - \triangle R_a \cos^2(\tan^{-1}(y/x) - \beta_a) \tag{4.2}$$

Where $\tan^{-1}(y/x)$ is the meridian, $\triangle R_a$ is the difference between the radius of curvature of the steepest and flattest meridian on the anterior cornea. R_{ao} is the anterior radius of curvature at the apex and β_a is the meridian containing the steepest radius of curvature of the anterior cornea.

The posterior cornea can be calculated in a similar way but with the inclusion of the posterior cornea offset at the anterior apex.

$$f(z)_p = -p_p z^2 + 2R_p z + (x + x_p)^2 + (y + y_p)^2 + p_p CCT - 2R_p CCT \tag{4.3}$$

Where x and y are the coordinates of the z location and x_a and y_a are the offset coordinates of the posterior apex from the anterior apex yet to be calculated. The CCT value is the central corneal thickness, which is the thickness of the cornea directly behind the anterior apex, and p_p is the asphericity factor of the posterior cornea. R_p is the posterior equivalent of the function relating the radius of curvature to meridian:

$$f(x,y)_{R_p} = R_{po} - \triangle R_p \cos^2(\tan^{-1}(y/x) - \beta_p) \tag{4.4}$$

By using the quadratic equation, the value of z can be denoted as a function of x and y:

$$f(x,y)_a = -2R_a + \frac{\sqrt{(2R_a)^2 + 4p_a(x^2+y^2)}}{-2p_a} \tag{4.5}$$

$$f(x,y)_p = -2R_p + \frac{\sqrt{(2R_p)^2 + 4p_p((x+x_p)^2 + (y+y_p)^2 + p_pCCT^2 - 2R_pCCT)}}{-2p_p} \tag{4.6}$$

The thickness of the cornea can then be evaluated by subtracting the posterior function from the anterior function, resulting in a thickness function defined by x and y.

$$f(x,y)_t = f(x,y)_a - f(x,y)_p \tag{4.7}$$

Using the newly created thickness function, the thinnest part of the cornea can be defined as the point where the differential is equal to 0:

$$f'(x,y)_t = 0 \tag{4.8}$$

The position of the posterior apex, in order to define the thinnest location in the correct position, can be determined by calculating x_p and y_p at:

$$f'(x_o, y_o) = 0 \tag{4.9}$$

Where x_o and y_o are the desired coordinates of the cornea's thinnest location.

The resulting model is an accurate 3 dimensional model cornea, which correctly models the offset of the thinnest location relative to the anterior apex by positioning the posterior apex appropriately.

4.4.4 Model Parameters

In order to generate a model cornea for interrogation it is first necessary to obtain parameters for the model. There have been a number of investigations into the the parameters of the human cornea, most notably Kiely [125]; however, for the purposes of this model the parameters outlined by Dubbleman [126] offer a more complete set. The parameters obtained from this investigation are listed in table 4.6 and form the basis for the model cornea.

In addition, the offset parameter of the thinnest location from the anterior apex is obtained from Ashwin et al [134] as it is absence in Dubblemans study. The CCT thickness is calculated by an average of thickness values obtained for each layer of the tear film and cornea previously described (table 4.4 and table 4.5).

Model Parameter	Value	Units	Reference
Anterior Corneal Radius of Curvature (R_a)	7870	µm	[126]
Anterior Corneal Asphericity (p_a)	0.82	-	[126]
Anterior Corneal Steepest Meridian (β_a)	95	°	[126]
Anterior Corneal Radius of Curvature Range ($\triangle R_a$)	-160	µm	[126]
Posterior Corneal Radius of Curvature (R_p)	6690	µm	[126]
Posterior Corneal Asphericity (p_p)	0.62	-	[126]
Posterior Corneal Steepest Meridian (β_p)	97	°	[126]
Posterior Corneal Radius of Curvature Range ($\triangle R_p$)	-325	µm	[126]
Posterior Corneal Apex x offset (x_o)	435	µm	[134]
Posterior Corneal Apex y offset (y_o)	442	µm	[134]
Central Corneal Thickness (CCT)	582	µm	Section 4.4.2

Table 4.6: Model cornea parameters.

4.4.5 Model Analysis

4.4.5.1 Anterior Cornea

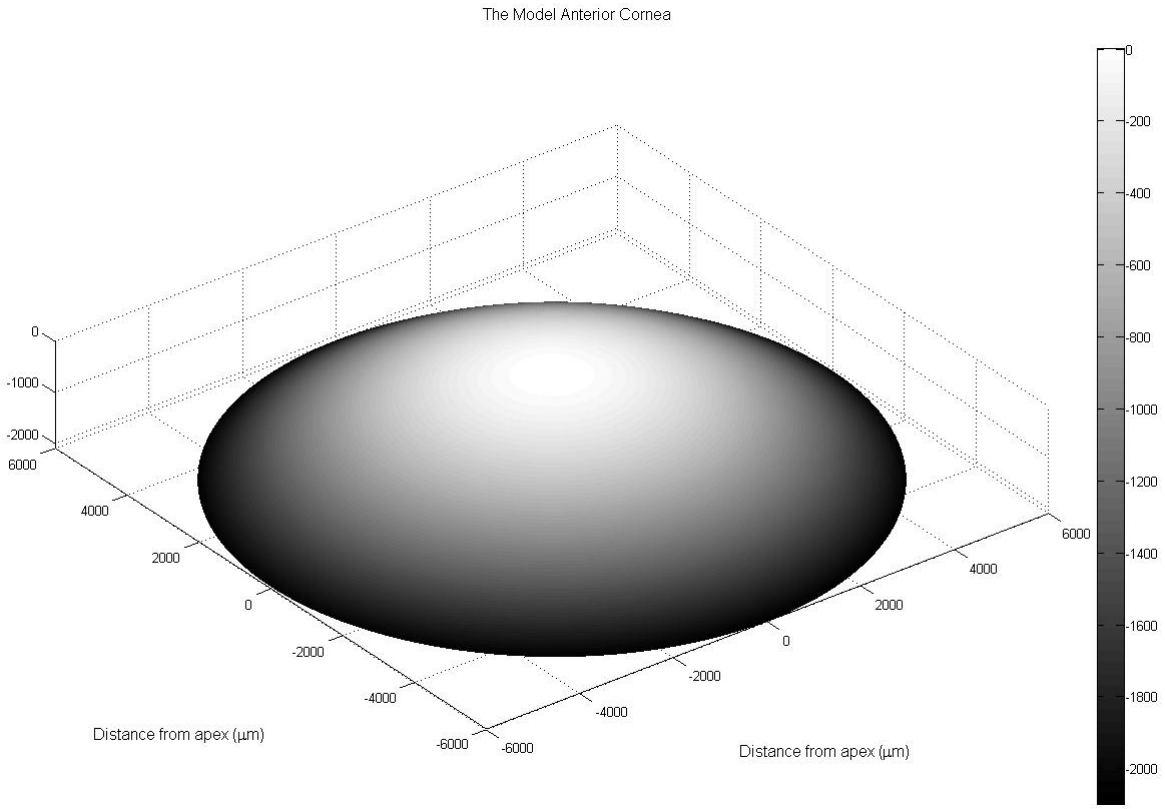

Figure 4.8: Anterior corneal surface.

Figure 4.8 shows the model's anterior corneal contour as a surface plot. The plot is centred on the anterior cornea's apex and displays the vertical displacement of each point of the corneal surface from the apex.

4.4.5.2 Posterior Cornea

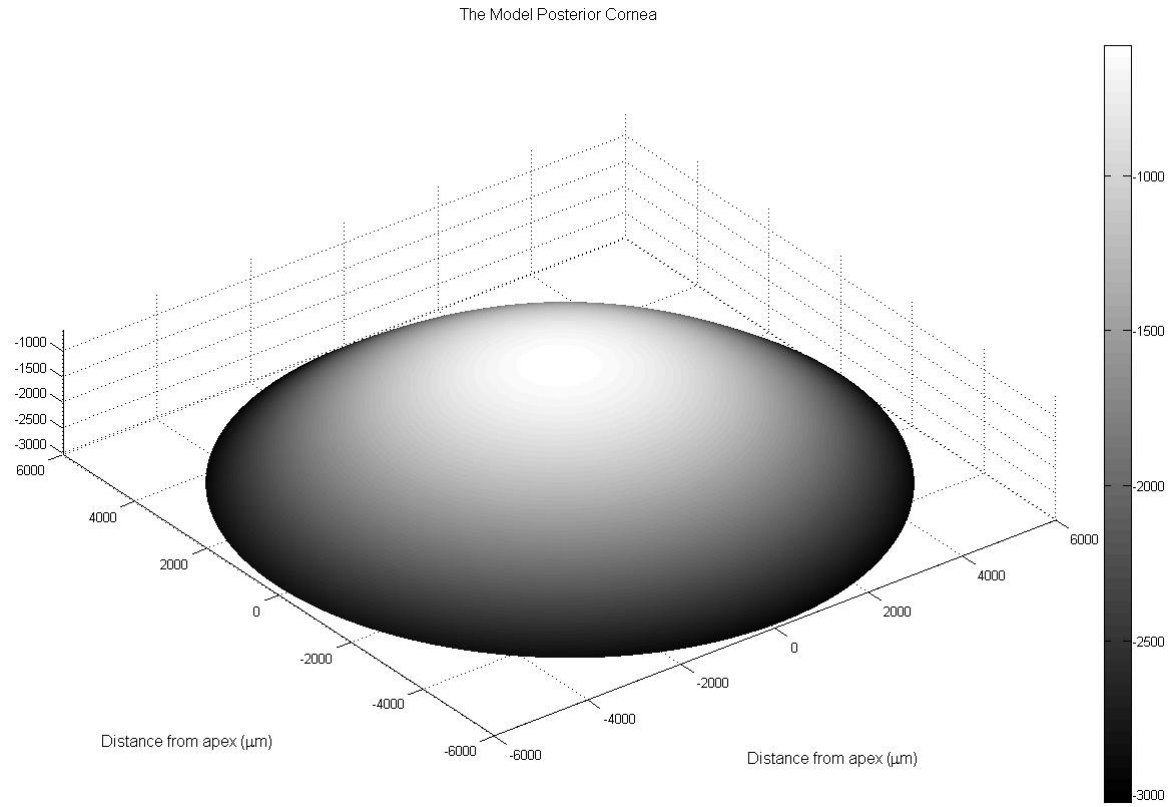

Figure 4.9: Posterior corneal surface.

Figure 4.9 shows the model's posterior corneal surface. The plot displays the vertical displacement of each point of the posterior cornea's contour from the anterior cornea's apex.

4.4.5.3 Corneal Cross Section

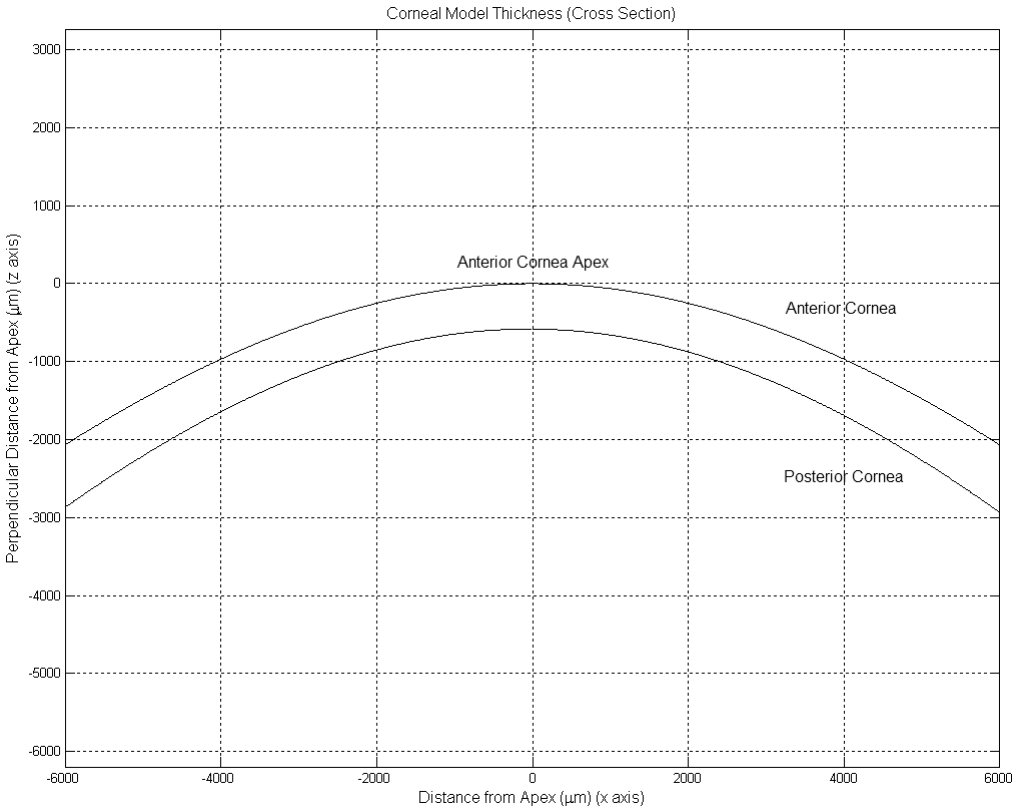

Figure 4.10: Cross section of the model cornea.

Figure 4.10 shows the cross section of the model cornea constructed by the anterior and posterior corneal surfaces. The model is centred on the anterior corneal apex.

4.4.5.4 Corneal Thickness

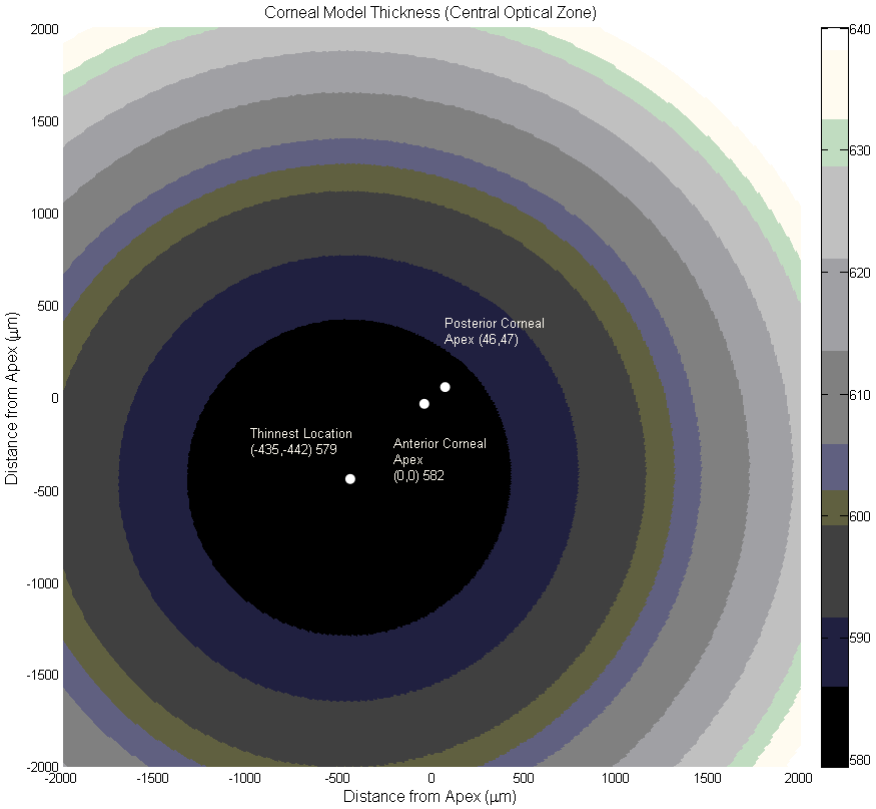

Figure 4.11: Model right cornea thickness map.

Figure 4.11 shows the thickness map of the central optical zone[3] obtained from the model cornea. The thickness at the apex is 582 µm and the thickness at the thinnest point, located at (-435,-442), is 579 µm. The thickness map displayed in this figure is a map of the a normal right cornea, the location of the thinnest point is inferotemporal[4] in accordance with Ashwin's [134] findings.

[3]The central optical zone is the central 3-4mm zone on the cornea centred round the anterior apex.
[4]Positioned down and towards the temple.

4.4.5.5 Corneal Thickness Range

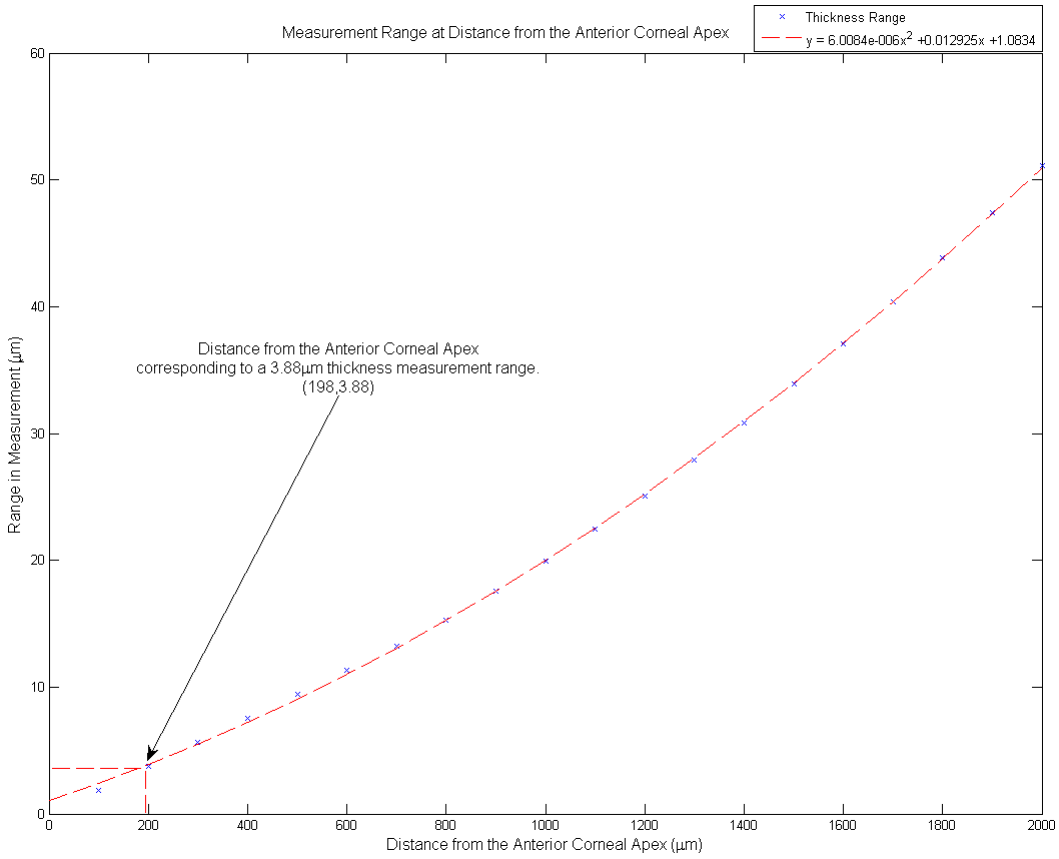

Figure 4.12: Model cornea thickness measurement range as a function of distance from the model cornea's anterior apex. Where the range is calculated with the maximum and minimum potential thickness measurements at the specificed distance from the apex.

Figure 4.12 shows the range[5] in thickness values as a function of the displacement from the model's anterior apex. The smaller the measurement variation the more localised it is. Also represented on the figure is a quadratic line of best fit, the equation was determined using Matlab (Mathworks, USA) with a generic curve fitting function. Using this equation the point at which the potential range in measurement is equal to the resolution of the pachymeter can be calculated (3.88 µm); resulting in a value of 198 µm from the anterior corneal apex.

This then suggests that the pachymeter would be unable to resolve corneal thickness differences in an area around the corneal apex consisting of a 198 µm radius. It also forms the translational alignment tolerance for the alignment system.

[5]The range in thickness values refers to the potential difference in corneal thickness measurment when measuring within a specified area round the corneal apex. As the thickness of the cornea increases with the distance from corneal apex, the larger this distance is the greater the potential range in thickness measurement.

4.4.5.6 Corneal Misalignment

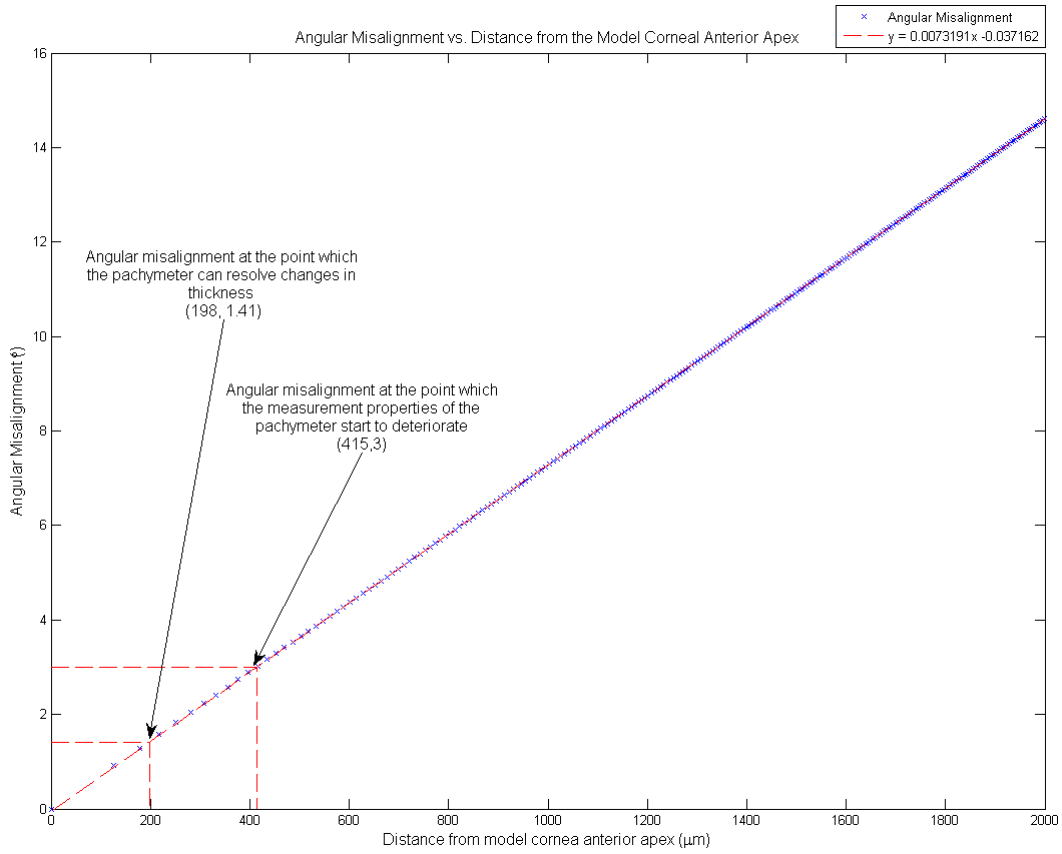

Figure 4.13: Anterior cornea gradient as a function of the distance from the model cornea's apex.

Figure 4.13 describes the angular misalignment of the anterior corneal surface as a function of the displacement from the apex. When the measurement is laterally displaced from the anterior corneal apex angular misalignment is induced due to the curved surface of the cornea. Thus it is important to quantify the angular misalignment induced by lateral movements of the eye's optical axis relative to the measurement axis.

In this regard, the 198 µm calculated previously corresponds to a angular misalignment of 1.41°. Conversely the 3°angular misalignment tolerance calculated in the device specifications correspond to 415 µm displacement from the anterior apex.

4.4.6 Discussion

The majority of corneal models position the posterior apex directly behind the anterior apex. This results in the thinnest part of the cornea lying directly behind the anterior apex; however, the thinnest part of the cornea is actually offset from this position. Whilst modelling the cornea in this manner is advantageous for investigating the eyes' optical properties it provides a false representation of the thickness of the cornea in the central optical zone.

The model cornea constructed in this research concentrates on the geometric properties of the cornea, thus incorporating the offset of the thinnest part of the cornea from the anterior apex. It has achieved this by offsetting the posterior apex from the anterior apex in order to place the thinnest part of the cornea in the desired location.

The introduction of the offset has made the model open to inaccuracies not present in other models. The offset of the posterior apex causes a sharper increase in corneal thickness at the periphery, in the meridian opposite to the thinnest location. Contrary to this, the model is more accurate in the central optical zone, arguably, this is more important for assessing central thickness. The greatest source of error can be attributed to the acquisition of model parameters from different sources. However, there still remains continuity, as all sources use the same method of measurement, and the majority of model parameters come from one source.

The main aim in the creation of the geometric mathematical model cornea was to allow the measurement properties of the v360 pachymeter to be related to an actual cornea in order to gauge alignment tolerance specification specific to the eye. In this regard, the results suggest that 3°of misalignment, caused by the curved surface of the anterior cornea, would be located at 415 µm from the anterior corneal apex. A radius of 198 µm round the anterior apex would also incorporate a thickness measurement range of 3.88 µm, the corresponding angular misalignment at this point would be 1.41°.

The alignment tolerance based on the resolution measurement parameter offers a smaller tolerance for the alignment system. An area round the corneal apex with a radius of 198 µm should then be used for the translation tolerance. On the otherhand, the angular alignment tolerance of 1.41°is too large for the alignment system to detect microsaccadic movement. Thus, it is suggested that the minimum microsaccadic movement should be used for the angular alignment tolerance, this would mean an angular alignment tolerance of 0.17°.

The model provides a valuable tool in relating thickness measurements to the alignment area on the cornea. This is very important in the context of this research as the model can be manipulated and interrogated at will, something which is difficult to achieve in a human eye.

4.4.7 Conclusions

The purpose of the mathematical model cornea was to relate the measurement properties obtained from the device specific specifications to alignment tolerances for an alignment system.

The device specific specifications outlined 2 potential sources for specification: firstly, the displacement from the anterior apex in which the instrument would be unable to resolve differences in corneal thickness; secondly, the angle of misalignment at which the measurement properties of the pachymeter start to deteriorate.

The v360 pachymeter has a resolution of 3.88 µm, this corresponds to an area round the corneal apex with a radius of 198 µm. The corresponding angular misalignment at this point is 1.41°. An angular misalignment of 3°was determined to lie 415 µm from the anterior corneal apex. The specification based on the v360 pachymeter's resolution is the narrower alignment tolerance.

However, both sets of results do not suggest an angular misalignment tolerance smaller than the microsaccade detection criteria of the alignment system. Thus the angular misalignment tolerance is based on the minimum microsaccade magnitude of 0.17°.

Chapter 5

JEDEye Alignment/Tracking

5.1 Chapter Overview

This chapter describes the construction and evaluation of an eye tracking technique capable of both tracking and alignment.

The chapter first describes the conception of an eye tracking technique, based on Purkinje Image tracking, capable of resolving microsaccades and quantifying the orientation of the eye's optical axis.

The construction of the system, designed to implement the technique, is detailed from the hardware considerations through to the development of tracking algorithms.

The system is evaluated by investigations in to safety, accuracy and comparison with other forms of eye tracking.

The chapter concludes on the capablities of the tracking system and its ability to facilitate alignment of the eye's optical axis with an imaging axis.

5.2 Introduction

The development of an eye tracking system is an integral aspect of the research for two reasons: firstly, it allows the identification of the factors responsible for misalignment; secondly, in order to correct alignment, misalignment needs to be quantified.

The literature review on eye tracking techniques highlighted one particular technique able to directly assess the misalignment of the eye's optical axis relative to a measurement axis, and track the eye to the required accuracy. Purkinje eye tracking uses reflections from the anterior cornea and the posterior lens, which, when viewed at an angular displacement from the eye's optical axis appear to separate. While there are commercial Purkinje trackers available [108], their bulky apparatus and manner of tracking do not lend themselves to instrument alignment. There have been research based Purkinje systems which image the eye [3], as apposed to the mechanical means proposed by Cornweet and Crane [109]; however these instruments are used to determine the angular misalignment of the lens relative to the cornea, rather than track eye movement. There is thus a requirement for a novel Purkinje Image tracking system which makes use of imaging techniques for the purposes of tracking and alignment.

While the purpose for developing an eye tracking system, in the context of this research, is to identify the eye movements responsible for misalignment, the development of this tracking system yields other advantages. A tracking system which directly identifies the optical axis and quantifies eye movement relative to this axis partially fulfills the requirements of the alignment system. Due to this, the tracking system is developed with a view to use the technique to perform alignment.

5.3 Specifications

To develop a tracking and alignment system capable of achieving the desired level of performance, it is first necessary to produce a set of specifications. The specifications for the tracking and alignment system can be considered separately. The purpose of tracking the eye is to acquire the raw data necessary for alignment correction, it is then the responsibility of the alignment technique to communicate how to correct this misalignment to the user. There is also a third set of specifications relating to the positioning of the alignment/tracking system dictated by the composition of the v360 pachymeter. These composition specifications ensure that the proposed technique will allow integration in the pachymeter without interference with the measurement hardware. The sources used for deriving the specifications are in literature review (Chapter 2), device specific specifications (Section 4.3) and the model cornea (Section 4.4) discussed in previous chapters.

1. Tracking

1.1 - The tracking technique must be based on Purkinje Image tracking, allowing detection of the eye's optical axis by imaging Purkinje Image I and Purkinje Image IV.

1.2 - The tracking technique must resolve eye and head movements relative to the optical axis of the eye thus determining misalignment.

1.3 - The tracking technique must be able to resolve eye rotation from head movement.

1.4 - The tracking technique must be able to detect microsaccadic/saccadic eye movements ranging from 0.17°to 20°.

1.5 - The tracking technique must be able to optically resolve changes in Purkinje Image position in the order of 0.017 mm. Using an approximation of the distance between the Purkinje Image imaging plane and the eye's centre of rotation, and the minimum desired detectable eye rotation, the magnitude of lateral movement induced by this movement can be determined.

1.6 - The tracking technique must sample in excess of 10 Hz in order to fulfill the nyquist criterion for the detection of saccadic eye movement.

1.7 - The tracking technique must be safe to use, thus in accordance with commercial tracking systems, maximum IR exposure to the eye must be below 10 mW/cm^2 [135, 136, 137].

2. Self Alignment

2.1 - The alignment technique must be able to detect alignment of the eye's optical axis with the measurement axis to within 198 µm laterally and 0.17°rotationally.

2.2 - The alignment system must be able to determine the magnitude of misalignment.

2.3 - The alignment system must be able to communicate the degree of required correction to the user or operator in a manner which enables them to perform correction. This information must be clearly presented in order to achieve a quick response from the user.

2.4 - Once in alignment, the alignment system must maintain alignment.

3. Composition

3.1 - The wavelength of the tracking illumination sources must be different from that used in the pachymeter (670 nm) to ensure no confusion in the measurement signal.

3.2 **-** The tracking illumination sources must lie outside the 10 mm diameter pachymeter beam path to prevent obstruction.

3.3 **-** The tracking illumination sources must be positioned in front of the system and at 50 mm from the corneal apex to allow the pachymeter to perform its measurement.

5.4 Design and Development

This section describes the development of a Purkinje eye alignment/tracker from conception to its implementation as an eye alignment/tracking tool. For convenience the development is separated into 4 parts:

- Tracking principle.
- Illumination.
- Hardware design.
- Software design.

5.4.1 Tracking Principle

5.4.1.1 Image Formation

The Purkinje Images are reflections from each of the refracting components in the eye; in terms of eye tracking, Purkinje Images I and IV are of primary concern as they provide both the rotational and translational information of the eye's movement. Purkinje Image I is a virtual image made visible by the convex surface of the anterior cornea while Purkinje Image IV is a real and inverted image emanating from the posterior lens surface.

Although the source of Purkinje Image IV is the posterior lens, the reflection refracts through the anterior lens, posterior cornea and the anterior cornea before becoming visible to the observer, thus the surface which Purkinje Image IV represents is often referred to as the equivalent mirror of these surfaces. Due to the transparent nature of the eye, the reflected light from the equivalent mirror is less than 1% of the intensity of Purkinje Image I; however, due to the anatomical structure of the eye the virtual Purkinje Image I and the real Purkinje Image IV are formed in the same focal plane and at similar distances from the optical axis.

5.4.1.2 Eye Rotation

Purkinje Images I and IV provide two points along the optical axis separated by a finite distance; when viewing these points through varying angular misalignments they appear to move relative to each other. As angular misalignment increases, the magnitude of the distance between the Purkinje Images will also increase. The opposite is the case when reducing angular misalignment.

The magnitude of eye rotation (θ_{mag}) can be determined by calculating the horizontal (θ_{hm}) and vertical (θ_{vm}) components of eye rotation[1]:

$$S_h = ccs \sin \theta_{hm} \tag{5.1}$$

$$S_v = ccs \sin \theta_{vm} \tag{5.2}$$

$$\theta_{mag} = \sqrt{\theta_{hm}^2 + \theta_{vm}^2} \tag{5.3}$$

Where S_h and S_v are the measured horizontal and vertical separations of Purkinje Image I and their corresponding Purkinje Image IV. The *ccs* value is the distance between the centres of curvature of the anterior cornea and the equivalent mirror.

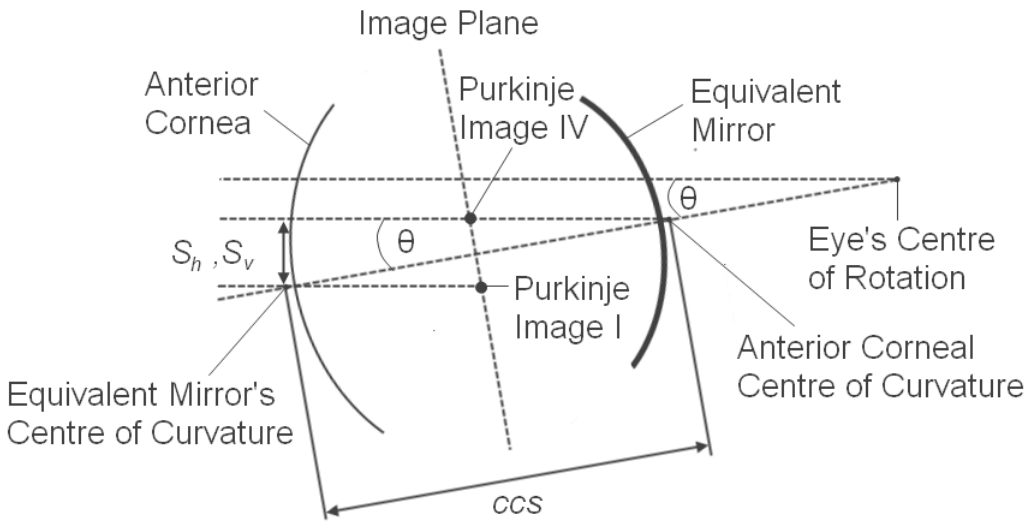

Figure 5.1: Determination of eye rotation using Purkinje Image I and Purkinje Image IV.

Figure 5.1 describes how the Purkinje Images can be used to determine eye rotation, explaination of how the *ccs* is contained within section 5.4.1.4. The choice on which

[1] These angular measurements refer to the rotational movement of the eye and are not related to the angular properties of the eye's structure

separation vallue to use is dependent on the plane in which the Purkinje Images are being assessed, in the horizontal plane the separation value will be denoted as S_h, while in the vertical plane the separation value will be S_v.

5.4.1.3 Eye Translation

Eye translation provokes a different response in the Purkinje Images, when the eye translates (due to head movement) the images appear to move in the same direction through the same magnitude. Thus the measurement of eye translation is performed by comparing the position of Purkinje Image I with its previous position.

5.4.1.4 Central Curvature Separation (*ccs*)

The *ccs* is the distance between the centre of curvature of the anterior cornea and the centre of curvature of equivalent mirror responsible for generating Purkinje Image IV. In current commercially available Purkinje Image trackers this measurement is either approximated or measured beforehand. This is not a viable approach in the context of this research as it prevents immediate use of the proposed alignment technique.

In order to make Purkinje Image tracking viable, a direct measurement of the *ccs* value is required. This measurement is achieved by the use of 2 existing techniques which make use of the Purkinje Images to measure physical properties of the eye, namely, keratometry and phakometry.

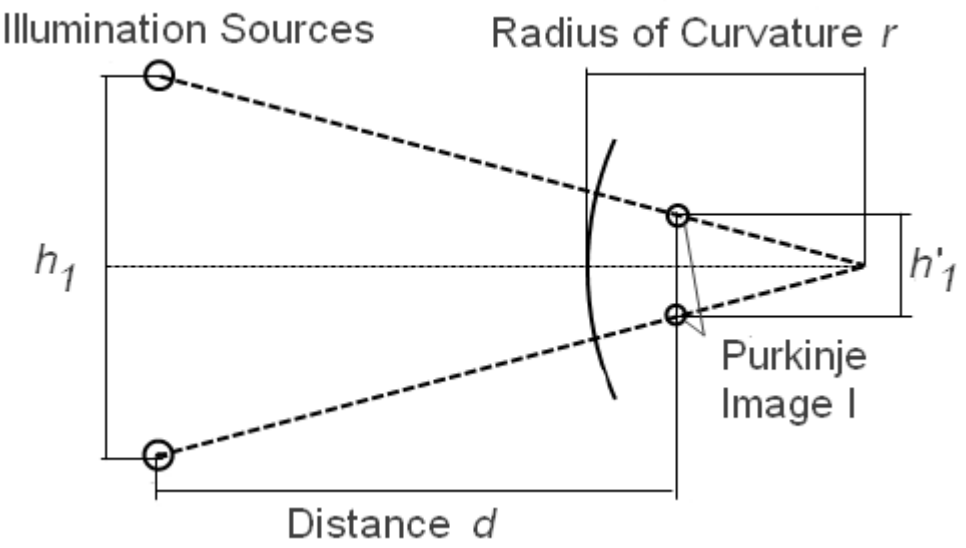

Figure 5.2: The principle of keratometry.

The Purkinje Images are used in the measurement of corneal curvatures, this technique is referred to as keratometry and is dipicted in figure 5.2. The separation between 2 Purkinje Images I (h_1') is proportional to the separation between 2 illumination sources (h_1), the distance between object and image (d) and the radius of curvature of the anterior cornea (r).

$$m = \frac{h_1'}{h_1} \tag{5.4}$$

$$r = \frac{2dm}{1 - m^2} \tag{5.5}$$

Specifically, the ratio of h_1' over h_1 refers to the magnification (m) of the object and the image as described in equation 5.4. The radius of curvature of the anterior cornea (r) can subsequently be found with equation 5.5 [10].

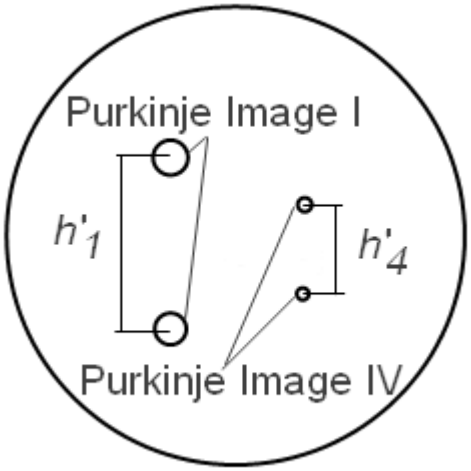

Figure 5.3: The formation of the Purkinje Images when invoked with 2 illumination sources for phakometry calculations.

The keratometry method can be extended to measure the radius of curvature of the refracting surface forming Purkinje Image IV, this technique is referred to as phakometry. Although Purkinje Image IV is reflected from the posterior lens it refracts through the anterior lens and the cornea before becoming visable to the user. Thus phakometry actually measures an imaginary refractive surface termed the equivalent mirror. The appearance of Purkinje Image I and Purkinje Image IV as formed by 2 illumination sources is shown in figure 5.3.

$$r'_4 = r\left(\frac{h'_4}{h'_1}\right) \tag{5.6}$$

The radius of the equivalent mirror (r'_4) is then calculated with the separation between Purkinje Images IV (h'_4), the separation between Purkinje Images I (h'_1) and the radius of curvature of the anterior cornea (r) determined by keratography (equation 5.6).

Although this does not directly measure the central curvature separation the radius of curvatures for both the anterior cornea and the equivalent mirror can be used to approximate the distance. Modelling the anterior cornea as a convex mirror and the equivalent mirror as a concave mirror the focal point of these two mirrors can be calculated by:

$$f_{r_1} = \frac{r_1}{2} \tag{5.7}$$

$$f_{r'_4} = \frac{r'_4}{2} \tag{5.8}$$

Figure 5.4 depicts structural assumptions used to calcuate the *ccs* value. As Purkinje Image I and Purkinje Image IV are formed in the same image plane, this image plane can be used as a datum to calculate the *ccs* separation. The distance between the image plane and the apex of each mirror is then equivalent to the focal length of that mirror.

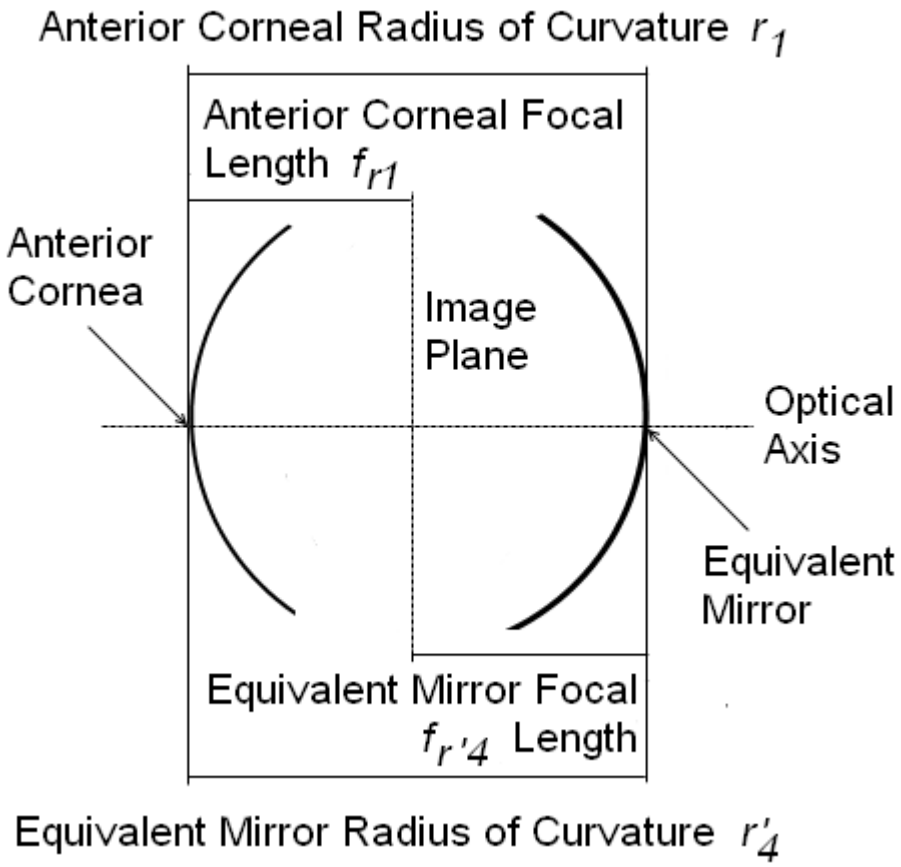

Figure 5.4: Diagram showing the structural assumptions used to calculate the *ccs* value.

The focal length of each mirror can then be related to the corresponding radius of curvature by equations 5.7 and 5.8. Thus the *ccs* value can be calculated using equation 5.9.

$$ccs = f_{r_1} + f_{r'_4} = \frac{1}{2}\left(r_1 + r'_4\right) \tag{5.9}$$

5.4.2 Illumination

The illumination sources used to invoke the Purkinje Images for alignment/tracking purposes warrant the most consideration. Not only must they be visible inside the pupil, they must also be distinct from each other. In addition to this, multiple illumination sources must be used to measure the *ccs* while also remaining in the constraints of the composition specifications detailed earlier in the chapter. Thus, in designing the illumination array for the generation of the Purkinje Images two steps were taken: firstly, a method of approximating the position of the Purkinje Image relative to the illumination was calculated; secondly, an appropriate illumination array was designed to both identify alignment and allow the *ccs* measurement.

5.4.2.1 Purkinje Image Position

Parameters

Table 5.1 lists the eye parameters used for the Purkinje Image position approximations, all data is taken from Gullstrand's model eye. It would also have been possible to use parameters obtained from the model cornea; however, the data would have consisted of only corneal parameters, the lens parameters would have have to be referenced from another source. For the purposes of continuity all parameters were obtained from one source.

Eye Parameter		
R_{ca}	0.0078m	Anterior cornea vertex radius
R_{cp}	0.0065m	Posterior cornea vertex radius
R_{la}	0.0102m	Anterior lens vertex radius
R_{lp}	-0.006	Posterior lens vertex radius
ct	0.00055m	Central corneal thickness
al	0.02386m	Axial length
acd	0.00305m	Anterior chamber depth
lt	0.004m	Lens thickness
nc	1.3771	Cornea refractive index
na	1.3374	Aqueous humour refractive index
nl	1.420	Lens refractive index
nv	1.336	Vitreous humour refractive index

Table 5.1: Eye parameters used for Purkinje Image position approximation.

Incident light on any optical system undergoes 3 transitions when travelling through the system, translation, refraction and mirroring. Translation refers to the translation of the ray through a medium of constant refractive index, while, refraction refers to the deviation of the ray's course when intersecting an interface of changing refractive index. Mirroring is the same as refraction, however, it describes the passage of the ray back through the system. Each of these transitions can be modelled by matrices, the combination of these matrices forms a system matrix which describes all the components within the optical system. This approach has been implemented on the eye using a selection of basic parameters, allowing the positions of the Purkinje Images to be approximated relative to the illumination source (the approach is detailed in [110]).

Refraction Matrix

$$P = \begin{bmatrix} 1 & -RP \\ 0 & 1 \end{bmatrix} \tag{5.10}$$

In which RP is the power of the refracting element calculated in the following equation with n and n', the refractive indexes of the medium in front and behind the refracting surface, and the radius of curvature R:

$$RP = \frac{n' - n}{R} \tag{5.11}$$

Mirror Matrix

$$M = \begin{bmatrix} 1 & F \\ 0 & 1 \end{bmatrix} \tag{5.12}$$

In which F is the focal point of the refracting element.

Translation Matrix

$$T = \begin{bmatrix} 1 & 0 \\ \frac{d}{n'} & 1 \end{bmatrix} \tag{5.13}$$

In which d is the height of the incident ray above the optical axis measured in metres, and n' is the refractive index of the material to the right of the interface (assuming standard ray tracing convention).

System Matrix

$$S = P_n.T_{n-1:n}.P_{n-1}...P_2.T_{1:2}.P_1 = \begin{bmatrix} a & b \\ c & d \end{bmatrix} \tag{5.14}$$

The combination of these matrices cumulate to form a system matrix in which a incident ray of light can be mapped from object plane to the image plane by one single matrix.

The system matrix can then be interrogated to determine the magnification ratio.

$$m = \frac{1}{a - \frac{b}{V}} \tag{5.15}$$

Where V is vergence determined by the distance between the object and plane of interest and the refractive index of the medium as it travels through before intercepting with that plane.

Purkinje Image System Matrices

Using approximations for the parameters of the anterior and posterior cornea, and the anterior and posterior lens the positions of Purkinje Image I and IV can be evaluated with reference to the position of the illumination sources.

As Purkinje Image I is a reflection from the anterior cornea its system matrix is formed by a mirror matrix.

$$S_I = \begin{bmatrix} 1 & \frac{2}{R_{ca}} \\ 0 & 1 \end{bmatrix} = \begin{bmatrix} 1 & 256.4103 \\ 0 & 1 \end{bmatrix} \tag{5.16}$$

Where the focal point of the anterior cornea modelled as a convex mirror is $\frac{2}{R_{ca}}$ in which R_{ca} is the radius of curvature of the anterior cornea at the apex.

The system matrix for Purkinje Image IV is more complicated as the incident light ray first has to refract and translate through the anterior and posterior cornea followed by the anterior lens and then the lens. After which the ray is mirrored by the posterior lens and is required to refract and translate through the lens and the cornea again before finally emerging from the eye. Thus the system matrix for Purkinje Image IV is modelled as follows:

$$S_{IV} = P_{ca}.T_c.P_{cp}.T_{acd}.P_{la}.T_l.M_{lp}.T_l.P_{la}.T_{acd}.P_{cp}.T_c.P_{ca} = \begin{bmatrix} -1.4597 & -336.1802 \\ -0.0034 & -1.4597 \end{bmatrix} \tag{5.17}$$

Where P_{ca} refers to the refraction matrix at the anterior cornea and T_c refers to the translation through the cornea. P_{cp} refers to the refraction matrix at the posterior cornea. T_{acd} refers to the translation through the anterior chamber. P_{la} refers to the refraction matrix at the anterior lens, T_l refers to the translation through the lens and finally M_{lp} refers to the mirror matrix at the posterior lens.

Calculations

The specifications state that the illumination sources must lie outside the pachymeter beam path and be positioned in front of the pachymeter. This results in a object height (h_1) of 0.01m and a distance (d) of 0.05m.

Defining vergence as:

$V = -1/d$

The magnification ratio for Purkinje Images I and IV can then be determined using the equation 5.15 and the relevant matrix coefficients, table 5.2 describes the image height of Purkinje Image I and Purkinje IV above and below the eye's optical axis.

Parameter	Value(mm)
h_1	10
d	50
h'_1	0.72
h'_4	-0.55

Table 5.2: Purkinje Image height.

Table 5.2 shows the calculated values from the matrix approach (full calculations can be found in Appendix C) and the corneal parameters outlined in table 5.1. The calculations suggest a Purkinje Image I height of 0.72 mm and a Purkinje Image IV image height of -0.55 mm. These images then span a total area of 1.27 mm and since the minimum pupil diameter is approximately 2 mm (as in figure 5.5), the Purkinje Images should always appear within a regular pupil, allowing them to be imaged and tracked.

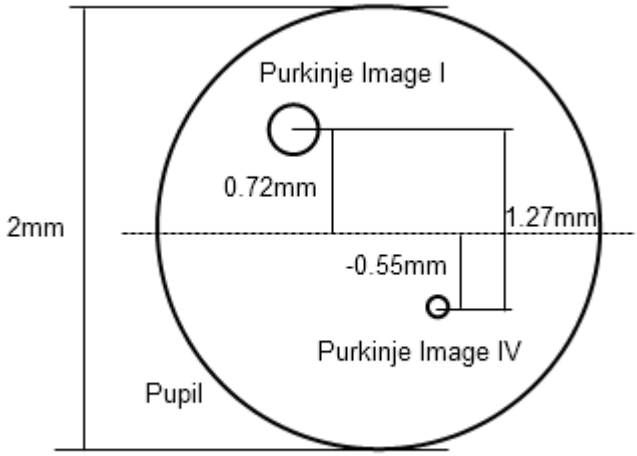

Figure 5.5: Purkinje Image positions as calculated using a distance (d) of 50 mm and an object height (h_1) of 10 mm.

5.4.2.2 Illumination Arrangement

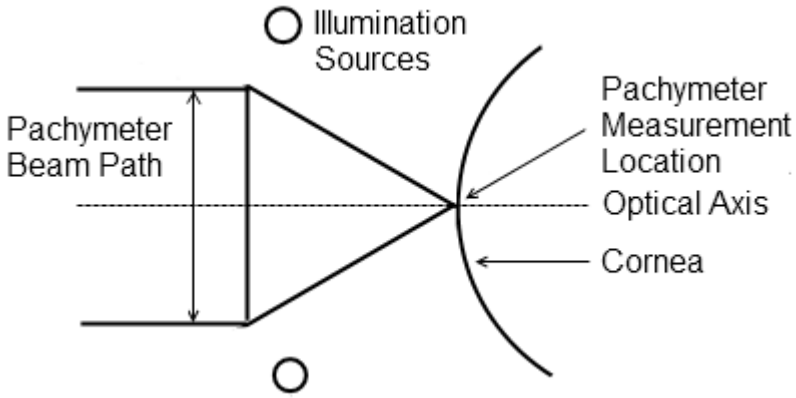

Figure 5.6: Illumination source arrangement considerations. Illumination sources lie outside the pachymeter beam path and does not interfere with the Pachymeter measurement.

The illumination source arrangement refers to the positioning of the light sources around the pachymeter's beam path. This arrangement requires the illumination sources to be positioned in such a way that the Purkinje Images they invoke do not interfere with the Pachymeter's measurement, but also still identify alignment. This is described pictorially in figure 5.6.Two potential solutions were proposed:

Ring Array

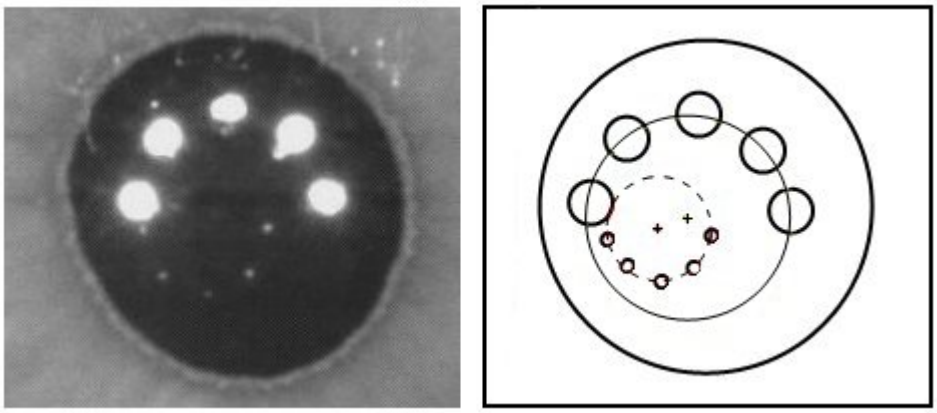

Figure 5.7: Eye image acquired with the ring array LED composition. The solid circle is constructed with the centre points of Purkinje Image I and the dashed circle is constructed with the centre points of the Purkinje Image IV. Misalignment is then defined by the positional magnitude difference of the two centre points.

The ring array arrangement was based on an instrument designed to measure the ocular misalignments in the eye [3]. It is constructed with a semi-circular light array consisting of 5 LEDs, figure 5.7 shows the formation of the Purkinje Images as invoked by the array. The misalignment is calculated from the separation of the circle centres as constructed with Purkinje Images I and Purkinje Images IV. The circles are fitted to the Purkinje Images in software.

Cross Array

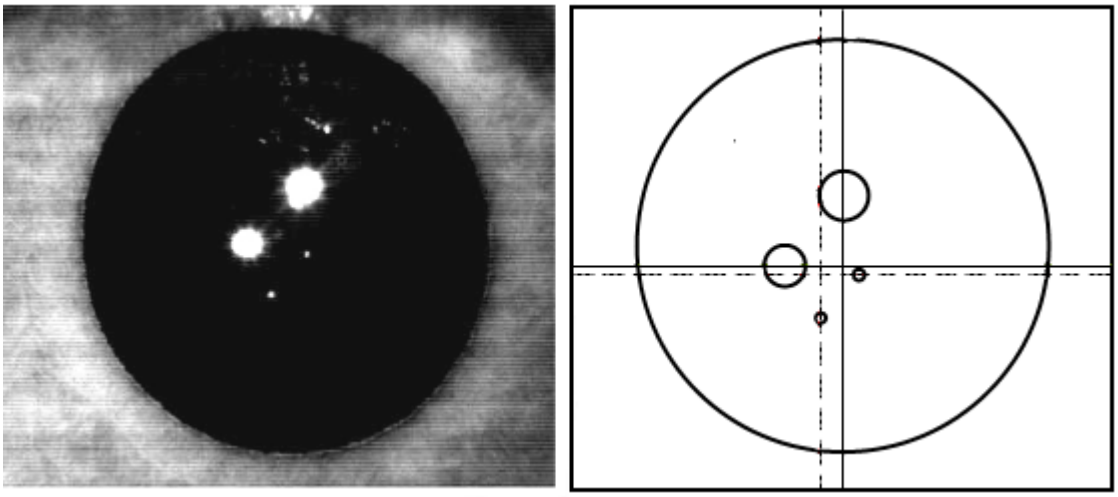

Figure 5.8: Eye image acquired with the cross array LED composition. The solid lines intersect Purkinje Images I and the dashed lines intersect Purkinje Images IV. The positional magnitude between the intersection of the two pairs of lines signifies misalignment.

The cross array arrangement consisted of two illumination sources placed orthogonally to each other. This arrangement allowed the vertical and horizontal components of eye rotation to be calculated separately while indicating alignment when both sets of images are aligned.

Although both formations allow both tracking and alignment identification, the cross arrangement produced a less convoluted image. It also meant that fewer light sources were directed into the eye reducing the levels of IR exposure.

5.4.3 Hardware

5.4.3.1 Imaging Device

The imaging device used for the JEDEye alignment/tracking system is a UEye UI-1540-M USB camera (IDS Imaging, Germany) with a pixel density of 1280 x 1024 pixels. This camera has a 1/2" CMOS sensor and is capable of imaging at 25 frames per second (fps) at full resolution. IDS imaging, the supplier of the UEye camera, also provide additional software which allows manipulation of the imaging parameters.

The camera also includes LabVIEW (National Instruments, USA) compatible drivers allowing direct access to the camera functionality.

5.4.3.2 Optical Arrangement

The optical arrangement for the Purkinje tracking system requires the imaging of the eye whilst also allowing the user to view a graphical display. Figure 5.9 describes the optical arrangement of the JEDEye alignment/tracker system.

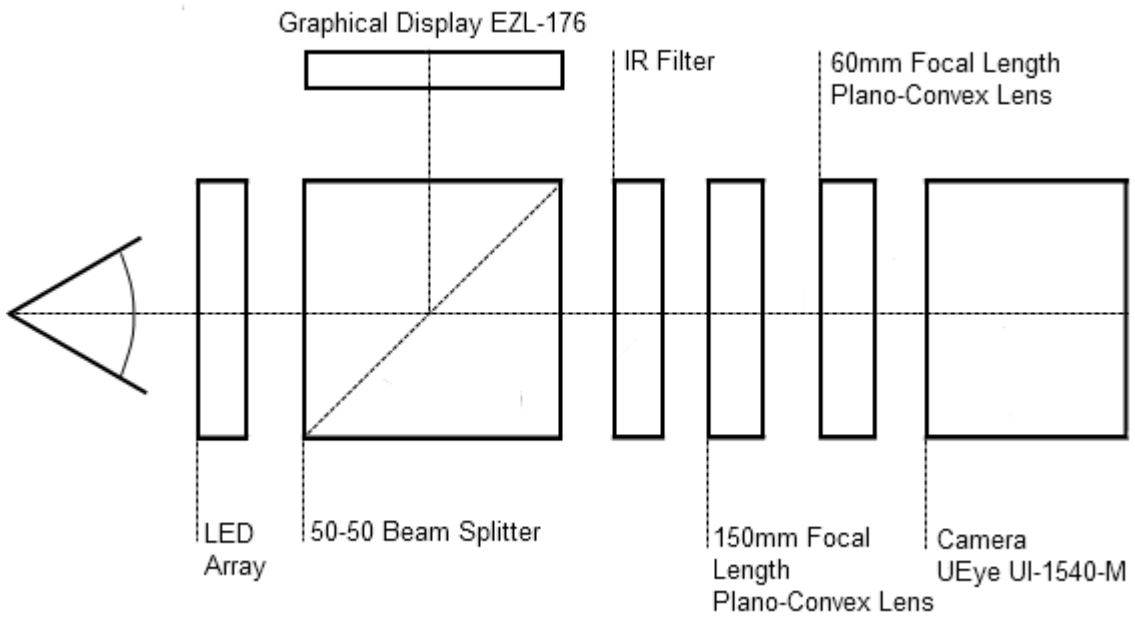

Figure 5.9: Optical arrangement of the Purkinje tracking system allows both the user to observe a graphical display and the operator to image the subject, this is achieved by means of a beam splitter. The lens array allows a fixed focal length for the system while the IR filter ensures that only IR light is able to reach the camera.

5.4.3.3 Graphical Display

The graphical display unit is included in the design to overlay both fixation targets and alignment correction notifications to the user. For the purposes of eye tracking the display

allows a number of different targets to be displayed in a consistent set up. In terms of eye alignment, the graphical display communicates the required movements of the user in order to achieve alignment.

The graphical display unit itself is a EZL-176 SMART (4D Systems, Austrialia) serial display module display with 28x35mm active area and 176x220 pixel density. The display is controlled via a serial TTL interface via a host controller.

5.4.3.4 Illumination Source

The illumination source is made up from two 3 mm LEDs (OSRAM, SFH 4350) positioned as in the cross arrangement (figure 5.8). Typical peak wavelength is 850nm with emission angle +/- 13°IR LEDs are used for both maximum dilation of the pupil and comfort for the user.

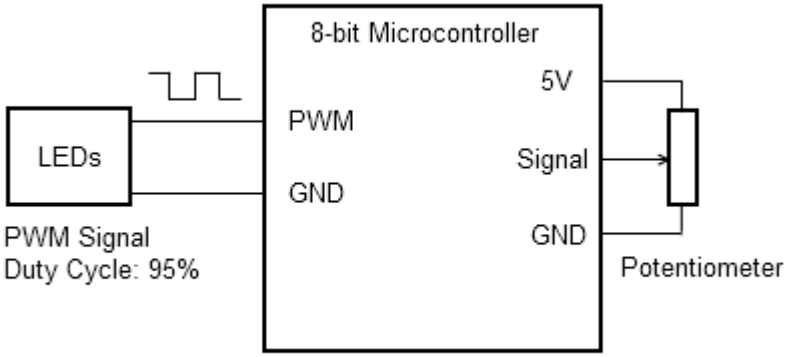

Figure 5.10: Illumination source driving circuit.

The LEDs are driven by a Pulse Width Modulated (PWM) signal via a host controller. The duty cycle of the PWM signal is determined by potentiometer connected to an analogue input on the host controller, the circuit is detailed in Figure 5.10.

5.4.4 Software

The software written to control the JEDEye alignment/tracker is written in LabVIEW (National Instruments, USA). The program acquires images from the camera and then processes these to determine the positions of the Purkinje Images. Once the misalignment of the eye from the alignment axis has been determined then the corrected position for the fixation target is communicated to the host controller (Arduino UNO (Arduino, Italy)). The host controller controls the position of the fixation target on the graphical display depending on the instructions received from the LabVIEW program. Instructions are sent from LabVIEW to the host controller via a software serial interface. The host controller also controls the brightness of the illumination sources via a PWM (Pulse Width Modulated) signal; this is performed independently from the LabVIEW program. All programming for the Arduino development board is performed in the Arduino IDE (release 0022, 24/12/2010) in C++.

The tracking software consists of 4 components:

- Overriding software architecture, this controls the graphical user interface and algorithm sequencing.
- Pupil detection algorithm.
- Purkinje reflection detection algorithm.
- Purkinje reflection filter algorithm.

5.4.4.1 Software Architecture

The overall sequencing of the tracking algorithm is performed in a state machine architecture. Essentially, the algorithm is broken down into a set of sequential steps in which the decision of progression is determined by the outcome of the previous step.

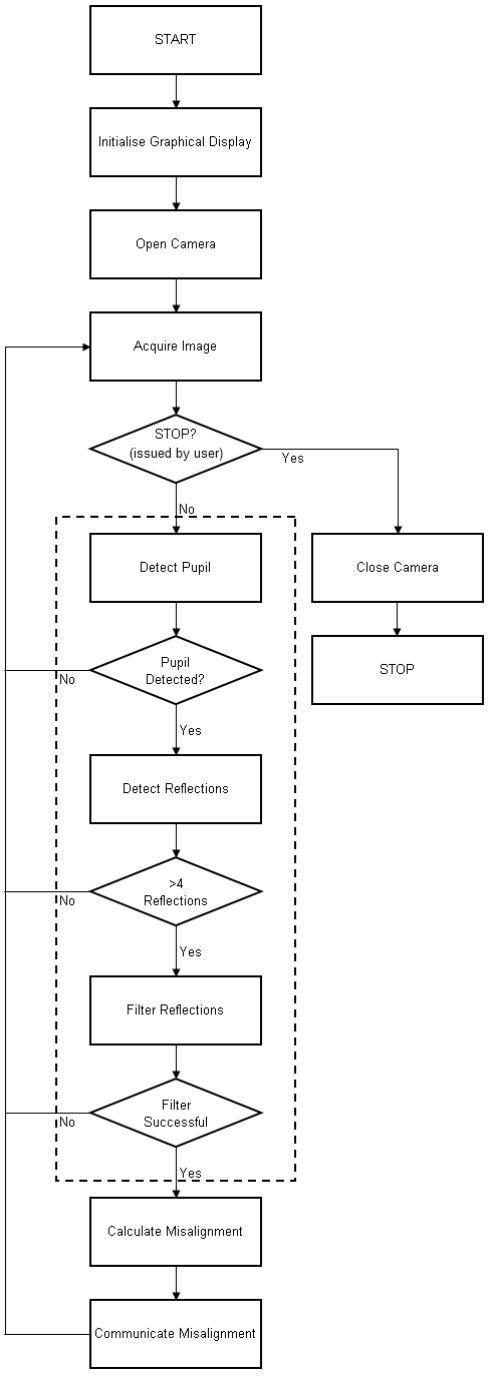

Figure 5.11: Tracking algorithm state diagram.

Figure 5.11 depicts the flow diagram used for the program algorithm. The tracking aspect of algorithm is split into 3 steps, pupil detection, Purkinje detection and Purkinje filtering.

The successful detection of the Purkinje Images is dependent on the success of all 3 of these steps. In the event that one of the tracking steps fails the program will proceed to acquire the next image until the program is notified otherwise.

All data acquired during the tracking session is stored to a tab delimited text file, the data consists of the calibrated coordinates of both sets of Purkinje Images and the pupil centre. Processing of the data is also done within the program and displayed as the total rotational and translational misalignment from the optical axis.

The program code is written in LabVIEW with a combination of built in functions acquired from the Vision Development Module and custom built functions built with LabVIEW's core functions. Images are acquired via LabVIEW's GigE driver and a selection of LabVIEW VI's acquired from IDS Imaging specifically written for image acquisition with LabVIEW from their imaging hardware.

5.4.4.2 Pupil Detection Algorithm

The detection of the pupil is required for this form of Purkinje Image tracking in order reduce the relevant image area for the detection of the Purkinje Images. Although the iris does not obstruct the view of Purkinje Image I it does prevent the detection of Purkinje Image IV if it stops the chief ray from the illumination source intersecting the lens. Thus Purkinje Image IV is only visible in the pupil which means imaging of the iris is redundant.

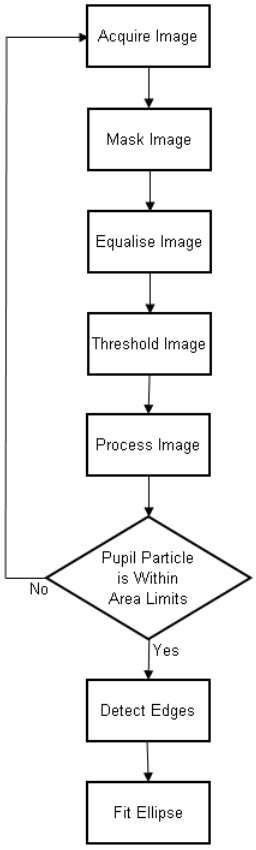

Figure 5.12: Pupil detection code flow diagram.

The eye image is masked, processed, thresholded and filtered to remove any particles which are not likely to be the pupil. An ellipse is then fitted to the remaining object. Depending whether the ellipse is a good fit, evaluated by the number of edge points used to fit the ellipse and the residual error between the actual edge point and the fitted ellipse, the algorithm will determine if the pupil detection has been successful.

Image Mask

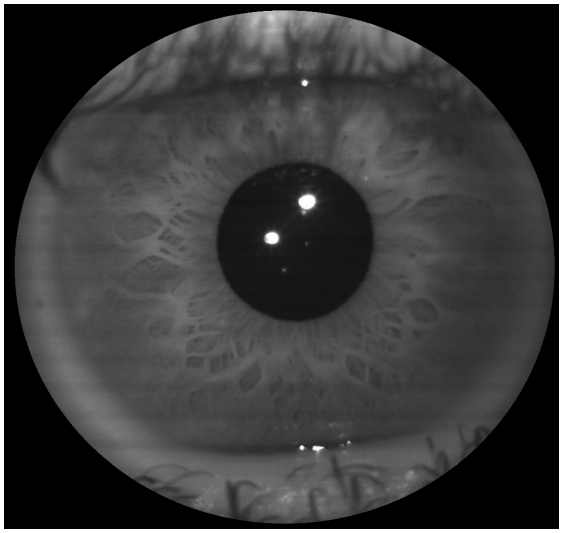

Figure 5.13: Pupil detection image mask.

Using the Mask function from LabVIEW's Vision Development Module the image is initially masked round the outskirts of the iris, this removes sections of the image which provide no information on the position of either the pupil or the Purkinje Images.

Equalise Image

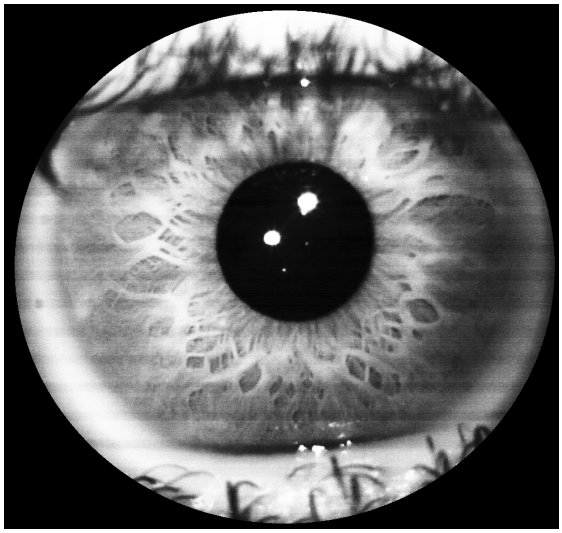

Figure 5.14: Pupil detection equalise image.

Using the Equalize look up table from LabVIEW's Vision Development Module the gray-scale image is remapped to the full 8 bit range, the function normailses the image allowing more consistent processing across multiple subjects.

Threshold

Figure 5.15: Pupil detection threshold image.

Using the Threshold function from LabVIEW's Vision Development Module a manual threshold is applied to the image to extract the dark pupil region. The threshold value was determined empirically, however having the images equalised allows a single value to be used across multiple subjects.

Binary Morphology

To enhance the image, and to remove unwanted particles, a series of binary morphological operations are performed using LabVIEW's Vision Development Module's in built functions. Initially the Remove Border Particles function is used to remove particles which touch the borders of the image, if particles are detected touching the border they are considered unlikely to be the pupil. The Close Objects function is then used to clean up the image, this function performs a binary dilation followed by an erosion. Finally, as the bright Purkinje Images are not included in the threshold step the dark region of the pupil is left incomplete, thus the Fill Holes function is used to complete the pupil in preparation for the Area Filter and elliptical fitting.

Area Particle Filter

The LabVIEW Particle Filter function allows the filtration of particles on a number of parameters. For extraction of the pupil, a simple area filter was used to remove particles which did not have an area between 3.14mm^2 and 50.27mm^2. The threshold limits equate to a minimum pupil diameter of 2mm and a maximum pupil diameter of 8mm.

Elliptical Fitting

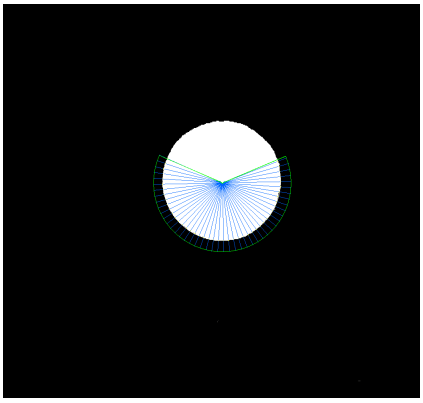

Figure 5.16: Pupil detection ellipse fitting.

In the event of multiple particles remaining in the image, a custom filter is used to determine the particle closet to the centre of the image and thus the most likely pupil particle. LabVIEWs IMAQ Spoke function is then used to determine the location of the pupil radial points. The function places a circular Region of Interest (ROI) at the centre of the potential pupil particle, the radius of the ROI extends out beyond the particle. The spoke function then projects a series a of lines from the ROI's centre point to the circumference, the location of the radial points are determined by the changes in intensity along the search lines. These radial points are then entered into an elliptical fitting function where the points which produce the best fit ellipse are used, thus the pupil ROI is determined.

5.4.4.3 Purkinje Detection Algorithm

Once the acquired image is reduced to the pupil, the image is processed again to isolate reflections within the pupil which are potentially the Purkinje Images.

The method first processes the image with a Sobel edge detection, then thresholds the image and finally performs a series of binary morphological operations to prepare the image for analysis.

Original Image

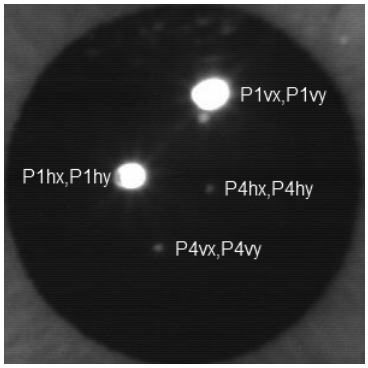

Figure 5.17: Purkinje Image notation used to for the Purkinje Image detection algorithm.

Figure 5.17 shows a sample image acquired for the Purkinje processing stage, using the cross arrangement of the LEDs. Each Purkinje Image is assigned specific notations for their coordinates. P1vx and P1vy are the x and y coordinates of the vertical Purkinje Image I, the corresponding Purkinje Image IV is denoted as P4vx and P4vy. In the same manner P1hx and P1hy refer to the horizontal Purkinje Image I, the corresponding Purkinje Image IV has coordinates P4hx and P4hy.

Sobel Edge Detection

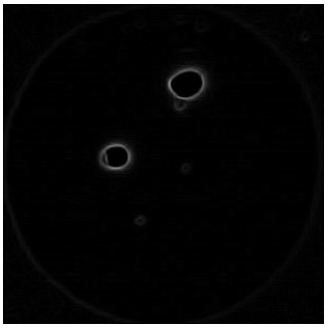

Figure 5.18: Purkinje detection Sobel edge filter.

The Sobel edge detection function is an in built LabVIEW function which highlights areas of the image with high intensity differences.

Threshold

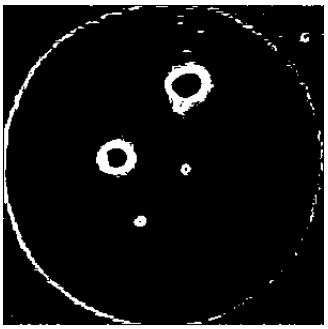

Figure 5.19: Purkinje detection threshold.

A manual threshold is then performed on the image to reduce it to a binary image in preparation for the morphological operations. The threshold value is found empirically.

Binary Morphology

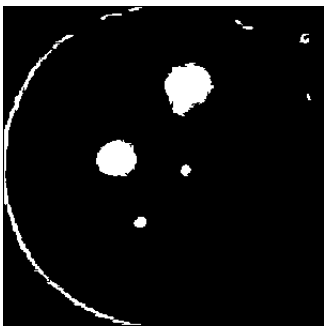

Figure 5.20: Purkinje detection binary morphology.

To complete the image processing, 3 morphological operations are performed. Firstly any particles touching the image edges are removed using LabVIEWs Reject Border Particles. Secondly, to fill in the centre of the particles, left behind by the Sobel edge detection, the Fill Holes function is used. Finally to tidy the image the Proper Open function is performed.

5.4.4.4 Purkinje Filter Algorithm

The resulting image from the Purkinje image processing algorithm is a collection of reflections which include the Purkinje Images. Purkinje Image I is relatively distinct from the rest of the reflections due to their size; however, Purkinje Image IV are far more allusive because they are of a similar size and intensity as reflections caused by eye lashes.

To obtain the correct Purkinje Images for eye tracking a custom Purkinje filter is used which analyse size, shape and position of the remaining particles. The relevant information for the Purkinje filter is generated by LabVIEWs Particle Analysis function.

The filter is split into two sections: detection of Purkinje Image I and detection of Purkinje Image IV.

5.4.4.5 Purkinje Image I Filter

Figure 5.21 describes the Purkinje Image I filter presented in a flow diagram. The correct Purkinje Images I are judged on their roundness, area and the gradient of the line joining them.

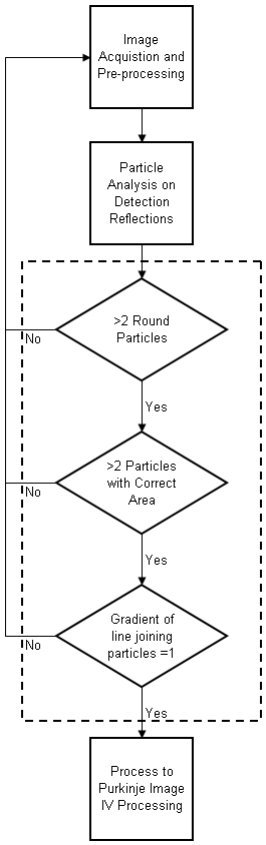

Figure 5.21: Purkinje Image I detection flow diagram.

Roundness

One of the measurements produced in the Particle Analysis is the Elongation Factor (also referred to as aspect ratio), which is a ratio of the particles bounding rectangles height and width. Essentially, the closer this value is to one the squarer the particle (or circular in this case). Thus particles which have a Elongation Factor higher than the threshold value are rejected. This stage of the filtering is prone to the detection of rogue Purkinje images as elliptical particles spread across the diagonal of the bounding box result in false positives. In this case the following filtering stages are used to filter these images.

Area

The second filter step thresholds the area of the particles, the upper and lower thresholds have been determined empirically.

Gradient

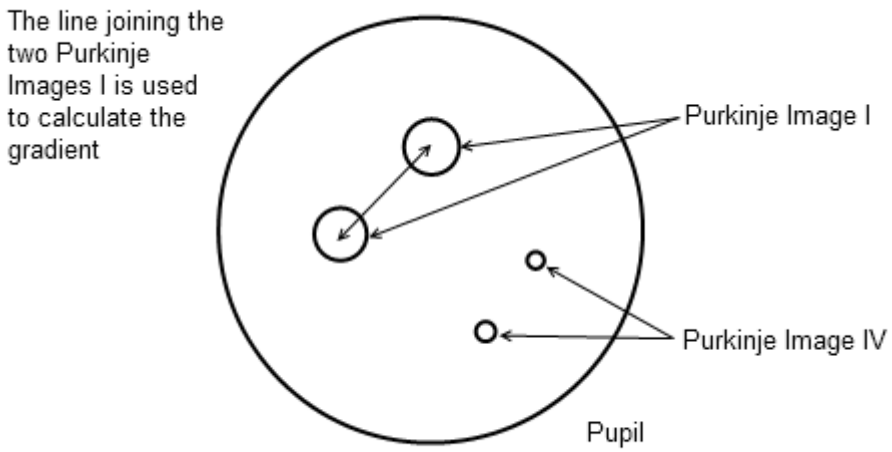

Figure 5.22: Line used for the gradient filter for Purkinje Image I.

As Purkinje Images are invoked in the eye by the instrument, their appearance can be controlled. In the case of the proposed set up there is a definitive gradient of the line joining both Purkinje Images I. Thus, potential Purkinje Image I points are split into pairs, where the gradient of the line joining them is determined. If a pair of potential Purkinje Images I falls within the gradient limits then they are deemed Purkinje Images I.

5.4.4.6 Purkinje Image IV Filter

Figure 5.23 presents the processing steps taken in the Purkinje Image IV filter. The correct Purkinje Image IV images are isolated from other reflections based on 5 criteria, position, length, gradient, proximity and a comparison factor.

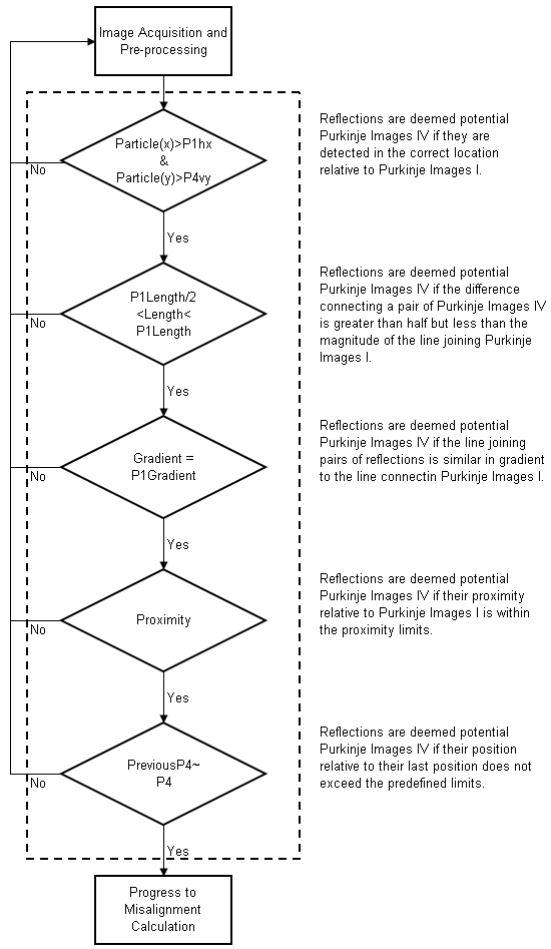

Figure 5.23: Purkinje Image IV filter flow diagram.

Position

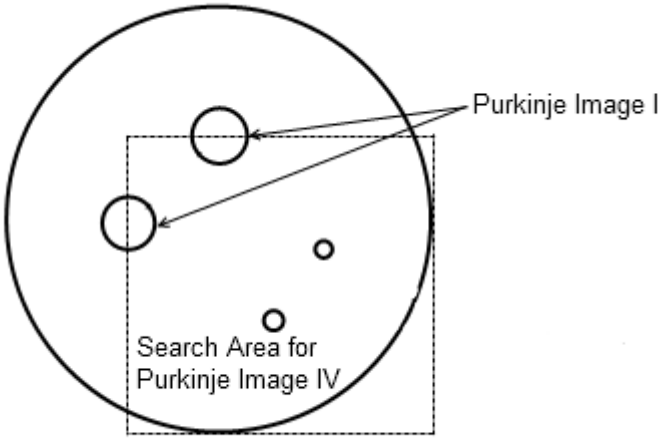

Figure 5.24: Diagram describing position filter.

Generally, both Purkinje Images IV occupy similar locations relative to Purkinje Image I when the subject looks straight ahead. The first stage of the Purkinje detection filter is then to filter out detected particles on this premise. Specifically, particles are considered potential Purkinje Images IV if their x coordinate is greater than the horizontal Purkinje Image I x coordinate (P1hx) and greater than the vertical Purkinje Image y coordinate (P1vy) (greater because the y axis is inverted with respect to general convention), as shown in figure 5.24.

Length

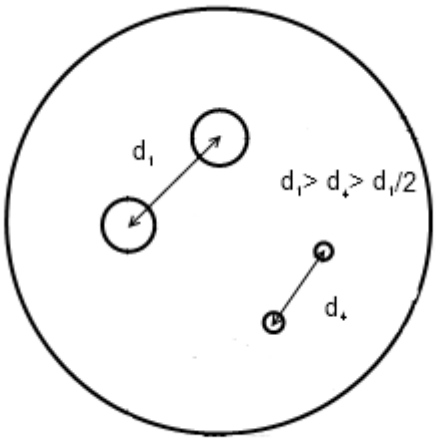

Figure 5.25: Diagram describing length filter.

The remaining particles are then organised into every possible combination of pairs and their separation calculated. The anatomical structure of the eye prevents the distance between 2 Purkinje Images IV being greater than the distance between the corresponding Purkinje Images I. Particles are then rejected if they are smaller than half the distance between the two Purkinje Images I or greater than the distance between the 2 Purkinje Images I.

Gradient

A gradient filter is then used to determine potential Purkinje Image IV pairs. There is a slight difference to the gradient filter used for Purkinje Image I. Where Purkinje Image I was compared to a gradient value determined by the instrument set up, the Purkinje Image IV gradient is compared to the gradient of the line joining the Purkinje Images I. Pairs of particles are then rejected if the gradient of the line joining them falls outside the threshold set with the Purkinje Image I gradient.

Proximity

Proximity refers to the distance between Purkinje Image I and its alternative Purkinje Image IV. Potential Purkinje Images IV are determined if the distance between (P1vx, P1vy) and (P4hx, P4hy) is equivalent to the distance between (P1hx, P1hy) and (P4vx, P4vy). This relationship is due to the parallel nature of the two sets of Purkinje Images.

Comparison Factor

The final filter is a comparison factor which compares the potential Purkinje Images IV to the previous Purkinje Images IV. If the movement is considered too great relative to their previous position then the potential Purkinje Images IV are rejected, thus leaving the correct Purkinje Images IV.

5.4.4.7 Host Controller

The Arduino UNO development board acts as the host controller and is responsible for two primary functions: firstly, it controls the intensity of the illumination source via a PWM signal; secondly, it relays serial commands from the Central Processing Unit (CPU) to the graphical display via a software serial communication.

In terms of the software, the programmed Arduino board performs the relative measures to initialise the graphical display so that it is ready for instruction.

5.4.4.8 Graphical User Interface

It is essential for any graphical user interface to quickly overlay the relevant information to the operator in a manner which provokes the correct response from the operator. In terms of the JEDEye alignment/tracking system it is imperative that the interface makes the operator aware of the movements of the eye and the degree of misalignment from the measurement axis. The operator also has to be informed that the correct Purkinje Images are being used to monitor eye movement.

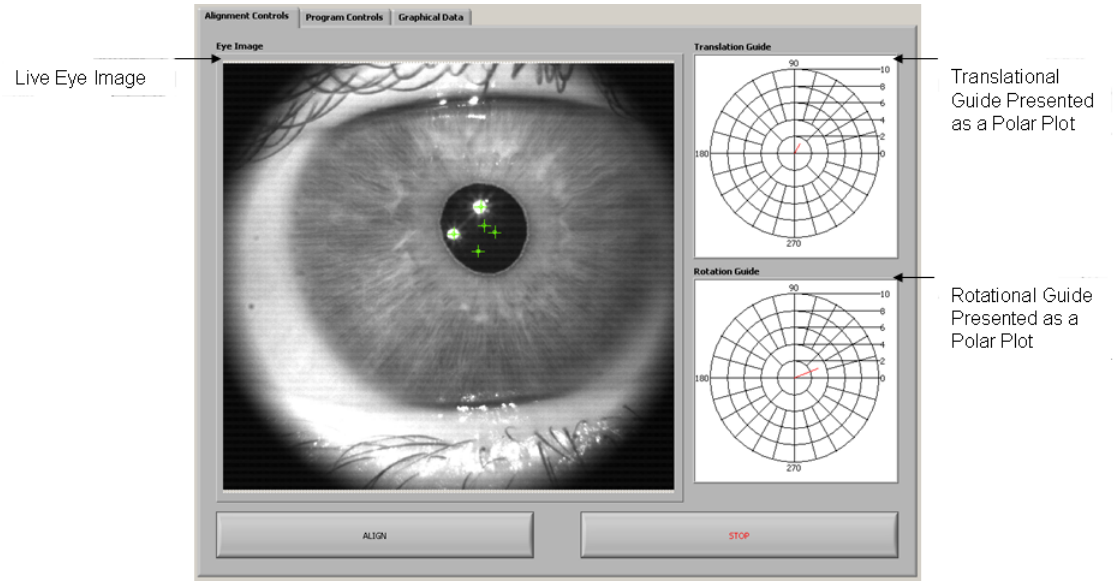

Figure 5.26: Graphical User Interface.

Figure 5.26 shows the graphical user interface used for the tracking system. The interface includes a live feed from the camera with an overlay of the detected Purkinje Images and pupil centre, this allows quick assessment of the validity of the tracking data. Misalignment data is then communicated to the operator by two polar plots, one showing the total translation misalignment while the other demonstrates the total rotational misalignment.

5.4.5 JEDEye Device Summary

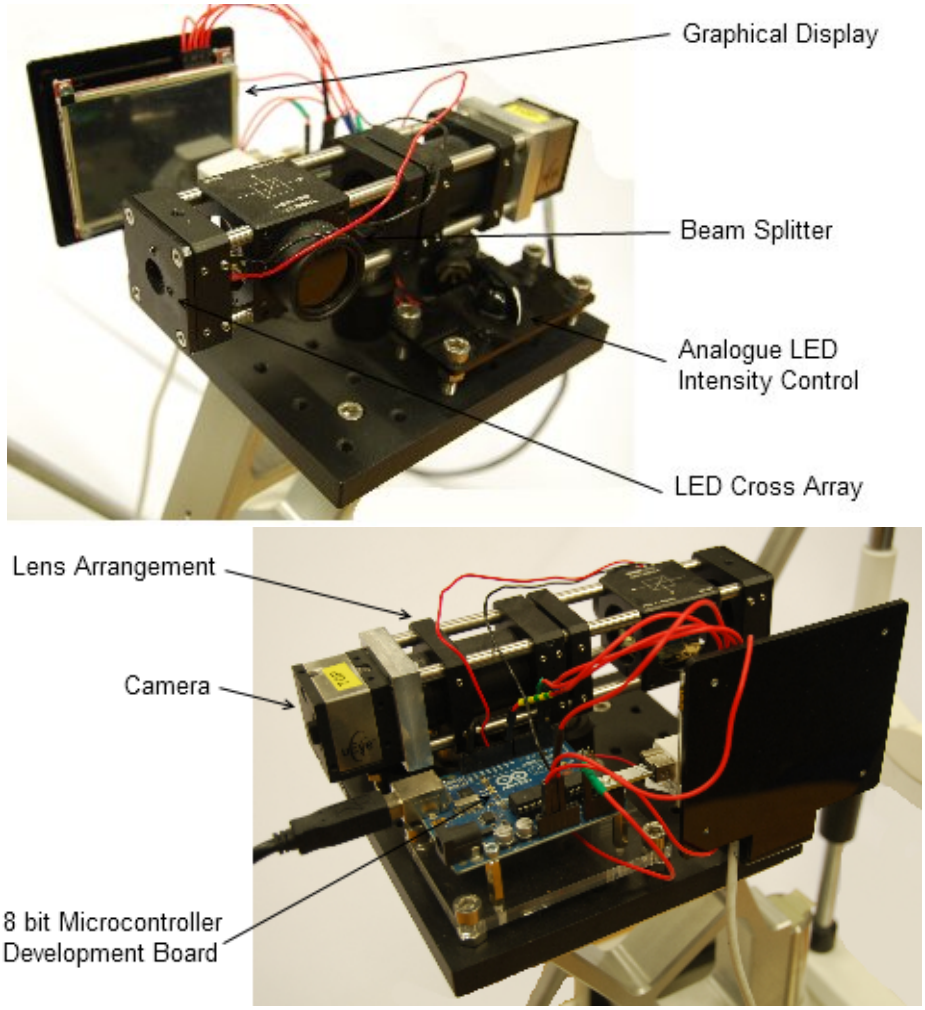

Figure 5.27: JEDEye device image.

Figure 5.27 shows the JEDEye alignment/tracker device. The device has a theoretical accuracy of 0.01 mm/pixel governed by the sensor and optical arrangement. At this pixel resolution the system has the ability to acquire images at 20 Hz, the software is also written to allow real time processing at this sampling frequency.

5.5 Evaluation

5.5.1 Safety

The development of any clinical instrument which interacts with the subject requires the instrument to be safe. While the developed eye tracking/alignment system has been designed for integration into a clinical instrument, first and foremost it is to be used as research tool to monitor the eye's movement during alignment. Thus for these research investigations it is imperative that the instrument is deemed safe.

The components of the developed eye tracking system are similar to those found in commercial eye tracking systems, with the major similarity being in the type of illumination source. IR light is used to illuminate the eye due to the eyes' lack of sensitivity in this wavelength range, for this reason, it is also the major safety concern as the amount of exposure to this wavelength goes unnoticed by the subject. The maximum irradience level for save exposure to the eye in the 720-1400 nm spectrum is 10 mW/cm^2 [135, 136, 137]; providing the irradiance level of the developed eye tracking system is less then this level the system can be deemed safe.

In regards to the novel eye tracking system, the irradenice is affected by two factors; firstly, as the LEDs are not coherent sources the magnitude of the irradience level is subject to the proximity of the user to the illumination source; secondly, the efficiency of the output of the LEDs is dependent on temperature. During longer durations of illumination, the temperature of the LEDs will change affecting the efficiency of their output. With these two factors in mind the safety of the illumination sources is tested in two separate experiments. The irradience of the illumination source is measured relative to the distance away from them, and the irradience of the illumination source is measured relative to time in the aligned position.

5.5.1.1 Aim

The objective of the safety experiment is to determine the power output of the illumination sources as a function of time and distance. Safety is then determined by comparing the maximum power output in each case with the maximum permissible exposure of 10 mW/cm^2.

Hypothesis

Maximum Power Irradience Level < 10 mW/cm^2

5.5.1.2 Method

As the power output of the illumination sources is dependent on two factors, duration and distance. The maximum power output was determined by two methods.

Duration

The power output of the illumination sources was measured with an optical power meter (Thorlabs, PM100D) using the S132C 700-1800 nm probe, factory calibrated prior to purchase. The probe was positioned at the focal point of the tracking system and aligned normally to the instrument axis. Alignment was performed by eye with the aid of the camera placed within the system. To ensure the probe was positioned normally to the illumination sources the probe was first pushed flat to the illumination array and then reversed along an optical rail until at the focal point.

Prior to data collection the voltage output from the probe was zeroed and the illumination sources turned off for an hour to allow the LEDs to cool to room temperature. The probe was then exposed to the illumination source for 900 s (15 mins) under dark conditions. The probe sampled the power output at 100 Hz and averaged the reading every 100 samples.

Distance

Initial set up of the experiment is as the duration set up.

Measurements of the power output were then read between distances of 0 and 100 mm at 5 mm increments. The order in which the measurements were acquired was randomly assigned. This process was repeated 3 times resulting in a total of 63 measurements.

5.5.1.3 Results

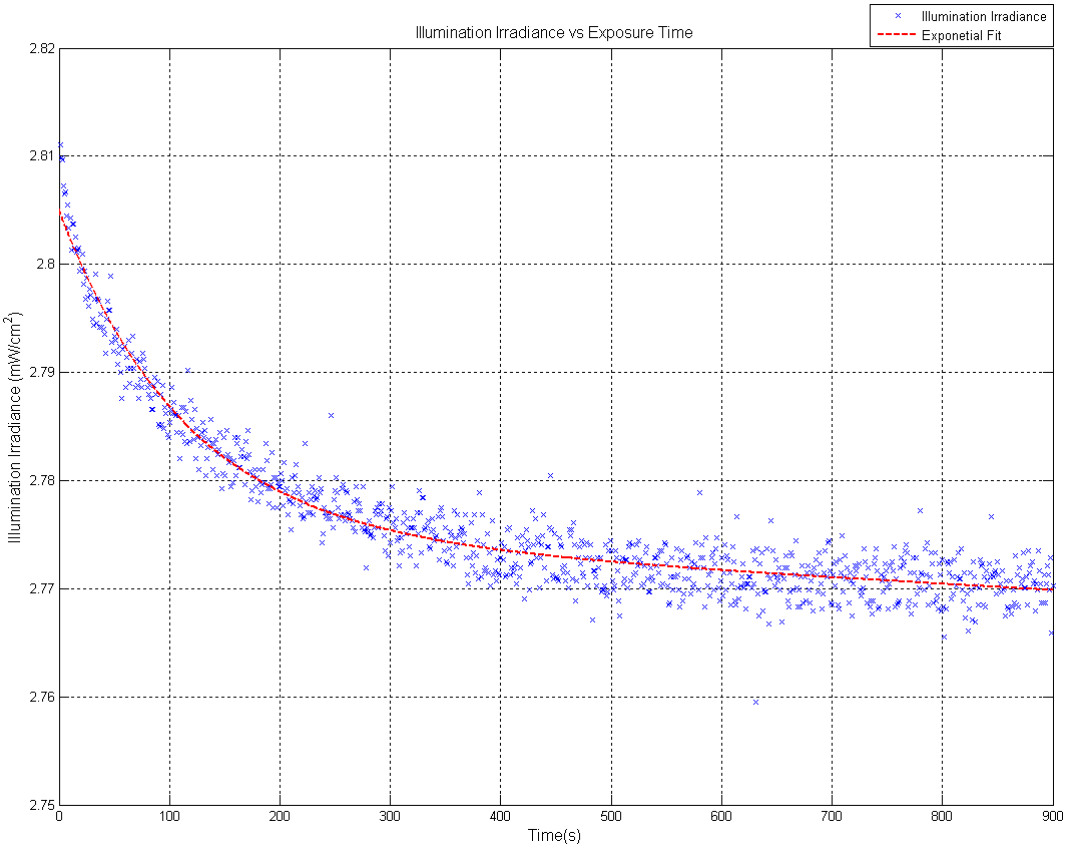

Figure 5.28: Illumination source power output vs exposure.

Figure 5.28 shows the power output of the illumination sources contained in the light array as a function of time. The data shows a general decreasing trend in irradiance over time. The maximum power out is charted at at the start of the time period and has a value of 2.81 mW/cm^2, this is 3.5 factors of safety below the 10 mW/cm^2 safety limit.

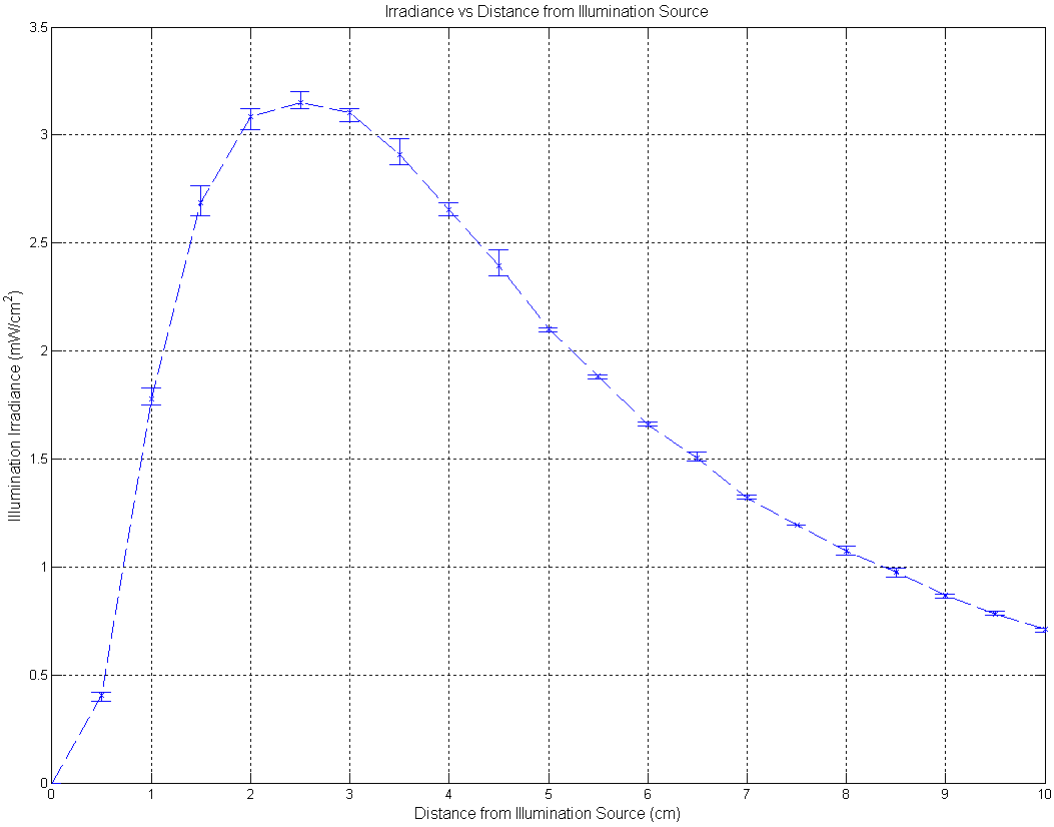

Figure 5.29: Illumination source power output vs distance from illumination source.

Figure 5.29 shows the power output from the illumination sources contained within the light array as a function of the distance from the illumination sources. The maximum measured value is 3.2 mW/cm^2 located at 25 mm away from the illumination sources, this is 3 factors of safety below the 10 mW/cm^2 safety limit.

5.5.1.4 Discussion

Head mounted eye trackers using a similar lighting arrangement found maximum power outputs of 0.8 mW/cm^2[138] which is smaller than the maximum power output found in this study. This suggests that the arrangement of the illumination source and the manner in which they are driven causes a higher exposure of the eye to IR radiation. However, the results do suggest 3 factors of safety, making the JEDEye alignment/tracker safe in its current form.

The investigation into the safety of the system was originally proposed to monitor the power output of the illumination sources in circumstance other than alignment. Of particular concern was the thermal efficiency of the LEDs, and whether, during long periods of active use the increase in temperature would result in unsafe levels of irradiance. In regards to this, the study suggests that the current driving of the LEDs causes a decrease in power output over time, thus maximum power output occurs at the beginning of the alignment procedure.

The power output described as a function of the distance away from the illumination sources suggests that there is an increase in power output at a point closer to the instrument than the optimum position for alignment, however this is still below the safety limit.

5.5.1.5 Conclusion

The maximum power output emitted by the light array positioned in front of the JEDEye alignment\tracker was 3.2 mW/cm^2 located at 25 mm away from the illumination sources, 3 factors of safety below the 10 mW/cm^2 safety limit.

The maximum output from the illumination sources over a 15 min time period was 2.81 mW/cm^2 which occurred at the beginning of the data collection, 3.5 factors of safety below the 10 mW/cm^2 safety limit.

As neither of the results suggest power outputs greater than the safety limit the JEDEye alignment/tracker device can be considered safe in its current format.

5.5.2 Accuracy

When developing a novel eye tracking system it is important to quantify the accuracy with which it determines the position of the eye, this information is integral to the evaluation of the system and allows comparison to the original specifications. The accuracy of the system can be partially approximated by the capabilities of the hardware, these approximations form a theoretical limit of the system. However, it is rare for any device to perform to its theoretical limits, inevitably there are systematic errors contained within the instrument which have a cumulative effect on accuracy.

The origins of these systematic errors can be traced to 2 main areas, hardware and software. Software provides the most significant source of unknown systematic error as the tracking algorithms are custom built to the application. Hardware is manufactured externally and so its performance and tolerances are documented. It is then in the interpretation of the acquired sample data (images of the eye); which is achieved through the tracking algorithm, that produces inaccuracies in the system. It is also important to note that unknown errors may also manifest themselves in the final error thus reiterating the importance of accuracy evaluation by the determination of systematic error.

One method to determine the systematic error is to compare the recorded readings with known readings. In the case of eye tracking this presents a difficult task. The eyes' movement, as well as the head's movement, causes the eyes to be relatively unstable, making precise positioning difficult. This obstacle can be overcome by the elimination of the eye to quantify movement and the use of an alternative artifact which possess the same trackable features. The artifact allows manipulation to an exact position and precise knowledge of the dimensions. The systematic error observed in the accuracy evaluation is then truly the systematic error and any increased error in the eye tracking will be as a result of the eye rather than the system.

5.5.2.1 Aim

The objective of the experiment is to quantify the systematic error in eye tracking data acquired with the JEDEye alignment/tracker. The systematic error is composed of 2 sources, offset error and gain error.

Offset error in the JEDEye alignment/tracker is defined as offset constant between the measured value and the actual value.

Gain error in the JEDEye alignment/tracker is defined as error value which is dependent on the magnitude of the actual value.

5.5.2.2 Methods

A model eye (Ocular Instruments, Germany) was imaged in different rotational and translational positions. From the acquired images the positions of the Purkinje Images induced in the model eye by the JEDEye system were recorded and used to calculate the orientation of the model, this allows comparison with the actual orientation.

All images were analysed with the JEDEye alignment\tracker principle.

The model eye was rotated using a dual stage goniometer with 0.167° resolution and +/-5° range. Translational movements were performed with a 3 axis linear stage with micrometer attachment, each axis of movement had 0-25 mm travel and 0.01 mm resolution. Translation was only performed in the x (horizontal) and y (vertical) direction, the z axis was used to manipulate the model eye into the correct focal plane.

For each mode of movement 21 data points were acquired; in this experiment 4 modes of movement are considered, rotation in the horizontal and vertical planes and translation in the horizontal and vertical planes. Rotational data was acquired in a range of +/-5° with an incrementation factor of 0.5°, while translational data was acquired in a range of +/-4 mm with an incrementation factor of 0.4mm, each measurement was repeated 3 times.

Initial alignment to the system was achieved with an optical cage system. Finer adjustments of alignment was achieved by translating the model until the x coordinate of the vertically located Purkinje Image I and the y coordinate of the horizontally located Purkinje Image I were the same as the coordinates of the central sensor pixel.

All measured values were then compared to the actual values of rotational and translational misalignment to determine the offset and gain error of the system.

Figure 5.30 shows the 5 axis model eye rotation and translation stage used to manipulate the position of the model relative to the JEDEye alignment\tracker.

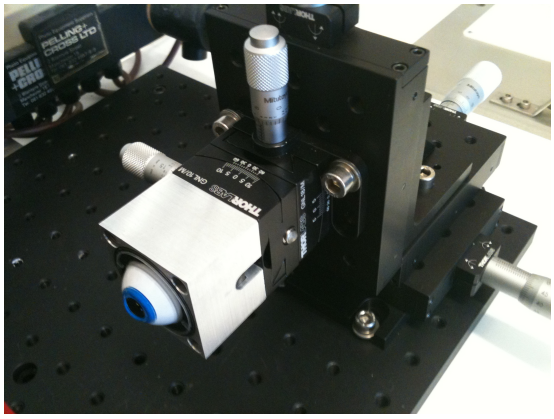

Figure 5.30: Model eye rotation stage.

Figure 5.31 shows the experimental set up with the JEDEye alignment\tracker aligned with the model eye and its rotation stage.

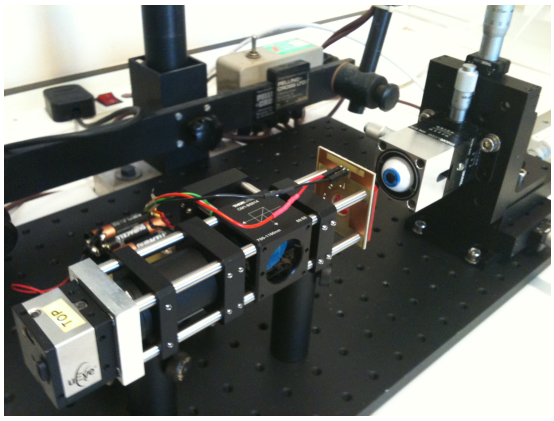

Figure 5.31: Accuracy experimental setup.

5.5.2.3 Results

Horizontal Rotation

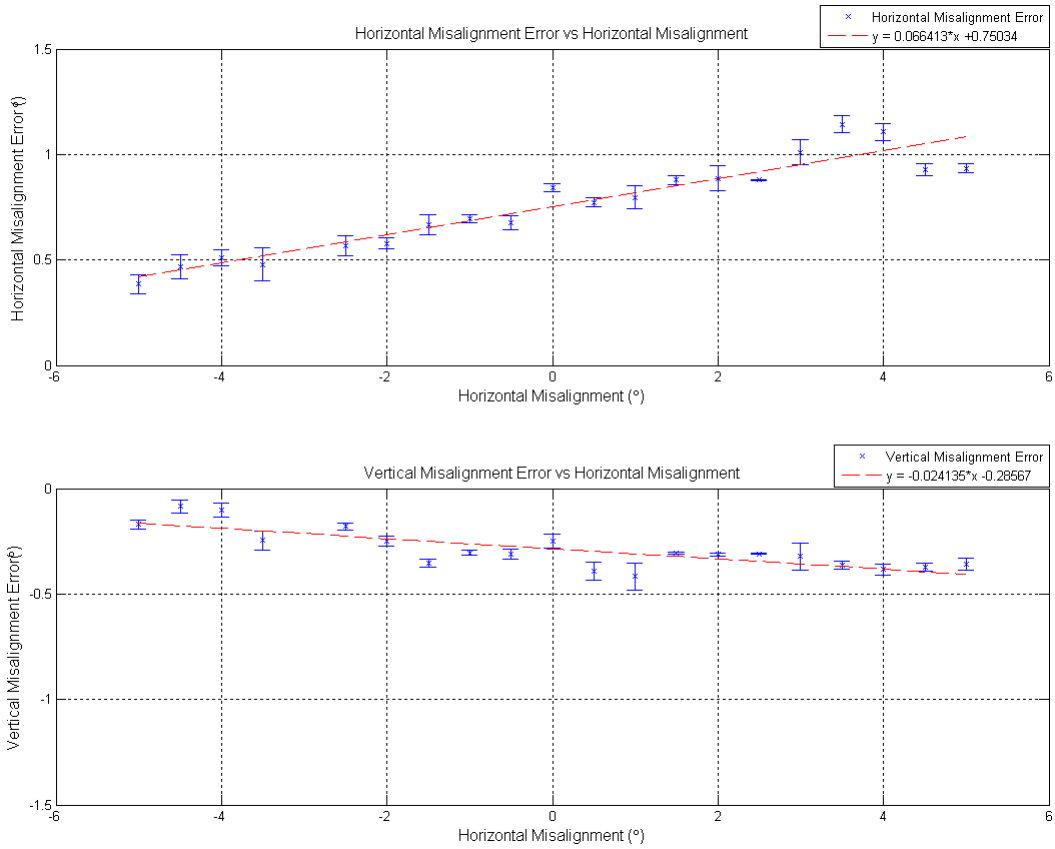

Figure 5.32: Horizontal rotational error.

Figure 5.32 shows the rotational error of the JEDEye technique when the model eye is rotated horizontally. The figure shows both the measured horizontal and vertical rotation when rotating in this axis. Theoretically, the measured rotation in the vertical direction is 0, however the results show -0.29° offset error and a small -0.02° component of gain error in this direction. The components of error in the horizontal direction are 0.75° offset error and 0.07° gain error.

Vertical Rotation

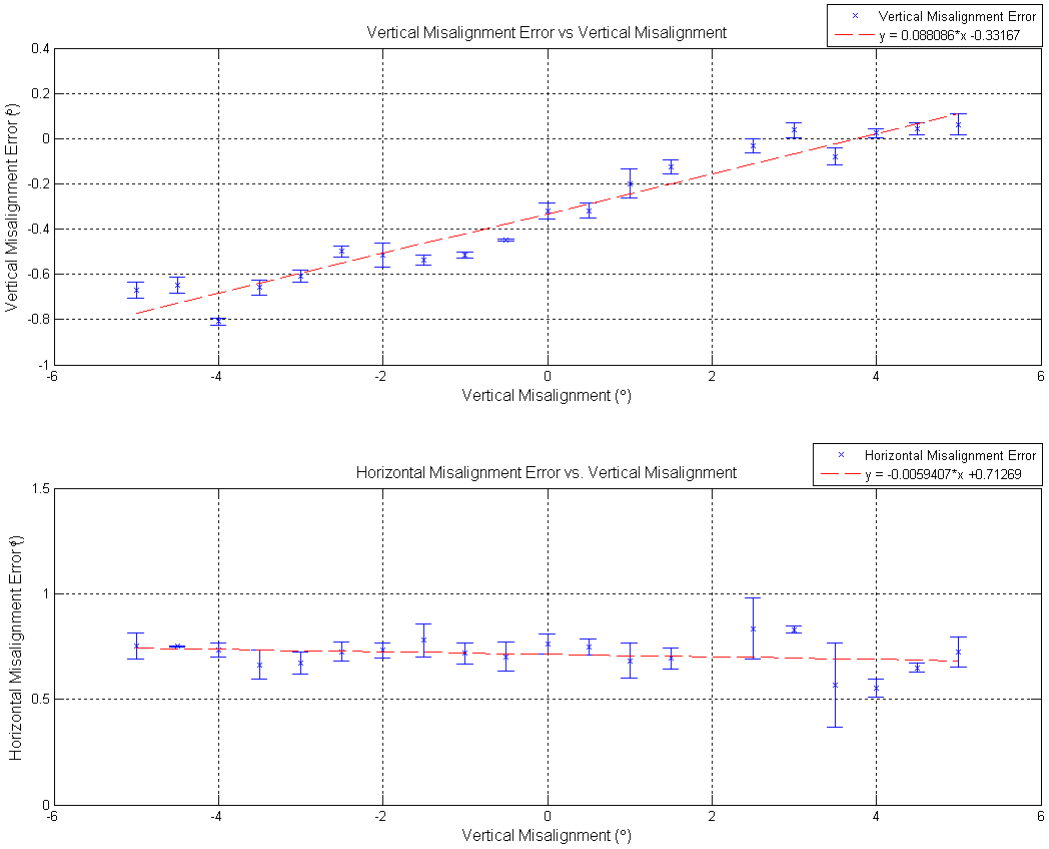

Figure 5.33: Vertical rotational error.

Figure 5.33 shows the rotational error of the JEDEye technique when the model eye is rotated vertically. The figure shows both the measured vertical and horizontal rotation when rotating in this axis. Theoretically, the measured rotation in the horizontal direction is 0, however the results show 0.71° offset error and a small -0.006° component of gain error in this direction. The components of error in the vertical direction are 0.33° offset error and 0.09° gain error.

Translation

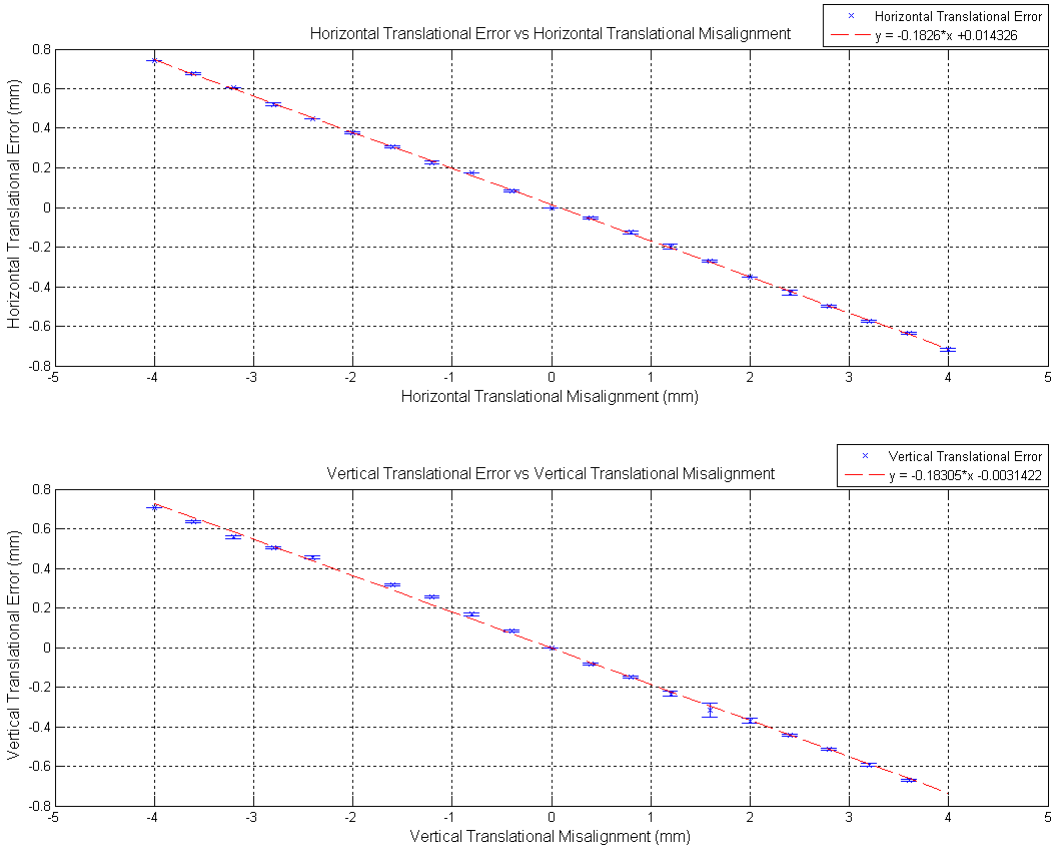

Figure 5.34: Translational error.

Figure 5.34 shows the translational error calculated from the experiment. Translation in the horizontal direction yields a 0.014 mm offset error and -0.18 mm gain error. Translation in the vertical direction yields the same gain error of -0.18 mm and an offset error of -0.003 mm.

Summary

Horizontal Rotation	**Gain (°)**	**Offset(°)**
Horizontal	0.066	0.75
Vertical	-0.024	-0.29
Vertical Rotation		
Horizontal	0.088	-0.33
Vertical	0.0059	0.71
Translation		
Horizontal	-0.18	0.014
Vertical	-0.18	-0.0031

Table 5.3: Error summary.

Figure 5.3 gives a summary of all the errors in the JEDEye technique calculated from the experiment.

5.5.2.4 Discussion

The results from the accuracy study into the JEDEye alignment/tracking system suggests relatively large components of offset error. However, close inspection of the results suggest that the error does not lie in the JEDEye system. There are 2 predominant reasons for this: firstly, the offset error is not symmetrical for each axis of rotation, the horizontal direction is slightly larger. Secondly, the component of offset error in the static axis of rotation is similar to that found in the manipulated axis of rotation for the alternative rotation. To explain in greater detail, when rotating horizontally the offset error was measured as 0.75°, while rotating vertically the horizontal offset error was measured at 0.71°, suggesting the error can be attributed to the model eye.

One potential reason for this offset error is that the model eye contains misaligned ocular surfaces; although the data sheet contains measurements and tolerances on the positions of the lenses on the model's optical axis it does not detail the alignment of the surfaces. Thus misalignment of this nature would manifest itself in the offset error but not in the gain error, a property of the results.

Although this misalignment is unenviable in the JEDEye accuracy assessment it demonstrates conditions which will be encountered when measuring the orientation of human eyes. In this regard, the tracking system demonstrates capabilities in the assessment of what would be angle α[2]. In addition to this, the offset error by itself does dictate the accuracy of the tracking system as the definition of the optical axis is the alignment of the Purkinje Images, by definition, any offset detected is a displacement from the optical axis.

The results obtained from the JEDEye alignment/tracking system in regard to the translational measurements show a larger gain error when compared to the offset error. This can be partly attributed to the way in which the translation is measured, the movement of Purkinje Image I dictates the translational movement and as the the initial alignment of the model eye was performed with the aid of Purkinje Image I it stands to reason there should be no offset error. The gain error obtained during translation of the model eye is a more notable result, the gain error shows that the more the eye translates from the alignment axis the higher the uncertainty in the measurement recorded with the JEDEye system.

Potentially, the reason for this error lies in the movements of the Purkinje Images. During rotation Purkinje Image I translates slightly. This movement is irrelevant when quantifying rotation as it is the separation between Purkinje Image I and Purkinje Image IV which is used to determine rotation. Also as both Purkinje Image I and Purkinje Image IV are induced by the same illumination source any translation movement performed by Purkinje Image I is reproduced in Purkinje Image IV. The rotational misalignment caused by the translation of the eye thus causes added movements of Purkinje Image I which is seen as translation by the JEDEye system.

[2] difference in angle between the optical axis and the visual axis

Errors of this nature may not manifest themselves in actual eye measurements as the rotational misalignment caused by translation would not occur. An actual eye would compensate for this rotational misalignment by maintaining fixation on an alignment target during translation, thus negating the added error of rotation to translation misalignment.

Comparing the accuracy of this tracking system with other tracking systems which make use of the Purkinje Images highlights consistencies in the magnitude of error. The first version of the Purkinje system as described by Cornsweet and Crane suggest accuracies of 0.5° - 1° with a resolution of 0.167° [109] which is in line with the JEDEye system. However there are differences in approach, Cornsweet and Crane use 1 pair of Purkinje Images and mirror the reflections down onto a 4 quadrant photo detector, eye movement is then determined by the movement of these mirrors to keep the reflections on the photo detectors. The original Purkinje tracking system also used approximations for the separation between the centres of curvatures which form the Purkinje Images. The Purkinje System described in this report images the entire eye and extracts the locations of the Purkinje Images, this allows determination of the not only the eye movements but the properties of the eye which allow calculation of central curvature separation thus negating the need for approximations.

It should also be mentioned that no calibration was needed to relate the positions of the Purkinje Images to the rotation of the eye, a necessity for many other systems which investigate gaze direction, this allows instantaneous identification of the orientation of the eye.

5.5.2.5 Conclusions

The offset error value for horizontal and vertical rotation was found to be +/-0.75° and +/-0.33° respectively, the gain error was determined to be +/-0.066° for horizontal rotation while gain error in vertical rotation was found to be +/-0.088°. In terms of translation the offset error value for horizontal and vertical translation was found to be +/-0.014 mm and +/-0.0031 mm respectively while the gain error was +/-0.18 mm in both directions.

The results suggest that the offset error can be partly attributed to the model eye. When rotating in the horizontal direction the offset error was found to be +/-0.75°; however, an offset error of +/-0.71° was found in the horizontal direction when rotating the model eye vertically. This then suggests an actual offset error of +/-0.04° in the horizontal direction. The same offset error of +/-0.04° can be found in the vertical rotation by applying the same principle.

The technique is required to resolve eye rotations of 0.17°, the accuracy results suggest that it has the ability to do this thus the technique fulfills the required specifications.

5.5.3 Tracking Comparison

There are technical issues with Purkinje image tracking using the JEDEye system which warrants comparisons with other techniques. The imaging of Purkinje Image IV is made difficult due to the low intensity of this reflection. Pupil tracking negates this problem and is by far the most reliable feature of the eye to track. If the low intensity of Purkinje Image IV does become a significant problem then it is important to investigate alternative methods.

Eye tracking performed with Purkinje Image I and the pupil centre (P1PC) is a very popular form of eye tracking with a number of devices making use of the technique [112, 113, 114, 115, 117]. The JEDEye alignment\tracker is based on Purkinje Image tracking [107, 108] which is an uncommon tracking technique; however, for the purposes of eye alignment it is a more attractive method. Its preference is due to its identification of the optical axis and its ability to monitor head movement and eye rotation independently. P1PC also has the ability to resolve head movements from eye rotations; however, the alignment axis which it identifies is the visual axis.

While the visual axis is an equally valid alignment axis as the optical axis, the way in which it is identified in P1PC tracking is subject to variation. This variation is due to two factors: firstly the pupil is not a uniform shape, thus determination of its centre point is subject to variation; secondly, the centre point of the pupil is said to deviate during dilation and constriction, as much as 0.6 mm in some cases [22].

The stimulus for pupil constriction/dilation is not just a matter of illumination, there are several other factors which influence this response such as accommodation. However, in typical alignment procedures, where the subject is required to fixate on a target for a relatively short period of time, it is questionable whether the amount of constriction/dilation would cause a significant shift in pupil centre location. More importantly, it is unclear whether the variation induced in tracking recordings as a result of the pupil's irregular shape and centre point deviation would significantly affect the precision in alignment.

While Purkinje Image tracking is also subject to natural deviation due to the accommodation of the lens, the magnitude of this deviation is small in comparison. In addition to this it does not suffer the variation induced by tracking an irregular shape as the Purkinje Images are invoked by the JEDEye alignment/tracker.

Both these techniques share a common characteristics which lend themselves to comparison. All reference points required to track the eye for both techniques are present in the same focal plane. The anatomical structure of the eye causes Purkinje Image I and Purkinje Image IV to fall in the same focal plane, which lies very close to the pupil. Also, the LEDs used to invoke the Purkinje Images are IR, these lights are outside the visible light spectrum and thus are not visible to the human eye.

The investigation then aims to evaluate and compare P1PC with the JEDEye technique on 5 criteria:

Pupil Centre Location - determination of the pupil centre location relative to the optical axis allows quantification of the offset of the visual axis from the optical axis.

Pupil Diameter - analysis of pupil diameter allows the amount of pupil constriction/dilation to be assessed during typical alignment conditions.

Pupil Fitting Error - determination of the error associated with fitting an elliptical shape to the pupil allows the quantification of the variance induced in pupil tracking as a result of this error.

Pupil Centre Movement - analysis of the pupil centre movement relative to pupil diameter allows the quantification of pupil centre movement during pupil constriction/dilation and thus the error induced while tracking this feature.

Tracking Comparison - comparison of the overall variances obtained from tracking data collected with both techniques allows the significance of the difference caused by the tracking the pupil to be determined.

5.5.3.1 Aim

The overall aim of the investigation is determine if the use of P1PC tracking causes a significant difference in tracking variance due to the pupil when compared to JEDEye alignment/tracking.

$H_o = \sigma_{P1PC} = \sigma_{PI}$

$H_a = \sigma_{P1PC} \neq \sigma_{PI}$

Pupil Centre Location

Determine the average location of the pupil centre relative to the optical axis defined by Purkinje Image I and IV.

Pupil Diameter

Determine the range in pupil diameter under typical alignment circumstances.

Pupil Fitting Error

Determine the range in error of elliptical shape fitting to the pupil.

Pupil Centre Movement

Determine the significance of correlation between pupil diameter and pupil centre movement.

$H_o = r = 0$

$H_a = r \neq 0$

5.5.3.2 Method

Rotational eye movements were measured using the JEDEye alignment/tracker. The JEDEye alignment/tracker detects the Purkinje Images as well as the pupil centre. This allows tracking by both methods on the same acquired images.

A total of 16 (mean age 31, SD +/- 11) subjects were asked to fixate on a black dot (6´ resolution), all subjects were naive to the purpose of the experiment. The same recording was used to analyse the difference in eye rotation variance obtained with P1PC methods and JEDEye tracking. For all subjects the subject's right eye was measured.

Exclusion Criteria

To ensure normality, subjects were only considered for the study if they passed the following criteria:

- No underlying eye conditions, such as dry eye or kerataconus.
- Do not wear contact lenses.
- Could identify the target to be used in the study.
- Subjects who had their vision corrected with glasses were allowed also long as they could see the target without their glasses.

Data Analysis

The entire set of data was processed using an algorithm written in National Instruments LabVIEW programming environment. The algorithm detects, isolates and extracts the coordinates of the Purkinje Images and pupil centre location. The algorithm also recorded the major and minor axes of the ellipse fitted to the pupil to find the centre location as well as the residual error in this fit. For JEDEye tracking, rotation was calculated by first performing phakometry calculations followed by analysis on the separation of the Purkinje Images. For P1PC tracking rotation was determined by the separation between Purkinje Image I and the Pupil Centre. All statistical analysis was performed with Matlab.

Pupil Centre Location

In order to determine the pupil centre location relative to the optical axis the location of the optical axis had to be obtained. This was achieved by determining the intersection between the lines formed by Purkinje Image I and their corresponding Purkinje Images IV. The vector between this point and the Pupil Centre location was then determined.

Pupil Diameter Range

The range in pupil diameter was determined by averaging the minor and major diameters obtained with the elliptical fitting of the pupil. This was done for every frame of the recording, after which the average diameter was determined along with the range of Pupil Diameter.

Pupil Fitting Error

To determine the error in the elliptical fit of the pupil the sum of the residual error in the fit was recorded for each frame in each recording. The residual error is calculated by the least squares difference between the detected pupil radial point and the corresponding fitted ellipse radial point as calculated by LabVIEW's elliptical fitting algorithm.

$$ResidualError = \sqrt{\sum e_i^2}$$

Where e_i is the difference between the detected pupil radial point and the corresponding fitted ellipse radial point at the i_{th} point used to fit the ellipse.

For analysis the average Residual Error was obtained along with the range in this error.

Pupil Centre Movement

To determine the significance of Pupil Centre movement as a result of constriction/dilation a regression ANOVA was used to analyse the correlation between pupil diameter and the magnitude of the separation between the pupil centre and optical axis determined by the pupil centre location analysis. In this case the optical axis served as reference point in which to chart the movement of the pupil centre during constriction/dilation.

The regression ANOVA was decided on for these results as it allows the significance of the relationship between the two variables to be assessed.

Tracking Comparison

To statistically test the difference in variation caused by the use of Pupil tracking in the P1PC technique and PI tracking a paired t-test was performed. Rotation data for each recording was only used if rotation information could be obtained for P1PC and PI tracking in the same frame. Tracking data was ignored for either technique if the tracking data was not present for the alternative technique.

The paired t test was decided on for these particular results as tracking data was essentially obtained from the same subject. The investigation is concerned with the difference in tracking data variation due to the inclusion of pupil tracking in P1PC tracking, thus it is the difference with-in subjects which is of interest, making the paired t test appropriate.

5.5.3.3 Results

Pupil Centre Location

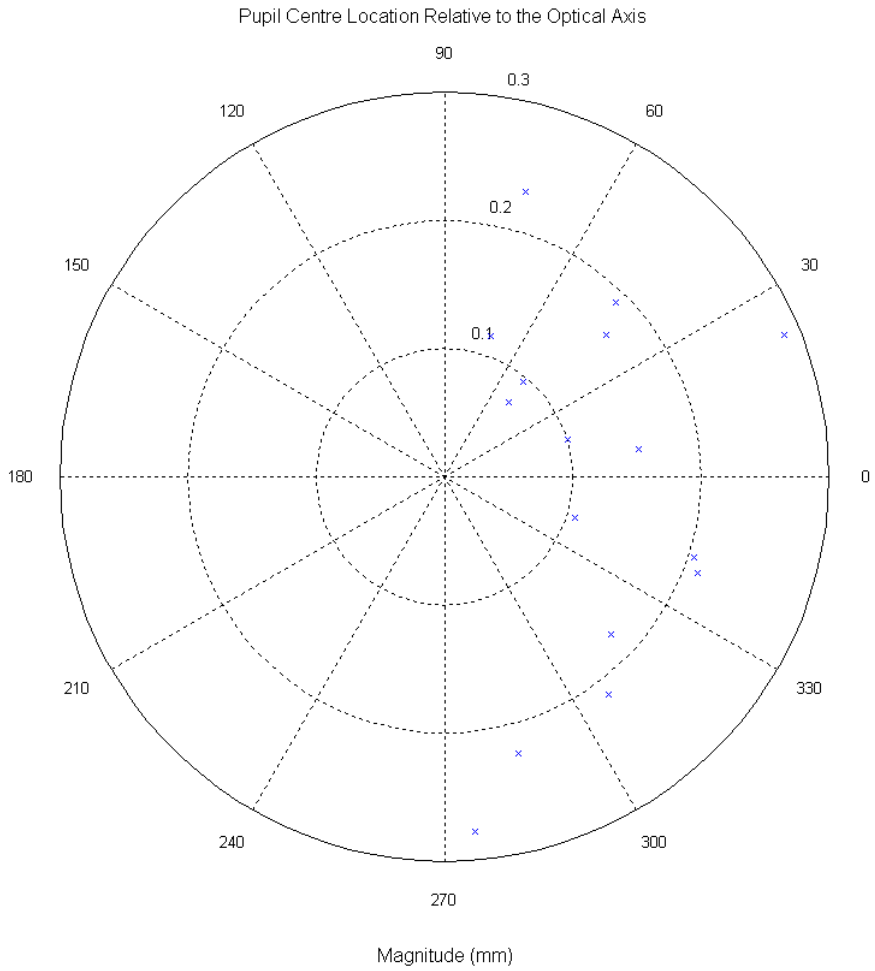

Figure 5.35: Pupil centre location relative to the optical axis in subjects' right eyes.

Figure 5.35 shows the position of the pupil centre relative to the optical axis defined by the Purkinje Images for all 16 subjects. Average magnitude from the optical axis was 0.18 mm with a maximum average of 0.29 mm and a minimum average of 0.08 mm. Results show a tendency for the pupil centre to lie nasally when compared to the optical axis.

Pupil Diameter Range

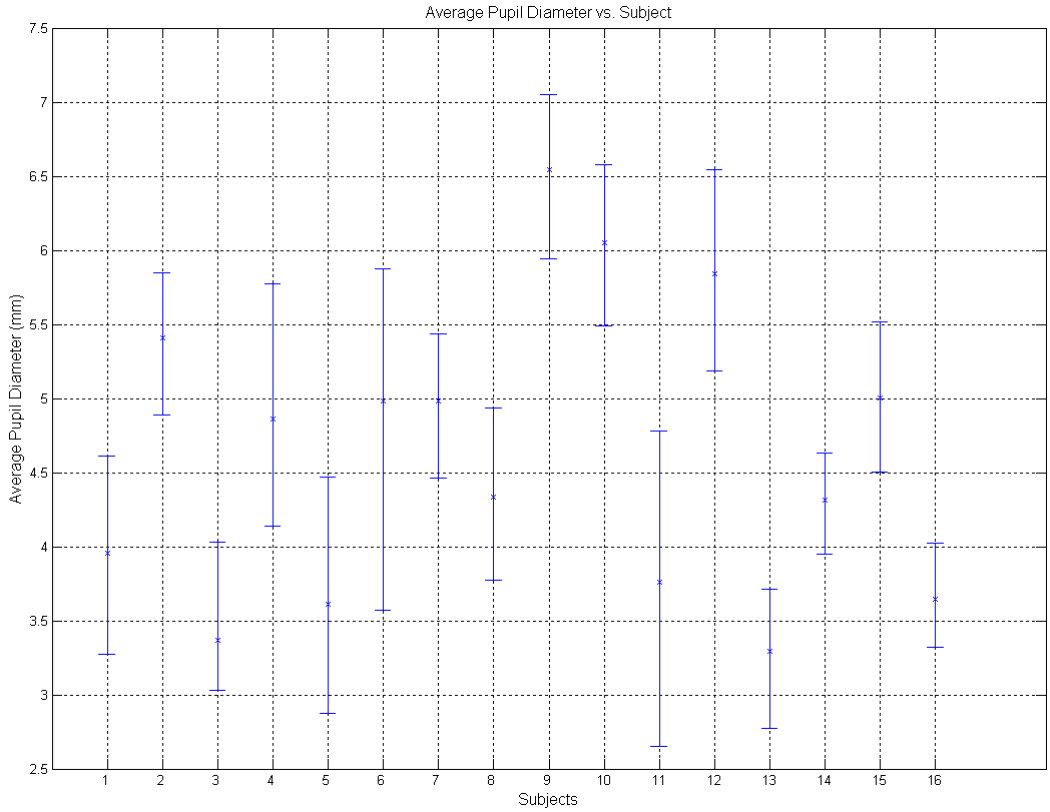

Figure 5.36: Range of pupil diameter during fixation for 60s.

Figure 5.36 demonstrates the range in pupil diameter during fixation for 60 s. The error bars indicate the maximum and minimum pupil diameter values. The results state that the average diameter for the pupil under the experiment conditions was 4.62 mm, while the average range in pupil diameter was 1.25 mm. The maximum range in pupil diameter was recorded as 2.3 mm while the minimum range was 0.68mm.

Pupil Fitting Error

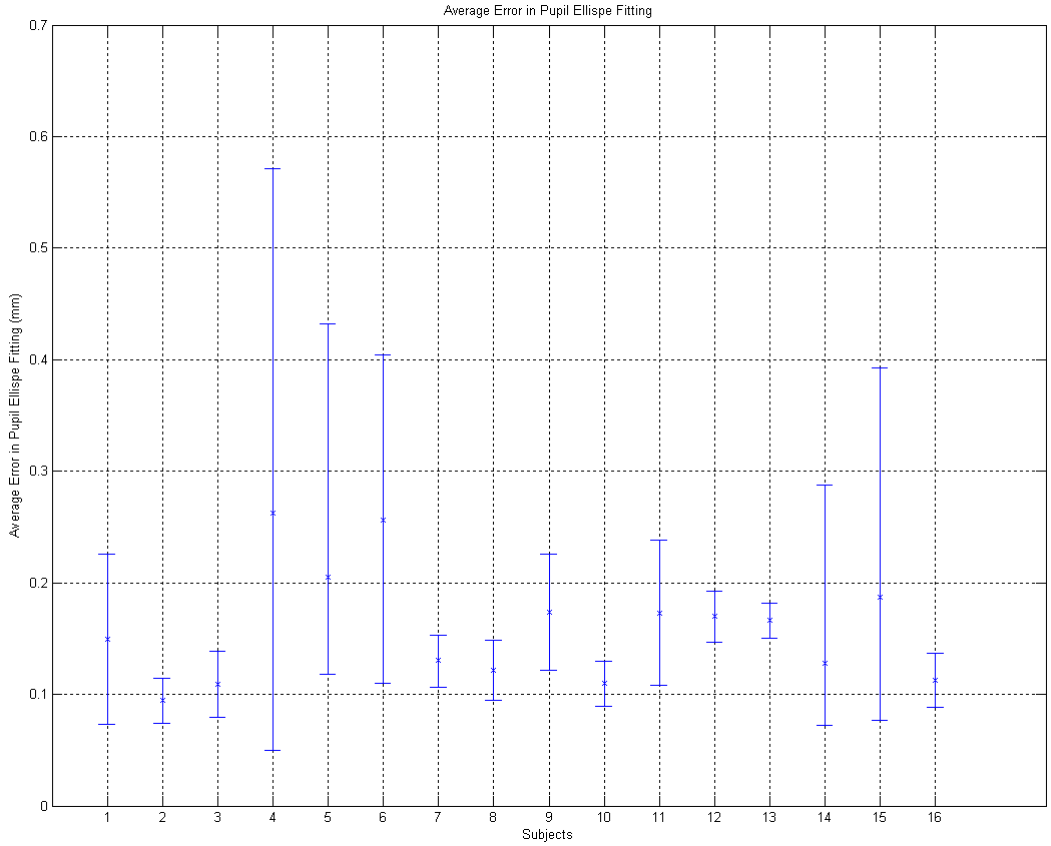

Figure 5.37: Residual error pupil ellipse fitting.

Figure 5.37 shows the residual error in the algorithm used an ellipse to the pupil. The average error was recorded as 0.16 mm while the maximum average error across all subjects was 0.26 mm, the minimum average error was recorded at 0.09 mm.

Pupil Centre Movement

The following graph is a typical representation of the relationship between the pupil centre location relative to the optical axis and pupil diameter obtained from the experiment. The results only suggest minor correlation. The graphical data from all other subjects can be found in Appendix D

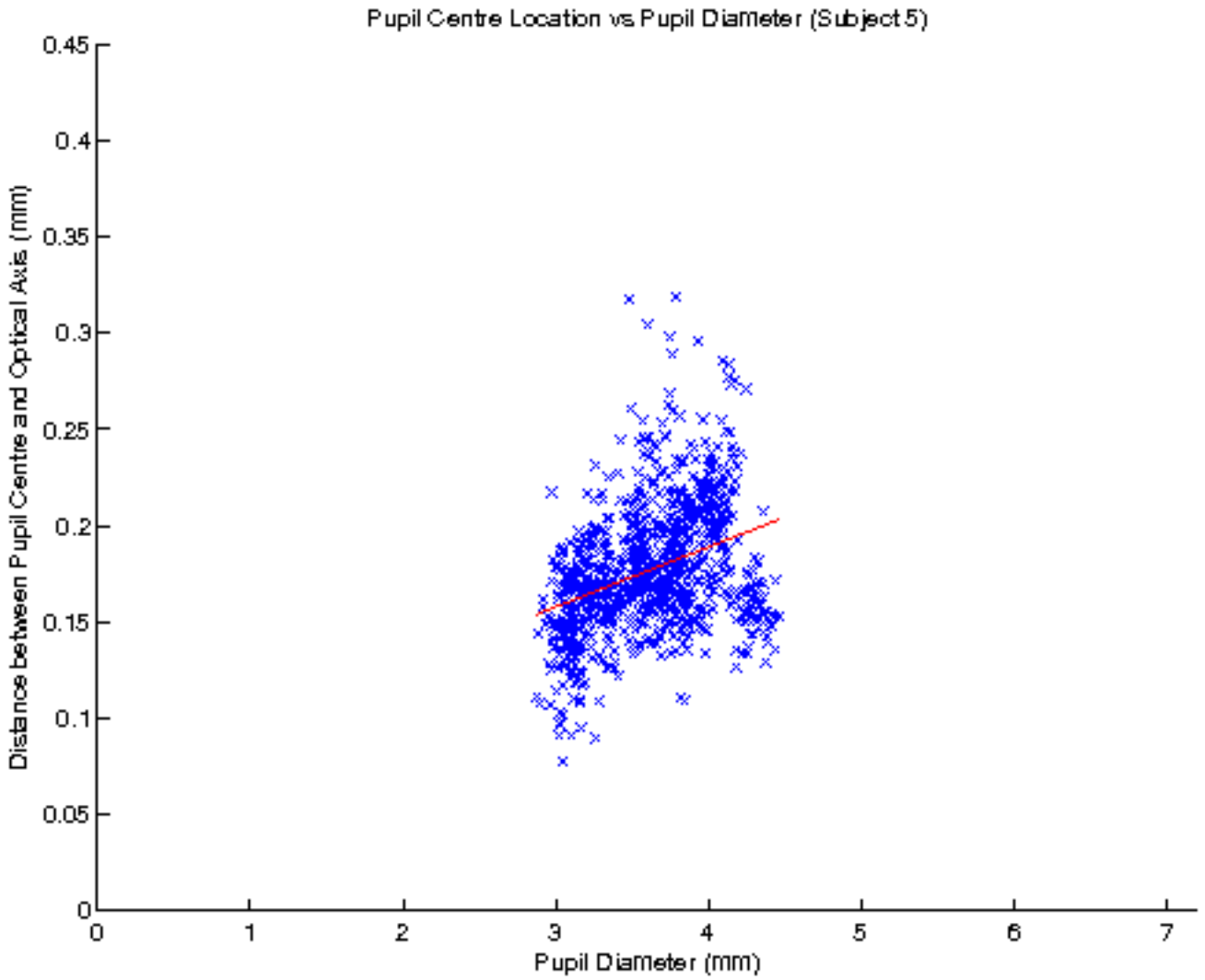

Figure 5.38: Correlation between pupil diameter and the position of the pupil centre relative to the optical axis (Subject 5)

Statistical Analysis

Subjects	r	r^2	F value	p value
1	0.69	0.47	821.14	0.00
2	0.18	0.03	41.97	0.00
3	0.21	0.04	56.97	0.00
4	0.61	0.37	532.54	0.00
5	0.31	0.11	120.01	0.00
6	0.16	0.03	23.37	0.00
7	0.41	0.17	195.65	0.00
8	0.43	0.19	335.59	0.00
9	0.34	0.12	195.64	0.00
10	0.34	0.12	199.09	0.00
11	0.13	0.02	9.96	0.00
12	0.15	0.02	30.45	0.00
13	0.4	0.16	268.93	0.00
14	0.32	0.1	34.41	0.00
15	0.05	0.00	3.16	0.08
16	0.04	0.00	2.13	0.15

Table 5.4: ANOVA regression analysis describing the statistical significance of the correlation between pupil centre movement and pupil diameter.

Table 5.4 shows the ANOVA analysis for the correlation between pupil diameter and pupil centre location relative to the optical axis. In 14 of the 16 subjects the variation in pupil centre location relative to the optical axis due to pupil diameter was found to be significant, however, in the majority of cases the coefficient of correlation suggests poor linear correlation.

Tracking Comparison

Subject	JEDEye Tracking Average Eye Rotation (°)	P1PC Tracking Average Eye Rotation (°)	Difference (D)	$\sqrt{(D)^2}$
1	0.45	0.38	0.07	0.07
2	0.23	0.24	-0.01	0.01
3	0.14	0.21	-0.07	0.07
4	0.25	0.23	0.02	0.02
5	0.46	0.41	0.05	0.05
6	0.36	0.61	-0.25	0.25
7	0.25	0.3	-0.05	0.05
8	0.25	0.16	-0.09	0.09
9	0.24	0.23	0.01	0.01
10	0.32	0.19	0.13	0.13
11	0.29	0.26	0.03	0.03
12	0.39	0.55	-0.16	0.16
13	0.26	0.18	0.08	0.08
14	0.37	0.36	0.01	0.01
15	0.13	0.19	-0.06	0.06
16	1.63	0.28	1.35	1.35
Mean	0.38	0.30	0.08	0.15
Standard Deviation	0.35	0.1	0.1	0.06
Total Mean	0.3		-	-
Total Standard Deviation	0.26		-	-
Samples	16			
t statistic	0.89			
t critical	2.13			
p value	0.83			

Table 5.5: Statistical data for the two tailed paired t test for the tracking comparison.

The obtained p-value of 0.83 is greater than the 0.05, thus the null hypothesis is accepted and there is no statistically significant difference between tracking data acquired with P1PC tracking and tracking data acquired with the JEDEye tracker due to the pupil, in typical alignment conditions.

Power Analysis

In order to determine the power of the statistical test performed on the tracking comparison a power analysis was undertaken. This analysis is based on the approach outlined by Barker and Li [139] in which two experimental parameters are used to estimate the power of the sample. These parameters are the effect size and the correlation coefficient. The effect size refers to the determined difference between two variables in a study, while the correlation refers to the strength of the relationship between the two tested variables.

The effect size (ES) is calculated by the mean difference between the observed results ($\bar{D}$) divided by the standard deviation of all the results (SD)[139]:

$$ES = \frac{\bar{D}}{SD}$$

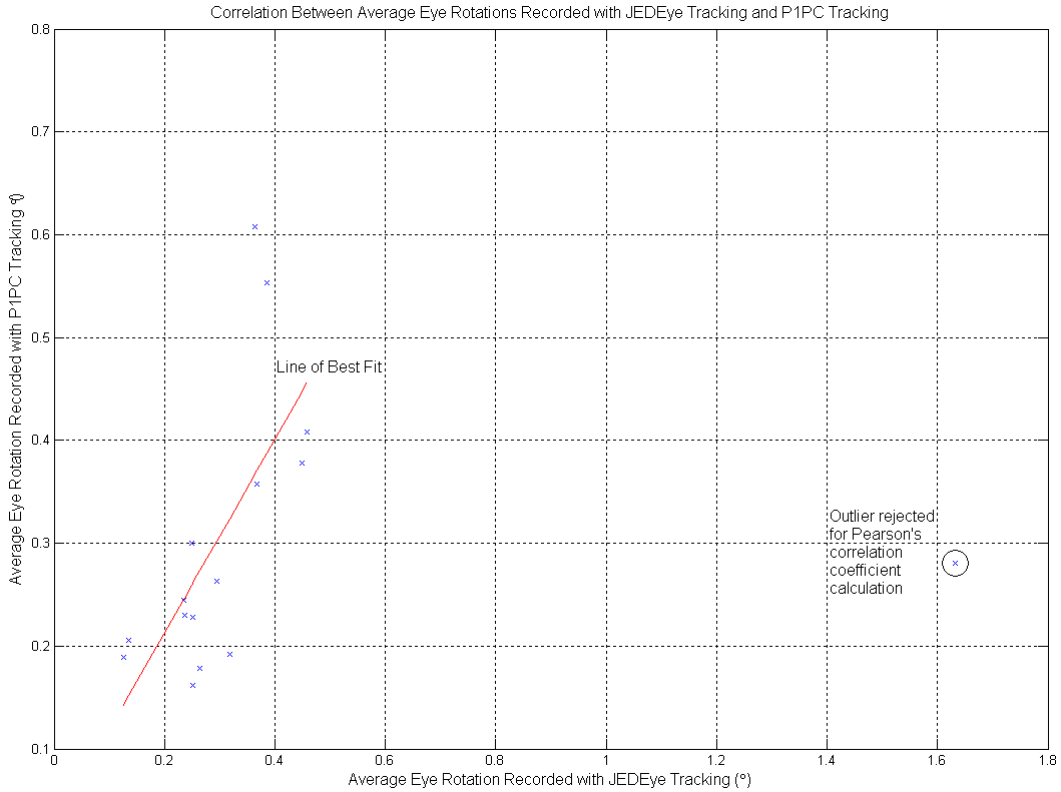

Figure 5.39: Correlation graph for the average eye rotations obtained with JEDEye tracking and P1PC tracking.

Figure 5.39 is a graphical representation of the correlation between the average eye rotation recorded with both JEDEye tracking and P1PC tracking. For the purposes of the power calculation the outlier is ignored and the remainder of the data is used to perform the calculation. Table 5.6 shows the Pearson's correlation coefficient calculated for the data, it suggests that high eye magnitudes of average eye movements is detected by both forms of tracking.

Pearson's Correlation Coefficient (r)
0.68

Table 5.6: Pearson Correlation coefficent for the data set.

The power of the statistical test can thus be calculated using an effect size (ES) of 0.58, a correlation coefficient (r) of 0.68 and a sample size (n) of 16.

Specifcally for the paired t-test power calculation, the effect size (ES) is adjusted due to the effect the correlation has on the statistical power [139, 140, 141]:

$$ES_{adj} = \frac{ES}{\sqrt{1-r}}$$

The t value is then calculated:

$$t = \frac{ES_{adj}}{\sqrt{\frac{2}{n}}}$$

The z score for the power value is then calculated by a comparison of the t value and the t_{cv} critical value. The t_{cv} is obtained from the Student's t distrubtion with a nomial criterion level of 0.05 and 15 degrees of freedom (df).

$$Power = z\left(\frac{t - t_{cv}}{\sqrt{1 + \frac{t_{cv}^2}{2df}}}\right)$$

$$Power = 78\%$$

The power calculation suggests that the experiment has a 78% chance of achieving statistical significane based on a ES of 0.58, a r of 0.68 and a sample size of 16. Although this lower than the standard power of 80% it is still sufficient to detect statistical differences if differences are present.

5.5.3.4 Discussion

The purpose of the experiment was to determine if there was significant difference between tracking data obtained with P1PC techniques and JEDEye tracking. It was hypothesised that due to the variation in the central pupil position, attributed to constriction/dilation, an increase in the standard deviation of P1PC data would be recorded. However, it was unclear whether this variance would appear in typical alignment conditions as it was questionable whether these circumstances would provoke pupil constriction/dilation.

The results suggest that there is no significant difference in the standard deviation between tracking data acquired with the two tracking methods. These results can be attributed to a number of reasons, the most obvious being that the pupil size and centre position remained stable during tracking. Other reasons lie in the JEDEye tracking technique, it is assumed that this technique is more stable in comparison to P1PC methods as it does not require pupil tracking. However, the results could be interpreted as JEDEye tracking is subject to equal amounts of variation as P1PC tracking. There is evidence to support this as pupil constriction/dilation is related to accommodation: accommodation is the mechanism in which the lens changes shape to re-focus an object on the fovea. Purkinje Image IV is formed from the posterior lens surface thus is subject to this movement. During accommodation it is largely the anterior lens which changes shape; however, as Purkinje Image IV is formed after refraction through the anterior lens the position of this image is affected. This then is potentially one of the reasons no significant difference was found between the 2 tracking methods.

Additional results obtained in the experiment suggest that the Purkinje Images remain stable relative to the pupil centre during constriction/dilation. The movement of the pupil centre during constriction/dilation was measured relative to the eye's optical axis, defined by the Purkinje Images. In 14 out 16 cases there was a significant change in central pupil position relative to pupil diameter. If the Purkinje Images were subject to the same types of movement during constriction/dilation this statistic would not be so strong. There have also been studies which chart the movement of the pupil centre with constriction/dilation [142, 22, 143] adding validity to the present results. Wilson [22] observed a shift of 0.6 mm in pupil centre location during constriction while Park [142] observed an average shift of 0.37 mm with 88.5% experiencing magnitudes in shift greater than 0.2 mm.

The results on pupil diameter range offer contradictory results. Wyatt [143] in his assessment of the human pupil suggests average pupil diameters of 3.09 mm in light conditions and 4.93 mm during dark conditions, a range of 1.84 mm. His study investigated an age range of 22-71 with an average age of 32.8. Present results suggest a range of pupil diameter under constant illumination conditions of 1.25 mm, 68% of the total range when compared to Wyatt's results. While the experiments differ in illumination conditions, the comparison serves to indicate how much the pupil can be expected to change size during constant illumination alignment conditions when compared to the total range in pupil diameter as determined in Wyatt's study. The comparison suggests that even with constant illumination the pupil will still move through 68% of its entire range due to other factors, factors which would be present in all alignment procedures.

Wyatt [143] also details the average magnitude in difference between the pupil centre and limbal centre as 0.34 mm, a larger average than suggested in these results. However this may be down to the difference in reference point with the comparison suggesting that the limbal centre lies slightly more temporally than the optical axis.

In all subjects, there was error present in the fitted ellipse to the pupil, interestingly the error was very similar to the deviation of the pupil centre from the optical axis. These results highlight the unique shape of each pupil commented on in other studies [144, 143], though again this did not cause significant difference in tracking results obtained with each tracking method.

Ultimately the decision on the most appropriate tracking method for alignment is dependent on the required axis of alignment. While the results show that there is variation in central pupil position relative to pupil diameter, this variation is not significantly greater than variation in JEDEye tracking, where the pupil is ignored. Thus the tracking method is dependent on whether the measurement system requires visual axis alignment (P1PC) or optical axis alignment.

Conclusion

The overall aim of the experiment was to determine if the variation induced in the P1PC tracking data by the pupil was significant when compared to the JEDEye system. This variation in pupil centre location is attributed to two factors: the variation caused by fitting an ellipse to the irregular shape of the pupil and the deviation of its centre during constriction/dilation. However, the results suggest that despite these sources of variance there was no significant difference found between tracking data obtained with P1PC tracking and JEDEye tracking under typical alignment circumstances.

Contrary to this 14 out of 16 subjects demonstrated that the variance in pupil centre location is significantly related to pupil diameter. The results also suggest that pupil centre location relative to the optical axis averaged 0.18 mm +/- 0.06 (0.08 mm - 0.29 mm). The range in pupil diameter averaged 1.25 mm +/- 0.46 (0.68 mm -2.3 mm). Finally the error in the elliptical fit to the pupil averaged 0.16 mm +/- 0.05 (0.26 mm - 0.09 mm).

The results demonstrate that there is error in the elliptical fit to the pupil and that the pupil centre does move due to constriction/dilation; however, it does cause significant differences in tracking data obtained with the P1PC technique when compared to the JEDEye method. Even though there is no significant difference in the tracking methods the fact that the pupil centre moves with constriction/dilation means that it is unsuitable for alignment, thus backing Purkinje Image tracking as the most suitable tracking for alignment.

Chapter 6

Fixation Studies

6.1 Chapter Overview

The purpose of the chapter is to determine the potential for an optimum fixation target to minimise eye rotation, and to investigate fixation as a method of stable alignment.

In order to determine the magnitude of eye movement during fixation the JEDEye alignment/tracker was used to monitor the eye's movement while fixating on a number of different targets. There are a vast number of targets which can be used for fixation, with each target having a number of permutations. Due to this, the study was split into 5 sub categories, type, size, movement, colour and concentration; with the aim to determine the optimum value for each category and merge them into an optimum fixation target for the reduction of eye movement.

Using this newly acquired eye tracking data, taking in reference to the fixation target, the stability of the eye during fixation was also analysed. This assessment allows the validity of eye fixation to induce a stable eye in ophthalmic equipment to be determined.

The chapter concludes by outlining the optimum target or strategy for fixation and the main factors for misalignment during fixation.

6.2 Introduction

Ophthalmic instruments measuring physical parameters of the eye attempt to keep the eye stable by instructing the patient to fixate on a target, the ability of the subject to fixate then dictates the stability of the eye. It was noted in the eye movements literature review (Chapter 2) that the type and magnitude of eye movement is influenced by the scene which the eye is regarding, the type of fixation target must then influence the subject's ability to fixate.

In the context of this research, this has 2 consequences: firstly, the influence of the fixation target on the magnitude of eye movement suggests an optimum target for the reduction of eye movement; secondly, the type and magnitude of eye movement performed during typical alignment procedures is still unclear and thus needs to be assessed. Both these points are important; an optimum target for the minimisation of eye movement is an attractive and yet simple concept, while knowledge of the magnitude of eye movements during fixation is important when designing the mechanism for alignment correction.

6.3 Target Type and Movement

The use of moving targets for increased eye stability seems a contradiction; however, there is argument to suggest that target movement may reduce eye movement. To understand the reasons why this might be the case we must first consider the movements of the eye which are produced during fixation. In total, there are said to be 3 eye movements associated with fixation: ocular tremor, ocular drift and microsaccades [145]. The appearance of the first two movements is unavoidable in fixation; however, due to their magnitude (depending on definition 2' - 12' [41]) they do not contribute enough significant movement to instigate misalignment; at least this is true when compared to the eye's larger movements. This then leaves the microsaccade, it has been suggested that microsaccades increase in frequency and amplitude when there is visual fading in the periphery of a subject's field of view [54, 55]. Fading is attributed to the Troxler effect [56], this effect is a component of visual perception in which images residing in the subject's peripheral field of view will start to fade and disappear if the image is sufficiently similar to its surroundings.

Figure 6.1: The Troxler effect: staring at the central cross for 20 - 30 s without blinking will cause the periphery of the image to fade.

It would then be logical to hypothesise that changes in the peripheral field of view would negate the requirement for microsaccades to 'refresh' the retina. Rolfs et al [61] goes on to demonstrate this with the use of changes in colour and luminance around a central fixation spot; both this, and interestingly auditory signals [146], diminish the frequency of microsaccades.

Figure 6.2: Movement illusion in static images [5].

Conversely, fixational eye movements are visible in illusions of movement in static images [5] as shown in figure 6.2, these particular images appear to move due to the small movements of the eye. This then reiterates the requirement for investigations into the reduction of eye movement by target movement as the opposite to this can be seen.

Movement of the target only forms one of many potential target parameters which may or may not influence the propagation of fixational eye movements during fixation. Target type is one such parameter, early investigations were principally concerned with simple fixation points [147, 148] while later investigations focused on colour and size [149] with significant differences found in both. More recent investigations have looked at the eye's movement, specifically microsaccades, when the subject is required to fixate on a target within a scene [150], though this was primarily to investigate saccadic generation. While target colour and size seem obvious parameters for investigations; target type does not, and yet this seems odd as the word target immediately conjures images of Bullseyes and Crosshairs. Why is it then that these images have a monopoly on targets? Do they have an inherent property which makes then suited to their function?

6.3.1 Aim

Determine if target type and movement affect a subject's ability to maintain steady fixation during a 60s time interval.

To test for significant differences in the mean standard deviation in eye rotation a null hypothesis and alternative hypothesis are formulated.

6.3.1.1 Null Hypothesis

$H_o = u_1 = u_2 = u_3...$

The null hypothesis states there is no significant difference in the mean standard deviation in eye rotation (u) between targets (denoted by the subtext $_n$).

6.3.1.2 Alternative Hypothesis

$H_a = u_1 \neq u_2 \neq u_3...$

The alternative hypothesis states that there is a statistically significant difference in eye rotation between targets.

6.3.2 Method

Translational and rotational eye movements were measured using the JEDEye tracking system which recorded the eye's movement for a 60s time period. In total 10 visual targets were used, 5 targets for target type, 4 targets for target movement and a blank control target consisting of a blank screen.

In total 20 subjects (mean age - 29, SD +/- 10, age range 22 - 62) were asked to look at 10 different targets for 60s at a time, the data from 4 subjects had to be rejected due to too frequent blinking or eye lash occlusion of the Purkinje Images, the frequency of blinking observed in these subjects was significantly higher than in other subjects thus led to a decrease in data, consequently the results from these subjects were incomparable to other subjects. A time period of 60s was chosen as this would allow adequate time for an optometrist to perform a single diagnostic measurement on a number of devices. The purpose of the experiment was explained to each of the subjects. The subjects were told to look at the centre of each target and maintain this fixation as best they could. Subjects were allowed to blink at their convenience. In all cases the subject's right eye was recorded. The targets were presented randomly. Subjects were notified when the recording was about to begin and when it ended, after which they were allowed to sit back from the apparatus and have a short break. All 10 recordings for each subject were recorded in the same session. The recordings were taken in a darkened room with only the subject and the examiner present. Experiments were performed at random times throughout the day.

Exclusion Criteria

To ensure normality, subjects were only considered for the study if they passed the following criteria:

- No underlying eye conditions, such as dry eye or kerataconus.
- Do not wear contact lenses.
- Could distinguish between 2 targets to be used in the study.
- Subjects who had their vision corrected with glasses were allowed also long as they could see the target without their glasses.

6.3.2.1 Target Type

Figure 6.3: The types of targets used in the target type experiment (actual size)

Figure 6.3 shows the types of targets used in the target type experiment, an additional blank target was also used as the control. From left to right, Bullseye, Crosshairs, Spot, Hypno-Wheel and Maltese Cross. All targets have an angular subtense of $200'$ relative to the subject. People with 20/20 vision can resolve angular subtenses of $5'$, thus these targets are comfortabley viewable for subjects.

6.3.2.2 Target Movement

A series of targets were used to assess the subjects response to target movement; including a rotating Hypno-Wheel, a Flashing and Rotating Maltese Cross and a Pulsating Dot.

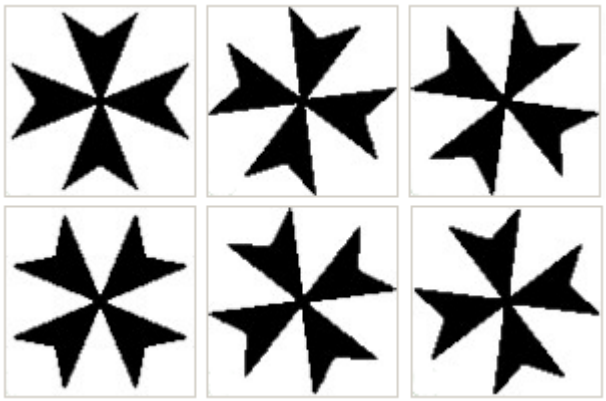

Figure 6.4: Frames used for the Rotating Maltese Cross, frames are cycled through at a rate of 2 Hz.

Figure 6.4 shows the individual frames used for the Rotating Maltese Cross. Additional frames for the Hypno-Wheel and the Pulsating Dot are included in Appendix E, frames were cycled through at a rate of 2 Hz.

6.3.2.3 Data Processing

The entire set of data was processed using an algorithm written in the National Instrument's LabVIEW programming environment. The algorithm detects, isolates and extracts the calibrated coordinates of the Purkinje Images. Rotation was then calculated using the JEDEye principle (Section 5.4.1) in Matlab. All acquired data was normalised to the first rotation value in the relevant data set. The standard deviation in eye rotation was then calculated, thus giving the average variation in eye rotation when looking at the relevant target. All statistical analysis was performed with the statistical analysis software package SPSS (IBM, New York, USA).

6.3.2.4 Statistical Analysis

To test the significance of the difference in mean standard deviation values, a repeated measures ANOVA was performed. The ANOVA [151] is similar to a paired t-test, however it allows comparison of multiple groups of data rather than just two. The advantage in using the repeated measures version of the ANOVA is that a within-subject comparison can be performed, thus negating random variance introduced by subject comparisons.

It is worth noting that the ANOVA, if there are significant differences, will not indicate where the significant differences lie. To do this, post-hoc tests should be performed to find the exact pair which the significant difference has emanated from. In this case, where significant differences are found, pairwise comparisons of all the potential pairs are performed. The pairwise comparisons take the form of paired t-tests in which every possible pair is analysed.

For valid results in tests of this nature it suggested a good sample size to aim for one which will result in 15 degrees of freedom (df) [152] for each target group. In statistical terms the degrees of freedom refers to the total number of independent scores or values, obtained experimentally, used to calculate a particular parameter. The total degrees of freedom for any experiment is the total number of independent scores minus the total amount of intermediate statistics used to calculate the specified parameter. In the case of this experiment a total of 20 subjects were used for each target, however 4 were rejected thus leaving 16 independent measures of eye movement. The degrees of freedom for each target group is then 16-1, as the sample mean is used to estimate the opulation mean.

For the target type set a single factor repeated measures ANOVA was performed to test if there was a statistically significant difference between the mean standard deviation in eye rotation.

The repeated measures ANOVA calculation makes an assumption of sphericity. Sphericity is defined as the equality of variances between each factor of the repeated measures ANOVA. For the repeated measures analysis the variance between each target must be the same; however, this assumption can be tested with the Mauchly's test and corrected

for if violated. The test determines if there is significant difference in the variances of each factor level.

All significance testing is performed to a 0.05 confidence level.

6.3.2.5 Additional Calculations

As the JEDEye system can monitor head movement as well as eye movement the total translational movement of the eye was decomposed into two factors: translational movement due to the head and translational movement due to eye rotation. Lateral head movement and eye rotation are not similar quantities, thus eye rotation was converted into lateral movement using an approximation of the distance between the corneal apex and the eye's centre of rotation. Analysis of the data consisted of the total translational movement made up of the percentage induced by eye rotation and the percentage induced by head movement.

6.3.3 Results

6.3.3.1 Target Type

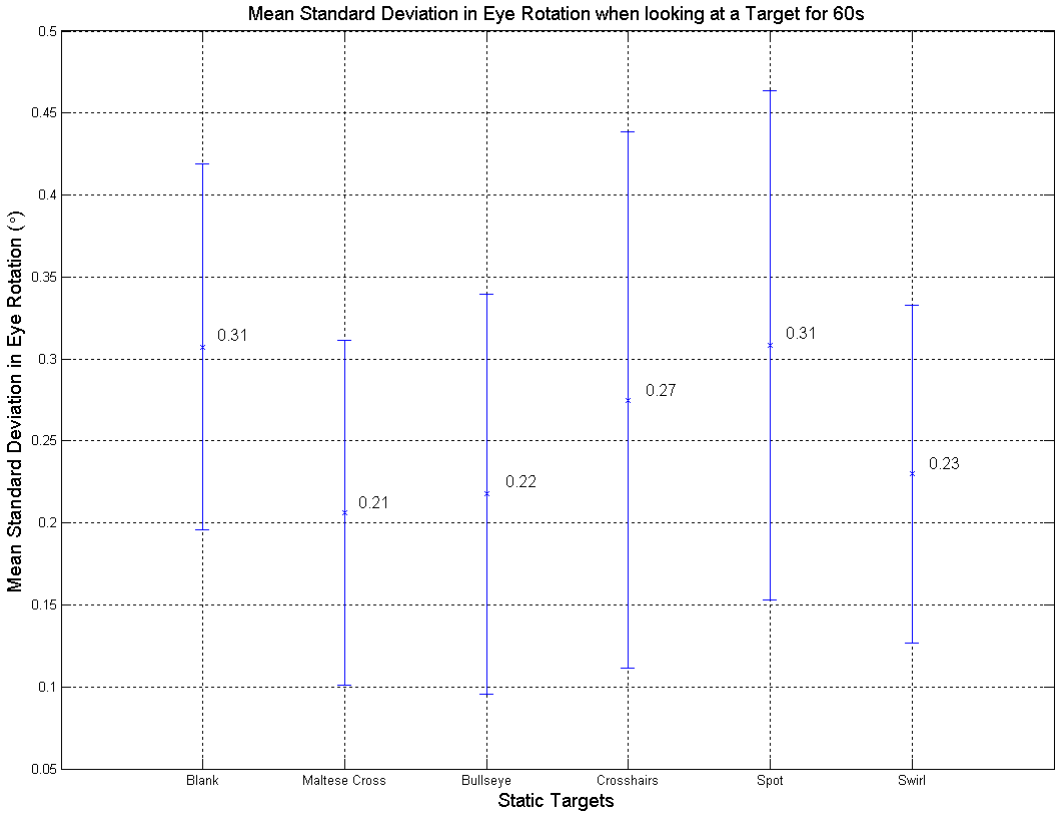

Figure 6.5: Mean standard deviation in eye rotation when regarding 5 static targets independently for 60s. The error bars indicate 1 standard deviation from the mean.

Figure 6.5 shows the mean standard deviation in eye rotation when looking at 5 different targets and a blank control. All targets, apart from the Spot (0.31°), showed a decrease in eye rotation when compared with the Blank control target. The smallest deviation in eye rotation is found in the Maltese Cross (0.21°), followed closely by the Bullseye (0.22°).

6.3.3.2 Statistical Analysis

Table 6.1 shows the sphericity test on this data set. This is to determine if adjustment to the significance level is required for the repeated measures ANOVA test. The test is performed to a confidence level of 0.05. The test suggests that sphericity can be assumed as there is no significant differences between the variances of each factor level.

Data Set	Mauchly's W	df	Significance
Target Type	.254	14	0.217

Table 6.1: Mauchly's test of sphericity for target type.

Table 6.2 shows the repeated measures ANOVA performed on the target type data set. The results suggests that there is significant difference in the means.

Source	Type III Sum of Squares	df	Mean Square	F	Significance
Target Type	0.166	5	0.033	2.694	0.027

Table 6.2: Repeated measures ANOVA test for target type.

Table 6.3 is a selection of pairwise comparisons showing significant differences found between each of the targets. Only two of the targets (Maltese Cross and Bullseye) show significant differences from the Blank control, these two targets also show significant differences from the Spot.

Target 1	Target 2	Mean Difference	Std. Error	Significance
Control	Maltese Cross	0.101	0.032	0.006
Control	Bullseye	0.09	0.035	0.023
Maltese Cross	Spot	-0.102	0.037	0.015
Bullseye	Spot	-0.091	0.041	0.044

Table 6.3: Selection of pairwise comparisons taken from the target type data set.

6.3.4 Target Movement

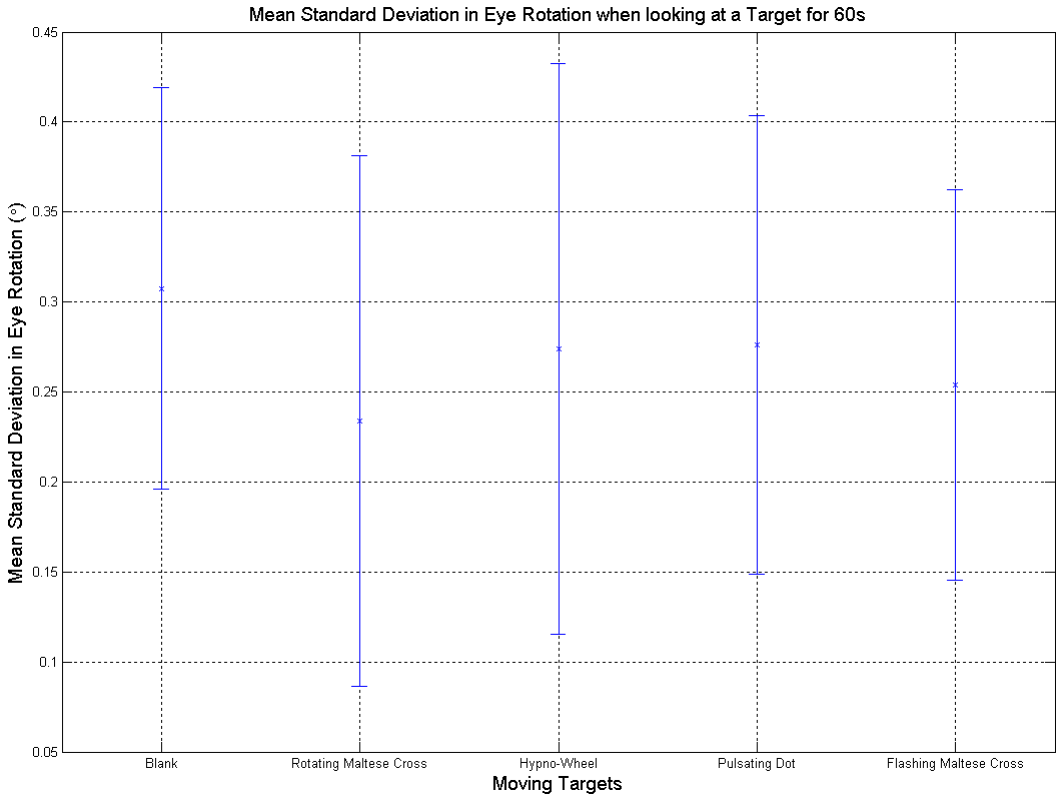

Figure 6.6: Mean standard deviation in eye rotation when regarding 4 moving targets independently for 60s. The error bars indicate 1 standard deviation from the mean.

Figure 6.6 shows the mean standard deviation in eye rotation when looking at 4 different moving targets and a blank control. All targets show a decrease in eye rotation when compared with the Blank control target. The smallest deviation in eye rotation is found in the Rotating Maltese Cross (0.24°).

6.3.4.1 Statistical Analysis

Table 6.4 shows the spherity test on this set of data, the results suggest sphericity can be assumed.

Data Set	Mauchly's W	df	Significance
Moving Target	.363	9	0.140

Table 6.4: Mauchly's test of sphericity for moving targets.

Table 6.5 shows the repeated measures ANOVA performed on the moving target data set. The results suggests that there is no significant difference in the means.

Source	Type III Sum of Squares	df	Mean Square	F	Significance
Moving Target	0.048	4	0.012	0.994	.418

Table 6.5: Repeated measures ANOVA test for moving targets.

6.3.4.2 Target Type and Movement Comparison

Table 6.6 shows a selection of pairwise statistics for the comparison on specific target means. Of interest is the difference between the stationary targets and the moving target counterparts, namely the Maltese Cross and its rotating and flashing counterparts. The Swirl, and its moving counterpart, the Hypno-Wheel are also included. The results suggest that there is no significant difference in average eye rotation when comparing a static target to its moving counterpart.

Target 1	Target 2	Difference	Std. Error	Significance
Maltese Cross	Rotating Maltese Cross	0.027	0.037	0.469
Maltese Cross	Flashing Maltese Cross	-0.043	0.044	0.350
Swirl	Hypno-Wheel	-0.006	0.036	0.878

Table 6.6: Selection of pairwise comparisons taken from the entire target data set.

6.3.4.3 Translational Movement

Target Type

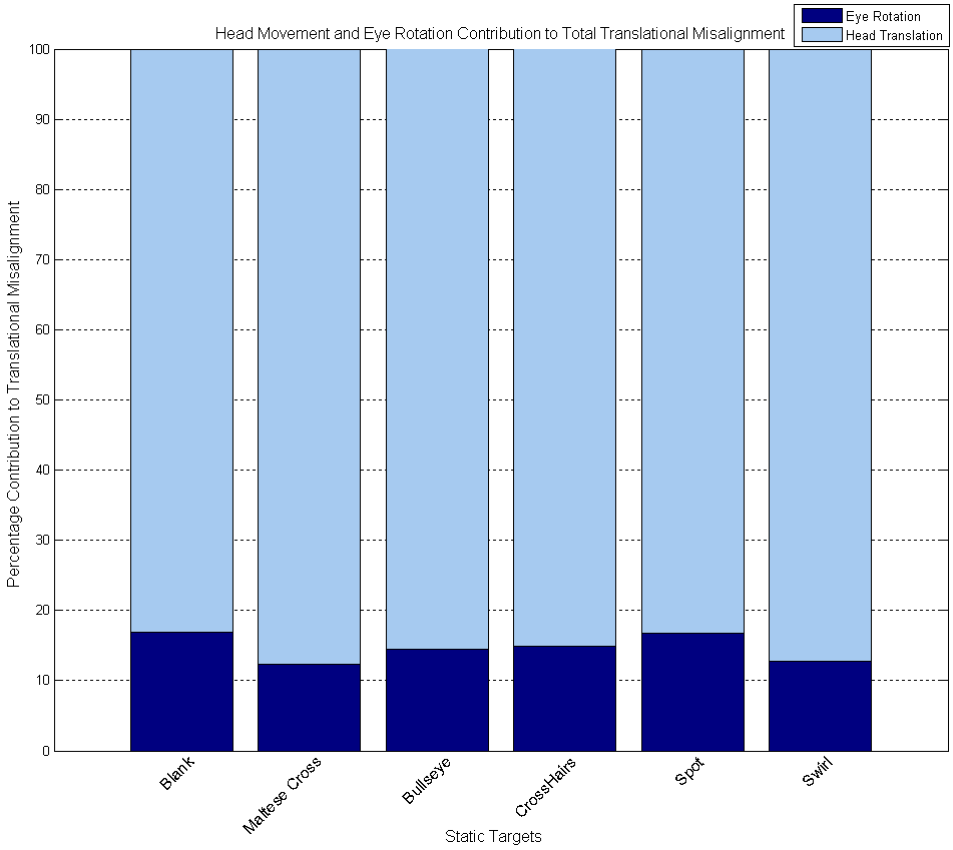

Figure 6.7: Translation percentages, target type.

Figure6.7 describes the total percentage of eye translation as caused by eye rotation and head movement. On average the results suggest that 79% of eye translation can be attributed to head movement.

Target Movement

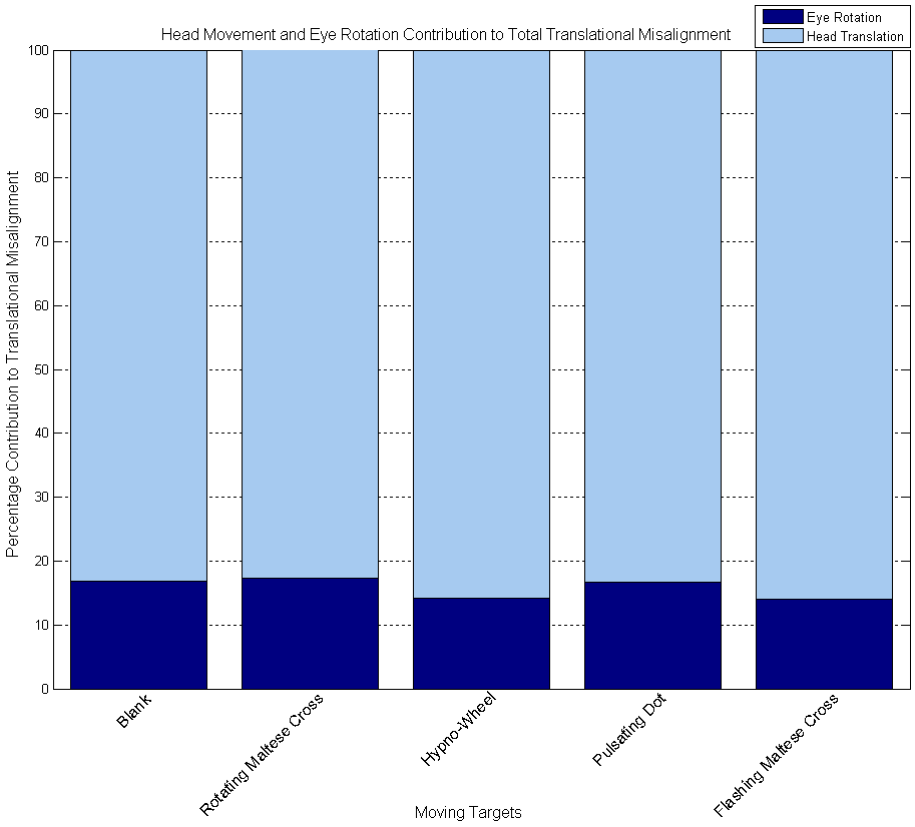

Figure 6.8: Translation percentages, target movement.

Figure 6.8 describes the total percentage of eye translation as caused by eye rotation and head movement. On average the results suggest that 79% of eye translation can be attributed to head movement.

6.3.5 Discussion

The results suggest eye movement amplitudes similar to microsaccades amplitudes found in Rolf et al [61] and Martinez-Conde et al [55], this suggests that the eye rotations induced during fixation were microsaccades and potentially form the source of variation.

The results from the target type data set suggest that there are significant differences between the induction of eye rotation and target type. Not only is the Maltese Cross and Bullseye significantly different from the Blank control, they are significantly different from other static targets such as the Spot and Swirl. The Maltese Cross is a popular target in ophthalmic accommodative research where the target is particularly suited to instigated the accommodation response and the results suggest valid reasons for this. The difference between static targets may arise due to the construction of the target. Both the Maltese Cross and the Bulleye have a definitive central point, something which is not clear in the Swirl and absent in the Spot. Contrary to this, the Crosshairs has a similar definitive central point; however, on average, it did not reduce eye movement as much as other targets.

The analysis of all the targets allowed some direct comparisons to be made between static targets and their moving counterparts. Specifically, this involved the Maltese Cross and the Swirl. The Maltese Cross had two moving counterparts, the Rotating Maltese Cross and the Flashing Maltese Cross. All the Cross targets were of the same area; however, the introduction of movement to the target did nothing to reduce eye rotation. The same outcome emerged from the Swirl and its Hypno-Wheel counterpart. It is important to remember that there were significant differences between the Maltese Cross and the Swirl, this backs up the hypothesis that target type does play a part in the reduction of eye rotation as this difference is maintained in the moving of these targets.

The question was posed in the introduction whether the introduction of movement round the periphery of the target centre would be therapeutic to the eye or whether it would be a source of distraction? The results offer no definite conclusion to this; in general the static targets induced the least amount of eye rotation, only the Rotating Maltese Cross delivered comparative results. The reason for this, as already suggested might be more to do with the type of target rather than its rotation.

It is important to remember when considering the results that the experiment investigated a limited range of each parameter. This is particularly significant in the movement parameter. There are a vast number of permutations to moving within a target, not only in the type of movement but also in the frequency. It may well be the case that a different speed of movement would have induced differing results; however, it is impossible to state this without investigating a larger range. What the results do allow discussion of is the comparison between movement and static targets, in which case the result suggest that static targets offer a greater reduction in eye rotation.

The use of Purkinje Image recording allowed the quantification of not only eye rotation but also of head translation. This allows total eye translation to be split into its eye and

head components. The results indicate that head movement provides the larger source of translation. This might be down to general discomfort when performing the tests, however as the chin-rest is standard piece ophthalmic equipment it would be reasonable to assume that the amount of comfort is similar to other ophthalmic conditions.

While the investigation aimed to determine the particular eye movements responsible for misalignment the results suggest that it is in fact head movement which is the major contributor to misalignment. This reiterates, and indeed increases, the importance of the alignment system's sensitivity to head movement.

6.3.6 Conclusion

Significant differences in eye rotation were found when subjects fixated on a range of static targets. Specifically, the Maltese Cross and the Bullseye induced less rotation (0.21°and 0.22°respectively) when compared to other targets. The remaining static targets showed no significant difference when compared to the Blank control (0.31°). The moving targets showed no significant differences in induced eye movement within their data set, which included the Blank control.

The entire range of targets was compared and analysed after significant differences were found between the means. Again the Maltese Cross and the Bulleye had significant differences from the control. The comparison of all targets allowed the direct comparison of the static targets with their moving counterparts. In both cases, the Maltese Cross and Swirl displayed no significant difference between them and their moving counterparts (Rotating Maltese Cross, Flashing Maltese Cross and Hypno-Wheel).

The results also suggest that the main contributor to translational eye movement is head movement, 79% of the total translational movement was attributed to the head.

6.4 Target Size

Target size is a logical target parameter worthy of investigation. If a target provokes more attention over a larger area then the eye is compelled to move through greater distances to analyse the image. However, when a subject is directed to look at the centre of a target it is debatable whether the subject will be able to ignore the outskirts of the image. In this case, larger movement required to search larger images would be suppressed. It is then important in the quest for an optimum fixation target that the relationship between target size and eye movement is investigated.

6.4.1 Aim

Determine if target size effects a subject's ability to maintain steady fixation during a 60s time interval.

Hypothesises are formulated as in section 6.3.1

6.4.1.1 Null Hypothesis

$H_o = u_1 = u_2 = u_3...$

6.4.1.2 Alternative Hypothesis

$H_a = u_1 \neq u_2 \neq u_3...$

6.4.2 Method

Translational and rotational eye movements were measured using a JEDEye tracking system which recorded the eye's movement for a 60s time period. In total 6 visual targets of different size were used.

In total 20 subjects (mean age - 29, SD +/- 10, age range 22 - 62) were asked to look at 6 different targets for 60s at a time, the data from 4 subjects had to be rejected due to too frequent blinking or eye lash occlusion of the Purkinje Images. The purpose of the experiment was explained to each of the subjects. The subjects were told to look at the centre of each target and maintain this fixation as best they could. The targets were presented randomly. Subjects were notified when the recording was about to begin and when it ended, after which they were allowed to sit back from the apparatus and have a short break. All 6 recordings for each subject were recorded in the same session. The recordings were taken in a darkened room with only the subject and the examiner present. Experiments were performed at random times throughout the day.

Exclusion Criteria

To ensure normality, subjects were only considered for the study if they passed the following criteria:

- No underlying eye conditions, such as dry eye or kerataconus.
- Do not wear contact lenses.

- Could distinguish between 2 targets to be used in the study.
- Subjects who had their vision corrected with glasses were allowed also long as they could see the target without their glasses.

6.4.2.1 Target Size

Figure 6.9: Dot size targets used for the target size experiment (actual size)

Figure 6.9 shows the different target sizes used for the target size experiment, from left to write Dot(200′), Dot(100′), Dot(50′), Dot(25′), Dot(13′) and Dot(6′), where the bracketed numbers refers to the angular subtense each target has to the eye in minutes of arc. [1]

6.4.2.2 Data Processing

The entire set of data was processed using an algorithm written in the National Instrument's LabVIEW programming environment. The algorithm detects, isolates and extracts the calibrated coordinates of the Purkinje Images. Rotation was then calculated using the JEDEye principle in Matlab. All acquired data was normalised to the first rotation value in the relevant data set. The standard deviation in eye rotation was then calculated, thus giving the average variation in eye rotation when looking at the relevant target. All statistical analysis was performed with the statistical analysis software package SPSS.

6.4.2.3 Statistical Analysis

A total of 20 subjects were used for each target, however 4 were rejected thus leaving 16. The degrees of freedom for the subplot is then 16-1, fulfilling the sample size requirement.

For the target type set a single factor repeated measures ANOVA was performed to test if there was a statistically significant difference between the mean standard deviation in eye rotation for each target.

To test the assumption of sphericity a Mauchly's test is performed on the data.

All significance testing is performed to a 0.05 confidence level.

6.4.2.4 Additional Calculations

The total amount of eye translation was recorded as percentages of eye translation caused by head movement and eye rotation.

In addition to this the correlation between fixation deviation and target size can be correlated to investigate the significance of the relationship. To perform this analysis the Pearson's correlation coefficient was calculated.

[1] For reference people with 20/20 vision can resolve angular subtenses of 5′

6.4.3 Results

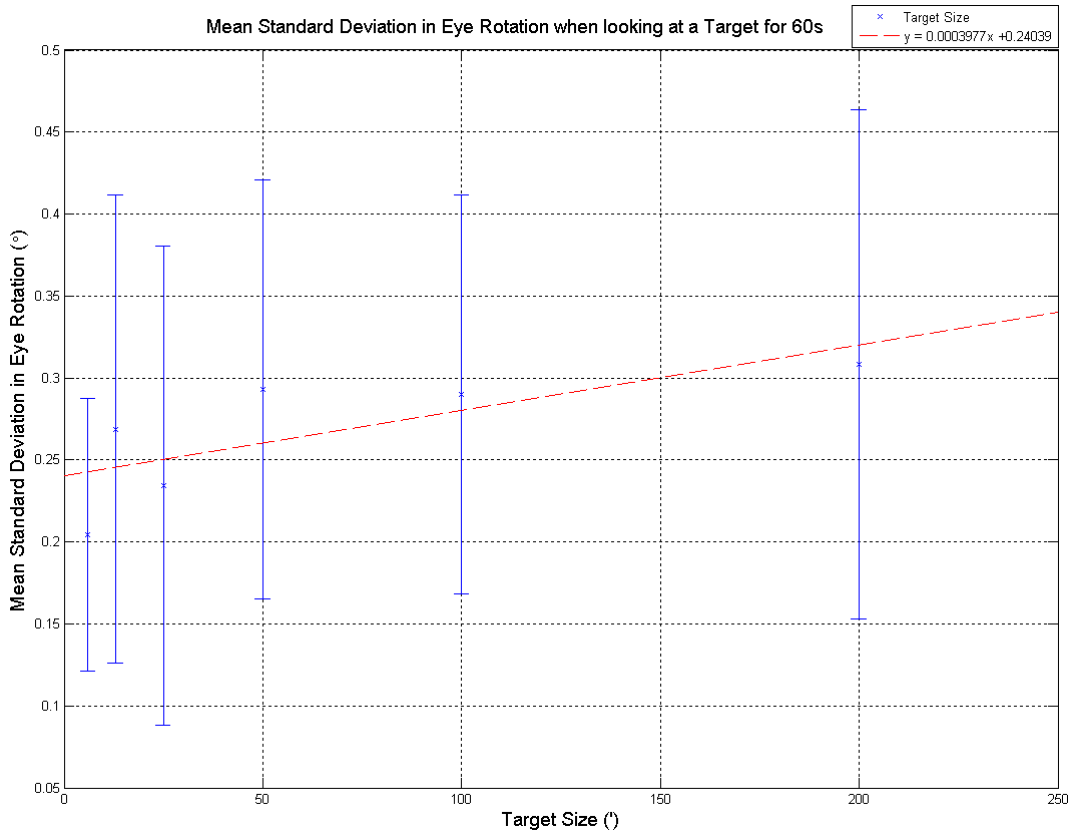

Figure 6.10: Mean standard deviation in eye rotation when regarding 6 targets of different size independently for 60s. The error bars indicate 1 standard deviation from the mean.

Figure 6.10 shows the mean standard deviation in eye rotation when looking at 6 targets differing in size. Dot(6′) induces the smallest amount of eye rotation (0.20°) while Dot(200′) induces the most (0.31°).

6.4.3.1 Statistical Analysis

As the target size fixation parameter is the only quantitative parameter, it allows the correlation between target size and average fixation distribution to be analysed. To statistically test whether fixation distribution is correlated to target size the Pearsons' correlation coefficient was calculated and tested at the 0.05 significance level.

$H_o : r = 0$

$H_a : r \neq 0$

Table 6.7 shows the calculated Pearson's correlation coefficient and the corresponding p-value. The correlation coefficient suggests a slight correlation; however, the p-value suggests that this relationship is not significant.

Pearson's Correlation Coefficient (r)	p-value
0.74	0.09

Table 6.7: Target size correlation analysis.

Table 6.8 shows the sphericity test on the target size data set, the results suggest sphericity can be assumed.

Data Set	Mauchly's W	df	Significance
Size Targets	.370	14	0.533

Table 6.8: Mauchly's test of sphericity for size targets.

Table 6.9 shows the repeated measures ANOVA performed on the target size data set. The results suggests that there is no significant difference in the means.

Source	Type III Sum of Squares	df	Mean Square	F	Significance
Size Targets	0.127	5	0.025	2.183	.065

Table 6.9: Repeated ANOVA test for size targets.

6.4.3.2 Translation

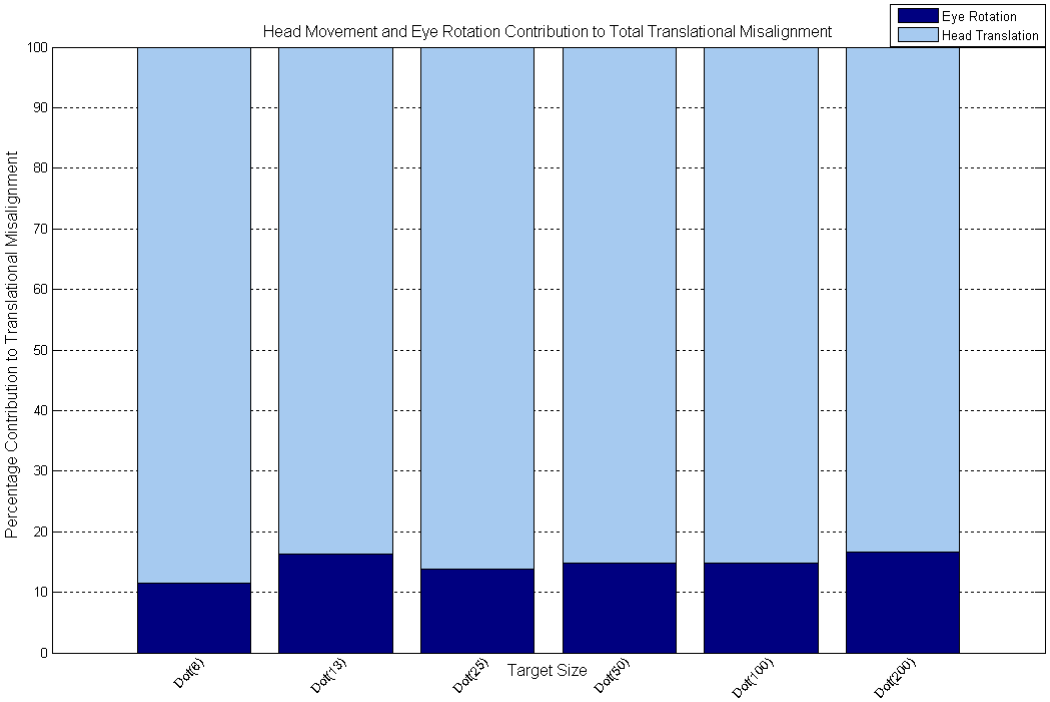

Figure 6.11: Percentage translation, size targets.

Figure 6.11 describes the total percentage of eye translation as caused by eye rotation and head movement. On average the results suggest that 86% of eye translation can be attributed to head movement.

6.4.4 Discussion

As with the target type and movement data (section 6.3), set the results suggest eye movement amplitudes similar to microsaccade amplitudes found in Rolf et al [61] and Martinez-Conde et al [55].

Target size is assumed to have a strong correlation with the reduction of eye movement, however the results suggest no significant correlation, and no significant differences between target sizes. Contrary to this, the target size which invoked the least amount of eye movement was the smallest target.

The experimental results from the target type and movement investigation alluded to the subject's ability to ignore the periphery of the image and highlighted the importance of the central construction of the image; specifically, the presence of a definitive central point. This could then be the reason why the smallest fixation point induced the smallest amount of eye movement. Interestingly, in comparison with the Maltese Cross (0.21°) and the Bullseye (0.22°) the Dot(6′) (0.20°) target showed a reduction in eye movement.

However, the fact that no significant differences were found between the target sizes brings this hypothesis into question. As target size increases, the absence of a central fixation point becomes more apparent, yet the results suggest no significant difference between targets.

The lack of variation potentially stems from the experimental procedure rather than the targets themselves. Each subject was requested to maintain fixation on the central portion of the image. While this instruction may have unintentionally biased the results it still allows interesting discussion on the mechanism of fixation. In attempting to maintain fixation on the central part of the target the subject was able to suppress movements of the eye to the periphery of the larger targets.

The consequence of this, in regards to the optimum alignment target, is that the periphery of the target goes largely unnoticed. This is due to the subjects ability to suppress larger eye movements when instructed to do so.

It is also worth noting the resolution of the eye; patients and subjects who have 20/20 vision can resolve images with angular subtenses of 5'. The majority of targets used within these studies made angular subtenses of approximately 200' with the subject, thus for the majority of subjects the size of the target was well within their visual capabilities. The hypothesis that the periphery of the target goes largely unnoticed ,and that it is in fact the centre part of the target which is of importance, is then not without evidence. The target size study attempted to investigate the relationship between visual acuity and fixation, however, a significant relationship was not found. It may be the case that a target size study using the Maltese Cross may suggest different results.

Similarly to the previous study on target type and movement the results suggest a large component of misalignment caused by the head. This reiterates the importance in the requirement of the alignment system to monitor and compensate for head movement.

6.4.5 Conclusion

The purpose of the study was to determine if target size had an impact on the amount of eye movement performed during a 60 s period. The results suggest that within the target size range there was no significant difference between target sizes. However, the best performing target, Dot(6') reduced average eye movement to 0.20°, this amount is smaller than the Maltese Cross (0.21°) and Bulleye (0.22°) results found in the target type/movement experiment.

There was also little correlation (0.74) found between target size and average eye rotation.

6.5 Target Colour

Colour vision is an interesting aspect of sight, what we perceive as colour is made visible to use by the photosensitive cone cells on the retina. There are three types of cone cell, each one responsible for detecting either long, middle or short wavelengths of light [7]. The peak wavelength for eye sensitivity is 555nm, which we perceive as green; however, in darker conditions retinal sensitivity changes to rod vision, these rod cells are more sensitive to shorter wavelengths of light [7]. Spectral sensitivity is also dependent on age, sensitivity to blue light decreases with age as a results of the wavelengths increasing absorption in the eye's lens [7]. As the eye is stimulated differently by varying colours it has the potential to behave differently as a result of the colour it observes. Together with the psychological aspect of colour and its affect on mood, the effect of colour on the eye's stability is an interesting and essential study.

Previous studies into colour undertaken in the 1960s have suggested that colour does have a significant impact on the eye's movement. Fender [153] found differences in fixational movements as a result of colour. Steinman [57] found that red invoked the least fixational eye movement while white caused the most; the difference was found to be 0.07°.

The aim of this experiment then is to investigate the affect of colour on the amount of eye movement caused during fixation. If significant differences are found then coloured targets can be used to reduce eye movement during diagnostic procedures, if not, the coloured target parameter can be ignored.

6.5.1 Aim

Determine the effect of colour on average eye rotation during a 60s time period.

Hypothesises are formulated as in section 6.3.1

6.5.2 Null Hypothesis

Ho = $u_1 = u_2 = u_3...$

6.5.3 Alternative Hypothesis

Ha= $u_1 \neq u_2 \neq u_3...$

6.5.4 Method

Translational and rotational eye movements were measured using the JEDEye tracking system which recorded the eye's movement for a 60s time period. In total 7 visual targets were used consisting of 1 blank control target and white, black, blue, green, red and yellow coloured targets.

In total 18 subjects (mean age - 30, SD +/- 11, age range 22 - 63) were asked to look at 10 different targets for 60s at a time, the data from 2 subjects had to be rejected due to too frequent blinking or eye lash occlusion of the Purkinje Images. The purpose of the experiment was explained to each of the subjects. The subjects were told to look at the centre of each target and maintain this fixation as best they could. The targets were presented randomly. Subjects were notified when the recording was about to begin and when it ended, after which they were allowed to sit back from the apparatus and have a short break. All 7 recordings for each subject were recorded in the same session. The recordings were taken in a darkened room with only the subject and the examiner present. Experiments were performed at random times throughout the day.

Exclusion Criteria

To ensure normality, subjects were only considered for the study if they passed the following criteria:

- No underlying eye conditions, such as dry eye or kerataconus.
- Do not wear contact lenses.
- Could distinguish between 2 targets to be used in the study.
- Subjects who had their vision corrected with glasses were allowed also long as they could see the target without their glasses.

6.5.4.1 Colour Targets

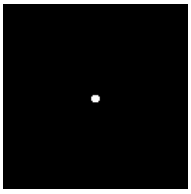

Figure 6.12: Target used in the colour fixation experiment.

Figure 6.12 is representative of the coloured targets used in the experiment, all had a black background with the exception of the black target which had a white background. The colours used in the targets were: black, blue, green, red, white and yellow.

6.5.4.2 Data Processing

The entire set of data was processed using an algorithm written in the National Instrument's LabVIEW programming environment. The algorithm detects, isolates and extracts the calibrated coordinates of the Purkinje Images. Rotation was then calculated using the JEDEye principle in Matlab. All acquired data was normalised to the first rotation value in the relevant data set. The standard deviation in eye rotation was then calculated, thus giving the average variation in eye rotation when looking at the relevant target. All statistical analysis was performed with the statistical analysis software package SPSS.

6.5.4.3 Statistical Analysis

A total of 18 subjects were used for each target, however 2 were rejected thus leaving 16. The degrees of freedom for the subplot is then 16-1, fulfilling the sample size requirement.

For the coloured target set a single factor repeated measures ANOVA was performed to test if there was a statistically significant difference between the mean standard deviation in eye rotation for each target.

To test the assumption of sphericity a Mauchly's test is performed on the data.

All significance testing is performed to a 0.05 confidence level.

6.5.4.4 Additional Calculations

The total amount of eye translation was recorded as percentages of eye translation caused by head movement and eye rotation.

6.5.5 Results

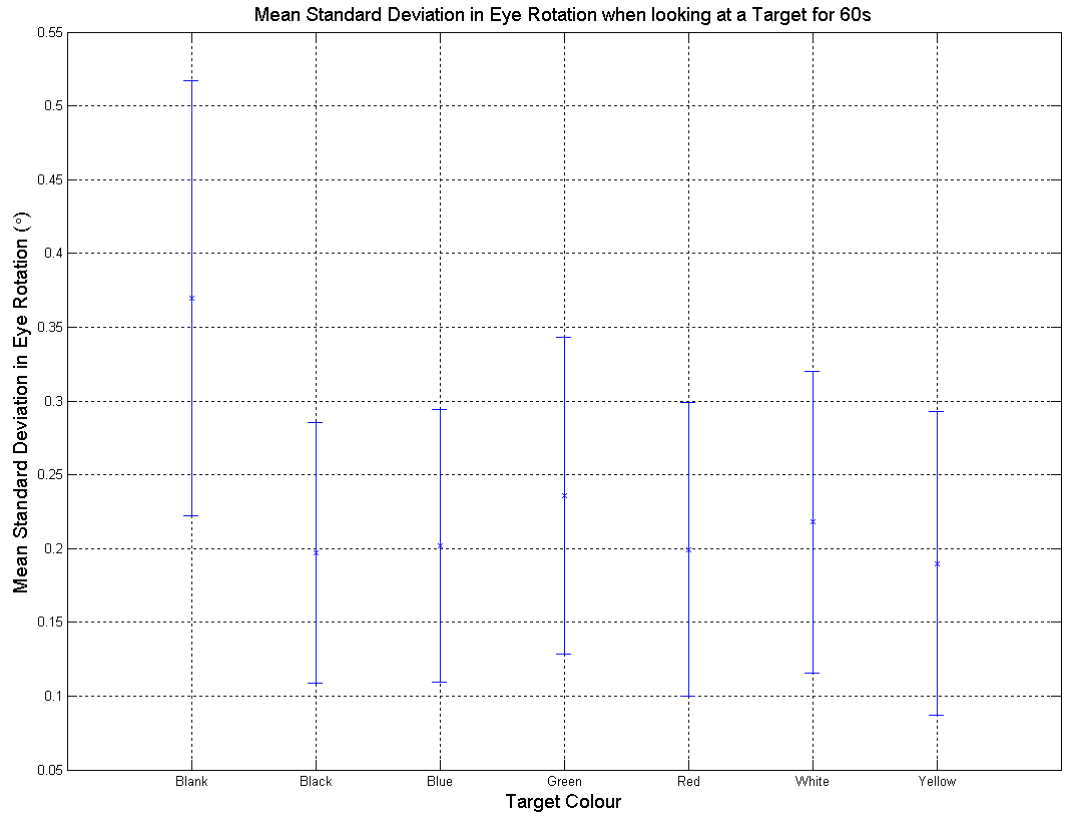

Figure 6.13: Mean standard error in eye rotation when regarding the coloured targets independently for 60s. The error bars indicate the standard error in the means.

Figure 6.13 shows the mean standard error in eye rotation when regarding each of the 7 targets independently. All coloured targets suggest a reduction in eye rotation when compared to the Blank (0.37°) control target. The smallest deviation in eye rotation was performed when subjects were required to look at the Yellow target (0.19°). However, all the coloured targets Black (0.20°), Blue (0.20°), Green (0.24°), Red (0.20°), White (0.22°) and Yellow (0.19°) were within a 0.05°range.

6.5.5.1 Statistical Analysis

Table 6.10 shows the spherity test on this set of data, the results suggest sphericity cannot be assumed. In order to correct the significance value the Greenhouse - Geisser calculation is performed.

Data Set	Mauchly's W	df	Significance
Colour Targets	0.014	20	0.000

Table 6.10: Mauchly's test of sphericity for data set.

Table 6.11 shows the repeated measures ANOVA performed on the coloured target data set. The results suggests that there is significant difference in the target means. However, closer inspection of the results suggests that this significant difference is due to the control.

Source	Type III Sum of Squares	df	Mean Square	F	Significance
Colour Targets	0.386	2.92	0.132	9.754	0.000

Table 6.11: Repeated ANOVA for data set with control.

Table 6.12 shows the repeated measures ANOVA duplicated, this time excluding the control. The results suggest that there is no significant difference in the reduction of eye rotation as a result of target colour.

Source	Type III Sum of Squares	df	Mean Square	F	Significance
Colour Targets	0.023	2.77	0.008	1.003	0.396

Table 6.12: Repeated measures ANOVA for data set without control.

6.5.5.2 Translation Movement

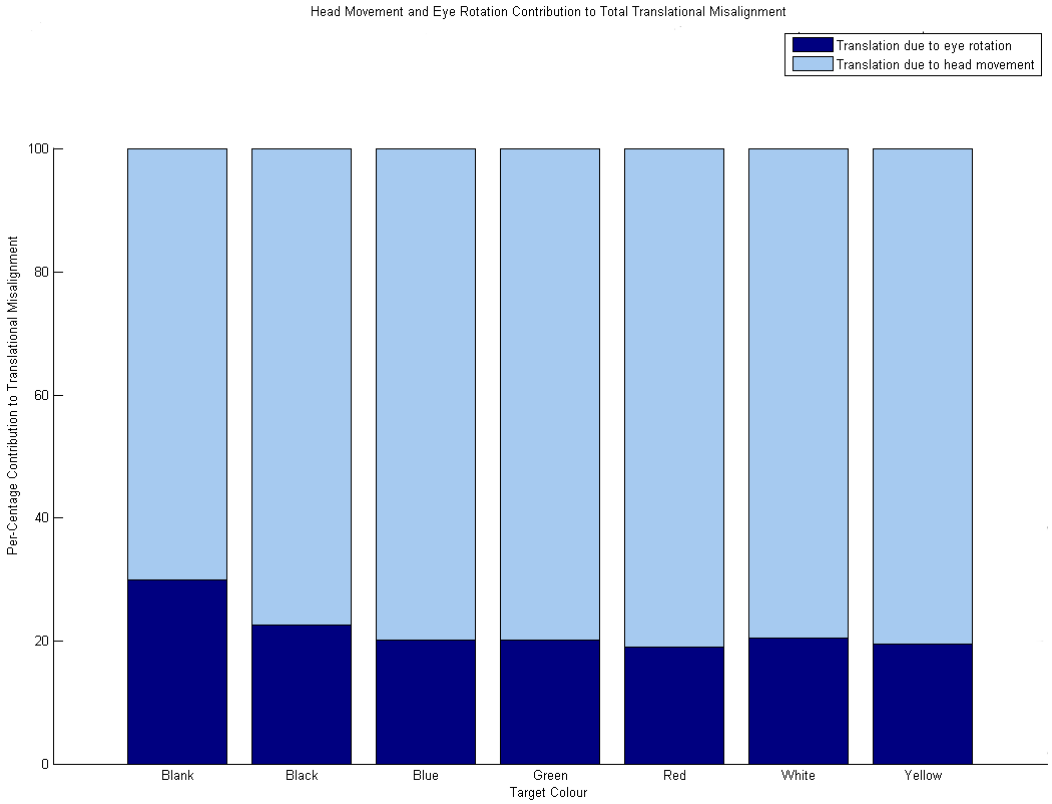

Figure 6.14: Percentage translational movement as performed by the head and the eye.

Figure 6.14 demonstrates the components of translational movements performed while staring at the targets. The information is represented as the total translation made up of percentages of the two contributing factors: eye rotation and head movement. The average contribution of eye rotation to translational movement was 22% where as the head, on average, contributes 78% to translation.

6.5.6 Discussion

The statistical analysis of the results suggest that there is no significant difference in the mean standard standard deviation in eye rotation when regarding targets of differing colour. Average eye movements for all coloured targets fell within a 0.05° range, previous studies reporting differences of 0.07° [149] have found this to be significant. The only significant differences obtained in this experiment was due to the difference from the control.

The are several potential reasons for these results, the most likely of them is attributed to target size. In order to isolate the colour variable for investigation, the target size and shape had to remain constant throughout the experiment. The target shape and size chosen was determined to invoke the smallest amount of eye movement in previous studies. It was then hypothesised that the combination of this target with an optimum colour would further reduce average eye movement; however, the results show this not to be the case, at least in the colour range studied.

The colour variable itself is an ambiguous quantity, it was noted at several points in the experiment that the subject disagreed with the target colour suggested. It is unlikely that the question of colour perception offset the results, as no significant differences were found between the Black target and the other coloured targets within the subject. The Black target is essentially no colour therefore all subjects would have perceived it the same.

The results also suggest that optical factors such as chromatic aberration had no consequence on the amplitude of average eye rotation when regarding each of the colours. The differences in refraction through the eye due to the wavelength of light results in the failure to focus all colours on a single focal plane. This would not have been problem for colours which match the peak sensitivity for either of the three cone cells. However, eye instability may have been induced as a result of colours which stimulated all three of the cone cells.

Analysis on the translational contribution to eye movement suggests that 78% can be attributed to head movement, this is in agreement with previous studies.

Within the range of colours investigated there was no significant difference between them. The results are attributed to the target size limiting the average eye movement, suggesting that the type and size parameters are more important in defining an optimum fixation target. Investigations performed with larger targets over a larger range of colours have the potential to allow significant differences to be demonstrated; however, it is unlikely that they would provoke smaller average rotations than found in this study, thus serving no advantage.

6.5.7 Conclusion

The aim of the experiment was to determine the effect of target colour on the average amplitude of eye rotation. Within the range of colours investigated there was no significant difference in the reduction of eye rotation. The lowest average rotation was obtained with the Yellow target (0.19°) while the highest average rotation was achieved with the Green target (0.24°). Average rotations for all targets fell within a 0.05° range, previous studies have suggested that a 0.07° difference is statistically significant; however, it is not the case in this study.

It is then concluded that the target colour parameter is not as significant as type and size in the definition of an optimum fixation target, thus this parameter can be ignored.

6.6 Concentration

There is currently debate on the role of microsaccades and the mechanisms by which they are inhibited. Their primary role is thought to aid fixation and to prevent the occurrence of image fading in the periphery of the subjects field of view [54, 55], a characteristic of vision known as the Troxler effect [56]. However, there have been suggestions that during high concentration tasks such as threading a needle and shooting microsaccades are suppressed to aid in the completion of the task [154, 155]. There have been results contradicting this with an increased number of microsaccades found in the performance of high-acuity visual tasks [156]. Other results have shown that microsaccades can be suppressed even with a simple change of instruction when fixating on the target [57] (instruction was changed from "fixate" to "hold"). Differences in the results have been attributed to the duration of the experiment, with microsaccades said to aid fixation initially, while introducing error the longer the experiment goes on [157].

Interestingly, there are a number of alignment techniques which aim to keep the eye still by asking them to look at blurred targets, thus attempting to achieve the opposite of high acuity. This method is also used in accommodative tasks to relax the eye before instigating accommodation [158, 159]. There is logic to this, if microsaccades are in-fact fixational movements, does eliminating a clear target in which to fixate render microsaccades unnecessary?

Even if there is only a casual link to the suppression of microsaccades and concentration, which ever side of the scale this may lie, it is worth evaluating its potential for use in eye diagnostics. High or low concentration tasks can easily be introduced to the instrument hardware/software making it a simple but yet effective tool.

6.6.1 Aim

Determine the effect of concentration on eye rotation during a 60s time period.

Hypothesises are formulated as in section 6.3.1

6.6.1.1 Null Hypothesis

Ho = $u_1 = u_2 = u_3...$

6.6.1.2 Alternative Hypothesis

Ha= $u_1 \neq u_2 \neq u_3...$

6.6.2 Method

Translational and rotational eye movements were measured using the JEDEye tracking system which recorded the eye's movement for a 60s time period. In total 4 visual targets were used consisting of 1 control target, a high concentration target, a blurred target and a static target.

In total 18 subjects (mean age - 30, SD +/- 11, age range 22 - 63) were asked to look at 4 different targets for 60s at a time, the data from 2 subjects had to be rejected due to too frequent blinking or eye lash occlusion of the Purkinje Images. The purpose of the experiment was explained to each of the subjects. The subjects were told to look at the centre of each target and maintain this fixation as best they could, the subjects received additional instruction on the concentration target in which they were required to respond to the target. The targets were presented randomly. Subjects were notified when the recording was about to begin and when it ended, after which they were allowed to sit back from the apparatus and have a short break. All 4 recordings for each subject were recorded in the same session. The recordings were taken in a darkened room with only the subject and the examiner present. Experiments were performed at random times throughout the day.

Exclusion Criteria

To ensure normality, subjects were only considered for the study if they passed the following criteria:

- No underlying eye conditions, such as dry eye or kerataconus.
- Do not wear contact lenses.

- Could distinguish between 2 targets to be used in the study.
- Subjects who had their vision corrected with glasses were allowed also long as they could see the target without their glasses.

6.6.2.1 Concentration Targets

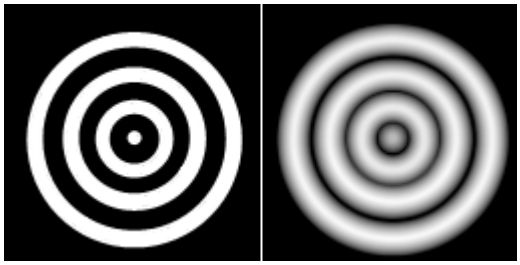

Figure 6.15: Static and blurred image targets used for the concentration experiment.

Figure 6.15 shows the static Bullseye and its corresponding Blurred Bullseye image. The experiment also included a control which consisted of a blank black screen as well as movie design to provoke a response from the subject. The blurred target was created using the static Bullseye blurred using a blurring function in a standard image processing package.

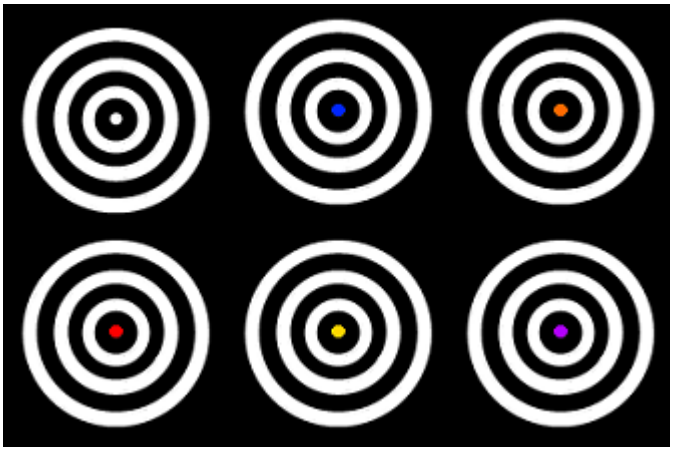

Figure 6.16: Bullseye images used for the concentration movie.

Figure 6.16 shows the images used for the concentration Bullseye movie designed to stimulate a response from the subject. Subjects were required to press a button when the centre of the target turned white, they were asked to do this as quickly as possible. The colours changed randomly and through different time periods thus requiring constant concentration. A base frame rate of approximatley 1 Hz was used however random time changes were produced by maintianing displayed frames for longer than a single frame.

6.6.2.2 Data Processing

The entire set of data was processed using an algorithm written in the National Instrument's Labview programming environment. The algorithim detects, isolates and extracts the calibrated coordinates of the Purkinje Images. Rotation was then calculated using the JEDEye principle in Matlab. All acquired data was normalised to the first rotation value in the relevant data set. The standard deviation in eye rotation was then calculated, thus giving the average variation in eye rotation when looking at the relevant target. All statistical analysis was performed with the statistical analysis software package SPSS.

6.6.2.3 Statistical Analysis

A total of 20 subjects were used for each target, however 4 were rejected thus leaving 16. The degrees of freedom for the subplot is then 16-1, fulfilling the sample size requirement.

For the target type set a single factor repeated measures ANOVA was performed to test if there was a statistically significant difference between the mean standard deviation in eye rotation for each target.

To test the assumption of sphericity a Mauchly's test is performed on the data.

All significance testing is performed to a 0.05 confidence level.

6.6.2.4 Additional Calculations

The total amount of eye translation was recorded as percentages of eye translation caused by head movement and eye rotation.

6.6.3 Results

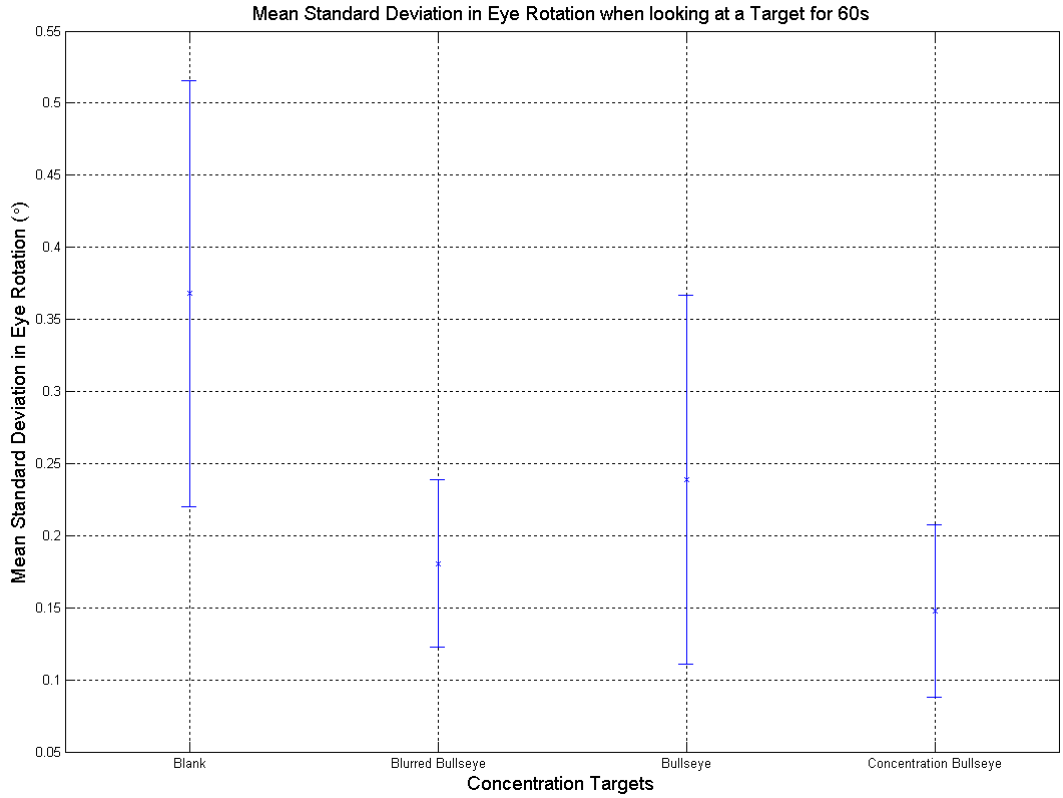

Figure 6.17: Mean standard error in eye rotation when regarding the concentration targets independently for 60s. The error bars indicate the standard deviation in the mean.

Figure 6.17 shows the mean standard deviation in eye rotation when regarding each of the 4 targets independently. All targets suggest a reduction in eye rotation when compared to the Blank (0.37°) control target. The smallest deviation in eye rotation was performed when subjects were required to look at the Concentration Bullseye (0.15°). The Blurred Bullseye (0.18°), as with the Concentration Bullseye performed better than the standard Bullseye (0.24°).

6.6.3.1 Statistical Analysis

Table 6.13 shows the spherity test on this set of data, the results suggest sphericity cannot be assumed. In order to correct the significance value the Greenhouse - Geisser calculation is performed.

Data Set	Mauchly's W	df	Significance
Concentration Targets	0.182	5	0.000

Table 6.13: Mauchly's test of sphericity for data set.

Table 6.14 shows the repeated measures ANOVA performed on the target type data set. The results suggests that there is significant difference in the target means.

Source	Type III Sum of Squares	df	Mean Square	F	Significance
Concentration	0.452	1.878	0.241	23.937	0.000

Table 6.14: Repeated ANOVA for data set.

Table 6.15 is a selection of pairwise comparisons showing significant differences found between each of the targets. Notable significant differences were found between the Blank control and the Concentration Bullseye**,** as well as between the standard Bullseye and the Blurred Bullseye and Concentration Bullseye respectively.

Target 1	Target 2	Mean Difference	Std. Error	Significance
Blank	Concentration Bullseye	0.220	0.033	0.000
Bullseye	Concentration Bullseye	0.091	0.022	0.001
Bullseye	Blurred Bullseye	0.058	0.025	0.037

Table 6.15: Selection of pairwise comparisons taken from the data set.

6.6.3.2 Translation Movement

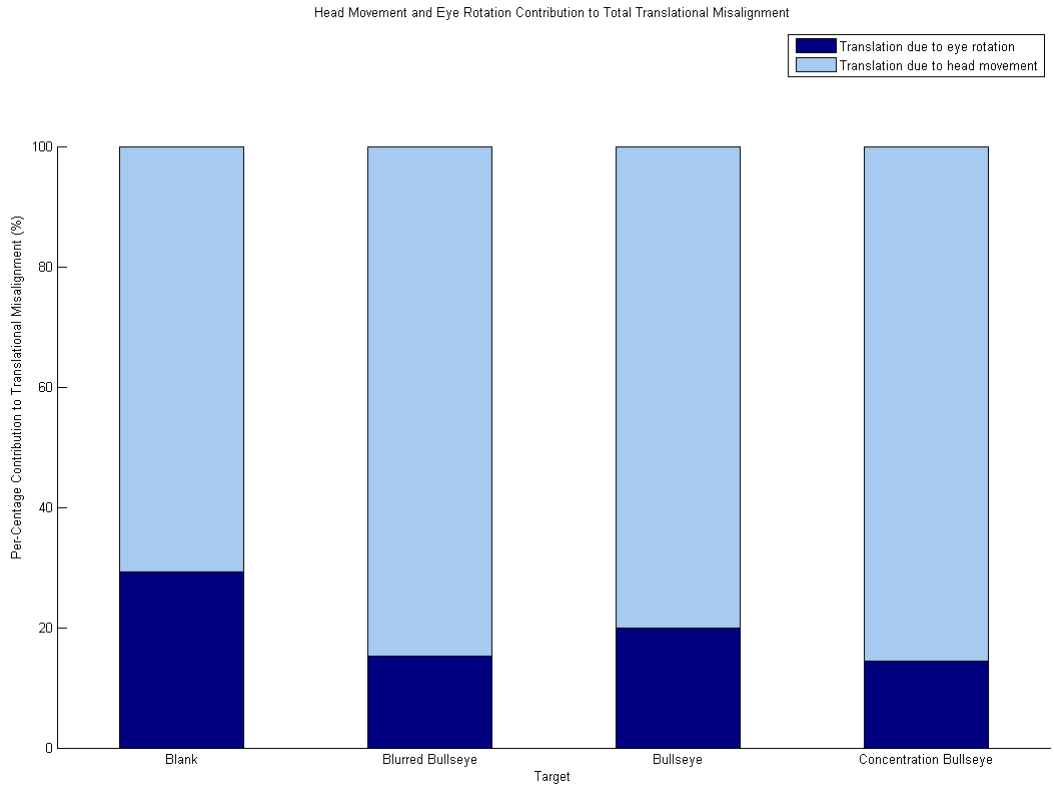

Figure 6.18: Percentage translational movement as performed by the head and the eye.

Figure 6.18 demonstrates the components of translational movements performed while staring at the targets. The information is represented as the total translation made up of percentages of the two contributing factors: eye rotation and head movement. The average contribution of eye rotation to translational movement was 20% where as the head on average contributes to 80% of translation.

6.6.4 Discussion

Although the experiment did not judge the distribution of fixation by the frequency of microsaccades the average amplitudes found are consistent with microsaccadic magnitudes, this means this experiment is comparable to previous studies. Previous investigations into microsaccades found that their frequency decreases when the subject is forced to perform high acuity tasks or, tasks which requires high concentration [155, 57]. The results found in this experiment are consistent with this; however, interestingly the results suggest both extremes of concentration reduce eye rotation. Both high concentration, as with the Concentration Bullseye**,** and low concentration as in the Blurred Bullseye**.**

What the results allude to is the voluntary nature of microsaccades, or rather the voluntary nature of microsaccadic suppression. Previous studies have shown that microsaccades can be suppressed with a simple verbal instruction [57] showing that their frequency is largely dependent on the subject. It is a possibility that the high concentration task warranted the conscious decision of the subject to prevent saccades; while, the blurred target did not warrant fixation at all and thus microsaccades were not required. The Bullseye target invoked fixation but the suppression of microsaccades was not invoked because their suppression was not required.

The results from the Blank control questions this theory, as in this case no fixation occurred due to the absence of a target. The case could be that the eye still required some reference to ensure that it stayed in the same location. Therefore the Blurred Bullseye still allowed the subject to be conscious of their eye movement where as the Blank control did not.

Inspection of the results also show less deviation in measurement between subjects when they regarded the Concentration Bullseye and the Blurred Bullseye. Statistically, this can be seen in the test of spherity, in which the difference in variances between targets was shown to be significant. This suggests that these targets provoke similar reductions in eye rotation, not only within subject comparisons but also between subject comparisons. The repercussions of this are that all subjects will reduce eye rotation to a similar level when the target warrants it; however, when regarding a target which does not warrant it the response will vary. This variation may be a consequence of a number of factors, such as the subject's concentration span.

Translation movements were recorded to assess the contributing factors to misalignment. In this analysis translation caused by eye rotation was compared to translation caused by head movement. On average 80% of the total movement of the eye can be attributed to head movement. This is in a agreement with previous fixational studies performed with the Purkinje eye tracker.

The Bullseye was chosen for this experiment because it could be used in all representations of concentration, from the Blurred Bullseye for lack of concentration, to the task dependent target for concentration. However, there are a number of targets or tasks which could have been used for this study, thus the results are representative of these particular targets. The targets used however, do fulfil each form of concentration, and so are no less valid.

As part of the Concentration Bullseye task the subject was required to push a button, thus, inducing movement into the recordings as a result of the button press. This movement was not performed when regarding the other targets. Even with this induced movement the Concentration Bullseye caused the lowest amount of average eye rotation suggesting that the movement did not adversely affect the results.

6.6.5 Conclusion

The aim of the experiment was to determine the effect of concentration on the reduction of eye rotation. In respect to this, the results suggest that concentration significantly reduces the amount of eye rotation performed when compared to a static target. The Concentration Bullseye induced an average of 0.15°eye rotation while the static equivalent Bullseye induced an average of 0.24°. Significant differences were also found between the Bullseye and the Blurred Bullseye (0.18°) suggesting that trying to prevent the eye from fixation also reduces eye rotation; however, the lowest average rotation still remained with the Concentration Bullseye. All targets showed a significant reduction in eye rotation when compared to the Blank control.

Translational analysis demonstrated that 80% of the total movement of the eye performed during the 60s can be attributed to the head while 20% can be attributed to eye rotation as a result of the fixation target. This is in agreement with previous studies performed with the JEDEye tracker.

6.7 Discussion

The purpose of the fixation studies was to investigate the possibilities of an optimum target for the reduction of eye movement. An optimum target is a valuable asset in the context of this research. Once the alignment system performs alignment it must then encourage the eye to remain stable, hence allowing repeatable measurements. Current methods of for eye stability rely on the subject's ability to maintain a steady gaze. Thus the investigation is valuable, not only in the search for an optimum target but in the assessment of the current approach.

There are numerous parameters involved in defining a target, thus the experiment isolated 5 factors which the literature has identified as having a significant effect. The study was then based on determining optimum values within these sub groups; with the overall aim to combine the optimum values to form an all inclusive optimum alignment target. This approach also means that there are a number of target variations absent from the study, as well as a reduced range in the variables which have been investigated. For these reasons, it is important to remember that when significant differences have been found, it is only present in the investigated range.

A by-product of the investigation into the potential of an optimum fixation target is information on the validity of fixation as a method of invoking eye stability, particularly when using popular targets. Ophthalmic instrumentation commonly use the Maltese Cross as a fixation target, but other renowned targets include Bullseyes and Crosshairs. Interestingly, the results suggest that the Maltese Cross reduces eye movement more than other targets confirming its status as the primary fixation target in optometry.

It is still unclear what exactly about targets such as the Bullseye and the Maltese Cross enable them to invoke a relatively stable eye. The results from the target size study, and the target movement study suggest that the periphery of these target goes largely unnoticed. This assumption is drawn from the absence of significant differences found in each of these studies. One similarity in the construction of the Maltese Cross and the Bullseye is the definitive central point, in addition to this, their construction seems to guide the eye to this position. This must then be an important factor in defining an optimum target.

Target movement was investigated to determine if movement of the target would reduce the requirement of eye movement. The are a vast number of permutations to movement in a target, including speed and type of movement. This experiment looked at a small range of movement and compared the movement to the images' static counterparts. It could well be the case that a different speed of movement would induce better stability in the eye; however, it is impossible to conclude this with out investigating a larger range of movement.

The range of targets which promoted the greatest eye stability was that of the concentration targets; the Concentration Bullseye and the Blurred Bullseye were responsible for the smallest amounts of eye rotations in any of the target parameters investigated. One

possible reason for this is that eye stability is increased as a consequence of the task rather than the target, thus, it is the way in which the target it looked at rather than how the target appears. The results then allude to a strong neurological aspect to fixation.

One of the examples used to warrant investigations into concentration was shooting. It was hypothesised that tasks such as these, which encourage high concentration, increase eye stability. Interestingly, common targets used in shooting are Bullseyes and Crosshairs. The strong association between these types of targets and fixation is then potentially due to the task which they are involved with rather than their appearance. Again this alludes to the importance of concentration in eye stability.

Arguably the most intriguing results from the fixation studies is the influence of head movement. In all the studies head movement was the major component of misalignment. It is important to remember that during the fixation recordings that the position of the instrument was not corrected, thus the head was allowed to drift out of alignment. While this situation would be uncommon in typical alignment procedures it highlights just how much head misalignment correction is needed in alignment.

6.8 Conclusion

The purpose of the fixation studies was to investigate the validity of eye stability methods in ophthalmic practices and investigate/determine the possibilities of an optimum target for eye stability.

Popular targets in ophthalmic research were found to significantly reduce eye rotation when compared to other targets, and the absence of targets. Out of the target type data set the Maltese Cross was found, on average, to reduce the greatest amount of eye rotation when compared to other targets.

However, the target which invoked the least amount of eye rotation was found to be the Concentration Bullseye followed closely by the Blurred Bullseye. The results then suggest it is the way the target is regarded rather than the appearance of the target which encourages eye stability. This then means that concentration in the form of a task must be used in the designed alignment process.

Chapter 7

JEDEye Alignment

7.1 Chapter Overview

The purpose of this chapter is to discuss the design and implementation of a self alignment strategy, and its evaluation against the original aims of the research.

The chapter first describes the development of a self alignment system which allows alignment to the optical axis of the eye. In doing this the JEDEye alignment/tracking system is used to track the eye and determine the position of eye's optical axis. The eye tracking information is used to communicate misalignment correction.

Following development of the system, the alignment method is tested against its original specifications to determine the validity of the proposed alignment philosophy.

The chapter concludes by evaluating the success of the self alignment system and philosophy by comparing the alignment system to the original aims of the research.

7.2 Introduction

To validate the alignment philosophy it is first necessary to design and develop a self alignment technique which allows the patient to align their optical axis with the measurement axis of the system. Chapter 5 described the design, development and the evaluation of a Purkinje tracking system capable of detecting the optical axis of the eye. Chapter 6 describes the investigation into fixation targets with the aim to determine an optimum target. There then remains one further requirement in the alignment system, the provision to allow the user to align themselves to the instrument without the assistance of an operator.

Out of all the parameters investigated in the fixation studies concentration was highlighted to be a contributing factor to the increase of eye stability during fixation. The design of the self alignment strategy has thus been centred on the involvement of the patient in the alignment process, forcing their concentration.

With the self alignment method designed and implemented, the next step is to evaluate its performance. The most important factor in its evaluation is whether it facilitates self alignment to the optical axis of the eye. Alignment can be judged against the original specifications of the system; if self alignment can be achieved the aims of the research have been meet, thus demonstrating the validity in the alignment philosophy.

7.3 Self Alignment and Evaluation

7.3.1 Aim

The aim of the investigation was to demonstrate the JEDEye alignment/tracker's ability to allow self alignment. The ability of the device to do this is evaluated by comparison to the original specifications. Specifically, alignment is achieved when rotational misalignment is less than 0.17°and translational misalignment is less than 0.198 mm (Specification 2.1).

The experiment also aims to determine the population ranges for the JEDEye's self alignment properties, namely, duration of self alignment and eye stability once in alignment. By calculating these values, the JEDEye system can be considered in the context of clinical use.

To answer the question of the self alignment system's effect on corneal thickness measurements, the corneal thickness measurement range is calculated from the eye stability calculation determined by the experiment. This variation in eye position is related to corneal thickness by means of the cornea model (Section 4.4).

7.3.2 Method

7.3.2.1 Self Alignment

Self alignment dictates the ability of a patient to move an instrument from an unaligned position to an aligned position, thereby permitting measurement. In order to achieve this, the instrument must perform 3 actions: calculate the magnitude of misalignment, communicate or perform alignment correction, and finally, identify alignment.

Misalignment Calculation

Misalignment of the eye's optical axis from the instruments measurement axis is comprised of 2 factors: eye rotation and head translation. While the eye must be rotated to ensure that the eye's optical axis is parallel with the measurement axis, the instrument as a whole must be moved so that both axes become collinear.

The JEDEye tracking/alignment system facilitates both rotational and translational measurements. By default, the JEDEye alignment/tracking system measures rotation relative to the optical axis, thus directly measuring the amount of rotational misalignment (figure 7.1). The amount of translational misalignment cannot be directly extracted from the tracking data; however, it can be inferred. By measuring the displacements of the vertical, and horizontally positioned Purkinje Images I relative to the centre of the image the translational misalignment can be measured (figure 7.2).

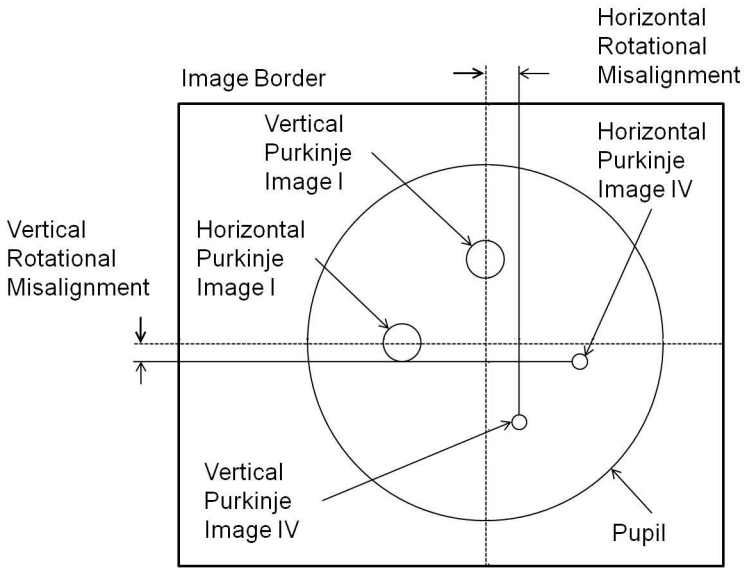

Figure 7.1: Rotational misalignment identification. The dashed lines intersect the centre of Purkinje Image I and thus represent the required position for Purkinje Image IV to achieve rotational alignment.

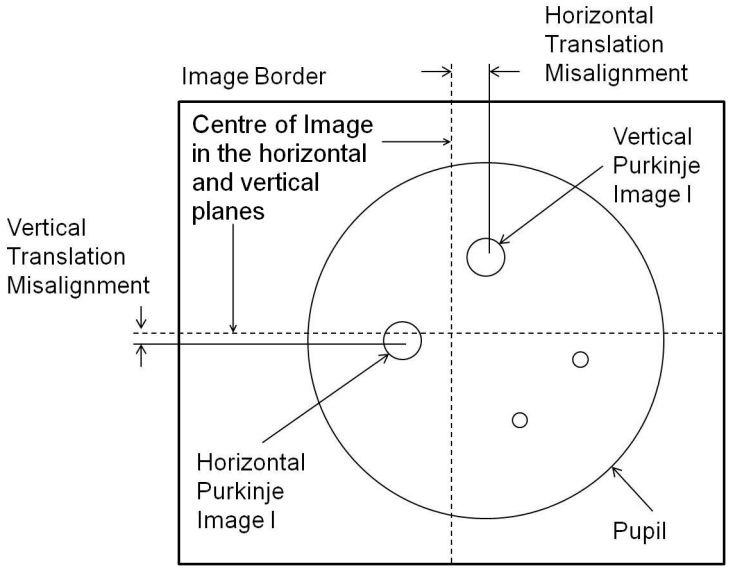

Figure 7.2: Translational misalignment identification. The dashed lines represent the centre of the image and thus the aligned position. In order to achieve alignment Purkinje Images IV must be inline with Purkinje Image I, while both Purkinje Images I must be positioned in the centre of the image.

Using these measurements, both components of misalignment can be quantified. The tracking aspect of the JEDEye alignment/tracking system then provides all the necessary data for alignment correction and identification.

Misalignment Correction

Misalignment correction involves either the instrument, or the patient manipulating the rotation of the eye and position of the head to achieve alignment. In the case of patient correction, the amount and direction of correction needs to be communicated by the instrument to the user.

While having the instrument perform all the alignment seems an attractive idea, there are 2 reasons why it is advantageous to involve the patient in the alignment process: firstly, the fixation studies have shown that concentration is a valuable tool in maintaining eye stability, in the fixation studies, concentration was invoked by performing a cognative task. In regards to self alignment, the alignment process can be thought of as the cognitive task. Secondly, by allowing the patient to manipulate the position of the instrument, the instrument is making use of the patient's dexterity rather than trying to perform alignment correction movements itself. It also coincides with the eventual aim for the instrument to become hand-held, thus the benefit of making the alignment system interactive is reiterated.

However, there are benefits in having the instrument perform some aspects of alignment, for example: the direction of gaze is largely controlled by the position of the fixation target, thus, rotational alignment correction can easily be induced in the eye by movement of the target. The alternative to manipulating the eye is to move the instrument; however, moving an instrument in response to potential eye rotations of 500°/s is a difficult task, and unnecessary.

The proposed method of alignment correction then involves both instrument alignment and patient alignment. Rotational misalignment caused by the eye is corrected for by movement of the fixation target, translational misalignment caused by head is corrected for by the patient.

Alignment Identification

The last aspect of self alignment is the identification of alignment. The optical axis of the eye can be defined by the closest alignment of the Purkinje Images, in the context of self alignment, the aligned position is when the Purkinje Images are aligned in the correct position relative to the instrument. Eye alignment can then be identified when the Purkinje Images appear as in figure 7.3.

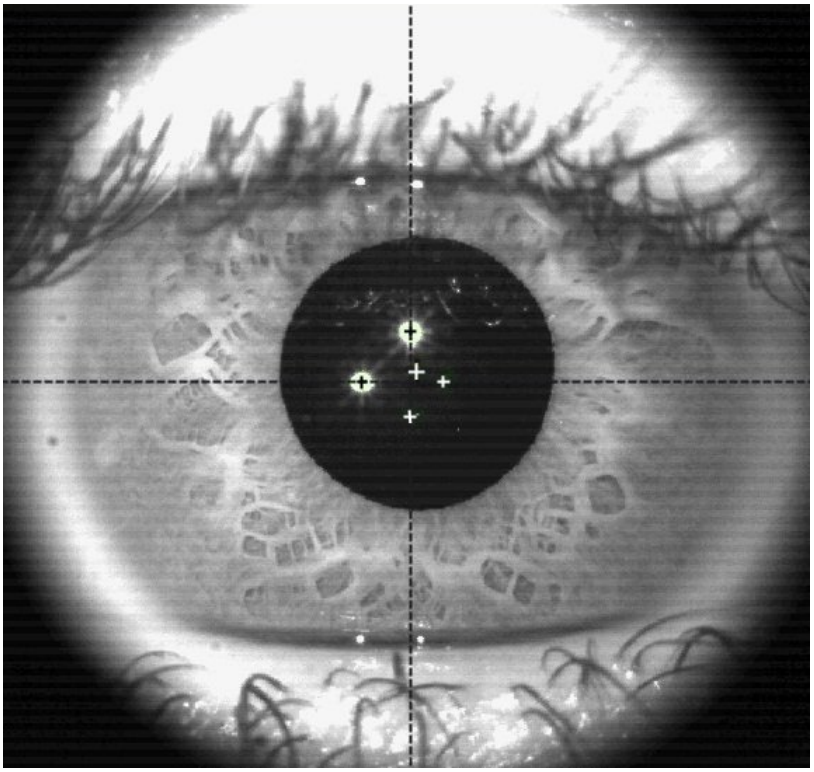

Figure 7.3: Appearance of the Purkinje Images when in the aligned position. The black crosshairs are overlaid on top of the Purkinje Images I while 2 of the white crosshairs are overlaid ontop of Purkinje Images IV. The central white crosshairs describes the position of the pupil centre. The dashed lines in the figure indicate the axes of the aligned position (centre of the image), as Purkinje Images I are positioned on these axes and Purkinje Images IV are inline with Purkinje Images I the image suggests alignment with the central imaging axes.

The aligned Purkinje Images dictate that the eye is rotationally aligned and the position of Purkinje Images I in the centre of their relevant alignment axis dictate that the instrument is in the correct position; the optical axis of the eye is then aligned with the central imaging axis of the instrument.

7.3.2.2 Self Alignment Procedure

The self alignment procedure designed to allow the patient to maneuver the instrument from and an unaligned position to the correct position consists of 5 steps:

- The patient must first move the instrument in order to place the eye at the focal plane of the imaging hardware.
- The JEDEye system then tracks the eye to calculate the initial amount of rotational misalignment.
- Rotational misalignment is then corrected for and translational misalignment is communicated to the patient.
- The patient then iteratively corrects for translational misalignment until in the correct position.
- The JEDEye alignment/tracking system identifies alignment.

Initial Alignment

In order for the JEDEye alignment/tracking system to quantify the initial amount of misalignment, the instrument must first be moved to position the eye in the instruments focal plane. The instrument allows this through a combination of methods. The optics within the JEDEye alignment/tracking system present a reflection of the subject's eye within the system; providing that this reflection is centred in the system the JEDEye system will be able to image the eye. The patient is then required to move the JEDEye device forwards until in the correct focal plane. The patient is notified when the eye is on the correct focal plane by a series of auditory signals. These auditory signals indicate that the tracking algorithm is able to detect the Purkinje Images and is thus able to track the eye. It can be assumed that if the algorithm is able to detect the Purkinje Images the eye is in the correct focal plane validating initial alignment.

Initial alignment is also partially undertaken in software. Performing a histogram analysis on the intensity of the pixels allows quantification of the standard deviation in pixel intensity. The larger the standard deviation the sharper the image appears; however as this value changes with the patient, additional initial alignment steps making use of the tracking algorithim are required.

Rotational Misalignment Correction

Once the instrument is in the correct position and can successfully detect the relevant tracking features the JEDEye system can then start calculating the amount of misalignment. The JEDEye alignment/tracker will then move the fixation target to the correct position on the graphical display unit in order to correct for the rotational misalignment.

Translational Misalignment Communication

In order for the subject to move the JEDEye system to correct for translational misalignment, the subject must first be notified of the direction and amount in which to move. The amount of misalignment is demonstrated to the subject by the displacement of a secondary target from the primary fixation target (used to correct for rotational misalignment in the previous step). This displacement then corresponds directly to the amount of translational displacement (figure 7.4).

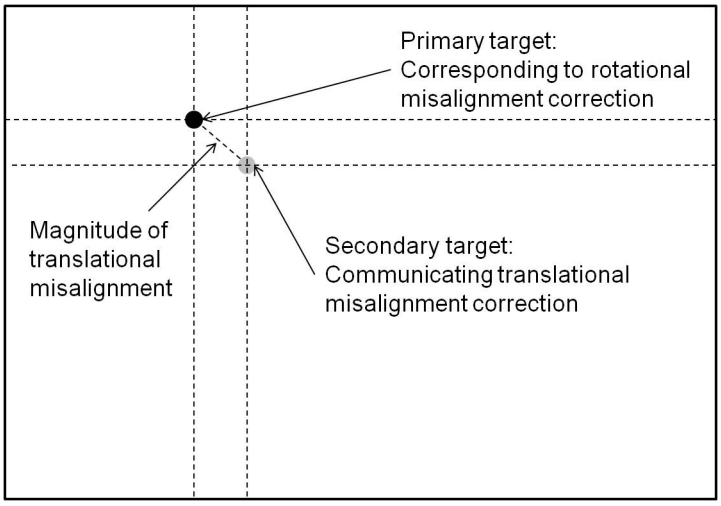

Figure 7.4: Translational misalignment communication.

Translational Misalignment Correction

To achieve alignment, the secondary target, corresponding to translational misalignment, must be positioned in the same location as the primary target. This then signifies that there is no translational misalignment. Providing the primary target is relatively stable the rotational misalignment is also corrected. Involving the patient in the alignment like this effectively gives the patient a task to perform, thus promoting the task dependent concentration desired.

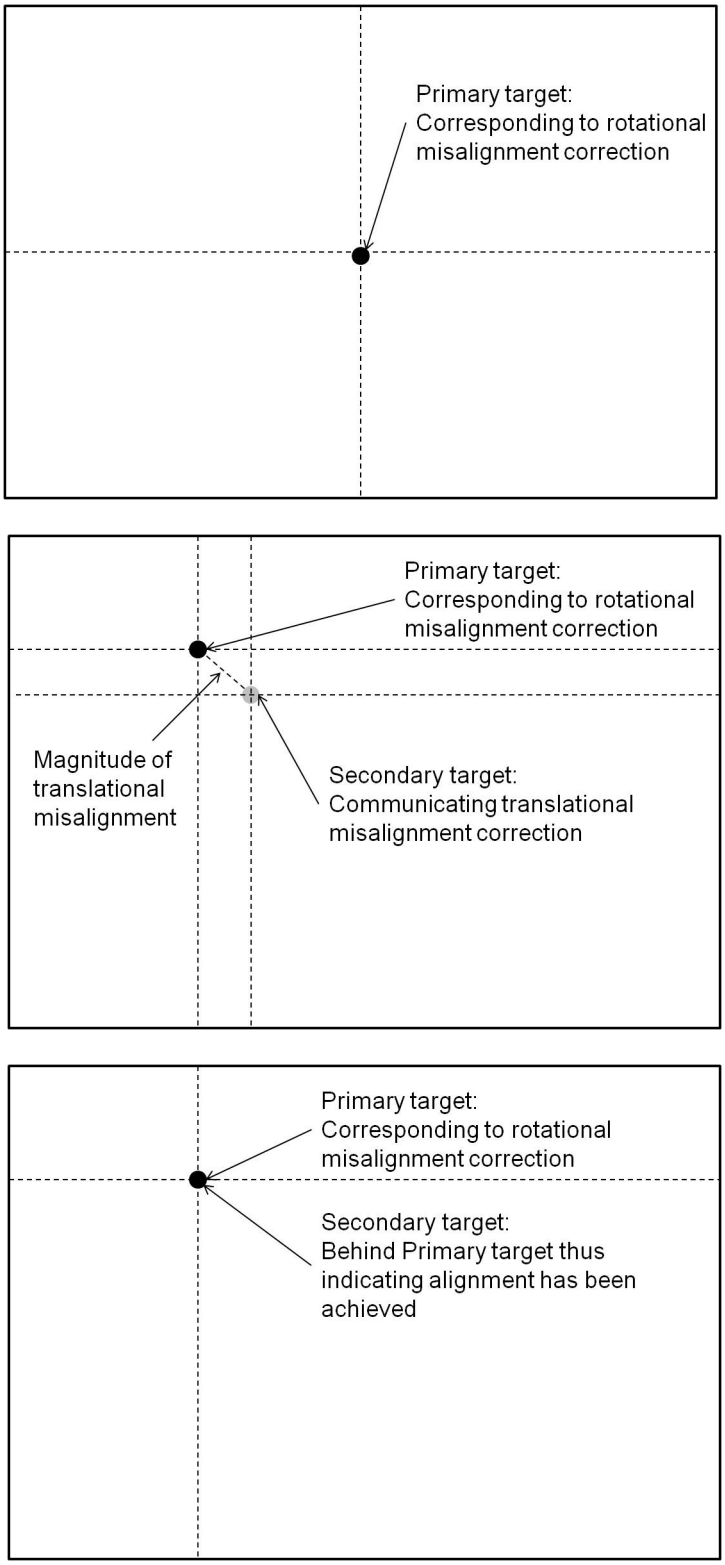

Figure 7.5: Patients view of translational misalignment correction. Top Image: starting location of the primary target, Middle Image: communication of translational misalignment, Bottom Image: both targets in the same position indicating alignment.

However, by moving the JEDEye system, the angular misalignment changes thus requiring correction. Correction is then constantly updated, this update of the position of the targets occurs at 1 Hz. With the JEDEye alignment/tracker sampling at 20 Hz it gives 20 data

points in which to calculate misalignment and make the appropriate corrections. The consequence of this is that the secondary target appears to 'chase' the primary target, adding a certain amount of complexity to the task.

Alignment Identification

While the user is attempting to maneuver the secondary target to the primary target the JEDEye alignment/tracker is analysing the tracking data to determine if at any point the eye reaches the alignment position. It does this by comparing the rotational misalignment and translational misalignment to the alignment tolerances set out in the specifications. Alignment is judged as successful if the subject is able to overlay the secondary target on the primary target in the correct location.

7.3.2.3 Procedure and Apparatus

The patient's ability to perform self alignment was recorded by the JEDEye alignment/tracking system. The system monitored the rotational and translational eye movements during a 60 s time period while the subject attempted to self align.

In total, 16 subjects performed self alignment with the JEDEye alignment/tracking system. Each subject had 3 attempts at aligning their optical axis with the imaging axis of the device using the self alignment strategy proposed. Prior to this, each subject recieved sufficient practice and explanation in order for them to comprehend the self alignment technique. The purpose of the experiment was explained to all subjects. All subjects received sufficient instruction to allow them to competently undertake the procedure.

Exclusion Criteria

To ensure normality, subjects were only considered for the study if they passed the following criteria:

- No underlying eye conditions, such as dry eye or kerataconus.
- Do not wear contact lenses.
- Could distinguish between the 2 targets to be used in misalignment correction display.
- Subjects who had their vision corrected with glasses were allowed also long as they could see the target without their glasses.

7.3.2.4 Processing

All tracking data was acquired with the JEDEye alignment/tracking system, which outputs the calibrated coordinates of the detected Purkinje Images. The following rotational calculations and statistical analysis was performed in MatLab.

7.3.2.5 Statistical Analysis

The statistical analysis consists of 3 calculations: percentage of subjects able to align, and the 95% confidence interval for time to alignment and alignment position variation. Subjects were considered to achieve alignment if they were able to align the JEDEye system within the alignment tolerance in 1 or all 3 runs. Calculation of the confidence interval was performed by calculating the mean and standard deviation of each parameter. The upper and lower limits were defined as the addition/subtraction of the standard deviation from the mean.

7.3.3 Results

The following graphs (figures 7.6 and 7.7) shows the typical reduction in rotational and translation misalignment as the subject performed self alignment. The initial misalignment is the subject looking directly down the centre of the instrument, approximately aligning their visual axis with the instrument axis. The initial misalignment alignment then serves as an approximation of angle alpha. Figure 7.6 is an example of a subject who was able to achieve alignment within the 60 s, figure 7.7 is an example of a subject who was unable to achieve alignment. The remainder of the graphical data is in Appendix D.

Rotational alignment correction is controlled by the JEDEye system, thus the graphs indicates substantial initial rotational alignment correction followed by smaller corrections caused by the subjects movement of the instrument. Translational misalignment correction is controlled by the subject, the graphs in this case shows a varied speed in the reduction of translational misalignment as the subject moves the instrument, attempting to achieve alignment.

7.3.3.1 Statistical Analysis

Self Alignment Statistical Analysis	
Subjects able to Align	
14/16	
95% Confidence Interval for Alignment Time	
Mean	28.6s
Lower Limit	16.5s
Upper Limit	40.8s
95% Confidence Interval for Rotational Alignment Variation	
Mean	0.036°
Lower Limit	0.03°
Upper Limit	0.044°
95% Confidence Interval for Translational Alignment Variation	
Mean	31.96µm
Lower Limit	20.64µm
Upper Limit	43.28µm

Table 7.1: Self alignment statistical analysis.

Table 7.1 shows the statistical analysis of the self alignment data acquired from the study. Of interest in the study was whether the system would facilitate alignment and how would the technique fare in the wider population. The table suggests that 14/16 of the sample group achieved alignment within the predefined alignment tolerances of 198 µm for translational and 0.17°for rotation, within this percentage of the population the 95% confidence interval for time to alignment was 16.5-40.8 s. The variation in alignment position is calculated from the eye tracking data acquired when the subject is in the aligned position, in this regard, the 95% confidence interval for rotation is 0.03°-0.044°, while the translational range is 20.64-43.28 µm.

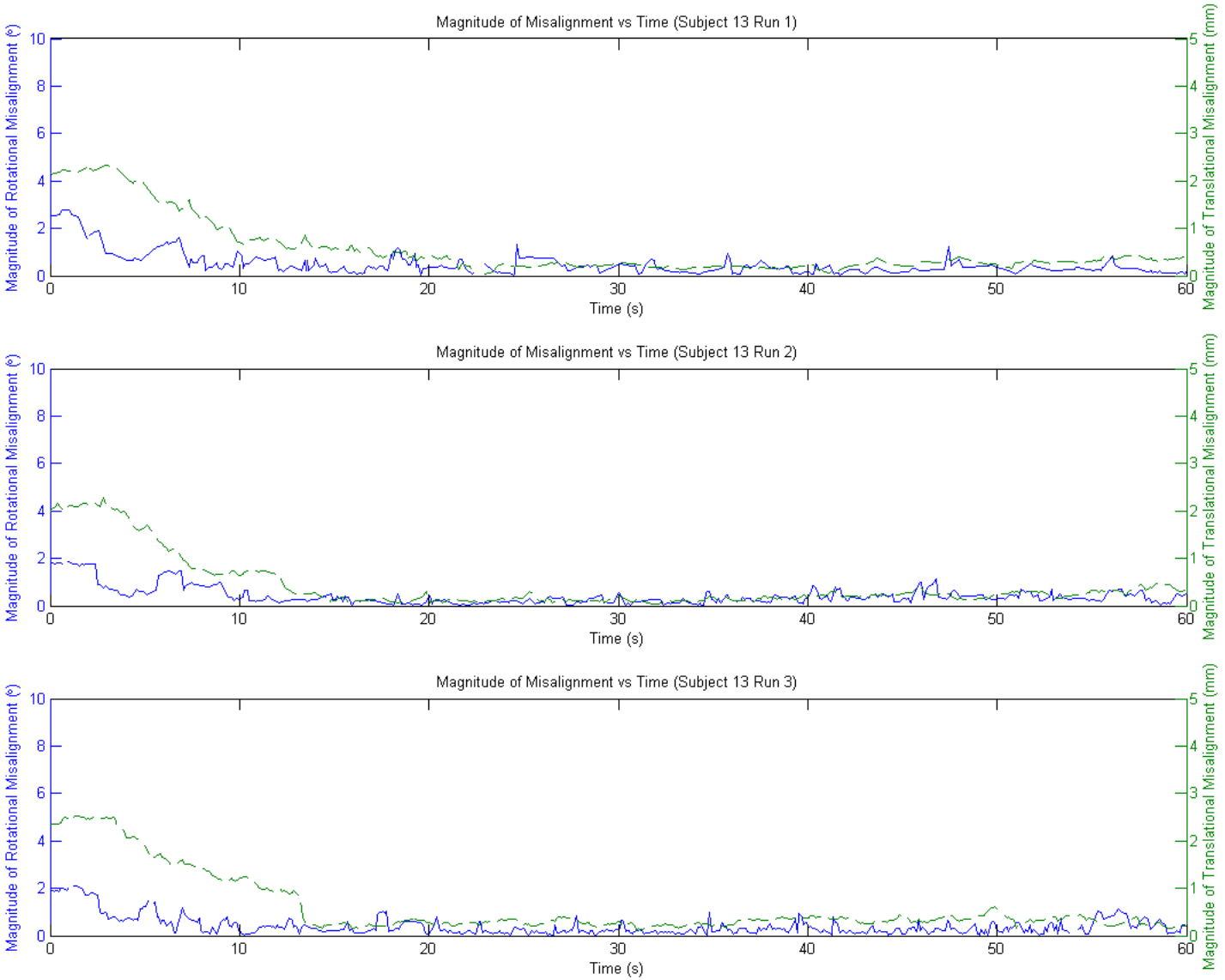

Figure 7.6: Aligned subject example (subject 13). The dashed line corresponds to the translational misalignment axis, while the solid line corresponds to the rotational misalignment axis. In all 3 runs the subject is able to lower their rotational and translational misalignment within 0.17 and 0.198 mm of the alignment position (centre of the captured image)

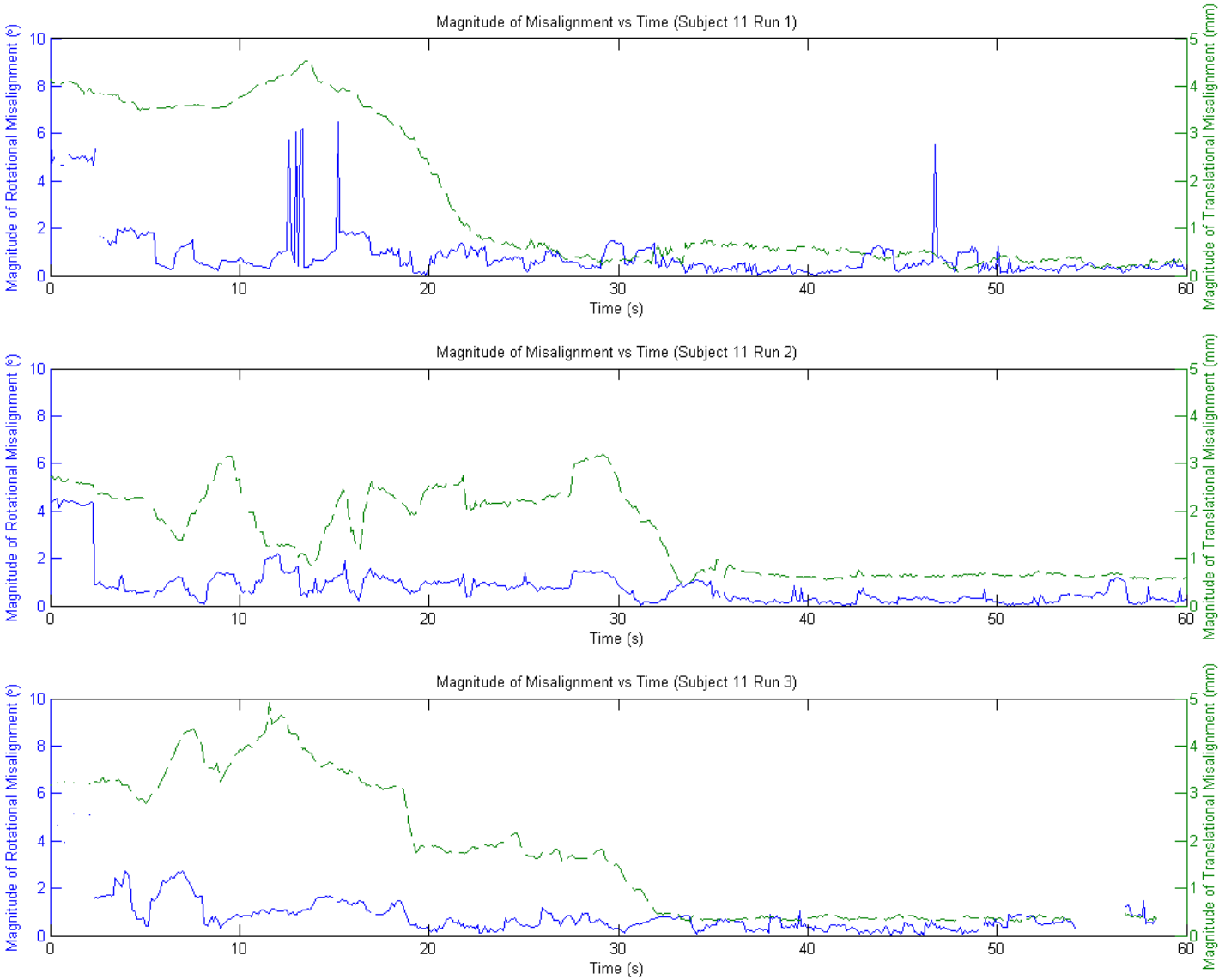

Figure 7.7: Misaligned subject example (subject 11). The dashed line corresponds to the translational misalignment axis, while the solid line corresponds to the rotational misalignment axis. In all 3 runs the subject is unable to lower their rotational and translational misalignment to within the alignment tolerances. The graphs indicate a gradual improvement to alignment but not sufficient improvement in the time period to achieve alignment to the specified tolerances.

7.3.3.2 Model Analysis

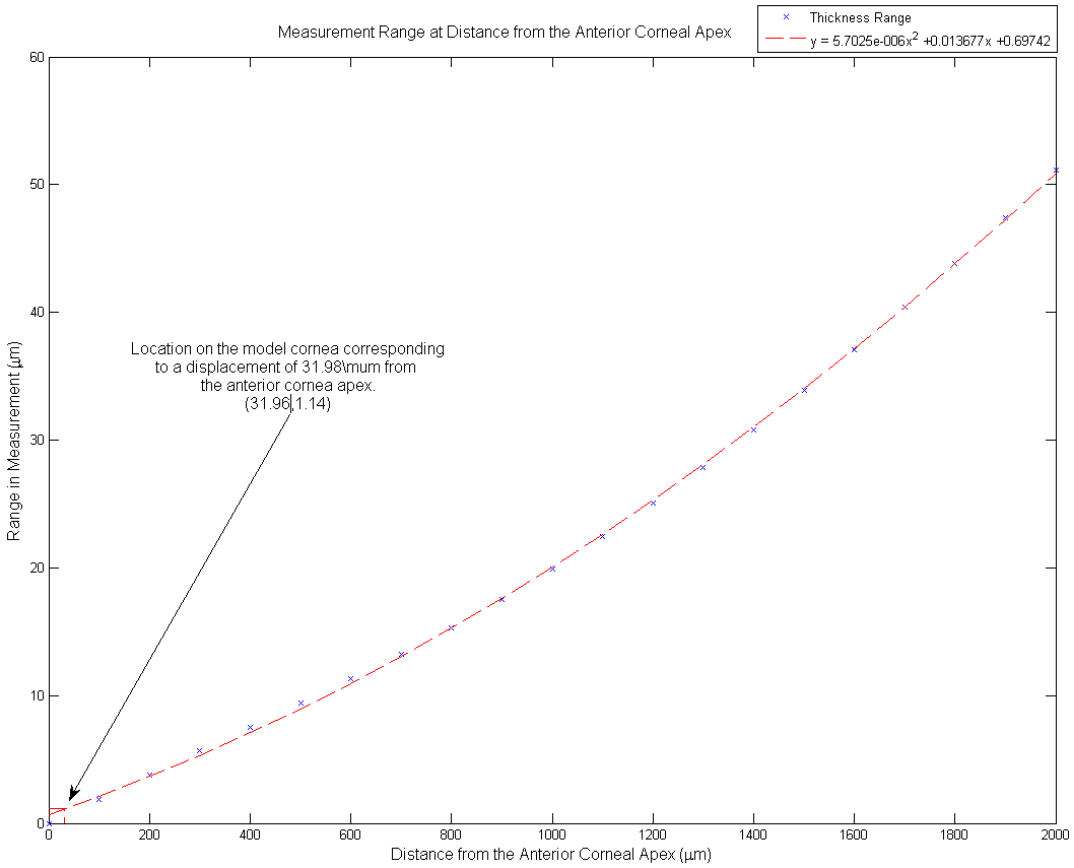

Figure 7.8: Model analysis of alignment position variation.

Figure 7.8 shows the model analysis of the alignment position variation. The model shows range in expected corneal thickness measurement as a function of the distance away from the cornea. Using the average translational misalignment determined in the self alignment study the model suggests a variation of 31.96µm would result in a 1µm range in thickness measurement. This value is below the resolution of the pachymeter (3.88µm) meaning that the precision in the alignment system is better than the resolution in the pachymeter.

7.3.4 Discussion

The intention of the experiment was to demonstrate a self alignment technique using the JEDEye system which allowed the subject to move an instrument from an unaligned position to aligned position. In this regard, the results show that 14/16 subjects of the sample group were able to achieve alignment.

There are a number of reasons why the results are potentially skewed in favor, or indeed, against the ability of the subject to achieve self alignment. It is important when considering these reasons that a clear distinction is drawn between validating a technique and validating an instrument. The experiment aims to determine if the alignment strategy, using the JEDEye system, allows self alignment within the alignment tolerances, rather than the mechanism in which this is performed.

The subject was instructed to align the JEDEye system by first bringing the JEDEye alignment/tracker into the camera's focal plane, then subsequently, adjusting the height and lateral displacement of the instrument. In doing this, the subject was required to reach round the instrument, making this process awkward. For the alignment process to work the subject is required to remain relatively still, a task which is difficult if uncomfortable. However, as the majority of subjects were still able to align it suggests that the arrangement did not have a negative influence on the results, at least not in their ability to align. It may be the case that this arrangement affected the speed and stability of alignment, although this is impossible to conclude without comparison to alternative methods.

Ideally, an alternative method would be a hand-held version of the JEDEye system, as the intended instrument for integration is desired to be hand-held. A hand-held device would arguably be an easier device to maneuver as it would be lighter, more responsive and move with the head (if resting on the forehead). Head movement is an important point, the fixation studies in Chapter 6 suggest that head movement is a major component of misalignment, thus misalignment correction is potentially more stable in a hand-held version of the JEDEye instrument.

The communication of alignment correction is another potential source of variation related to the instrumentation. Specifically, the speed in which correction information was overlaid to the subject. To add robustness to the tracking system, and in keeping with the information obtained in the Chapter 2 (Anatomy, Mechanics and Physical Dyanmics of the Eye), misalignment correction was communicated at 1 Hz. The reasoning behind this was that this speed was considered comfortable for the subject to both comprehend the amount of misalignment and perform correction. In addition to this, the tracking system samples at 20 Hz, thus for every update, 20 samples were used to calculate the amount of alignment correction. Through observations during the experiment, it was often apparent that the subject expected a much quicker response to their movement, thus, at first, they were unable to correlate the instrument movement with secondary target movement. The consequence of this was the inability to achieve alignment as quickly as other subjects; however, its seems appropriate at this point to reiterate the difference between validating a technique and instrument. The speed at which the instrument communicates

misalignment is an area of development, this alignment strategy used a speed based upon eye movement literature; however this may not be the optimum setting for misalignment correction.

Another important factor in the communication of alignment, relating to the apparatus, is the subject's perception of the alignment targets. Each subject within the sample group will see the targets with varying clarity, influencing their ability to perform the fixation task. While this variation may not be prominent in a group of subjects with emmetropic vision the variation will be more severe in larger sample populations. Again, arguably this is another aspect of development which concerns the final instrument rather than the technique itself. However, the sample group used in this experiment was not limited to emmetropes and the results still suggest that self alignment can be achieved using the proposed strategy.

The sample group is worth considering in any experiment involving human subjects, in this case, the point for discussion comes from the source of the group. The task dependent nature of the alignment system potentially suits subjects who can understand and appreciate the task better than others. In regards to this experiment, all subjects were university personnel and thus were potentially better equipped to understand, appreciate and perform the task. In order to accommodate a larger population there are a number of ways which the alignment task could be better communicated; however, this strays from the object of the exercise. The point of the experiment was not test the intuitiveness of the strategy but to prove that self alignment can be achieved with the JEDEye system.

Practice would produce similar effects to intuitiveness in the results, although this is a more controllable variable. The greatest endeavor was made to allow similar amounts of time for the subject to practice before the acquisition of data. However it was deemed that valid data could only be acquired if the subject fully understood the self alignment procedure, thus while practicing times may differ all data was acquired from the point where the subject fully comprehended the self alignment process. The consequence of this is that all subjects started their 3 runs from the same level of understanding.

The data acquired for the rotational and translational alignment variances are recordings of eye movement when the eye was identified as being in the aligned position. This method of analysis highlights the advantage in this method of alignment. By only using data from the aligned position the variation is immediately biased in favor of self alignment; however, this highlights the self validation aspect of eye tracking in alignment procedures. The ability of the JEDEye system to identify the times when the eye is in the correct position distinguishes this method of alignment with other methods of alignment. It allows the intended instrument for integration to validate the measurement at the time of measurement as well as instruct the instrument when the eye is in the correct position before the measurement. The eye tracking data thus gives the ability to distinguish between aligned data and misaligned data.

The self alignment technique attempted to use concentration as a method to encourage eye stability. However, by involving a task which incorporated target movement the eye

was constantly encouraged to move. When concentration was outlined in Chapter 6 as a valid approach in the reduction of eye movement, concentration was maintained at a single location. The difficulty in reproducing this in the self alignment procedure comes from the need for the subject to correct misalignment. Observations of the experiment suggest that the misalignment correction was constantly required because of slight movements of the head and eye, thus the patient was never given the opportunity to maintain fixation. While the instrument moves independently to the head, this will be an inescapable feature of self alignment; however, as head movement forms the major component of misalignment a hand-held version of the device resting on the forehead would negate alot of this movement, potentially allowing concentration fixation at a single location. The fact that the system constantly corrects for misalignment is in fact an advantage of the system and is one of the main sources of its novelty.

Ultimately the research is concerned with facilitating self alignment of the subject's optical axis with the imaging axis. In answer to this, a strategy has been proposed using the custom built JEDEye system which allows 14/16 subjects of the sample group to achieve alignment. While there are equally as many reasons for skewed results both in favor and against this statement, these are developmental concerns and do not invalidate the technique itself.

7.3.5 Conclusion

The purpose of the self alignment study was to investigate whether self alignment of the subject's optical axis and the central imaging axis could be achieved with the JEDEye alignment/tracking technique. Alignment was determined when the subject was able to maneuver the JEDEye instrument to within the predefined alignment tolerances of 198 μm and 0.17°.

In this respect, 14/16 subjects of the sample group were able to achieve alignment with the proposed method in 1 or all of their runs.

Within this percentage, calculation of the 95% confidence interval for alignment time suggests that once tracking commences alignment can be achieved in 16.5-40.8 s, with an average of 28.6 s +/- 12.44 s.

Again within the population which could achieve alignment, the 95% confidence interval suggests that the alignment variation ranges from 0.03-0.043°(mean 0.037°+/- 0.007) rotationally and 20.64-43.28 μm translationally (mean 32 μm +/- 11.6 μm).

Applying this positional variation to the geometric model cornea suggests that the range in thickness measurement would be approximately 1 μm, meaning that the precision in the alignment technique is better than the resolution of the pachymeter (3.88 μm).

The results from the experiment suggest that self alignment with the proposed strategy and the JEDEye alignment/tracking technique can be achieved within the alignment tolerances set in the specification, thus proving the system as a valid method of precise self alignment to the eye's optical axis.

Chapter 8

Conclusions

8.1 Summary

The orginial aims of the reseach stated the desire to create a self alignment technique capable of aligning a patient's optical axis with a central measurement axis or imaging axis. In order to achieve these objectives, the research first had to identify parameters and specifications for self alignment, develop a technique capable of performing to these specifications and finally design a prototype to facilate the testing of the developed alignment technique. The thesis has achieved this in the following steps:

Reviewed the axes of the eye commonly used for alignment in ophthalmic instrumentation. The review highlighted the natural variation in alignment to these axes caused by the eye's anatomy (Section 2.4).

Reviewed eye movements and identified the most likely contributors to misalignment during eye alignment procedures. The review also highlights the dynamic properties of these movements enabling their consideration in the design of the self alignment technique. The review outlined microsaccades as the most likely contributor to misalignment (Section 2.7).

Reviewed current eye tracking techniques based on the suitability of their use in alignment. This review outlined Purkinje Image tracking as the most suitable form of tracking due to its high accuracy and the ability to detect an approximation of the eye's optical axis (Chapter 3).

Designed and developed a novel Purkinje Image tracking technique which makes use of imaging techniques rather than mechanical solutions. This development included design of the optical arrangement, illumination and the construction of custom tracking algorithms designed to extract rotation data. The design of the system and the algorithm also allows the measurement of physical parameters of the eye. Due to this, the system can measure the curvatures necessary to extract rotation data directly, thus not requiring calibration or prior knowledge of the geometry of the eye (Section 5).

Discussed the ability of the Purkinje tracking system and the thus the alignment technique to identify multiple axes of alignment including the visual axis. This then demonstrates the potential for the alignment technique to be used as a standard alignment methodology across ophthamology, reducing unknown variation in diagnostic measurements attributed to the variation in alignment techniques (Section 7.3.4).

The thesis has also described the construction of a geometric model cornea which accurately models the offset of the thinnest point of the cornea relative to the corneal apex. This allows the range in corneal thickness to be calculated as a function of misalignment (Section 4.4).

Investigated the potential for an optimum alignment target in the reduction of eye rotation using the custom built Purkinje tracking system. The investigation determined that it is the manner in which the target is regarded rather than the target itself which plays an important role in the magnitude of eye rotation. Concentration in the form of a task was found to reduce eye movement when compared with static targets. The investigation also highlighted the significant impact of head movement during eye alignment; on average 80% (Section 6).

Designed a self alignment strategy which, using the JEDEye alignment/tracker, allows self alignment of the patent's optical axis with the central imaging axis of the device. The system makes use of the JEDEye's capabilities to resolve eye rotation from head translation and identify the eye's optical axis. The strategy also makes use of the task dependent concentration highlighted in the fixation studies to improve eye stability (Chapter 7).

The thesis has consequently tested the JEDEye alignment/tracker and the self alignment strategy demonstrating that 14/16 of a sample group was able to achieve alignment within 0.17°and 198 µm of the optical axis. Using the model cornea, the corresponding corneal thickness range was calculated at 1 µm. The thesis has thus designed, developed and tested a self alignment strategy with the ability to achieve alignment to the desired specifications, while also incorporating eye tracking into eye alignment taking advantage of its ability to quantify misalignment and validate measurements (Section 7.3).

8.2 Specification Assessment

The orginial aims and objectives of the research desired to investigate eye alignment as a whole, and, more specifically, develop an self alignment methodolgy which allows a patient to align their optical axis with a measurement or imaging axis.

In order to achieve this, a specification was established agaisnt which the device could be compared. These specifications were drawn from a series of reviews on the eye's anatomical structure, movement and the parameters for the device in which the technique is intended to be implemented (v360 pachymeter). The specifications, and their assessment, are detailed in table 8.1. Principally, the specifications outlined the requirement for the self alignment technique to determine alignment to within 0.198 mm and 0.17°(specification 2.1). Based on the investigations into fixation, it was also specified that the user must be involved in the alignment process to encourage concentration (specification 2.3). A technique was subsequently developed and prototyped which allowed 14/16 subjects to align themselves with the prototypes imaging axis, thus successfully meeting the orginal aims of the research.

Tracking Specifications	Assessment
1.1 - The tracking technique must be based on Purkinje Image tracking, allowing detection of the eye's optical axis by imaging Purkinje Image I and Purkinje Image IV.	The tracking technique used Purkinje Images I and IV inorder to track the eye and identify the eye's optical axis (Section 5.4.1).
1.2 - The tracking technique must resolve eye and head movements relative to the optical axis of the eye thus determining misalignment.	Using the cross illumination arrangement (Figure 5.8), the tracking technique was able to calculate both rotational and translational misalignment relative to an approximation of the eye's optical axis.
1.3 - The tracking technique must be able to resolve eye rotation from head movement.	The use of Purkinje Image tracking allowed the distinction between eye rotation and head translation to be made (Section 5.4.1).
1.4 - The tracking technique must be able to detect microsaccadic/saccadic eye movements ranging from 0.17°to 20°.	The tracking technique was unable to determine microsaccades from the eye movement data; however, average eye rotations calculated through out the fixation studies and alignment investigations produced variations in eye rotation suggestive of microsaccades.
1.5 - The tracking technique must be able to optically resolve changes in Purkinje Image position in the order of 0.017 mm, as a result of eye rotations of 0.17°. Using an approximation of the distance between the Purkinje Image imaging plane and the eye's centre of rotation, and the minimum desired detectable eye rotation, the magnitude of lateral movement induced by this movement can be determined.	The investigation into the accuracy of the Purkinje tracking technique (Section 5.5.2) and prototype such that changes in rotational changes of 0.04°can be detected thus within the required 0.17°.
1.6 - The tracking technique must sample in excess of 10 Hz in order to fulfill the nyquist criterion for the detection of saccadic eye movement.	The tracking technique sampled at 20 Hz.
1.7 - The tracking technique must be safe to use, thus in accordance with commercial tracking systems, maximum IR exposure to the eye must be below 10 mW/cm^2.	Investigations into the power output of the prototype (Section 5.5.1) suggests maximum power levels of 3.2 mW/cm^2, 3 factors of safety below the safety limit.

Table 8.1: Tracking specifications assessment.

Self Alignment Specifications	Assessment
2.1 - The alignment technique must be able to detect alignment of the eye's optical axis with the measurement axis to within 198 µm laterally and 0.17°rotationally.	The self alignment investigation (Section 7.3) demonstartes the ability of the technique to detect alignment when within the specified tolerance limits.
2.2 - The alignment system must be able to determine the magnitude of misalignment.	Using the Purkinje tracking technique described in this thesis the amount of rotational and translational misalignment was quantifable (Section 5.4.1).
2.3 - The alignment system must be able to communicate the degree of required correction to the user or operator in a manner which enables them to perform correction. This information must be clearly presented in order to achieve a quick response from the user.	Self alignment was achieved in 14/16 subjects (Section 7.3), in which misalignment was communicated to them by the methodology described in this thesis.
2.4 - Once in alignment, the alignment system must maintain alignment.	Concentration was used as a tool to maintain alignment once in the aligned position. This approach was successful in 14/16 subjects (Section 7.3).

Table 8.2: Self alignment specifications assessment.

Composition Specifications	Assessment
3.1 - The wavelength of the tracking illumination sources must be different from that used in the pachymeter (670 nm) to ensure no confusion in the measurement signal.	Illumination s sources had a peak wavelength of 850nm.
3.2 - The tracking illumination sources must lie outside the 10 mm diameter pachymeter beam path to prevent obstruction.	Illumination sources were placed at 10mm away from the imaging axis.
3.3 - The tracking illumination sources must be positioned in front of the system and at 50 mm from the corneal apex to allow the pachymeter to perform its measurement.	The front of the device was placed 50mm from the corneal apex.

Table 8.3: Composition specifications assessment.

8.3 Recommendations

Although the research fulfilled its primary objectives, there are many areas of the research undertaken which could be modified and investigated further. These aspects, and recommendations, are now discussed.

The most poignant recommendation involves the investigation of the alignment technique on measurement precision. The current technique described in this research facilitates self alignment and maintains alignment through concentration. However, the effect on corneal thickness measurement precision is infered from the geometric mathematical model cornea. A more powerful study would be to incorprate the self alignment system into a pachymeter and determine the change in measurement precision. This was not undertaken in this research due to the limitations in the changes which could be made to Lein's pachymeter and the safety issues surrounding the laser source used in Lein's equipment.

The manner in which alignment can be achieved can also be investigated further. There are many ways in which a task can be incorporated into the alignment procedure; the current research proposed a single technique as a proof of research philosophy, however this may not be the most efficient way to achieve alignment. The mechanism for correction could also be changed; this research proposed an iterative approach to misalignment correction in which an image was taken, misalignment calculated and correction performed. The mechanisim could be expanded further to allow prediction of eye movement based on previous time periods, thus providing a quicker response to misalignment..

Eye movement analysis would be another powerful, and a candidate for further investigation. The propsed tracking technique was theroretically capable of detecting microsaccades, and the average eye rotatations determined in the fixation studies was suggestive of microsaccades. However, the precise points at which microsaccades were performed was not clear from the data. The research would benefit from the determination of the type of eye movements performed during the alignment procedures, as well as the magnitude and frequency, as this information can be feed back into the alignment correction mechanism improving the corrective response.

All the recommendations discussed above concern the application of the research philosophy to real world use, thus this becomes the overriding reccommendation. Developmental changes to the software and hardware must be performed to allow the application of this technology, these changes are partially discussed in following sections.

8.4 Future Work

The design and development of the eye alignment technique, which makes use of eye tracking, is the initial step in the clinical application of the technique. Potential areas for future work are then centred round the conversion of the alignment principle to a mechanism which is integrated into a diagnostic device.

8.4.1 Integration

While the alignment technique has been shown to perform to the desired specifications it is still unlcear whether the system would improve the measurement of the v360 pachymeter. The first step in this analysis is the integration of the alignment technique in the v360 pachymeter. In this regard there are 2 areas of modification:

1. Hardware alterations

2. Software conversion and refinement

Currently the alignment technique and the v360 pachymeter are 2 separate entities, however the alignment device was designed in such a way to allow simple integration of the alignment technique into the device. The illumination sources used for the alignment technique were designed to lie outside the measurement beam path thus this stage of the integration would require only superficial modifications to the pachymeter. The optical integration warrants more consideration as the optical path must allow the measurement of corneal thickness, imaging of the eye and a graphical display for the subject to view and receive visual commands. While this is not an unreasonable set of specifications it does require significant alteration to the optics currently inside the v360 pachymeter.

The other major discrepancy in the integration of the alignment system to the measurement system is in the software. The 2 systems were written in 2 different programming languages thus not allowing direct integration. The measurement system was written in the C programming language and the alignment system was written in LabVIEW. While this initially seems a problem there is nothing in the alignment software which is unique to LabVIEW thus the equivalent functions can be found and used instead. This also means that new software can be written based on the architecture of the current software; it may also be the case that to incorporate the alignment software in the measurement software the measurement software must be rewritten thus not allowing direct integration anyway.

8.4.2 Clinical Testing

On completion of the integration of the alignment technique there is one further area of investigation. It would be interesting to determine the effect of the alignment system on the actual acquired measurement. This would allow evaluation of the repeatability and

stability of measurement. This experiment would consist of the correlation of measurement signal with the alignment position determined with the alignment technique. Depending on the results of this investigation the alignment system may have to be modified to determine the optimum alignment position if this is not the alignment of the Purkinje Images; however, the alignment technique is fully capable of doing this as it uses eye tracking. The study would then consist of correlating the position of the eye with the optimum return signal.

8.4.3 Further Applications

The requirement of the alignment device to track the eye and perform alignment to the optical axis has meant that the device has had to facilitate additional measurements of the eye. Specifically, as the alignment/tracking system is designed to allow the subject to use the instrument without prior measurements taken, the system has to perform these measurements at the time of tracking; because of this, the JEDEye system can be considered a measurement system in its own right in addition to its capabilities as an alignment and tracking system.

8.4.3.1 Keratometer

In order to allow Purkinje Image tracking the JEDEye alignment/tracking system must calculate the separation between the centre of curvatures of the anterior cornea and the equivalent mirror which generates Purkinje Image IV. To enable this, two illumination sources are used thus allowing the principle of keratometry to be applied. What the JEDEye system actually measures is a single radius of curvature value for the cornea which is slightly offset from the apex value.

8.4.3.2 Phakometer

Phakometry for the alignment system has to be performed for similiar reasons to keratometry. Similar to Keratometry, the use of 2 illumination sources allows the radius of curvature of the equivalent mirror to be deduced. The JEDEye alignment/tracker measures a single value of the radius of curvature of the equivalent mirror at the position of Purkinje Image IV.

8.4.3.3 Intraocular Lens (IOL) Alignment

As the JEDEye alignment/tracker is based on Purkinje Image tracking the system also has the limited capabilities of analysing the misalignment of IOLs. In fact IOLs actually produce a higher intensity Purkinje Image IV, firstly because they possess a higher refractive index then natural lenses; and secondly, because of their higher quality surface finish. In addition to this the appearance of Purkinje Image III is also improved.

8.4.3.4 Alignment Research Tool

As the JEDEye system is an alignment system it most suited area for future use is in the field of eye alignment. While the JEDEye system was designed to allow alignment to the optical axis of the eye, the design of the tracking algorithm produced some interesting consequences. By tracking the Purkinje Images and the pupil centre, and the additional control of the fixation target, the system actually allows tracking of 3 important alignment axes: optical axis, visual axis and the line of sight.

Maintaining the fixation target in the centre of the graphical display (in line with the imaging axis) and using Purkinje Image I as an approximation for the eye's nodal points the system can facilitate alignment to the visual axis.

Keeping the fixation target in the central position and using the geometric pupil centre as an approximation for the eye's pupil points the system can facilitate alignment to the line of sight.

The JEDEye system is then an alignment system that can also apply the advantages of tracking to any of the indicated alignment axes. It then becomes a powerful research tool as well as a candidate for an alignment standard.

An alignment system which uses the same method of alignment across different eye axes allows a more informed comparison of measurement techniques. It was discussed in the introduction to the thesis that there is ambiguity in alignment as each instrument uses a unique method of alignment. The alignment technique proposed in this research then would allow a single alignment technique across multiple instruments as well as the additional information on eye tracking; again reiterating its potential as a powerful research tool.

8.5 Concluding Remarks

The JEDEye system developed in this research describes a novel solution to optical axis alignment; however, the novelty of the system does not just lie in optical axis alignment. The system makes use of eye tracking technology to combine eye alignment with eye tracking, allowing the alignment system to go beyond identification of alignment. With the addition of tracking data the alignment system is able to quantify misalignment, thus allowing the amount of misalignment to be quantified. This results in the alignment system's ability to communicate or perform alignment correction, a capability which is demonstrated in this research. It also, with knowledge of the eye's position at the time of measurement, can validate position in which the measurement was taken.

The introduction to this thesis touched upon the growing need for manufacturers to develop portable devices, thus alignment must be performed in a completely new set of circumstances requiring a novel solution. One such manufacturer is Lein Applied Diagnostics who desire the v360 pachymeter to become hand-held for the purposes of glucose monitoring. The likely end user for a device such as this is a patient who is not trained in optometry, and is ignorant of the anatomy and physical axes of the eye, thus are unable to judge the success of the measurement and alignment. While the purpose of the thesis is not to extract the clinician from the diagnosis process it does aim to allow the patient to perform a measurement successfully with out the aid of the optician thus allowing the use of ophthalmic diagnostic equipment in other health care areas.

While the aims of this research was to facilitate the use ophthalmic equipment in areas other than vision care; the alignment system has further applications in ophthalmology. At the beginning of this research, the variety in alignment techniques was discussed as a consequences of the variation in measurement principles. This variation results in a certain amount of ambiguity between different instruments taking similar measurements, as well as the additional varaition due to the clinician's interpretation of the results. As the alignment technique proposed in this research facilitates alignment to multiple alignment axes, and can resolve the position of the eye at the time of measurement, it has the potential to be used across ophthalmic instrumentation as a standard alignment methodology, thereby permitting unbiased measurements.

The JEDEye alignment/tracker, with the proposed self alignment technique, is able to facilitate self alignment of an eye tracking device with the patent's optical axis. In doing this it highlights the potential of a hand-held version of the v360 pachymeter, incorporating the JEDEye technique, to achieve an aligned measurement of corneal thickness along the patient's optical axis. In achieving this, the thesis has outlined an alignment philosophy which incorporates eye tracking into eye alignment giving the alignment system the ability to both correct and validate alignment; this then allows applications of ophthalmic devices in health care areas other than vision care.

References

1. D A Robinson. A Method of Measuring Eye Movement Using a Scleral Search Coil in a Magnetic Field. *IEEE Transactions on Bio-Medical Electronics*, 10(4):137–145, 1963.

2. G B Arden and P A Constable. The electro-oculogram. *Progress in retinal and eye research*, 25(2):207–48, March 2006.

3. J Tabernero, A Benito, V Nourrit, and P Artal. Instrument for measuring the misalignments of ocular surfaces. *Optics Express*, 14(22):10945–10956, October 2006.

4. D J Daly. Ocular Property Measuring Apparatus and Method Therefor, US Patent 0078308 A1, 2007.

5. I Murakami, A Kitaoka, and H Ashida. A positive correlation between fixation instability and the strength of illusory motion in a static display. *Vision research*, 46(15):2421–31, July 2006.

6. A Duchowski. *Eye tracking methodology: theory and practice*. Springer, London, 2. ed. edition, 2007.

7. D A Atchison and G Smith. *Optics of the Human Eye*. Butterworth-Heinemann Medical, 2000.

8. J Schwiegerling. *Field guide to visual and ophthalmic optics*. SPIE Press, Bellingham, WA, 2004.

9. W F Harris. Optical axes of eyes and other optical systems. *Optometry and Vision Science*, 86(5):537–541, 2009.

10. A G Bennett and R B Rabbetts. *Clinical Visual Optics*. Butterworths, London; Boston, 1984.

11. J C Barry, R Effert, A Kaupp, and A Burhoff. Measurement of ocular alignment with photographic Purkinje I and IV reflection pattern evaluation. *Investigative Ophthalmology & Visual Science*, 35(13):4219–4235, 1994.

12. M C M Dunne, L N Davies, E A H Mallen, T Kirschkamp, and J C Barry. Non-invasive phakometric measurement of corneal and crystalline lens alignment in human

eyes. *Ophthalmic Physiological Optics*, 25(2):143–152, 2005.

13. P Rosales and S Marcos. Phakometry and lens tilt and decentration using a custom-developed Purkinje imaging apparatus: validation and measurements. *Journal of the Optical Society of America*, 23(3):509–520, 2006.

14. Y Nishi, N Hirnschall, A Crnej, V Gangwani, J Tabernero, P Artal, and O Findl. Reproducibility of intraocular lens decentration and tilt measurement using a clinical Purkinje meter. *Journal of Cataract and Refractive Surgery*, 36(9):1529–1535, 2010.

15. T Kirschkamp, M C M Dunne, and J C Barry. Phakometric measurement of ocular surface radii of curvature, axial separations and alignment in relaxed and accommodated human eyes. *Ophthalmic Physiological Optics*, 24(2):65–73, 2004.

16. G Smith and D A Atchison. *The Eye and Visual Optical Instruments*. Cambridge University Press, 1997.

17. C Cui and V Lakshminarayanan. The reference axis in corneal refractive surgeries: visual axis or the line of sight? *Journal of Modern Optics*, 50(11):1743–1749, 2003.

18. H Von Helmholtz. *Physiological Optics*, volume 3. Dover, 1866.

19. W F Harris. Visual axes in eyes that may be astigmatic and have decentred elements. *Ophthalmic physiological optics the journal of the British College of Ophthalmic Opticians Optometrists*, 30(2):204–207, 2010.

20. R A Schachar. Should the pupil be used as a fixed reference for instrument alignment? *Journal of Cataract and Refractive Surgery*, 31(11):2040–2041, 2005.

21. Y Yang, K Thompson, and S A Burns. Pupil location under mesopic, photopic, and pharmacologically dilated conditions. *Investigative Ophthalmology & Visual Science*, 43(7):2508–2512, 2002.

22. M A Wilson, M C Campbell, and P Simonet. Change of Pupil Centration with Change of Illumination and Pupil Size. *Optometry and Vision Science*, 69:129–136, 1992.

23. J C Barry and A Backes. Limbus versus pupil center for ocular alignment measurement with corneal reflexes. *Investigative Ophthalmology & Visual Science*, 38(12):2597–2607, 1997.

24. R A Applegate, L N Thibos, M D Twa, and E J Sarver. Importance of fixation, pupil center, and reference axis in ocular wavefront sensing, videokeratography, and retinal image quality. *Journal of cataract and refractive surgery*, 35(1):139–152, 2009.

25. A Tomlinson and C Schwartz. The Position of the Corneal Apex in the Normal Eye. *American Journal of Optometry & Physiological Optics*, 56:236–240, 1979.

26. R K Maloney. Corneal topography and optical zone location in photorefractive keratectomy. *Refrative Corneal Surgery*, 6(5):363–371.

27. R B Mandell. The Enigma of Corneal Contour. *Contact Lens Association of Ophthalmologists*, 18(4):267–273, 1992.

28. R B Mandell, C S Chiang, and S A Klein. Location of the major corneal reference points. *Optometry and Vision Science*, 72(11):776–784, 1995.

29. J M Wolfe, S J Butcher, C Lee, and M Hyle. Changing your mind: On the contributions of top-down and bottom-up guidance in visual search for feature singletons. *Journal of Experimental Psychology Human Perception and Performance*, 29(2):483–502, 2003.

30. E C Carter and R C Carter. Color and conspicuousness. *Journal of the Optical Society of America*, 71(6):723–729, Jun 1981.

31. A L Nagy and R R Sanchez. Critical color differences determined with a visual search task. *Journal of the Optical Society of America*, 7(7):1209–1217, 1990.

32. A L Yarbus. *Role of eye movements in the visual process.* {N}auka, 1965.

33. R H S Carpenter. *Movements of the eyes.* London, 1977.

34. W Becker. The neurobiology of saccadic eye movements. Metrics. *Reviews Of Oculomotor Research*, 3:13–67, 1989.

35. K.J Ciuffreda and B Tannen. *Chapter 2 , Eye movement basics for the Clinician.* 1995.

36. A T Bahill, D Adler, and L Stark. Most naturally occurring human saccades have magnitudes of 15 degrees or less. *Investigative Ophthalmology*, 14(6):468–469, 1975.

37. E Kowler and E Blaser. The accuracy and precision of saccades to small and large targets. *Vision Research*, 35(12):1741–1754, 1995.

38. H Collewijn, C J Erkelens, and R M Steinman. Binocular co-ordination of human vertical saccadic eye movements. *The Journal of Physiology*, 404(1):183–197, 1988.

39. L L Wheeless, R M Boynton, and G H Cohen. Eye-movement responses to step and pulse-step stimuli. *Journal of the Optical Society of America*, 56(7):956–960, 1966.

40. M G Saslow. Latency of saccadic eye movement. *Journal of the Optical Scoiety of America*, 57(8):1030 – 1033, February 1966.

41. H Collewijn and E Kowler. The significance of microsaccades for vision and oculomotor control. *Erasmus*, 8:1–21, 2008.

42. U Tulunay-Keesey. Fading of stabilized retinal images. *Journal of the Optical Society of America*, 72(4):440–7, April 1982.

43. G S Brindley. Two new properties of foveal after-images and a photochemical hypothesis to explain them. *The Journal of Physiology*, 164(1):168, 1962.

44. G C Higgins and K F Stultz. Frequency and amplitude of ocular tremor. *Journal of*

the Optical Society of America, 43(12):1136–40, December 1953.

45. C Bolger, S Bojanic, N F Sheahan, D Coakley, and J F Malone. Dominant frequency content of ocular microtremor from normal subjects. *Vision research*, 39(11):1911–5, June 1999.

46. J P Ryle, M Al-Kalbani, N Collins, U Gopinathan, G Boyle, D Coakley, and J T Sheridan. Compact portable ocular microtremor sensor: design, development and calibration. *Journal of Biomedical Optics*, 14(1):014021, 2011.

47. A Spauschus, J Marsden, D M Halliday, J R Rosenberg, and P Brown. The origin of ocular microtremor in man. *Experimental Brain Research*, 126(4):556–62, June 1999.

48. P Brown. A new clinical technique for demonstrating changes in eye acceleration during horizontal saccades in patients with partial internuclear ophthalmoplegias. *Journal of Neuro-Ophthalmology*, 1998.

49. N F Sheahan, D Coakley, F Hegarty, C Bolger, and J Malone. Ocular microtremor measurement system: design and performance. *Medical and Biological Engineering and Computing*, 31(3):205–212, 1993.

50. E Kowler. *Eye Movements and Their Role in Visual and Cognitive Processes*. Elsevier Science Ltd, 1990.

51. R M Steinman, G M Haddad, A A Skavenski, and D Wyman. Miniature eye movement. *Science*, 181(102):810–819, 1973.

52. M Rolfs. Microsaccades: small steps on a long way. *Vision research*, 49(20):2415–41, October 2009.

53. R W Ditchburn. *Eye-movements and visual perception*. Clarendon Press, 1973.

54. S Martinez-Conde, S L Macknik, and D H Hubel. The role of fixational eye movements in visual perception. *Nature reviews. Neuroscience*, 5(3):229–40, March 2004.

55. S Martinez-Conde, S L Macknik, X G Troncoso, and T A Dyar. Microsaccades counteract visual fading during fixation. *Neuron*, 49(2):297–305, January 2006.

56. I P V Troxler. *Über das Verschwinden gegebener Gegenstände innerhalb unseres Gesichtskreises*, volume II, pages 1–53. F. Fromann, Jena, Germany, 1804.

57. R M Steinman, R J Cunitz, G T Timberlake, and M Herman. Voluntary control of microsaccades during maintained monocular fixation. *Science*, 155(769):1577–1579, 1967.

58. E Gowen and R V Abadi. Saccadic instabilities and voluntary saccadic behaviour. *Experimental Brain Research*, 164(1):29–40, July 2005.

59. E Kowler and R M Steinman. Miniature saccades: eye movements that do not count. *Vision Research*, 19(1):105–108, 1979.

60. B J Winterson and H Collewijn. Microsaccades during finely guided visuomotor

tasks. *Vision Research*, 16(12):1387–1390, 1976.

61. R Rolfs, Mand Engbert. Toward a model of microsaccade generation : The case of microsaccadic inhibition. *Journal of Vision*, 8:1–23, 2008.

62. M Rolfs, J Laubrock, and R Kliegl. Shortening and prolongation of saccade latencies following microsaccades. *Experimental Brain Research*, 169(3):369–376, 2006.

63. E Kowler and R M Steinman. Small saccades serve no useful purpose: reply to a letter by R. W. Ditchburn. *Vision Research*, 20(3):273–276, 1980.

64. R Engbert. Microsaccades uncover the orientation of covert attention. *Vision Research*, 43(9):1035–1045, April 2003.

65. E Kowler. Eye movements: The past 25years. *Vision research*, (January), January 2011.

66. A M Bronstein and M A Gresty. Short latency compensatory eye movement responses to transient linear head acceleration: a specific function of the otolith-ocular reflex. *Experimental Brain Research*, 71(2):406–410, 1988.

67. R J Leigh and D S Zee. *The neurology of eye movements (Book/DVD). Fourth edition.* New York: Oxford University Press, 2006.

68. R M Steinman and H Collewijn. Binocular retinal image motion during active head rotation. *Vision Research*, 20(5):415–429, 1980.

69. H Collewijn, A J Martins, and R M Steinman. Compensatory eye movements during active and passive head movements: fast adaptation to changes in visual magnification. *The Journal of Physiology*, 340:259–286, 1983.

70. G E Grossman, R J Leigh, D J Lanska, S E Thurston, and L A Abel. Frequency and velocity of rotational head perturbations during locomotion. *Experimental Brain Research*, 70(3):470–476, 1988.

71. G R Barnes and R Smith. The effects of visual discrimination of image movement across the stationary retina. *Aviation space and environmental medicine*, 52(8):466–472, 1981.

72. I P Howard and B J Rogers. *Vergence Eye Movements*, chapter 10, pages 381–426. Oxford University Press, Clarendon Press, New York, Oxford, 1995.

73. E E Maddox. *The Clinical use of Prisms; and the Decentering of Lenses.* 1893.

74. D A Owens and H W Liebowitz. Accommodation, convergence, and distance perception in low illumination. *American Journal of Optometry and Physiological Optics*, 57(9):540–550, 1980.

75. S K Fisher, K J Ciuffreda, B Tannen, and P Super. Stability of tonic vergence. *Investigative Ophthalmology & Visual Science*, 29(10):1577–1581, 1988.

76. E F Fincham. Accommodation and convergence in the absence of retinal images.

Vision Research, 1(5-6):425 – 432, 1962.

77. M Alpern. Vergence and accommodation: I can change in size induce vergence movements? *AMA Arch Ophthalmol*, 60(3):355–357, 1958.

78. C Rashbass and G Westheimer. Disjunctive eye movements. *The Journal of Physiology*, 159(2):339, 1961.

79. C J Erkelens, R M Steinman, and H Collewijn. Ocular vergence under natural conditions. I. Continuous Changes of Target Distance Along the Median Plane. 236(1285):441–65, May 1989.

80. J R Carl and R S Gellman. Human smooth pursuit: stimulus-dependent responses. *Journal of Neurophysiology*, 57(5):1446–1463, 1987.

81. C J Erkelens. Coordination of smooth pursuit and saccades. *Vision Research*, 46(1-2):163–170, 2006.

82. H Kimmig, M Biscaldi, J Mutter, J P Doerr, and B Fischer. The initiation of smooth pursuit eye movements and saccades in normal subjects and in "express-saccade makers". *Experimental Brain Research*, 144(3):373–384, 2002.

83. D A Robinson. The mechanics of human smooth pursuit eye movement. *The Journal of Physiology*, 180(3):569–591, 1965.

84. A Tavassoli and D L Ringach. Dynamics of smooth pursuit maintenance. *Journal of Neurophysiology*, 102(1):110–118, 2009.

85. S G Lisberger, E J Morris, and L Tychsen. Visual motion processing and sensory-motor integration for smooth pursuit eye movements. *Annual review of neuroscience*, 10:97–129, January 1987.

86. S De Brouwer, M Missal, G Barnes, and P Lefèvre. Quantitative analysis of catch-up saccades during sustained pursuit. *Journal of Neurophysiology*, 87(4):1772–1780, 2002.

87. E Kowler and S P McKee. Sensitivity of smooth eye movement to small differences in target velocity. *Vision Research*, 27(6):993–1015, 1987.

88. L Schalén. Quantification of tracking eye movements in normal subjects. *Acta oto-laryngologica*, 90(5-6):404–413, 1980.

89. J Pola and H J Wyatt. Offset dynamics of human smooth pursuit eye movements: effects of target presence and subject attention. *Vision Research*, 37(18):2579–2595, 1997.

90. C H Meyer, A G Lasker, and D A Robinson. The upper limit of human smooth pursuit velocity. *Vision Research*, 25(4):561–563, 1985.

91. Omer Yilmaz, Nese Alagoz, Gokhan Pekel, Engin Azman, Ebru F. Aksoy, Hanefi Cakir, Ercument Bozkurt, and Ahmet Demirok. Intracorneal inlay to correct pres-

byopia: Long-term results. *Journal of Cataract and Refractive Surgery*, 37(7):1275 – 1281, 2011.

92. H Collewijn, F van der mark, and T C Jansen. Precise recording of human eye movements. *Vision Research*, 15(3):447–450, March 1975.

93. D A Robinson. The mechanics of human saccadic eye movement. *The Journal of Physiology*, pages 245–264, 1964.

94. E Grossman, R John Leigh, N Bruce, and J Lanska. Performance of the Human During Locomotion Vestibuloocular Reflex. *Neurophysiology*, 62(1):264–272, 1989.

95. E Paperno and D Semyonov. A new method for eye location tracking. *IEEE transactions on bio-medical engineering*, 50(10):1174–9, October 2003.

96. H Kasper and B J Hess. Magnetic search coil system for linear detection of three-dimensional angular movements. *IEEE transactions on bio-medical engineering*, 38(5):466–75, May 1991.

97. R S Remmel. An inexpensive eye movement monitor using the scleral search coil technique. *IEEE Transactions on Biomedical Engineering*, (4):388–390, 1984.

98. R H Schor and J M Furman. The "practical mathematics" of recording three-dimensional eye position using scleral coils. *Methods (San Diego, Calif.)*, 25(2):164–85, October 2001.

99. L R Young and D Sheena. Eye-movement measurement techniques. *The American psychologist*, 30(3):315–30, March 1975.

100. F Träisk, R Bolzani, and J Ygge. A comparison between the magnetic scleral search coil and infrared reflection methods for saccadic eye movement analysis. *Graefe's archive for clinical and experimental ophthalmology = Albrecht von Graefes Archiv für klinische und experimentelle Ophthalmologie*, 243(8):791–7, August 2005.

101. H Collewijn, J van der Steen, and R M Steinman. Human eye movements associated with blinks and prolonged eyelid closure. *Journal of neurophysiology*, 54(1):11–27, July 1985.

102. A Sprenger, B Neppert, S Köster, S Gais, C Kömpf, Dand Helmchen, and H Kimmig. Long-term eye movement recordings with a scleral search coil-eyelid protection device allows new applications. *Journal of neuroscience methods*, 170(2):305–9, May 2008.

103. M A Frens and J N van der Geest. Scleral search coils influence saccade dynamics. *Journal of Neurophysiology*, 88(2):692–8, August 2002.

104. OH Mowrer, TC Ruch, and NE Miller. The corneo-retinal potential difference as the basis of the galvanometric method of recording eye movements. *American Journal of Physiology*, 114:423, 1936.

105. A W North. Accuracy and Precision of Electro-Oculographic Recording. *Investigative Ophthalmology*, 4:343–8, June 1965.

106. B Shackel. Pilot study in electro-oculography. *British Journal of Ophthalmology*, 44(2):89, 1960.

107. H D Crane and C M Steele. Accurate three-dimensional eyetracker. *Applied Optics*, 17(5):691–705, March 1978.

108. H D Crane and C M Steele. Generation-V dual-Purkinje-image eyetracker. *Applied Optics*, 24(4):527, February 1985.

109. T N Cornsweet and H D Crane. Accurate two-dimensional eye tracker using first and fourth Purkinje images. *Journal of the Optical Society of America*, 63(8):921–8, August 1973.

110. C Langenbucher, Aand Jakob, S Reese, and B Seitz. Determination of pseudophakic accommodation with translation lenses using Purkinje image analysis. *Ophthalmic & physiological optics : the journal of the British College of Ophthalmic Opticians (Optometrists)*, 25(2):87–96, March 2005.

111. G Youssefi and F Moritz. Method and Apparatus for Eye Alignment, October 2004.

112. 3D Video-Oculugraphy, January 2011.

113. Arrington Research HMD Eye Trackign System, January 2011.

114. Chronos Vision C-ETD, January 2011.

115. Sr Research EyeLink II, January 2011.

116. ASL Head Mounted EyeTRAC6 Binocular, January 2011.

117. SMI iViewX Hi Speed, January 2011.

118. J N van der Geest and M A Frens. Recording eye movements with video-oculography and scleral search coils: a direct comparison of two methods. *Journal of Neuroscience Methods*, 114(2):185–95, March 2002.

119. M M J Houben, J Goumans, and J van der Steen. Recording three-dimensional eye movements: scleral search coils versus video oculography. *Investigative ophthalmology & visual science*, 47(1):179–87, January 2006.

120. H Deubel and B Bridgeman. Fourth Purkinje image signals reveal eye-lens deviations and retinal image distortions during saccades. *Vision research*, 35(4):529–38, February 1995.

121. Y. Le Grand. *Physiological Optics*. Springer-Verlag, Berlin, 1980.

122. W Lotmar. Theoretical Eye Model with Aspherics. *Journal of the Optical Society of America*, 61(11):1522, 1971.

123. H L Liou and N A Brennan. Anatomically accurate, finite model eye for optical modeling. *Journal of the Optical Society of America A*, 14(8):1684–1695, 1997.

124. R Navarro, J Santamaría, and J Bescós. Accommodation-dependent model of the

human eye with aspherics. *Journal of the Optical Society of America*, 2(8):1273–1281, 1985.

125. P M Kiely, G Smith, and L G Carney. The mean shape of the human corneal. *Optica Acta*, 29(8):1027–1040, 1982.

126. M Dubbelman, V A D P Sicam, and G L Van Der Heijde. The shape of the anterior and posterior surface of the aging human cornea. *Vision Research*, 46(6-7):993–1001, 2006.

127. J M Tiffany. Refractive index of meibomian and other lipids. *Current Eye Research*, 5(11):887–889, 1986.

128. J P Craig, P a Simmons, S Patel, and A Tomlinson. Refractive index and osmolality of human tears., October 1995.

129. A C Kooijman. Light distribution on the retina of a wide-angle theoretical eye. *Journal of the Optical Society of America*, 73(11):1544–1550, 1983.

130. S Barbero. Refractive power of a multilayer rotationally symmetric model of the human cornea and tear film. *Journal of the Optical Society of America A*, 23(7):1578–1585, 2006.

131. D R Korb. *The Tear Film*. Butterworth-Heinemann, Oxford, 2002.

132. G Smolin, C S Foster, D T Azar, and C H Dohlman. *Smolin and Thoft's The cornea: scientific foundations and clinical practice*. Lippincott Williams and Wilkins, Philadelphia, 2005.

133. S Patel, J Marshall, and F W Fitzke. Refractive index of the Human Corneal Epithelium and Stroma. *Journal of Refractive Surgery*, 11(2):100–105, 1995.

134. P T Ashwin, S Shah, S Pushpoth, L Wehbeh, and B Ilango. The relationship of Central Corneal Thickness (CCT) to Thinnest Central Cornea (TCC) in healthy adults. *Contact lens & anterior eye : the journal of the British Contact Lens Association*, 32(2):64–7, April 2009.

135. ICNIRP. ICNIRP GUIDELINES: Guidelines on the exposure to Broadband Incoherent Optical Radiation(0.38um to 5um). *Health Physics*, 73(3):539–554, 1997.

136. ICNIRP. ICNIRP GUIDELINES: Light-Emitting Diodes (LEDS) and Laser Diodes: Implications for Hazard Assessment. *Health Physics*, 78(6):744–752, 2000.

137. D Sliney and M Wolbarst. *Saftey with Lasers and other Optical Sources*. Plenum Press, New York, 1980.

138. J S Babcock and J B Pelz. Building a lightweight eyetracking headgear. *Proceedings of the Eye tracking research & applications symposium on Eye tracking research & applications - ETRA'2004*, pages 109–114, 2004.

139. B R Barker and Y Li. *Power Analysis for Experimental Research: A Practical Guide*

for the Biological, Medical and Social Sciences. Cambridge University Press, West Nyack, NY, USA, 2002.

140. W B Hays. *Statistics for the Social Sciences*. Holt, Rinehart and Winston, New York, 1973.

141. H Scheffe. *The Analysis of Variance*. Wiley, New York, 1959.

142. S H Park, M Kim, and C-K Joo. Measurement of pupil centroid shift and cyclotorsional displacement using iris registration. *Ophthalmologica. Journal international d'ophtalmologie. International journal of ophthalmology. Zeitschrift für Augenheilkunde*, 223(3):166–71, January 2009.

143. H J Wyatt. The form of the human pupil. *Vision research*, 35(14):2021–36, July 1995.

144. C Fedtke, F Manns, and A Ho. The entrance pupil of the human eye: a three-dimensional model as a function of viewing angle. *Optics express*, 18(21):22364–76, October 2010.

145. D F Fisher, R A Monty, and J W Senders. *Eye movements : cognition and visual perception*. L. Erlbaum Associates, Hillsdale, N.J, 1981.

146. M Rolfs, R Engbert, and R Kliegl. Crossmodal coupling of oculomotor control and spatial attention in vision and audition. *Experimental Brain Research*, 166(3-4):427–39, October 2005.

147. F Ratliff and L A Riggs. Involuntary motions of the eye during monocular fixation. *Journal of Experimental Psychology*, 40(6):687–701, December 1950.

148. R W Ditchburn and B L Ginsborg. Involuntary eye movements during fixation. *The Journal of physiology*, 119(1):1–17, January 1953.

149. R M Steinman. Effect of Target Size, Luminance, and Color on Monocular Fixation. *Journal of the Optical Society of America*, 55(9):1158, September 1965.

150. J Otero-Millan, X G Troncoso, S L Macknik, I Serrano-Pedraza, and S Martinez-Conde. Saccades and microsaccades during visual fixation, exploration, and search: Foundations for a common saccadic generator. *Journal of Vision*, 8(14), 2008.

151. R A Armstrong, S V Slade, and F Eperjesi. Statistical Review An introduction to analysis of variance (ANOVA) with special reference to data from clinical experiments in optometry. *Ophthalmic and Physiological Optics*, 20(3):235–241.

152. R A Armstrong, F Eperjesi, and B Gilmartin. The application of analysis of variance (ANOVA) to different experimental designs in optometry. *Ophthalmic and Physiological Optics*, 22(3):248–56, May 2002.

153. D H Fender. Variation of fixation direction with colour of fixation target. *The British Journal of Ophthalmology*, 39(5):294–7, May 1955.

154. R M Steinman, Z Pizlo, T I Forofonova, and J Epelboim. One fixates accurately in order to see clearly not because one sees clearly. *Spatial Vision*, 16(3-4):225–41, January 2003.

155. B Bridgeman and P Palca. The role of microsaccades in high acuity observational tasks. *Vision Research*, 20(9):813 – 817, 1980.

156. H Ko, M Poletti, and M Rucci. Fixational eye movements in a high-acuity visual task. *Journal of Vision*, 9(8):430, 2009.

157. R Engbert and R Kliegl. Microsaccades keep the eyes' balance during fixation. *Psychological Science*, 15(6):431, 2004.

158. E Gambra, Y Wang, J Yuan, P B Kruger, and S Marcos. Dynamic accommodation with simulated targets blurred with high order aberrations. *Vision Research*, 50(19):1922 – 1927, 2010.

159. P B Kruger and J Pola. Stimuli for accommodation: Blur, chromatic aberration and size. *Vision Research*, 26(6):957 – 971, 1986.

APPENDICES

Appendix A

Additional Geometric Model Cornea Calculations

A.1 Introduction

The thesis outlines an accurate geometric model cornea which primarily models the geometry of the cornea's central optical zone. With additional knowledge of the refractive properties of the cornea a selection of the cornea's optical properties can be investigated. Of particular interest in the context of this research is the amplitude of reflection from the anterior and posterior cornea.

The thesis states that the v360 pachymeter receives the highest amplitude in return signal from both the anterior corneal surface and the posterior corneal surface when aligned on the anterior apex. As the measurement becomes increasingly misaligned the amplitude in return signal starts to deteriorate; however, this deterioration is more extreme in the reflection from the posterior surface as the incident light is initially refracted through the cornea. The amount of reflection relative to the angle of incidence can be calculated using the Fresnel equations.

The consequence of this relationship is that the ratio of the reflected light from the anterior cornea over the posterior cornea is unique in the aligned position. The advantage in this is that the aligned position can potentially be identified using solely the measurement signal, in addition to this the amount of misalignment can be inferred by the drop in ratio.

To investigate the potential of a unique ratio at the aligned position a 2 dimensional version of the geometric model described in the thesis is interrogated using the refractive indicies of each layer of the cornea as additional parameters.

A.2 Aim

Determine the ratio of the reflections calculated from the models anterior surface over the reflection calculated from the model's posterior surface after refraction through the cornea.

A.3 Method

For a light ray traveling parallel to the eye's optical axis, the angle of incidence of the ray on the geometric model cornea was calculated. The ray was then traced through the different layers of the cornea and the angle of incidence calculated for the intersection with the posterior cornea. The magnitude of reflection was then calculated at the anterior and posterior cornea, using this the ratio of the anterior cornea reflection over the posterior cornea was determined. The ratios was then correlated with the distance away from the corneal apex.

A.4 Results

The simulation results found from the mathematical model suggest possible readings from an actual eye if the cornea was struck by a narrow beam of light running in parallel with the optical axis. Theoretically the mathematical model can produce results for any angle at which the light beam strikes the cornea providing that angle is known. The model does this by tracing the optical path of the light through the cornea to the endothelium – aqueous humour interface and then the reflection back through the cornea. Reflection and transmission coefficients are calculated using Fresnel equations. No consideration is given to the affects of absorption in each layer.

A.4.1 Peak to Peak Ratio

At each interface through the cornea a beam of light will reflect a certain amount of light depending on the angle of incidence and the refractive index of the two materials. The amount of light reflected has a direct correlation with the magnitude of change in refractive index between two materials, the larger the difference in refractive index the more incident light reflected. A similar relationship is found between the angle of incidence and reflection, the larger the angle of incidence the more light reflected from the interface. In particular the last relationship varies with the position at which the light beam strikes the cornea, in more peripheral regions the angle of incidence increases causing a higher percentage of the light to reflect and thus less transmitted light. The first interface between the air and the tear film provides the largest change in refractive index and therefore the highest peak, the second most prominent peak is formed by the interface between the endothelium and the aqueous humour, the distance between these peaks is then the corneal thickness at that particular point.

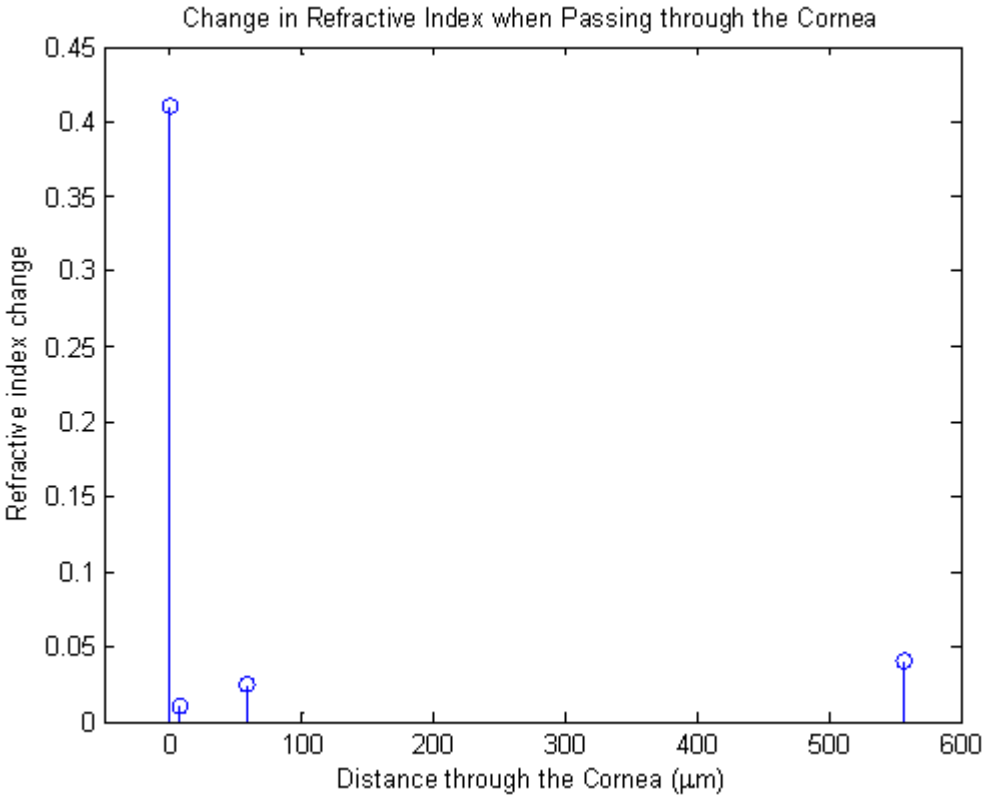

Figure A.1: Stem plot of the refractive index values at each layer of the cornea.

Figure A.1 describes the refractive indicies of each of the layers of the cornea used in the geometric model. The largest peak in the pachymeter return signal emanates from the anterior cornea, this is also the location of the largest refractive index change.

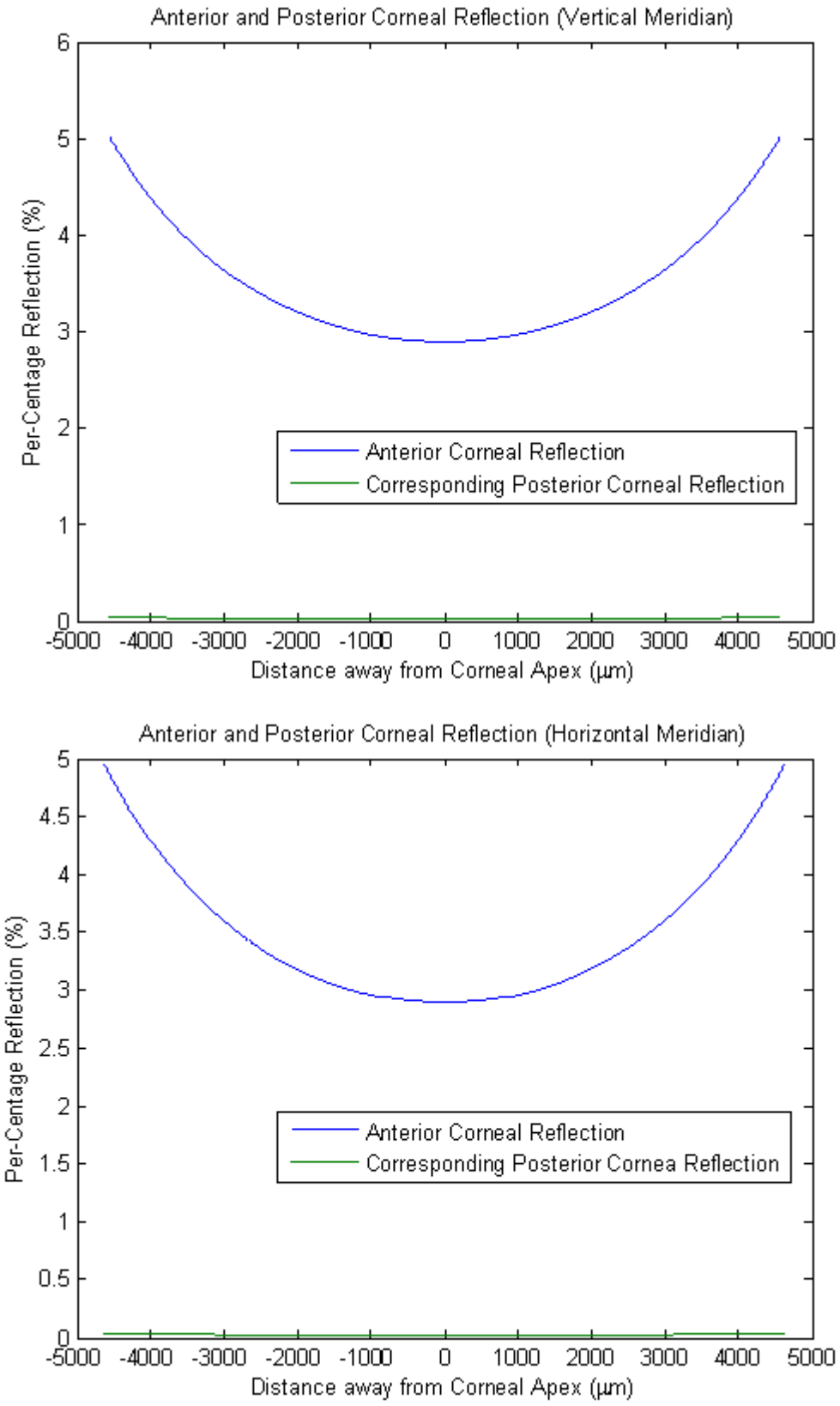

Figure A.2: Percentage reflection from the anterior cornea and the corresponding location on the posterior cornea for the vertical and horizontal meridians.

Figure A.2 shows the percentage reflection of incident light on both the anterior and posterior cornea in the vertical and horizontal meridians. The figure demonstrates the

large difference in reflections contributing to the difficulty in detection of the posterior interface. The figures also show the relatively small change in reflection from the posterior cornea when compared to the cornea as the ray moves away from the apex.

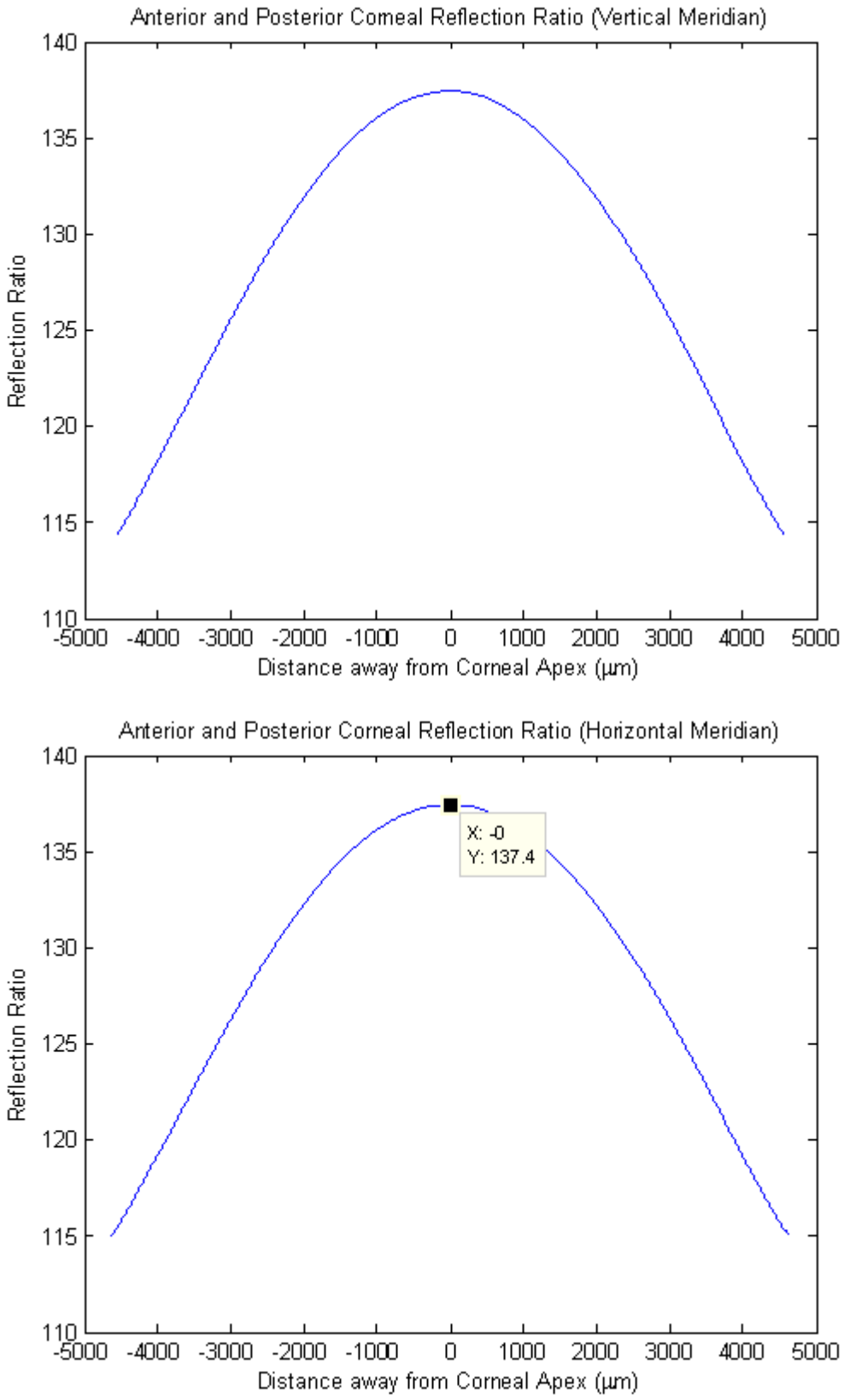

Figure A.3: The ratio of reflection from the anterior cornea over the posterior cornea, vertical and horizontal meridians.

Figure A.3 describes the ratio of the anterior reflection over the posterior reflection as a function of the distance away from the apex. The model suggests an alignment ratio of 134

in the aligned position. The figure also clearly indicates the drop in ratio as misalignment increases.

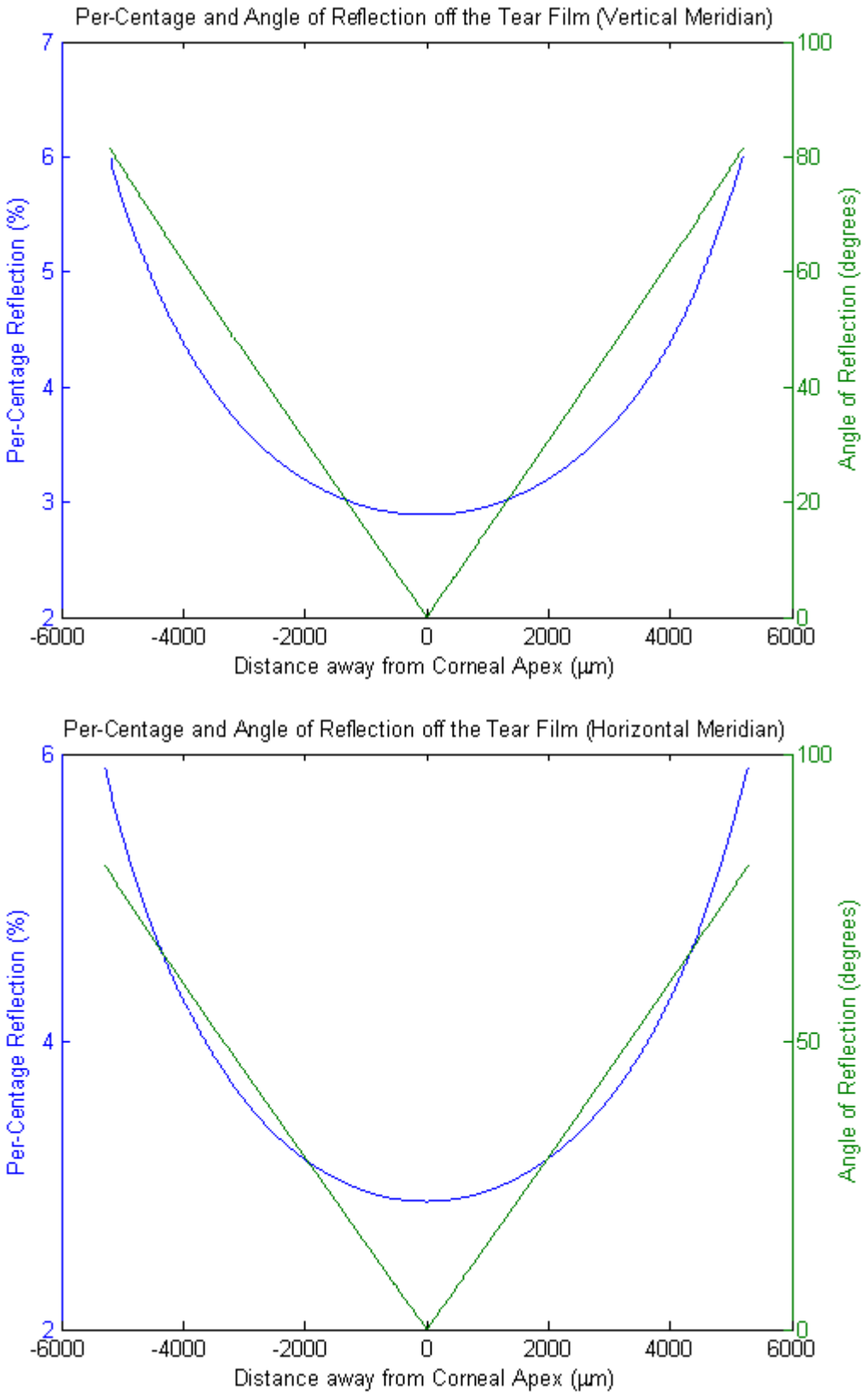

Figure A.4: Percentage and angle of reflection from the anterior cornea, vertical and horizontal meridians.

Figure A.4 shows the percentage reflection from the anterior cornea as a function of the distance away from the apex. The figure also shows the angle of reflection at each loca-

tion on the model's anterior cornea. It can be seen that the reflection increases as the misalignment from the apex increases, this due to the curved shape of the cornea.

A.5 Conclusions

The report summaries a multilayer anatomically accurate model cornea which simulates the reflection from the first and last interfaces contained with in the cornea assuming that each layer is homogeneous and there is a stable tear film. In reality these two assumptions are not viable as the tear film breaks up and thins between blinking. The stroma in particular is not a homogeneous medium as the refractive index actually decreases the closer it gets to the posterior interface. Due to these factors the signal from the posterior cornea is very poor in comparison to the signal from the anterior cornea, the suggested ratio of anterior peak divided by posterior peak would be highly variable, not just between person to person but in the individual. A potential solution to the problem which the dynamic nature of the tear film presents could lie in comparison of the first peak with the peak obtained from the corneal epithelium – stroma interface. There is a relatively large change in refractive index at this point leading to a noticeable peak; this particular peak should remain constant in the individual because this interface lacks the dynamic properties of the tear film. Again the lack of an datum to compare the readings would mean that a ratio would have to be predicted as the peak from the corneal epithelium - stroma interface would be dependent on transmission through the tear film. Another property which the model highlights is the increase in reflection off the tear film as the light strikes the cornea near the peripheral. The angle of reflection would also depend on the gradient of the cornea at the point of intersection. Monitoring the reflection from the tear film to track the eye rather than looking at the peak ratio means that the complex signal from the posterior cornea is no longer required. The problem then becomes the tear film break up and how this might affect the reflection coefficient from the anterior cornea. The model suggests a peak ratio of 137 would indicate alignment, but the ratio is based on a cornea with homogeneous layers and stable tear film, a way to compensate for the tear film would be to monitor the corneal epithelium – stroma interface, but as with the peak ratio there is no reliable datum. Other measures could include the monitoring of the reflection from the anterior cornea but again this can be highly variable due to the tear film.

Appendix B

Model Eye

REV	DCN	DESCRIPTION	DATE	BY
A	2632	CHANGE ITEM 4 GEOM. ADD DISTILLED TO NOTE 3	05/10/06	JR
B	3206	ADD DIMENSIONS. ADD NOTE 2. CHG MAT'L 5 TO RUBBER.	08/18/09	JR

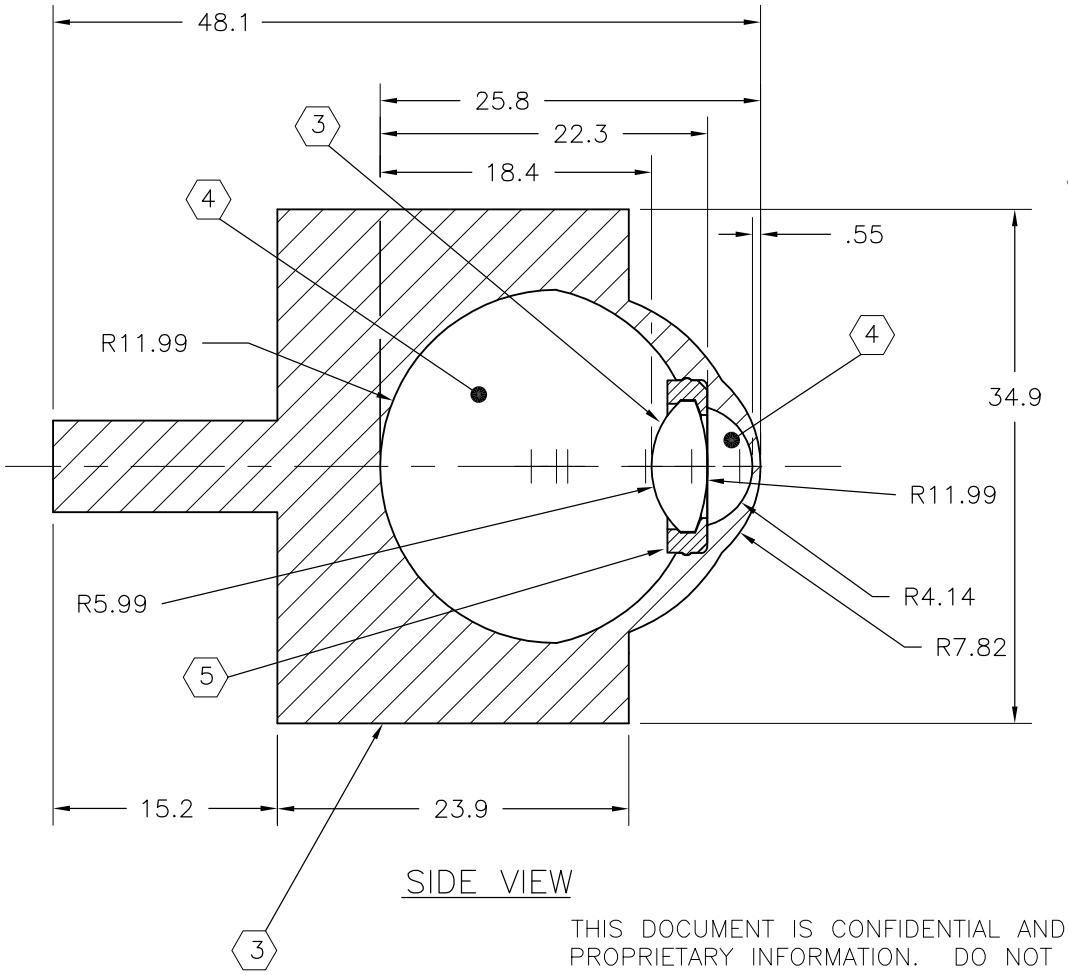

SIDE VIEW

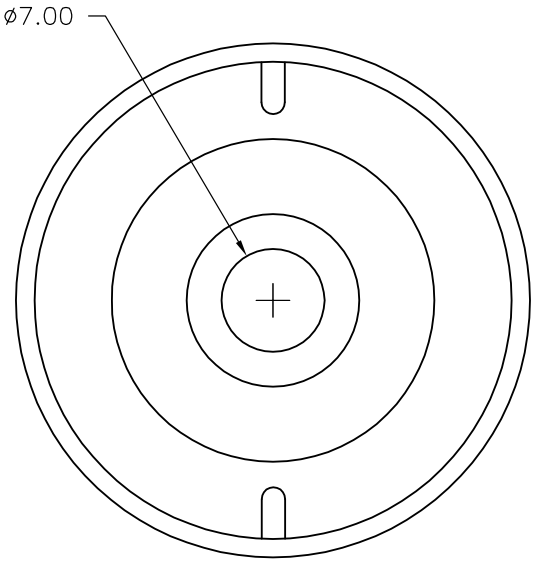

FRONT VIEW

NOTES:

1. ALL DIMENSIONS IN MM
2. (B) ALL TOLERANCES: .X=±.51, .XX=±.13, ANG=±.5°
3. PLASTIC
4. DISTILLED WATER
5. (B) RUBBER

OCULAR INSTRUMENTS, INC.

TITLE

OCULAR IMAGING EYE MODEL

DRAWN	J. RIEDEMANN	06/20/05	PRODUCT CLASS	SCALE	DRAWING NUMBER	REV
ENGR			860	2	OEMI-7	B
MFG						

Appendix C

Purkinje Image IV System Matrix Calculation

Calculations for of Purkinje Image IV system matrix and image height:

$$S_{IV} = P_{ca}.T_c.P_{cp}.T_{acd}.P_{la}.T_l.M_{lp}.T_l.P_{la}.T_{acd}.P_{cp}.T_c.P_{ca} = \begin{bmatrix} -1.46 & -336.18 \\ -0.0034 & -1.46 \end{bmatrix} \quad \text{(C.1)}$$

In which the matrices are constructed as follows:

$$P_{ca} = \begin{bmatrix} 1 & -RP_{ca} \\ 0 & 1 \end{bmatrix} = \begin{bmatrix} 1 & -(\frac{n_c-1}{Rca}) \\ 0 & 1 \end{bmatrix} = \begin{bmatrix} 1 & -(\frac{1.3771-1}{0.0078}) \\ 0 & 1 \end{bmatrix} = \begin{bmatrix} 1 & -48.35 \\ 0 & 1 \end{bmatrix}$$

$$T_c = \begin{bmatrix} 1 & 0 \\ \frac{ct}{n_c} & 1 \end{bmatrix} = \begin{bmatrix} 1 & 0 \\ \frac{0.00055}{1.3771} & 1 \end{bmatrix} = \begin{bmatrix} 1 & 0 \\ 0.0004 & 1 \end{bmatrix}$$

$$P_{cp} = \begin{bmatrix} 1 & -RP_{cp} \\ 0 & 1 \end{bmatrix} = \begin{bmatrix} 1 & -(\frac{n_a-n_c}{Rcp}) \\ 0 & 1 \end{bmatrix} = \begin{bmatrix} 1 & -(\frac{1.3374-1.3771}{0.0065}) \\ 0 & 1 \end{bmatrix} = \begin{bmatrix} 1 & 6.11 \\ 0 & 1 \end{bmatrix}$$

$$T_{acd} = \begin{bmatrix} 1 & 0 \\ \frac{acd}{n_a} & 1 \end{bmatrix} = \begin{bmatrix} 1 & 0 \\ \frac{0.00305}{1.3374} & 1 \end{bmatrix} = \begin{bmatrix} 1 & 0 \\ 0.0023 & 1 \end{bmatrix}$$

$$P_{la} = \begin{bmatrix} 1 & -RP_{la} \\ 0 & 1 \end{bmatrix} = \begin{bmatrix} 1 & -(\frac{n_l-n_a}{Rla}) \\ 0 & 1 \end{bmatrix} = \begin{bmatrix} 1 & -(\frac{1.42-1.3374}{0.0102}) \\ 0 & 1 \end{bmatrix} = \begin{bmatrix} 1 & -8.1 \\ 0 & 1 \end{bmatrix}$$

$$T_l = \begin{bmatrix} 1 & 0 \\ \frac{al}{n_l} & 1 \end{bmatrix} = \begin{bmatrix} 1 & 0 \\ \frac{0.004}{1.42} & 1 \end{bmatrix} = \begin{bmatrix} 1 & 0 \\ 0.0028 & 1 \end{bmatrix}$$

$$M_{lp} = \begin{bmatrix} 1 & \frac{R_{lp}}{2} \\ 0 & 1 \end{bmatrix} = \begin{bmatrix} 1 & -0.003 \\ 0 & 1 \end{bmatrix}$$

Appendix D

Graphical Data: Pupil Centre Movement

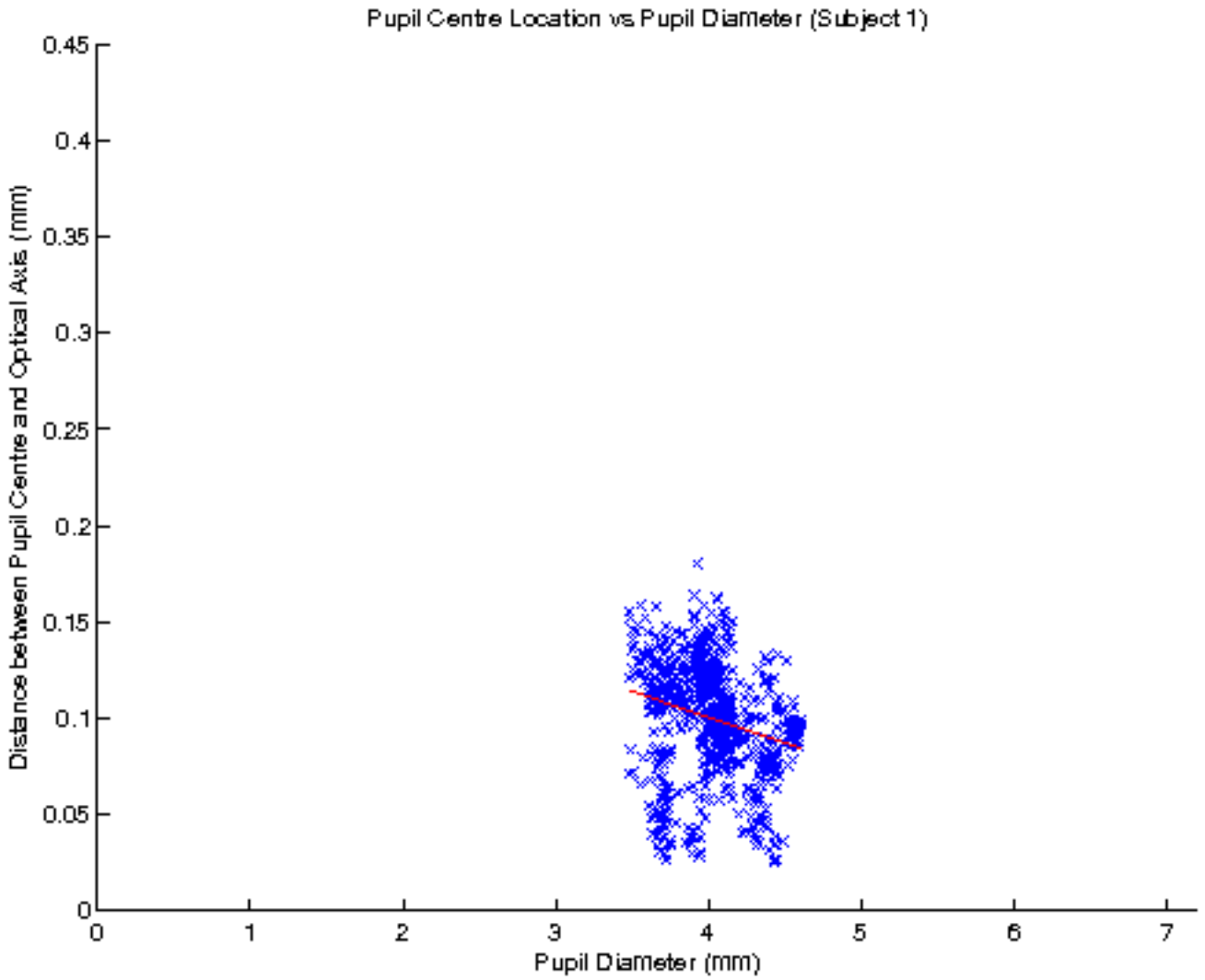

Figure D.1: Correlation between pupil diameter and the position of the pupil centre relative to the optical axis (Subject 1)

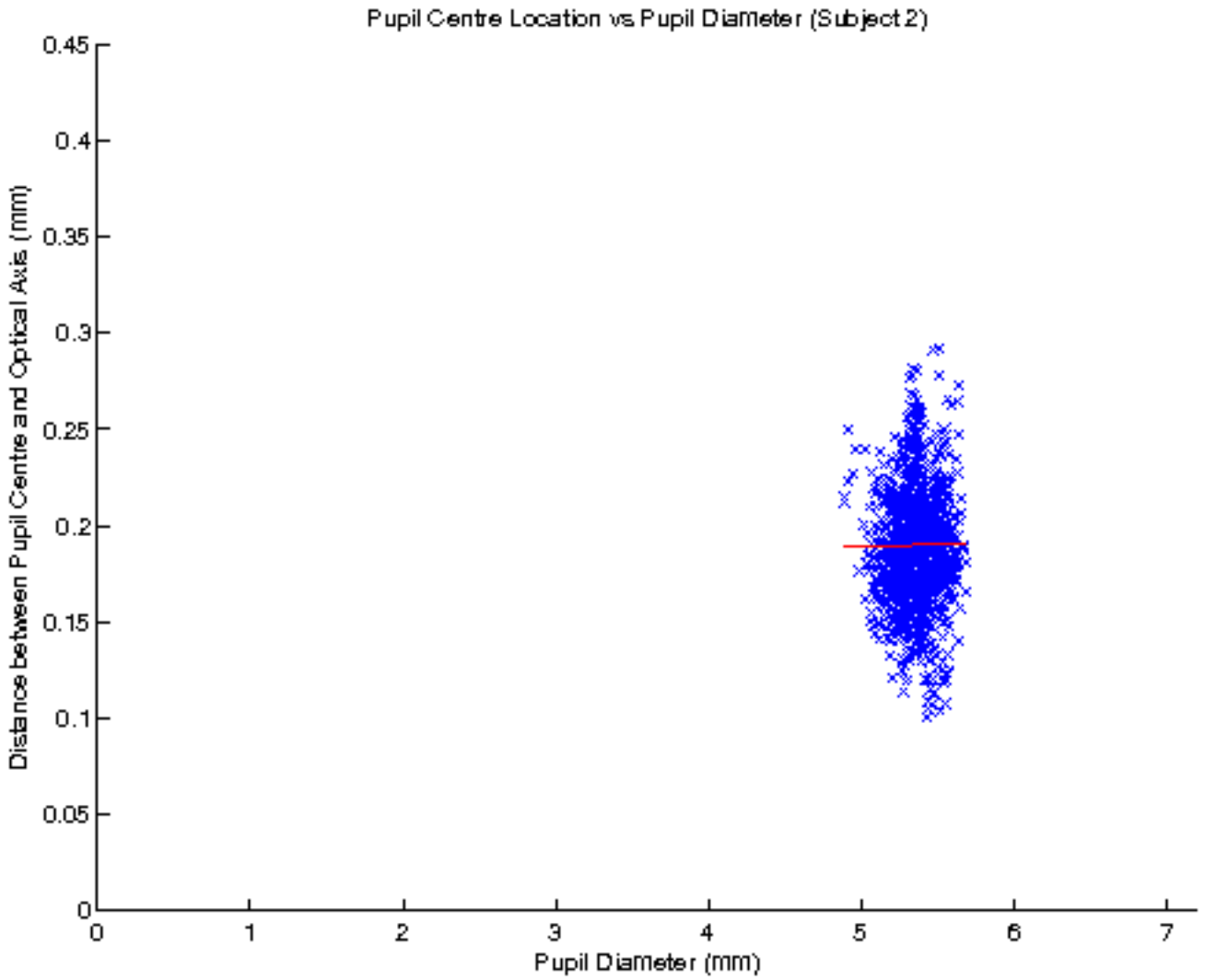

Figure D.2: Correlation between pupil diameter and the position of the pupil centre relative to the optical axis (Subject 2)

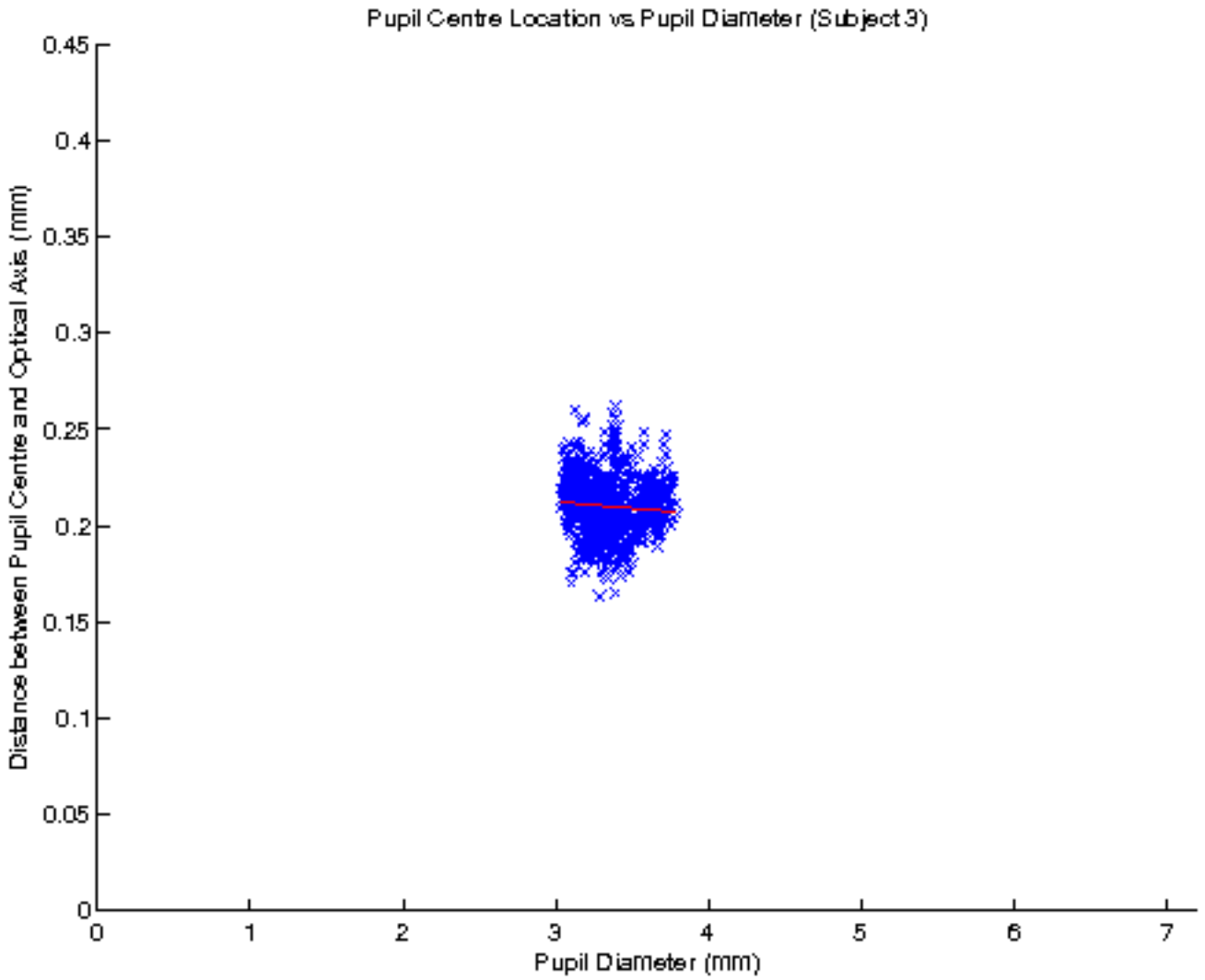

Figure D.3: Correlation between pupil diameter and the position of the pupil centre relative to the optical axis (Subject 3)

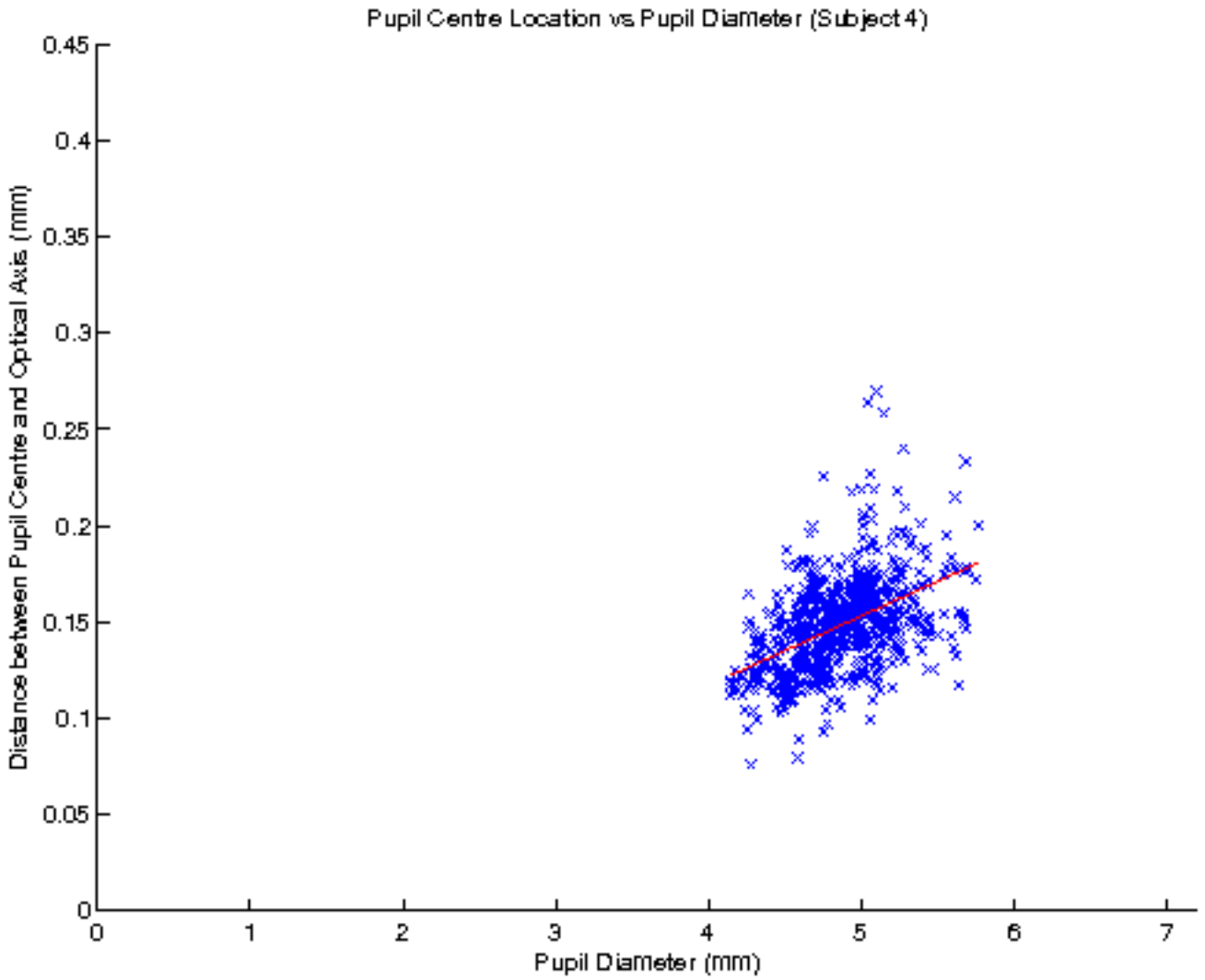

Figure D.4: Correlation between pupil diameter and the position of the pupil centre relative to the optical axis (Subject 4)

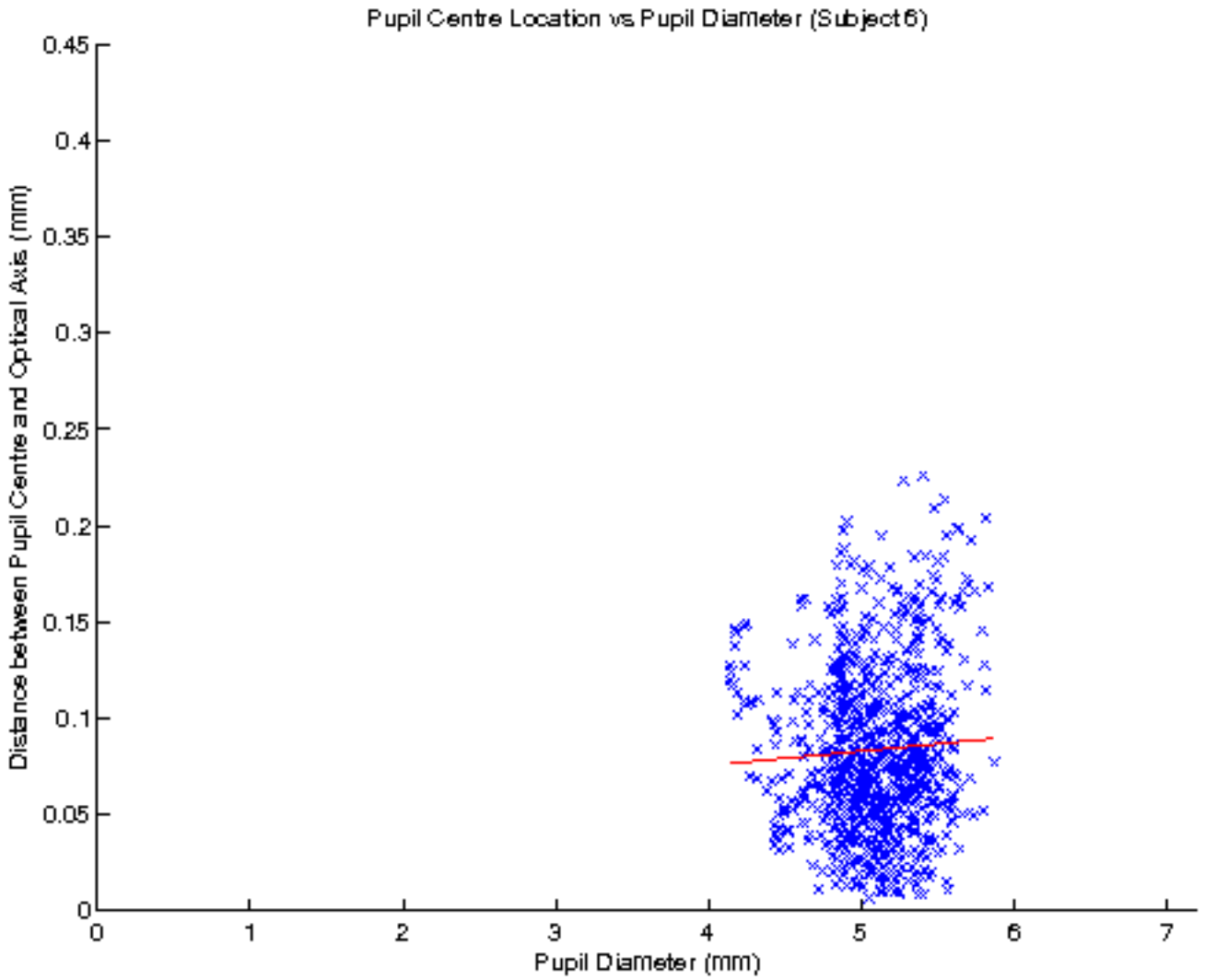

Figure D.5: Correlation between pupil diameter and the position of the pupil centre relative to the optical axis (Subject 6)

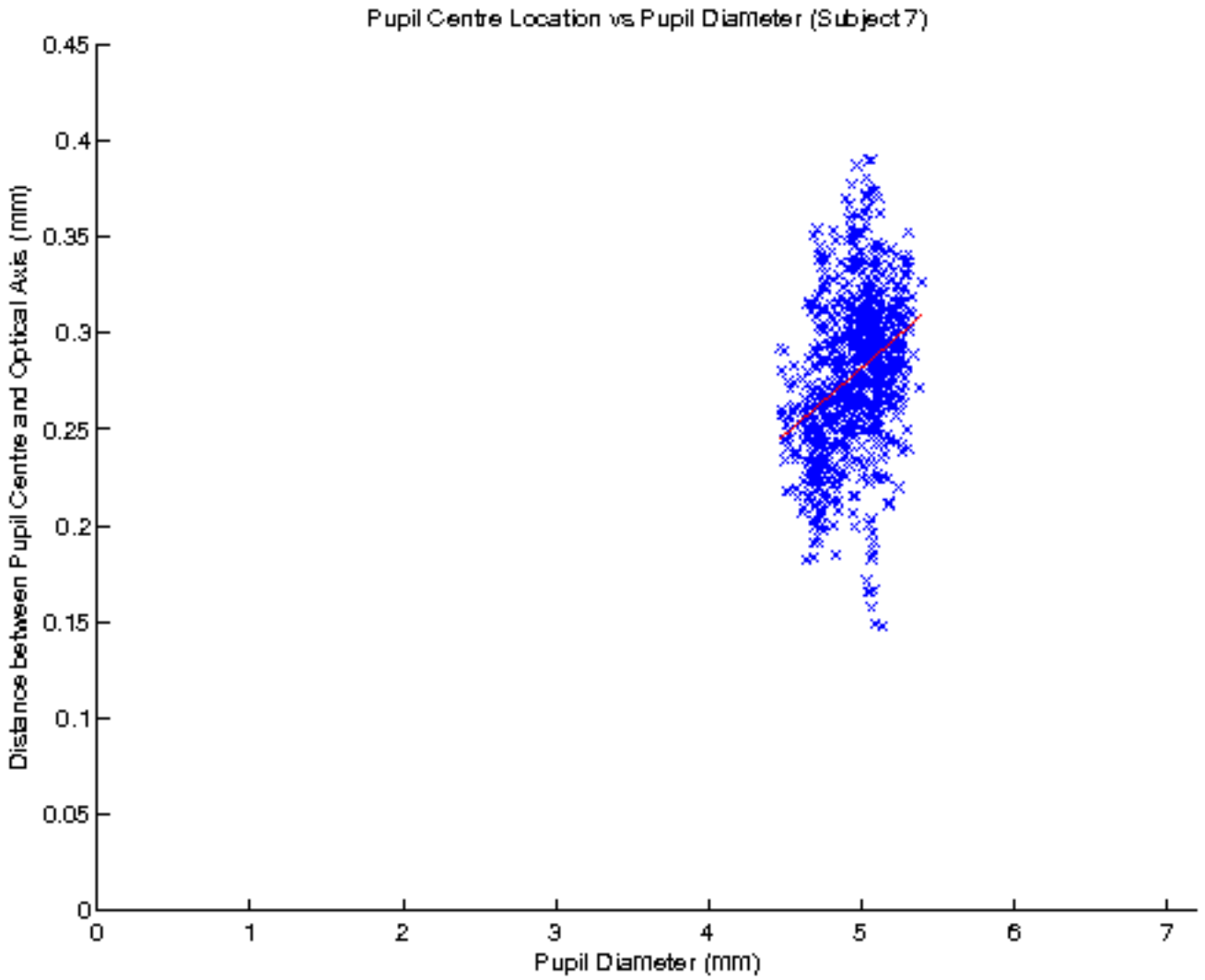

Figure D.6: Correlation between pupil diameter and the position of the pupil centre relative to the optical axis (Subject 7)

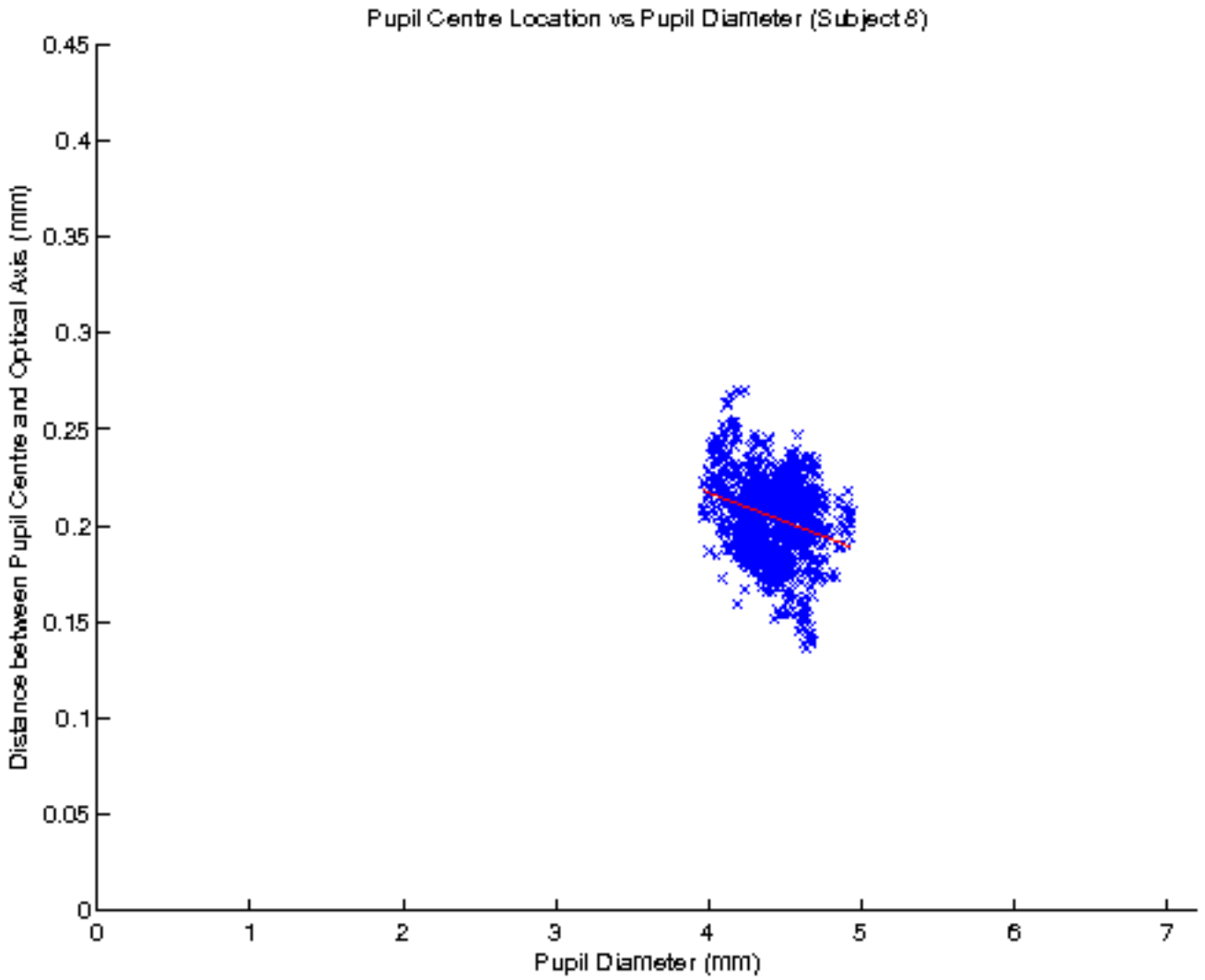

Figure D.7: Correlation between pupil diameter and the position of the pupil centre relative to the optical axis (Subject 8)

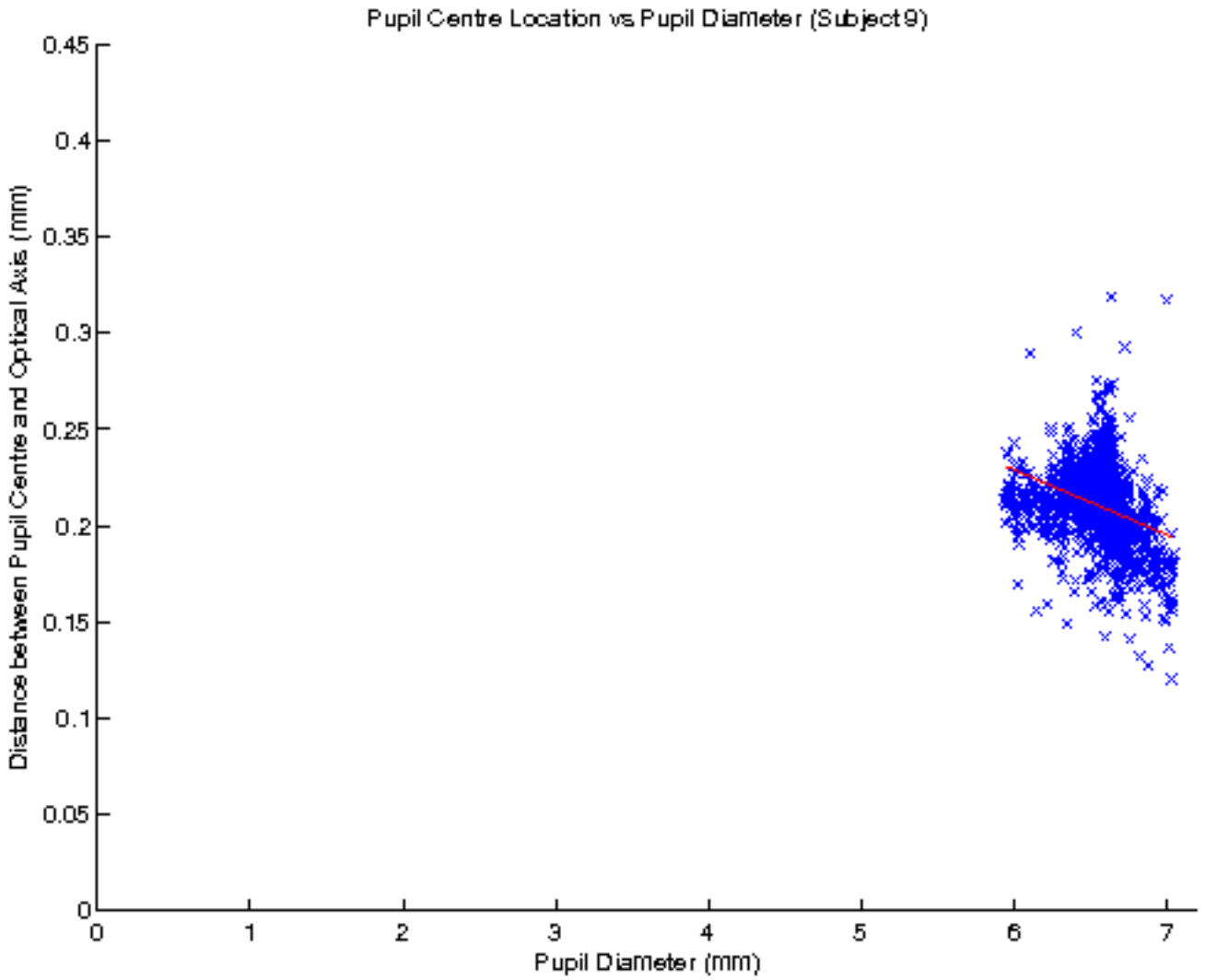

Figure D.8: Correlation between pupil diameter and the position of the pupil centre relative to the optical axis (Subject 9)

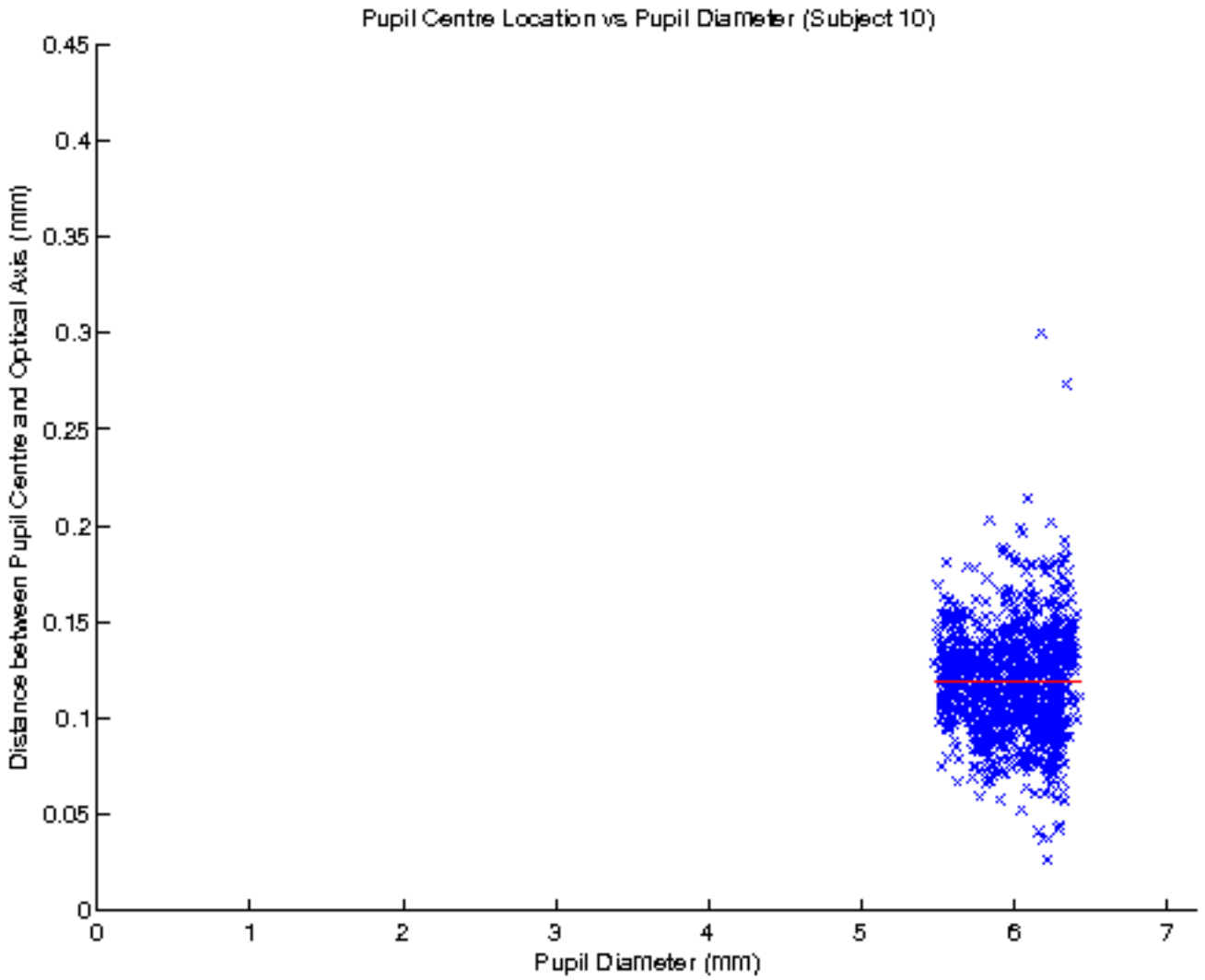

Figure D.9: Correlation between pupil diameter and the position of the pupil centre relative to the optical axis (Subject 10)

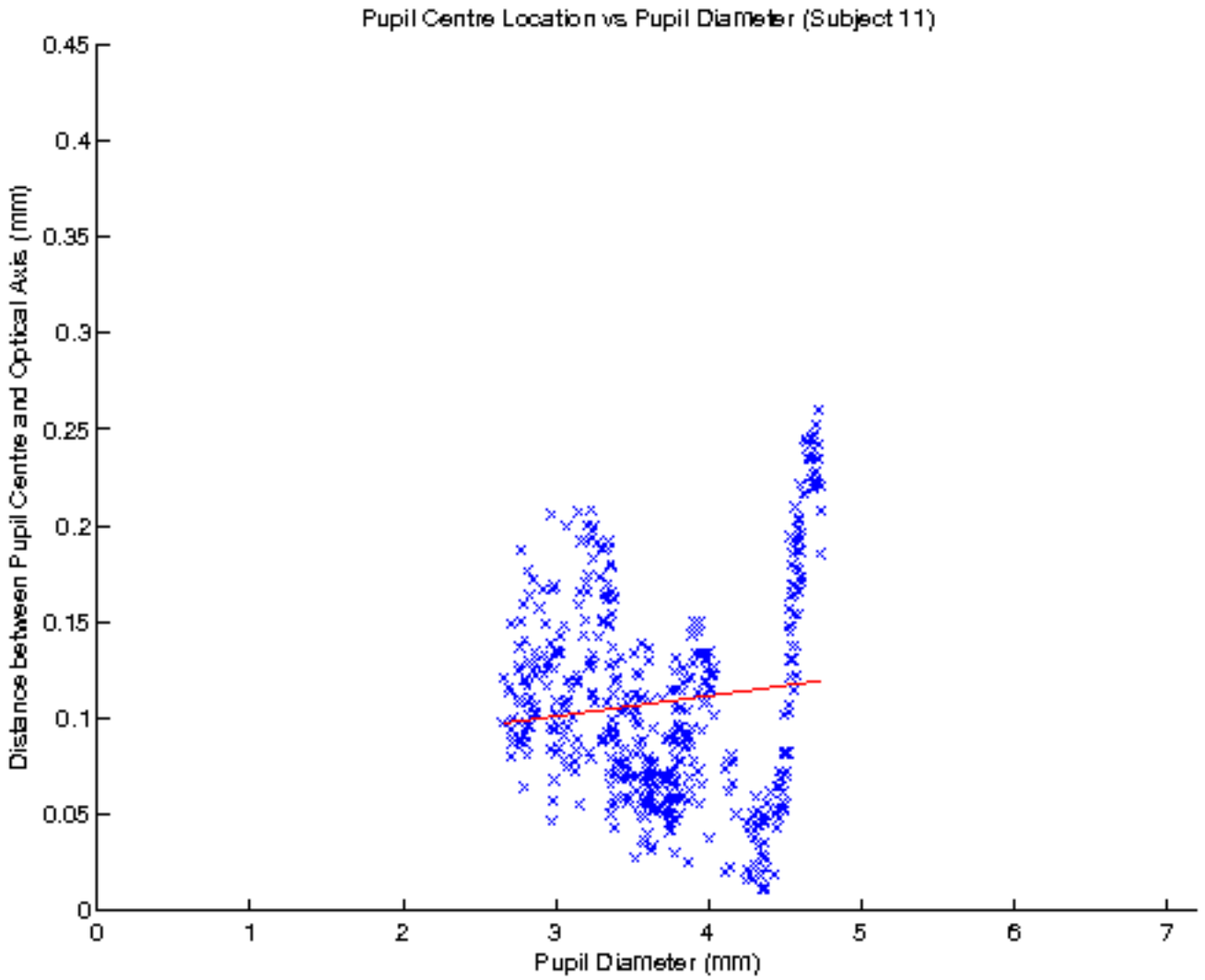

Figure D.10: Correlation between pupil diameter and the position of the pupil centre relative to the optical axis (Subject 11)

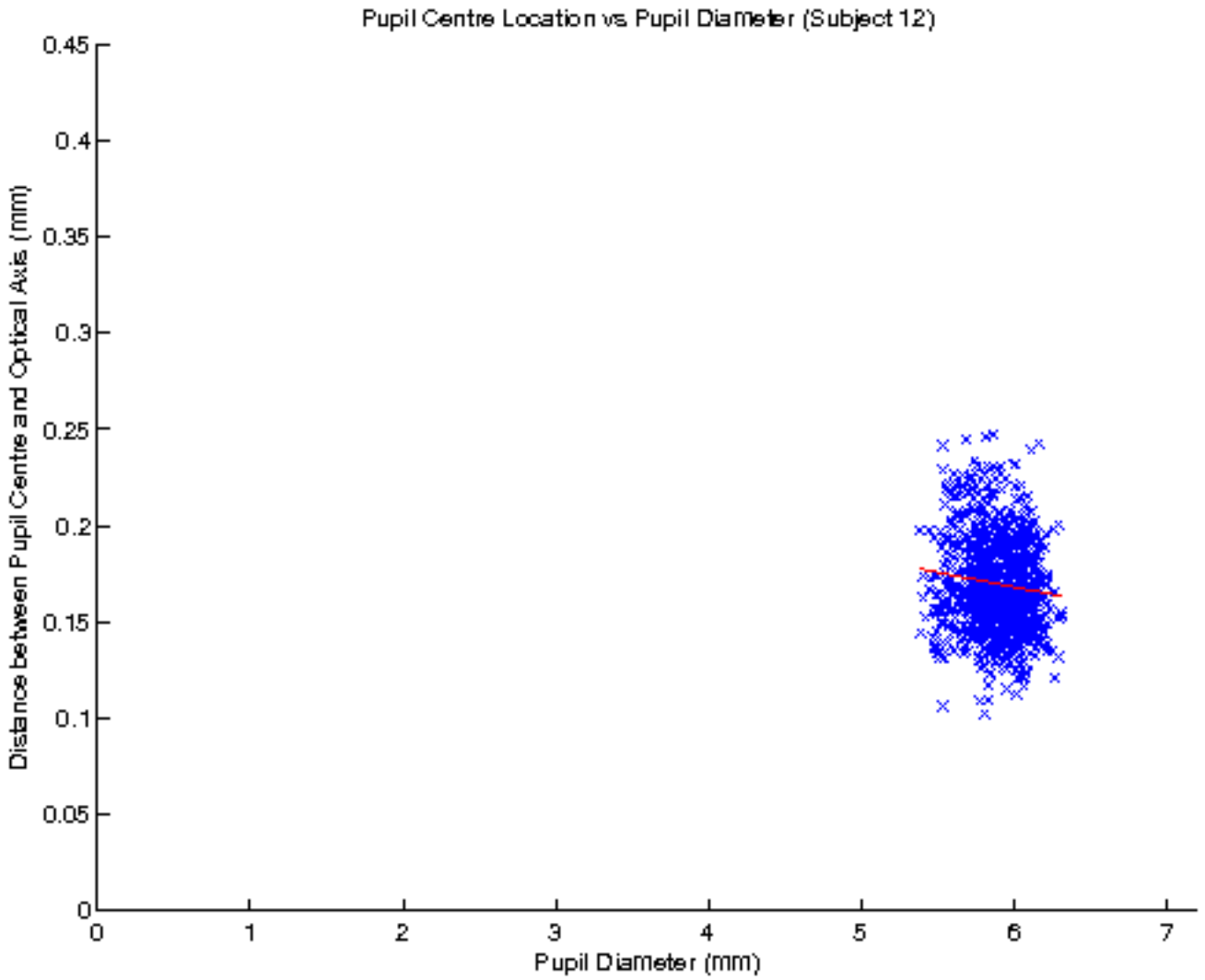

Figure D.11: Correlation between pupil diameter and the position of the pupil centre relative to the optical axis (Subject 12)

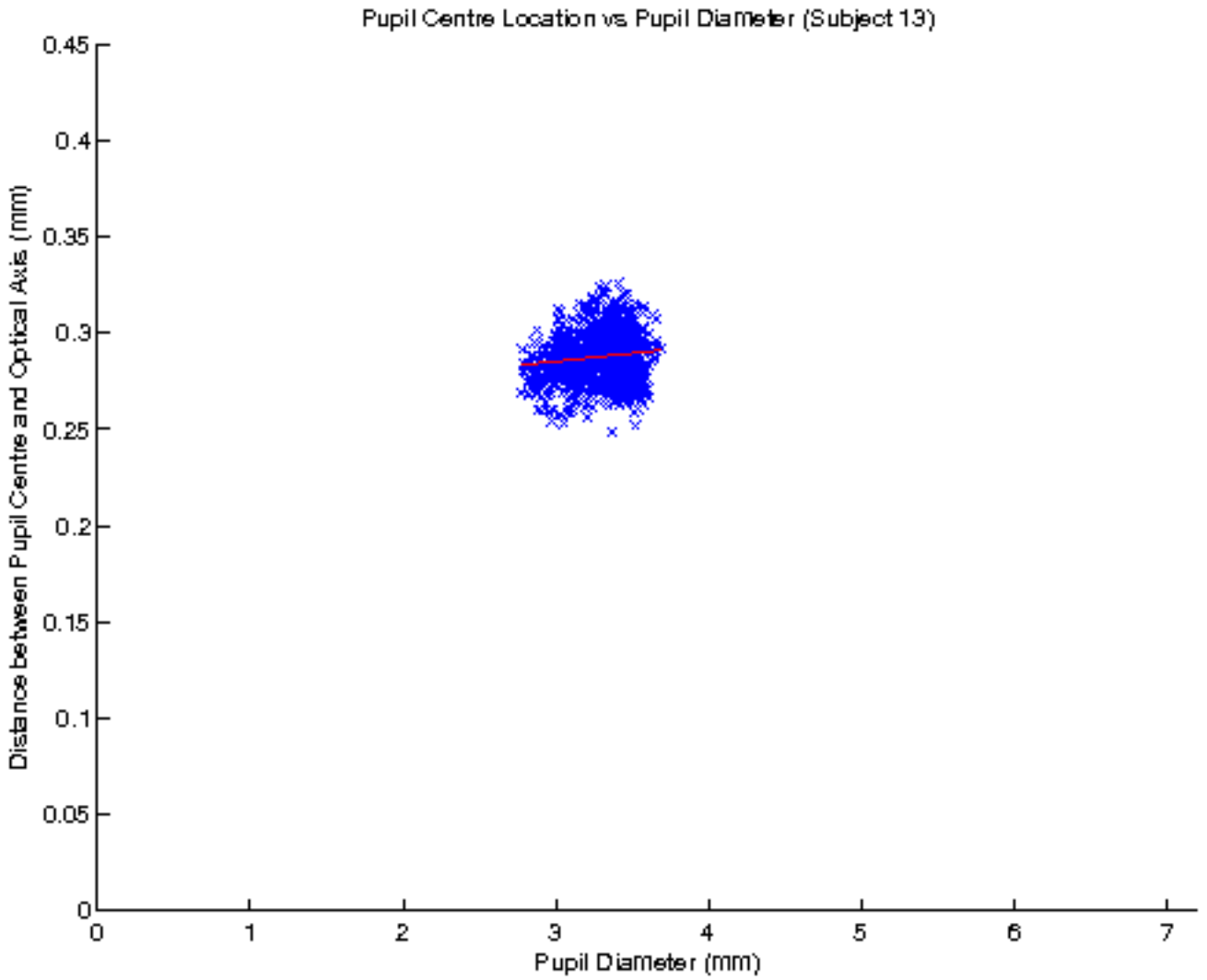

Figure D.12: Correlation between pupil diameter and the position of the pupil centre relative to the optical axis (Subject 13)

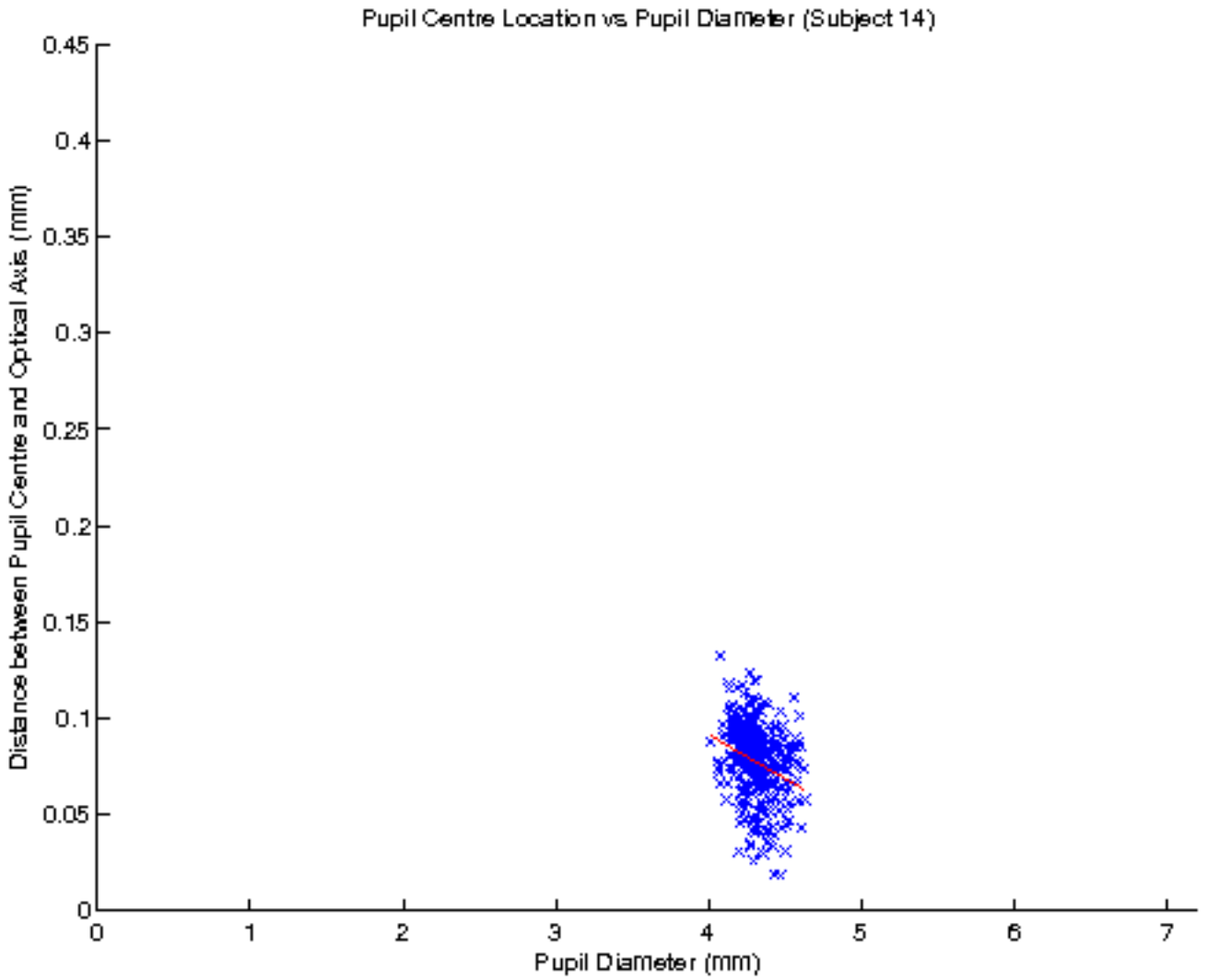

Figure D.13: Correlation between pupil diameter and the position of the pupil centre relative to the optical axis (Subject 14)

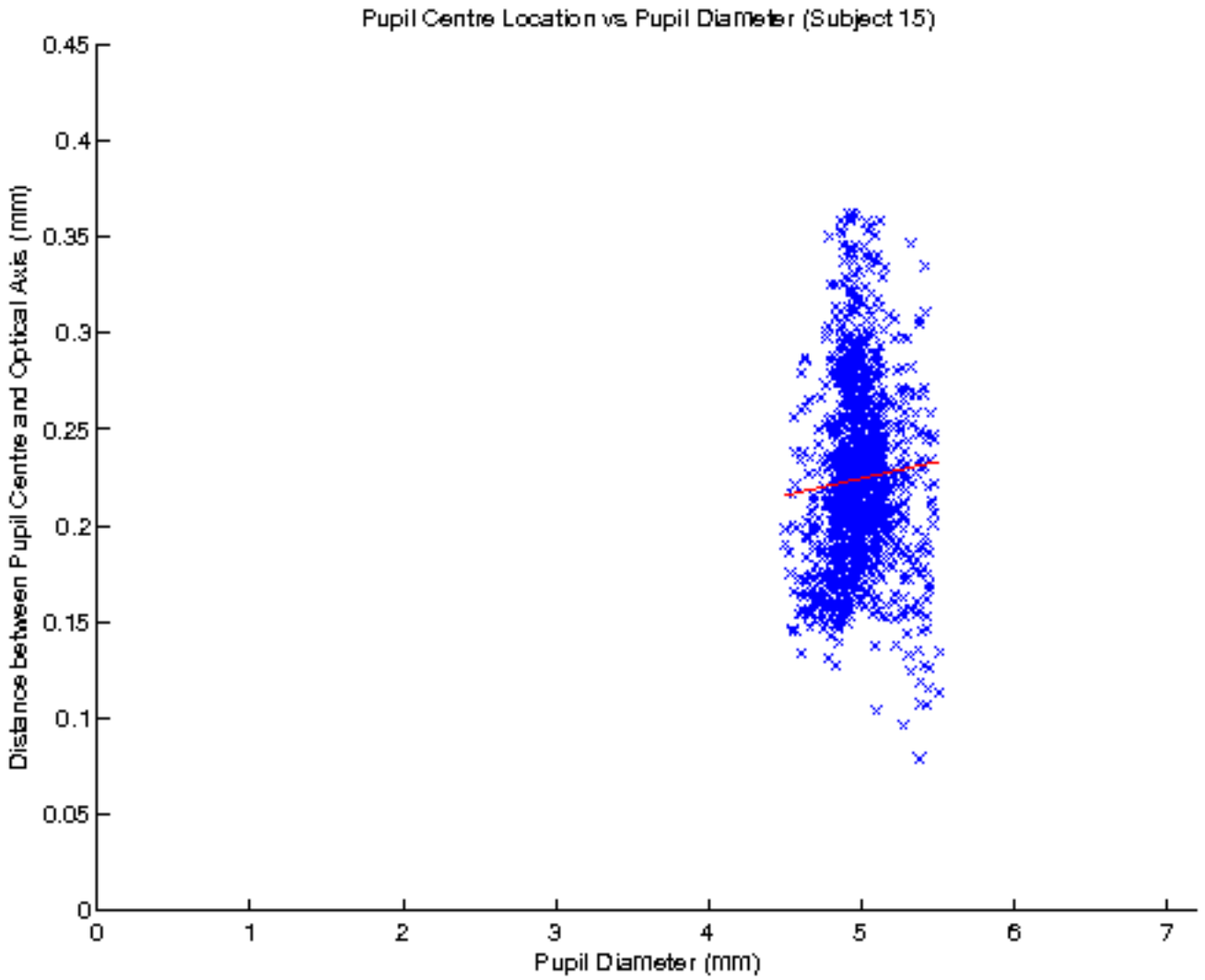

Figure D.14: Correlation between pupil diameter and the position of the pupil centre relative to the optical axis (Subject 15)

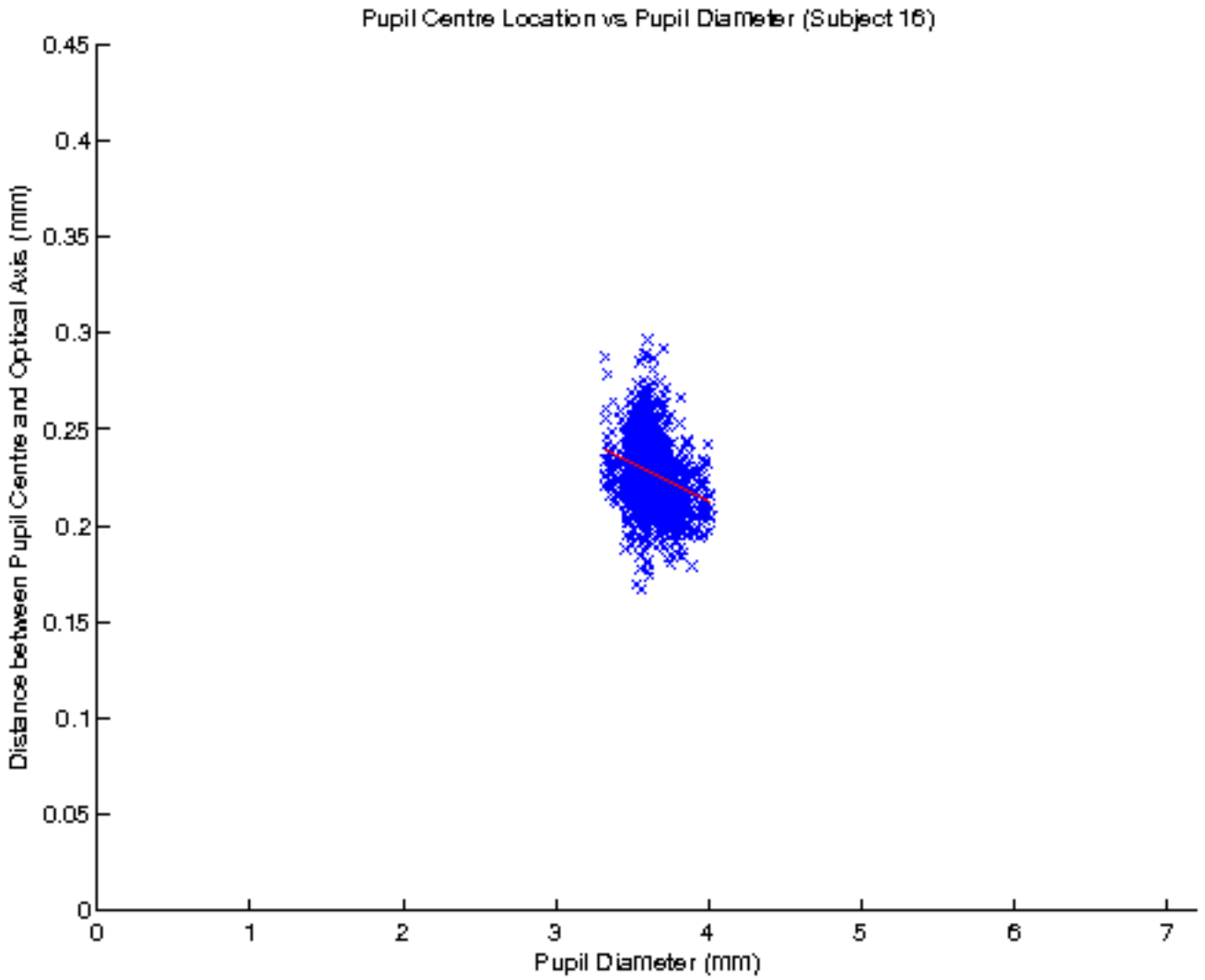

Figure D.15: Correlation between pupil diameter and the position of the pupil centre relative to the optical axis (Subject 16)

Appendix E

Moving Target Frames

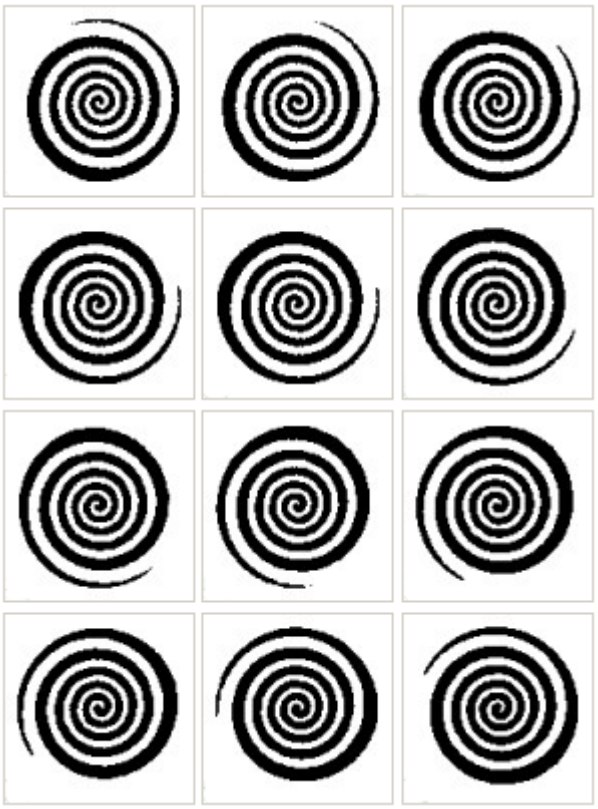

Figure E.1: Rotating Hyno-Wheel.

Figure E.2: Pulsating Dot.

Appendix F

Statistical Analysis

F.1 Target Type

The content of this appendices shows the SPSS output of the statistical analysis undertaken on the target type data set in the fixation studies. The output contains the raw data used for the calculations as well as the repeated measures ANOVA. The output also contains a list of the pairwise comparisons undertaken when searching for significant differences between targets.

```
GLM Blank MalteseCross Bullseye Crosshairs Spot Swirl
  /WSFACTOR=TargetType 6 Polynomial
  /METHOD=SSTYPE(3)
  /EMMEANS=TABLES(TargetType) COMPARE ADJ(LSD)
  /PRINT=DESCRIPTIVE
  /CRITERIA=ALPHA(.05)
  /WSDESIGN=TargetType.
```

General Linear Model

Notes

Output Created		2011-10-12T12:12:28.932
Comments		
Input	Active Dataset	DataSet0
	Filter	<none>
	Weight	<none>
	Split File	<none>
	N of Rows in Working Data File	16
Missing Value Handling	Definition of Missing	User-defined missing values are treated as missing.
	Cases Used	Statistics are based on all cases with valid data for all variables in the model.
Syntax		GLM Blank MalteseCross Bullseye Crosshairs Spot Swirl /WSFACTOR=TargetType 6 Polynomial /METHOD=SSTYPE(3) /EMMEANS=TABLES(TargetType) COMPARE ADJ(LSD) /PRINT=DESCRIPTIVE /CRITERIA=ALPHA(.05) /WSDESIGN=TargetType.
Resources	Processor Time	0:00:00.031
	Elapsed Time	0:00:00.017

```
[DataSet0]
```

Within-Subjects Factors

Measure:MEASURE_1

Target…	Dependent Variable
1	Blank
2	MalteseCross
3	Bullseye
4	Crosshairs

Within-Subjects Factors

Measure:MEASURE_1

Target...	Dependent Variable
5	Spot
6	Swirl

Descriptive Statistics

	Mean	Std. Deviation	N
Blank	.3074	.11157	16
MalteseCross	.2064	.10507	16
Bullseye	.2177	.12188	16
Crosshairs	.2749	.16370	16
Spot	.3085	.15524	16
Swirl	.2298	.10300	16

Multivariate Tests[b]

Effect		Value	F	Hypothesis df	Error df	Sig.
TargetType	Pillai's Trace	.508	2.274[a]	5.000	11.000	.119
	Wilks' Lambda	.492	2.274[a]	5.000	11.000	.119
	Hotelling's Trace	1.033	2.274[a]	5.000	11.000	.119
	Roy's Largest Root	1.033	2.274[a]	5.000	11.000	.119

a. Exact statistic

b. Design: Intercept
Within Subjects Design: TargetType

Mauchly's Test of Sphericity[b]

Measure:MEASURE_1

Within Subjects Effect	Mauchly's W	Approx. Chi-Square	df	Sig.	Epsilon[a]		
					Greenhouse-Geisser	Huynh-Feldt	Lower-bound
TargetType	.254	17.938	14	.217	.599	.765	.200

Tests the null hypothesis that the error covariance matrix of the orthonormalized transformed dependent variables is proportional to

a. May be used to adjust the degrees of freedom for the averaged tests of significance. Corrected tests are displayed in the Tests of

b. Design: Intercept
Within Subjects Design: TargetType

› an identity matrix.

›f Within-Subjects Effects table.

Tests of Within-Subjects Effects

Measure:MEASURE_1

Source		Type III Sum of Squares	df	Mean Square	F	Sig.
TargetType	Sphericity Assumed	.166	5	.033	2.694	.027
	Greenhouse-Geisser	.166	2.995	.055	2.694	.057
	Huynh-Feldt	.166	3.824	.043	2.694	.042
	Lower-bound	.166	1.000	.166	2.694	.122
Error(TargetType)	Sphericity Assumed	.922	75	.012		
	Greenhouse-Geisser	.922	44.919	.021		
	Huynh-Feldt	.922	57.367	.016		
	Lower-bound	.922	15.000	.061		

Tests of Within-Subjects Contrasts

Measure:MEASURE_1

Source	Target Type	Type III Sum of Squares	df	Mean Square	F	Sig.
TargetType	Linear	.000	1	.000	.014	.907
	Quadratic	.008	1	.008	.649	.433
	Cubic	.157	1	.157	14.459	.002
	Order 4	.000	1	.000	.017	.899
	Order 5	1.536E-5	1	1.536E-5	.001	.972
Error(TargetType)	Linear	.144	15	.010		
	Quadratic	.178	15	.012		
	Cubic	.163	15	.011		
	Order 4	.253	15	.017		
	Order 5	.183	15	.012		

Tests of Between-Subjects Effects

Measure:MEASURE_1
Transformed Variable:Average

Source	Type III Sum of Squares	df	Mean Square	F	Sig.
Intercept	6.363	1	6.363	165.848	.000
Error	.575	15	.038		

Estimated Marginal Means

TargetType

Estimates

Measure:MEASURE_1

Target Type	Mean	Std. Error	95% Confidence Interval	
			Lower Bound	Upper Bound
1	.307	.028	.248	.367
2	.206	.026	.150	.262
3	.218	.030	.153	.283
4	.275	.041	.188	.362
5	.308	.039	.226	.391
6	.230	.026	.175	.285

Pairwise Comparisons

Measure:MEASURE_1

(I) Target Type	(J) Target Type	Mean Difference (I-J)	Std. Error	Sig.[a]	95% Confidence Interval for Difference[a]	
					Lower Bound	Upper Bound
1	2	.101*	.032	.006	.033	.169
	3	.090*	.035	.023	.014	.165
	4	.033	.054	.557	-.083	.148
	5	-.001	.035	.976	-.076	.073
	6	.078*	.035	.044	.003	.153
2	1	-.101*	.032	.006	-.169	-.033
	3	-.011	.026	.674	-.067	.045
	4	-.068	.048	.176	-.171	.034
	5	-.102*	.037	.015	-.182	-.022
	6	-.023	.029	.426	-.084	.038
3	1	-.090*	.035	.023	-.165	-.014
	2	.011	.026	.674	-.045	.067
	4	-.057	.038	.154	-.139	.024
	5	-.091*	.041	.044	-.179	-.003

Based on estimated marginal means

*. The mean difference is significant at the .05 level.

a. Adjustment for multiple comparisons: Least Significant Difference (equivalent to no adjustments).

Pairwise Comparisons

Measure:MEASURE_1

(I) Target Type	(J) Target Type	Mean Difference (I-J)	Std. Error	Sig.[a]	95% Confidence Interval for Difference[a]	
					Lower Bound	Upper Bound
3	6	-.012	.025	.630	-.065	.041
4	1	-.033	.054	.557	-.148	.083
	2	.068	.048	.176	-.034	.171
	3	.057	.038	.154	-.024	.139
	5	-.034	.058	.572	-.157	.090
	6	.045	.040	.278	-.040	.130
5	1	.001	.035	.976	-.073	.076
	2	.102*	.037	.015	.022	.182
	3	.091*	.041	.044	.003	.179
	4	.034	.058	.572	-.090	.157
	6	.079	.038	.055	-.002	.159
6	1	-.078*	.035	.044	-.153	-.003
	2	.023	.029	.426	-.038	.084
	3	.012	.025	.630	-.041	.065
	4	-.045	.040	.278	-.130	.040
	5	-.079	.038	.055	-.159	.002

Based on estimated marginal means

*. The mean difference is significant at the .05 level.

a. Adjustment for multiple comparisons: Least Significant Difference (equivalent to no adjustments).

Multivariate Tests

	Value	F	Hypothesis df	Error df	Sig.
Pillai's trace	.508	2.274[a]	5.000	11.000	.119
Wilks' lambda	.492	2.274[a]	5.000	11.000	.119
Hotelling's trace	1.033	2.274[a]	5.000	11.000	.119
Roy's largest root	1.033	2.274[a]	5.000	11.000	.119

Each F tests the multivariate effect of TargetType. These tests are based on the linearly independent pairwise comparisons among the estimated marginal means.

a. Exact statistic

F.2 Target Movement

The content of this appendices shows the SPSS output of the statistical analysis undertaken on the target movement data set in the fixation studies. The output contains the raw data used for the calculations as well as the repeated measures ANOVA. The output also contains a list of the pairwise comparisons undertaken when searching for significant differences between targets.

```
GLM Blank RotatingMalteseCross HypnoWheel PulsatingDot FlashingMalteseCross
  /WSFACTOR=TargetMovement 5 Polynomial
  /METHOD=SSTYPE(3)
  /EMMEANS=TABLES(TargetMovement) COMPARE ADJ(LSD)
  /PRINT=DESCRIPTIVE
  /CRITERIA=ALPHA(.05)
  /WSDESIGN=TargetMovement.
```

General Linear Model

Notes

Output Created		2011-10-12T12:18:58.729
Comments		
Input	Active Dataset	DataSet1
	Filter	<none>
	Weight	<none>
	Split File	<none>
	N of Rows in Working Data File	16
Missing Value Handling	Definition of Missing	User-defined missing values are treated as missing.
	Cases Used	Statistics are based on all cases with valid data for all variables in the model.
Syntax		GLM Blank RotatingMalteseCross HypnoWheel PulsatingDot FlashingMalteseCross /WSFACTOR=TargetMovement 5 Polynomial /METHOD=SSTYPE(3) /EMMEANS=TABLES (TargetMovement) COMPARE ADJ (LSD) /PRINT=DESCRIPTIVE /CRITERIA=ALPHA(.05) /WSDESIGN=TargetMovement.
Resources	Processor Time	0:00:00.047
	Elapsed Time	0:00:00.016

[DataSet1]

Within-Subjects Factors

Measure:MEASURE_1

Target...	Dependent Variable
1	Blank
2	Rotating MalteseCross

Within-Subjects Factors

Measure:MEASURE_1

Target...	Dependent Variable
3	HypnoWheel
4	PulsatingDot
5	Flashing MalteseCross

Descriptive Statistics

	Mean	Std. Deviation	N
Blank	.3074	.11157	16
RotatingMalteseCross	.2339	.14760	16
HypnoWheel	.2740	.15855	16
PulsatingDot	.2762	.12740	16
FlashingMalteseCross	.2539	.10844	16

Multivariate Tests[b]

Effect		Value	F	Hypothesis df	Error df	Sig.
TargetMovement	Pillai's Trace	.315	1.379[a]	4.000	12.000	.299
	Wilks' Lambda	.685	1.379[a]	4.000	12.000	.299
	Hotelling's Trace	.460	1.379[a]	4.000	12.000	.299
	Roy's Largest Root	.460	1.379[a]	4.000	12.000	.299

a. Exact statistic

b. Design: Intercept
Within Subjects Design: TargetMovement

Mauchly's Test of Sphericity[b]

Measure:MEASURE_1

Within Subjects Effect	Mauchly's W	Approx. Chi-Square	df	Sig.	Epsilon[a]		
					Greenhouse-Geisser	Huynh-Feldt	Lower-bound
TargetMovement	.363	13.601	9	.140	.670	.830	.250

Tests the null hypothesis that the error covariance matrix of the orthonormalized transformed dependent variables is proportional to

a. May be used to adjust the degrees of freedom for the averaged tests of significance. Corrected tests are displayed in the Tests of

b. Design: Intercept
Within Subjects Design: TargetMovement

) an identity matrix.

)f Within-Subjects Effects table.

Tests of Within-Subjects Effects

Measure:MEASURE_1

Source		Type III Sum of Squares	df	Mean Square	F	Sig.
TargetMovement	Sphericity Assumed	.048	4	.012	.994	.418
	Greenhouse-Geisser	.048	2.681	.018	.994	.398
	Huynh-Feldt	.048	3.320	.015	.994	.409
	Lower-bound	.048	1.000	.048	.994	.334
Error(TargetMovement)	Sphericity Assumed	.727	60	.012		
	Greenhouse-Geisser	.727	40.217	.018		
	Huynh-Feldt	.727	49.799	.015		
	Lower-bound	.727	15.000	.048		

Tests of Within-Subjects Contrasts

Measure:MEASURE_1

Source	Target Movem…	Type III Sum of Squares	df	Mean Square	F	Sig.
TargetMovement	Linear	.007	1	.007	.640	.436
	Quadratic	.005	1	.005	.381	.546
	Cubic	.031	1	.031	5.236	.037
	Order 4	.006	1	.006	.316	.582
Error(TargetMovement)	Linear	.157	15	.010		
	Quadratic	.187	15	.012		
	Cubic	.087	15	.006		
	Order 4	.295	15	.020		

Tests of Between-Subjects Effects

Measure:MEASURE_1
Transformed Variable:Average

Source	Type III Sum of Squares	df	Mean Square	F	Sig.
Intercept	5.792	1	5.792	148.870	.000

Tests of Between-Subjects Effects

Measure:MEASURE_1
Transformed Variable:Average

Source	Type III Sum of Squares	df	Mean Square	F	Sig.
Error	.584	15	.039		

Estimated Marginal Means

TargetMovement

Estimates

Measure:MEASURE_1

Target Mo...	Mean	Std. Error	95% Confidence Interval	
			Lower Bound	Upper Bound
1	.307	.028	.248	.367
2	.234	.037	.155	.313
3	.274	.040	.190	.358
4	.276	.032	.208	.344
5	.254	.027	.196	.312

Pairwise Comparisons

Measure:MEASURE_1

(I) Target Movement	(J) Target Movement	Mean Difference (I-J)	Std. Error	Sig.[a]	95% Confidence Interval for Difference[a]	
					Lower Bound	Upper Bound
1	2	.074	.035	.054	-.001	.148
	3	.033	.048	.499	-.069	.136
	4	.031	.028	.284	-.029	.091
	5	.053	.037	.167	-.025	.132
2	1	-.074	.035	.054	-.148	.001
	3	-.040	.049	.424	-.144	.064
	4	-.042	.026	.126	-.098	.013
	5	-.020	.046	.668	-.118	.078
3	1	-.033	.048	.499	-.136	.069
	2	.040	.049	.424	-.064	.144
	4	-.002	.041	.958	-.089	.085
	5	.020	.034	.569	-.053	.094
4	1	-.031	.028	.284	-.091	.029

Based on estimated marginal means

a. Adjustment for multiple comparisons: Least Significant Difference (equivalent to no adjustments).

Pairwise Comparisons

Measure:MEASURE_1

(I) TargetMovement	(J) TargetMovement	Mean Difference (I-J)	Std. Error	Sig.[a]	95% Confidence Interval for Difference[a]	
					Lower Bound	Upper Bound
4	2	.042	.026	.126	-.013	.098
	3	.002	.041	.958	-.085	.089
	5	.022	.038	.565	-.058	.103
5	1	-.053	.037	.167	-.132	.025
	2	.020	.046	.668	-.078	.118
	3	-.020	.034	.569	-.094	.053
	4	-.022	.038	.565	-.103	.058

Based on estimated marginal means

a. Adjustment for multiple comparisons: Least Significant Difference (equivalent to no adjustments).

Multivariate Tests

	Value	F	Hypothesis df	Error df	Sig.
Pillai's trace	.315	1.379[a]	4.000	12.000	.299
Wilks' lambda	.685	1.379[a]	4.000	12.000	.299
Hotelling's trace	.460	1.379[a]	4.000	12.000	.299
Roy's largest root	.460	1.379[a]	4.000	12.000	.299

Each F tests the multivariate effect of TargetMovement. These tests are based on the linearly independent pairwise comparisons among the estimated marginal means.

a. Exact statistic

F.3 Target Type and Movement

The content of this appendices shows the SPSS output of the statistical analysis undertaken on the target type and movement data set in the fixation studies. The output contains the raw data used for the calculations as well as the repeated measures ANOVA. The output also contains a list of the pairwise comparisons undertaken when searching for significant differences between targets.

```
GLM Blank MalteseCross Bullseye Crosshairs Spot Swirl RotatingMalteseCross HypnoWheel Pul
satingDot FlashingMalteseCross
  /WSFACTOR=TypeandMovment 10 Polynomial
  /METHOD=SSTYPE(3)
  /EMMEANS=TABLES(TypeandMovment) COMPARE ADJ(LSD)
  /PRINT=DESCRIPTIVE
  /CRITERIA=ALPHA(.05)
  /WSDESIGN=TypeandMovment.
```

General Linear Model

Notes

Output Created		2011-10-12T12:23:07.045
Comments		
Input	Active Dataset	DataSet2
	Filter	<none>
	Weight	<none>
	Split File	<none>
	N of Rows in Working Data File	13
Missing Value Handling	Definition of Missing	User-defined missing values are treated as missing.
	Cases Used	Statistics are based on all cases with valid data for all variables in the model.
Syntax		GLM Blank MalteseCross Bullseye Crosshairs Spot Swirl RotatingMalteseCross HypnoWheel PulsatingDot FlashingMalteseCross /WSFACTOR=TypeandMovment 10 Polynomial /METHOD=SSTYPE(3) /EMMEANS=TABLES (TypeandMovment) COMPARE ADJ (LSD) /PRINT=DESCRIPTIVE /CRITERIA=ALPHA(.05) /WSDESIGN=TypeandMovment.
Resources	Processor Time	0:00:00.063
	Elapsed Time	0:00:00.031

```
[DataSet2]
```

Within-Subjects Factors

Measure:MEASURE_1

Type an...	Dependent Variable
1	Blank
2	MalteseCross
3	Bullseye
4	Crosshairs
5	Spot
6	Swirl
7	Rotating MalteseCross
8	HypnoWheel
9	PulsatingDot
10	Flashing MalteseCross

Descriptive Statistics

	Mean	Std. Deviation	N
Blank	.3003	.12273	13
MalteseCross	.2165	.11290	13
Bullseye	.2269	.12819	13
Crosshairs	.3115	.15990	13
Spot	.2850	.11498	13
Swirl	.2399	.09989	13
RotatingMalteseCross	.1891	.06723	13
HypnoWheel	.2455	.14823	13
PulsatingDot	.2368	.08214	13
FlashingMalteseCross	.2593	.11395	13

Multivariate Tests[b]

Effect		Value	F	Hypothesis df	Error df	Sig.
TypeandMovment	Pillai's Trace	.823	2.064[a]	9.000	4.000	.253
	Wilks' Lambda	.177	2.064[a]	9.000	4.000	.253
	Hotelling's Trace	4.644	2.064[a]	9.000	4.000	.253
	Roy's Largest Root	4.644	2.064[a]	9.000	4.000	.253

a. Exact statistic

b. Design: Intercept
Within Subjects Design: TypeandMovment

Mauchly's Test of Sphericity[b]

Measure:MEASURE_1

Within Subjects Effect	Mauchly's W	Approx. Chi-Square	df	Sig.	Epsilon[a]		
					Greenhouse-Geisser	Huynh-Feldt	Lower-bound
TypeandMovment	.001	57.314	44	.141	.474	.767	.111

Tests the null hypothesis that the error covariance matrix of the orthonormalized transformed dependent variables is proportional to

a. May be used to adjust the degrees of freedom for the averaged tests of significance. Corrected tests are displayed in the Tests of

b. Design: Intercept
Within Subjects Design: TypeandMovment

an identity matrix.

f Within-Subjects Effects table.

Tests of Within-Subjects Effects

Measure:MEASURE_1

Source		Type III Sum of Squares	df	Mean Square	F	Sig.
TypeandMovment	Sphericity Assumed	.173	9	.019	1.823	.072
	Greenhouse-Geisser	.173	4.263	.040	1.823	.135
	Huynh-Feldt	.173	6.905	.025	1.823	.094
	Lower-bound	.173	1.000	.173	1.823	.202
Error(TypeandMovment)	Sphericity Assumed	1.135	108	.011		
	Greenhouse-Geisser	1.135	51.161	.022		
	Huynh-Feldt	1.135	82.864	.014		
	Lower-bound	1.135	12.000	.095		

Tests of Within-Subjects Contrasts

Measure:MEASURE_1

Source	Typeand Movment	Type III Sum of Squares	df	Mean Square	F	Sig.
TypeandMovment	Linear	.012	1	.012	.618	.447
	Quadratic	.004	1	.004	.281	.606
	Cubic	.004	1	.004	.568	.465
	Order 4	.041	1	.041	6.596	.025

Tests of Within-Subjects Contrasts

Measure:MEASURE_1

Source	Typeand Movment	Type III Sum of Squares	df	Mean Square	F	Sig.
TypeandMovment	Order 5	.075	1	.075	14.725	.002
	Order 6	.001	1	.001	.060	.810
	Order 7	.028	1	.028	3.214	.098
	Order 8	.000	1	.000	.010	.921
	Order 9	.007	1	.007	.926	.355
Error(TypeandMovment)	Linear	.227	12	.019		
	Quadratic	.153	12	.013		
	Cubic	.090	12	.007		
	Order 4	.075	12	.006		
	Order 5	.062	12	.005		
	Order 6	.192	12	.016		
	Order 7	.105	12	.009		
	Order 8	.143	12	.012		
	Order 9	.088	12	.007		

Tests of Between-Subjects Effects

Measure:MEASURE_1
Transformed Variable:Average

Source	Type III Sum of Squares	df	Mean Square	F	Sig.
Intercept	8.194	1	8.194	183.685	.000
Error	.535	12	.045		

Estimated Marginal Means

TypeandMovment

Estimates

Measure:MEASURE_1

Type and Mo…	Mean	Std. Error	95% Confidence Interval	
			Lower Bound	Upper Bound
1	.300	.034	.226	.374
2	.216	.031	.148	.285
3	.227	.036	.149	.304
4	.311	.044	.215	.408
5	.285	.032	.215	.354
6	.240	.028	.180	.300
7	.189	.019	.149	.230

Estimates

Measure:MEASURE_1

Type and Mo…	Mean	Std. Error	95% Confidence Interval	
			Lower Bound	Upper Bound
8	.245	.041	.156	.335
9	.237	.023	.187	.286
10	.259	.032	.190	.328

Pairwise Comparisons

Measure:MEASURE_1

(I) Type and Movment	(J) Type and Movment	Mean Difference (I-J)	Std. Error	Sig.[a]	95% Confidence Interval for Difference[a]	
					Lower Bound	Upper Bound
1	2	.084*	.038	.046	.002	.166
	3	.073	.041	.101	-.017	.164
	4	-.011	.060	.856	-.143	.120
	5	.015	.031	.625	-.051	.082
	6	.060	.040	.158	-.027	.148
	7	.111*	.041	.019	.022	.201
	8	.055	.051	.307	-.057	.167
	9	.063	.035	.093	-.012	.139
	10	.041	.042	.349	-.051	.133
2	1	-.084*	.038	.046	-.166	-.002
	3	-.010	.030	.735	-.076	.055
	4	-.095	.057	.121	-.219	.029
	5	-.068*	.031	.046	-.135	-.001
	6	-.023	.032	.480	-.093	.047
	7	.027	.037	.469	-.052	.107
	8	-.029	.050	.569	-.137	.079
	9	-.020	.031	.523	-.088	.047
	10	-.043	.044	.350	-.139	.053
3	1	-.073	.041	.101	-.164	.017
	2	.010	.030	.735	-.055	.076
	4	-.085	.043	.071	-.178	.009
	5	-.058	.032	.097	-.128	.012
	6	-.013	.030	.677	-.079	.053
	7	.038	.040	.365	-.050	.125

Based on estimated marginal means

*. The mean difference is significant at the .05 level.

a. Adjustment for multiple comparisons: Least Significant Difference (equivalent to no adjustments).

Pairwise Comparisons

Measure:MEASURE_1

(I) Type and Movment	(J) Type and Movment	Mean Difference (I-J)	Std. Error	Sig.[a]	95% Confidence Interval for Difference[a]	
					Lower Bound	Upper Bound
3	8	-.019	.048	.707	-.124	.087
	9	-.010	.044	.824	-.105	.085
	10	-.032	.051	.539	-.144	.079
4	1	.011	.060	.856	-.120	.143
	2	.095	.057	.121	-.029	.219
	3	.085	.043	.071	-.009	.178
	5	.027	.052	.618	-.086	.140
	6	.072	.045	.137	-.026	.170
	7	.122*	.041	.011	.034	.211
	8	.066	.037	.101	-.015	.147
	9	.075	.054	.193	-.043	.193
	10	.052	.045	.271	-.046	.151
5	1	-.015	.031	.625	-.082	.051
	2	.068*	.031	.046	.001	.135
	3	.058	.032	.097	-.012	.128
	4	-.027	.052	.618	-.140	.086
	6	.045	.025	.097	-.010	.100
	7	.096*	.043	.047	.001	.190
	8	.039	.041	.356	-.050	.129
	9	.048	.032	.154	-.021	.117
	10	.026	.041	.543	-.064	.115
6	1	-.060	.040	.158	-.148	.027
	2	.023	.032	.480	-.047	.093
	3	.013	.030	.677	-.053	.079
	4	-.072	.045	.137	-.170	.026
	5	-.045	.025	.097	-.100	.010
	7	.051	.035	.178	-.027	.128
	8	-.006	.036	.878	-.084	.073
	9	.003	.026	.906	-.053	.059
	10	-.019	.034	.583	-.094	.056
7	1	-.111*	.041	.019	-.201	-.022
	2	-.027	.037	.469	-.107	.052
	3	-.038	.040	.365	-.125	.050
	4	-.122*	.041	.011	-.211	-.034
	5	-.096*	.043	.047	-.190	-.001

Based on estimated marginal means

*. The mean difference is significant at the .05 level.

a. Adjustment for multiple comparisons: Least Significant Difference (equivalent to no adjustments).

Pairwise Comparisons

Measure:MEASURE_1

(I) Type and Movment	(J) Type and Movment	Mean Difference (I-J)	Std. Error	Sig.[a]	95% Confidence Interval for Difference[a]	
					Lower Bound	Upper Bound
7	6	-.051	.035	.178	-.128	.027
	8	-.056	.041	.197	-.146	.034
	9	-.048	.030	.139	-.113	.018
	10	-.070*	.030	.040	-.136	-.004
8	1	-.055	.051	.307	-.167	.057
	2	.029	.050	.569	-.079	.137
	3	.019	.048	.707	-.087	.124
	4	-.066	.037	.101	-.147	.015
	5	-.039	.041	.356	-.129	.050
	6	.006	.036	.878	-.073	.084
	7	.056	.041	.197	-.034	.146
	9	.009	.039	.828	-.077	.094
	10	-.014	.035	.701	-.090	.063
9	1	-.063	.035	.093	-.139	.012
	2	.020	.031	.523	-.047	.088
	3	.010	.044	.824	-.085	.105
	4	-.075	.054	.193	-.193	.043
	5	-.048	.032	.154	-.117	.021
	6	-.003	.026	.906	-.059	.053
	7	.048	.030	.139	-.018	.113
	8	-.009	.039	.828	-.094	.077
	10	-.023	.028	.438	-.084	.039
10	1	-.041	.042	.349	-.133	.051
	2	.043	.044	.350	-.053	.139
	3	.032	.051	.539	-.079	.144
	4	-.052	.045	.271	-.151	.046
	5	-.026	.041	.543	-.115	.064
	6	.019	.034	.583	-.056	.094
	7	.070*	.030	.040	.004	.136
	8	.014	.035	.701	-.063	.090
	9	.023	.028	.438	-.039	.084

Based on estimated marginal means

*. The mean difference is significant at the .05 level.

a. Adjustment for multiple comparisons: Least Significant Difference (equivalent to no adjustments).

Multivariate Tests

	Value	F	Hypothesis df	Error df	Sig.
Pillai's trace	.823	2.064[a]	9.000	4.000	.253
Wilks' lambda	.177	2.064[a]	9.000	4.000	.253
Hotelling's trace	4.644	2.064[a]	9.000	4.000	.253
Roy's largest root	4.644	2.064[a]	9.000	4.000	.253

Each F tests the multivariate effect of TypeandMovment. These tests are based on the linearly independent pairwise comparisons among the estimated marginal means.

a. Exact statistic

F.4 Target Size

The content of this appendices shows the SPSS output of the statistical analysis undertaken on the target size data set in the fixation studies. The output contains the raw data used for the calculations as well as the repeated measures ANOVA. The output also contains a list of the pairwise comparisons undertaken when searching for significant differences between targets.

```
GLM six thirteen twentyfive fifty onehundred twohundred
  /WSFACTOR=TargetSize 6 Polynomial
  /METHOD=SSTYPE(3)
  /EMMEANS=TABLES(TargetSize) COMPARE ADJ(LSD)
  /PRINT=DESCRIPTIVE
  /CRITERIA=ALPHA(.05)
  /WSDESIGN=TargetSize.
```

General Linear Model

Notes

Output Created		2011-10-12T14:01:29.542
Comments		
Input	Active Dataset	DataSet0
	Filter	<none>
	Weight	<none>
	Split File	<none>
	N of Rows in Working Data File	16
Missing Value Handling	Definition of Missing	User-defined missing values are treated as missing.
	Cases Used	Statistics are based on all cases with valid data for all variables in the model.
Syntax		GLM six thirteen twentyfive fifty onehundred twohundred /WSFACTOR=TargetSize 6 Polynomial /METHOD=SSTYPE(3) /EMMEANS=TABLES(TargetSize) COMPARE ADJ(LSD) /PRINT=DESCRIPTIVE /CRITERIA=ALPHA(.05) /WSDESIGN=TargetSize.
Resources	Processor Time	0:00:00.015
	Elapsed Time	0:00:00.093

```
[DataSet0]
```

Within-Subjects Factors

Measure:MEASURE_1

Target…	Dependent Variable
1	six
2	thirteen
3	twentyfive
4	fifty

Within-Subjects Factors

Measure:MEASURE_1

Target...	Dependent Variable
5	onehundred
6	twohundred

Descriptive Statistics

	Mean	Std. Deviation	N
six	.2042	.08313	16
thirteen	.2689	.14249	16
twentyfive	.2343	.14624	16
fifty	.2933	.12774	16
onehundred	.2899	.12151	16
twohundred	.3085	.15524	16

Multivariate Tests[b]

Effect		Value	F	Hypothesis df	Error df	Sig.
TargetSize	Pillai's Trace	.488	2.094[a]	5.000	11.000	.143
	Wilks' Lambda	.512	2.094[a]	5.000	11.000	.143
	Hotelling's Trace	.952	2.094[a]	5.000	11.000	.143
	Roy's Largest Root	.952	2.094[a]	5.000	11.000	.143

a. Exact statistic

b. Design: Intercept
Within Subjects Design: TargetSize

Mauchly's Test of Sphericity[b]

Measure:MEASURE_1

Within Subjects Effect	Mauchly's W	Approx. Chi-Square	df	Sig.	Epsilon[a]		
					Greenhouse-Geisser	Huynh-Feldt	Lower-bound
TargetSize	.370	13.008	14	.533	.743	1.000	.200

Tests the null hypothesis that the error covariance matrix of the orthonormalized transformed dependent variables is proportional to

a. May be used to adjust the degrees of freedom for the averaged tests of significance. Corrected tests are displayed in the Tests of

b. Design: Intercept
Within Subjects Design: TargetSize

) an identity matrix.

)f Within-Subjects Effects table.

Tests of Within-Subjects Effects

Measure:MEASURE_1

Source		Type III Sum of Squares	df	Mean Square	F	Sig.
TargetSize	Sphericity Assumed	.127	5	.025	2.183	.065
	Greenhouse-Geisser	.127	3.714	.034	2.183	.087
	Huynh-Feldt	.127	5.000	.025	2.183	.065
	Lower-bound	.127	1.000	.127	2.183	.160
Error(TargetSize)	Sphericity Assumed	.873	75	.012		
	Greenhouse-Geisser	.873	55.715	.016		
	Huynh-Feldt	.873	75.000	.012		
	Lower-bound	.873	15.000	.058		

Tests of Within-Subjects Contrasts

Measure:MEASURE_1

Source	Target Size	Type III Sum of Squares	df	Mean Square	F	Sig.
TargetSize	Linear	.095	1	.095	6.866	.019
	Quadratic	.002	1	.002	.152	.702
	Cubic	.002	1	.002	.141	.713
	Order 4	.007	1	.007	.655	.431
	Order 5	.022	1	.022	2.687	.122
Error(TargetSize)	Linear	.207	15	.014		
	Quadratic	.209	15	.014		
	Cubic	.181	15	.012		
	Order 4	.153	15	.010		
	Order 5	.123	15	.008		

Tests of Between-Subjects Effects

Measure:MEASURE_1
Transformed Variable:Average

Source	Type III Sum of Squares	df	Mean Square	F	Sig.
Intercept	6.819	1	6.819	149.632	.000
Error	.684	15	.046		

Estimated Marginal Means

TargetSize

Estimates

Measure:MEASURE_1

Target Size	Mean	Std. Error	95% Confidence Interval	
			Lower Bound	Upper Bound
1	.204	.021	.160	.249
2	.269	.036	.193	.345
3	.234	.037	.156	.312
4	.293	.032	.225	.361
5	.290	.030	.225	.355
6	.308	.039	.226	.391

Pairwise Comparisons

Measure:MEASURE_1

(I) Target Size	(J) Target Size	Mean Difference (I-J)	Std. Error	Sig.[a]	95% Confidence Interval for Difference[a]	
					Lower Bound	Upper Bound
1	2	-.065	.037	.100	-.143	.014
	3	-.030	.045	.510	-.125	.065
	4	-.089*	.033	.018	-.160	-.018
	5	-.086*	.038	.039	-.166	-.005
	6	-.104*	.046	.040	-.203	-.005
2	1	.065	.037	.100	-.014	.143
	3	.035	.032	.304	-.035	.104
	4	-.024	.024	.331	-.076	.027
	5	-.021	.032	.523	-.090	.048
	6	-.040	.048	.420	-.141	.062
3	1	.030	.045	.510	-.065	.125
	2	-.035	.032	.304	-.104	.035
	4	-.059	.033	.091	-.129	.011
	5	-.056	.037	.154	-.134	.023

Based on estimated marginal means

a. Adjustment for multiple comparisons: Least Significant Difference (equivalent to no adjustments).

*. The mean difference is significant at the .05 level.

Pairwise Comparisons

Measure:MEASURE_1

(I) TargetSize	(J) TargetSize	Mean Difference (I-J)	Std. Error	Sig.[a]	95% Confidence Interval for Difference[a]	
					Lower Bound	Upper Bound
3	6	-.074	.041	.088	-.161	.012
4	1	.089*	.033	.018	.018	.160
	2	.024	.024	.331	-.027	.076
	3	.059	.033	.091	-.011	.129
	5	.003	.030	.912	-.061	.068
	6	-.015	.038	.694	-.096	.065
5	1	.086*	.038	.039	.005	.166
	2	.021	.032	.523	-.048	.090
	3	.056	.037	.154	-.023	.134
	4	-.003	.030	.912	-.068	.061
	6	-.019	.049	.709	-.123	.086
6	1	.104*	.046	.040	.005	.203
	2	.040	.048	.420	-.062	.141
	3	.074	.041	.088	-.012	.161
	4	.015	.038	.694	-.065	.096
	5	.019	.049	.709	-.086	.123

Based on estimated marginal means

a. Adjustment for multiple comparisons: Least Significant Difference (equivalent to no adjustments).

*. The mean difference is significant at the .05 level.

Multivariate Tests

	Value	F	Hypothesis df	Error df	Sig.
Pillai's trace	.488	2.094[a]	5.000	11.000	.143
Wilks' lambda	.512	2.094[a]	5.000	11.000	.143
Hotelling's trace	.952	2.094[a]	5.000	11.000	.143
Roy's largest root	.952	2.094[a]	5.000	11.000	.143

Each F tests the multivariate effect of TargetSize. These tests are based on the linearly independent pairwise comparisons among the estimated marginal means.

a. Exact statistic

F.5 Target Colour with Control

The content of this appendices shows the SPSS output of the statistical analysis undertaken on the target colour (with control) data set in the fixation studies. The output contains the raw data used for the calculations as well as the repeated measures ANOVA. The output also contains a list of the pairwise comparisons undertaken when searching for significant differences between targets.

```
GLM Blank Black Blue Green Red White Yellow
  /WSFACTOR=colour 7 Polynomial
  /METHOD=SSTYPE(3)
  /EMMEANS=TABLES(colour) COMPARE ADJ(LSD)
  /PRINT=DESCRIPTIVE
  /CRITERIA=ALPHA(.05)
  /WSDESIGN=colour.
```

General Linear Model

Notes

Output Created		2011-10-12T12:28:32.757
Comments		
Input	Active Dataset	DataSet4
	Filter	<none>
	Weight	<none>
	Split File	<none>
	N of Rows in Working Data File	16
Missing Value Handling	Definition of Missing	User-defined missing values are treated as missing.
	Cases Used	Statistics are based on all cases with valid data for all variables in the model.
Syntax		GLM Blank Black Blue Green Red White Yellow /WSFACTOR=colour 7 Polynomial /METHOD=SSTYPE(3) /EMMEANS=TABLES(colour) COMPARE ADJ(LSD) /PRINT=DESCRIPTIVE /CRITERIA=ALPHA(.05) /WSDESIGN=colour.
Resources	Processor Time	0:00:00.078
	Elapsed Time	0:00:00.031

[DataSet4]

Within-Subjects Factors

Measure:MEASURE_1

colour	Dependent Variable
1	Blank
2	Black
3	Blue
4	Green
5	Red

Within-Subjects Factors

Measure:MEASURE_1

colour	Dependent Variable
6	White
7	Yellow

Descriptive Statistics

	Mean	Std. Deviation	N
Blank	.3697	.14716	16
Black	.1972	.08842	16
Blue	.2019	.09224	16
Green	.2360	.10733	16
Red	.1994	.09972	16
White	.2178	.10245	16
Yellow	.1898	.10300	16

Multivariate Tests[b]

Effect		Value	F	Hypothesis df	Error df	Sig.
colour	Pillai's Trace	.803	6.809[a]	6.000	10.000	.004
	Wilks' Lambda	.197	6.809[a]	6.000	10.000	.004
	Hotelling's Trace	4.086	6.809[a]	6.000	10.000	.004
	Roy's Largest Root	4.086	6.809[a]	6.000	10.000	.004

a. Exact statistic

b. Design: Intercept
Within Subjects Design: colour

Mauchly's Test of Sphericity[b]

Measure:MEASURE_1

Within Subjects Effect	Mauchly's W	Approx. Chi-Square	df	Sig.	Epsilon[a]		
					Greenhouse-Geisser	Huynh-Feldt	Lower-bound
colour	.014	54.807	20	.000	.486	.616	.167

Tests the null hypothesis that the error covariance matrix of the orthonormalized transformed dependent variables is proportional to

a. May be used to adjust the degrees of freedom for the averaged tests of significance. Corrected tests are displayed in the Tests of

b. Design: Intercept
Within Subjects Design: colour

› an identity matrix.

›f Within-Subjects Effects table.

Tests of Within-Subjects Effects

Measure:MEASURE_1

Source		Type III Sum of Squares	df	Mean Square	F	Sig.
colour	Sphericity Assumed	.386	6	.064	9.754	.000
	Greenhouse-Geisser	.386	2.915	.132	9.754	.000
	Huynh-Feldt	.386	3.693	.104	9.754	.000
	Lower-bound	.386	1.000	.386	9.754	.007
Error(colour)	Sphericity Assumed	.593	90	.007		
	Greenhouse-Geisser	.593	43.720	.014		
	Huynh-Feldt	.593	55.399	.011		
	Lower-bound	.593	15.000	.040		

Tests of Within-Subjects Contrasts

Measure:MEASURE_1

Source	colour	Type III Sum of Squares	df	Mean Square	F	Sig.
colour	Linear	.143	1	.143	16.618	.001
	Quadratic	.080	1	.080	7.267	.017
	Cubic	.105	1	.105	14.566	.002
	Order 4	.036	1	.036	8.546	.010
	Order 5	.014	1	.014	2.680	.122
	Order 6	.007	1	.007	2.233	.156
Error(colour)	Linear	.129	15	.009		
	Quadratic	.166	15	.011		
	Cubic	.108	15	.007		
	Order 4	.064	15	.004		
	Order 5	.080	15	.005		
	Order 6	.046	15	.003		

Tests of Between-Subjects Effects

Measure:MEASURE_1
Transformed Variable:Average

Source	Type III Sum of Squares	df	Mean Square	F	Sig.
Intercept	5.939	1	5.939	144.841	.000
Error	.615	15	.041		

Estimated Marginal Means

colour

Estimates

Measure:MEASURE_1

colour	Mean	Std. Error	95% Confidence Interval	
			Lower Bound	Upper Bound
1	.370	.037	.291	.448
2	.197	.022	.150	.244
3	.202	.023	.153	.251
4	.236	.027	.179	.293
5	.199	.025	.146	.253
6	.218	.026	.163	.272
7	.190	.026	.135	.245

Pairwise Comparisons

Measure:MEASURE_1

(I) colour	(J) colour	Mean Difference (I-J)	Std. Error	Sig.[a]	95% Confidence Interval for Difference[a]	
					Lower Bound	Upper Bound
1	2	.172*	.043	.001	.080	.265
	3	.168*	.041	.001	.080	.256
	4	.134*	.033	.001	.064	.203
	5	.170*	.041	.001	.083	.257
	6	.152*	.033	.000	.081	.222
	7	.180*	.037	.000	.102	.258
2	1	-.172*	.043	.001	-.265	-.080
	3	-.005	.022	.830	-.051	.041
	4	-.039	.023	.119	-.089	.011

Based on estimated marginal means

*. The mean difference is significant at the .05 level.

a. Adjustment for multiple comparisons: Least Significant Difference (equivalent to no adjustments).

Pairwise Comparisons

Measure:MEASURE_1

(I) colour	(J) colour	Mean Difference (I-J)	Std. Error	Sig.[a]	95% Confidence Interval for Difference[a]	
					Lower Bound	Upper Bound
2	5	-.002	.021	.918	-.048	.043
	6	-.021	.030	.509	-.085	.044
	7	.007	.033	.828	-.064	.079
3	1	-.168*	.041	.001	-.256	-.080
	2	.005	.022	.830	-.041	.051
	4	-.034	.021	.124	-.079	.011
	5	.002	.020	.900	-.039	.044
	6	-.016	.020	.450	-.060	.028
	7	.012	.018	.516	-.027	.051
4	1	-.134*	.033	.001	-.203	-.064
	2	.039	.023	.119	-.011	.089
	3	.034	.021	.124	-.011	.079
	5	.037	.020	.094	-.007	.080
	6	.018	.024	.468	-.034	.070
	7	.046	.030	.141	-.017	.109
5	1	-.170*	.041	.001	-.257	-.083
	2	.002	.021	.918	-.043	.048
	3	-.002	.020	.900	-.044	.039
	4	-.037	.020	.094	-.080	.007
	6	-.018	.026	.487	-.073	.037
	7	.010	.027	.726	-.048	.067
6	1	-.152*	.033	.000	-.222	-.081
	2	.021	.030	.509	-.044	.085
	3	.016	.020	.450	-.028	.060
	4	-.018	.024	.468	-.070	.034
	5	.018	.026	.487	-.037	.073
	7	.028	.014	.066	-.002	.058
7	1	-.180*	.037	.000	-.258	-.102
	2	-.007	.033	.828	-.079	.064
	3	-.012	.018	.516	-.051	.027
	4	-.046	.030	.141	-.109	.017
	5	-.010	.027	.726	-.067	.048
	6	-.028	.014	.066	-.058	.002

Based on estimated marginal means

*. The mean difference is significant at the .05 level.

a. Adjustment for multiple comparisons: Least Significant Difference (equivalent to no adjustments).

Multivariate Tests

	Value	F	Hypothesis df	Error df	Sig.
Pillai's trace	.803	6.809[a]	6.000	10.000	.004
Wilks' lambda	.197	6.809[a]	6.000	10.000	.004
Hotelling's trace	4.086	6.809[a]	6.000	10.000	.004
Roy's largest root	4.086	6.809[a]	6.000	10.000	.004

Each F tests the multivariate effect of colour. These tests are based on the linearly independent pairwise comparisons among the estimated marginal means.

a. Exact statistic

F.6 Target Colour without Control

The content of this appendices shows the SPSS output of the statistical analysis undertaken on the target colour (without control) data set in the fixation studies. The output contains the raw data used for the calculations as well as the repeated measures ANOVA. The output also contains a list of the pairwise comparisons undertaken when searching for significant differences between targets.

```
GLM Black Blue Green Red White Yellow
  /WSFACTOR=colour 6 Polynomial
  /METHOD=SSTYPE(3)
  /EMMEANS=TABLES(colour) COMPARE ADJ(LSD)
  /PRINT=DESCRIPTIVE
  /CRITERIA=ALPHA(.05)
  /WSDESIGN=colour.
```

General Linear Model

Notes

Output Created		2011-10-12T12:29:42.256
Comments		
Input	Active Dataset	DataSet4
	Filter	<none>
	Weight	<none>
	Split File	<none>
	N of Rows in Working Data File	16
Missing Value Handling	Definition of Missing	User-defined missing values are treated as missing.
	Cases Used	Statistics are based on all cases with valid data for all variables in the model.
Syntax		GLM Black Blue Green Red White Yellow /WSFACTOR=colour 6 Polynomial /METHOD=SSTYPE(3) /EMMEANS=TABLES(colour) COMPARE ADJ(LSD) /PRINT=DESCRIPTIVE /CRITERIA=ALPHA(.05) /WSDESIGN=colour.
Resources	Processor Time	0:00:00.047
	Elapsed Time	0:00:00.015

[DataSet4]

Within-Subjects Factors

Measure:MEASURE_1

colour	Dependent Variable
1	Black
2	Blue
3	Green
4	Red

Within-Subjects Factors

Measure:MEASURE_1

colour	Dependent Variable
5	White
6	Yellow

Descriptive Statistics

	Mean	Std. Deviation	N
Black	.1972	.08842	16
Blue	.2019	.09224	16
Green	.2360	.10733	16
Red	.1994	.09972	16
White	.2178	.10245	16
Yellow	.1898	.10300	16

Multivariate Tests[b]

Effect		Value	F	Hypothesis df	Error df	Sig.
colour	Pillai's Trace	.307	.975[a]	5.000	11.000	.474
	Wilks' Lambda	.693	.975[a]	5.000	11.000	.474
	Hotelling's Trace	.443	.975[a]	5.000	11.000	.474
	Roy's Largest Root	.443	.975[a]	5.000	11.000	.474

a. Exact statistic

b. Design: Intercept
Within Subjects Design: colour

Mauchly's Test of Sphericity[b]

Measure:MEASURE_1

Within Subjects Effect	Mauchly's W	Approx. Chi-Square	df	Sig.	Epsilon[a]		
					Greenhouse-Geisser	Huynh-Feldt	Lower-bound
colour	.107	29.337	14	.010	.554	.692	.200

Tests the null hypothesis that the error covariance matrix of the orthonormalized transformed dependent variables is proportional to

a. May be used to adjust the degrees of freedom for the averaged tests of significance. Corrected tests are displayed in the Tests of

b. Design: Intercept
Within Subjects Design: colour

) an identity matrix.

)f Within-Subjects Effects table.

Tests of Within-Subjects Effects

Measure:MEASURE_1

Source		Type III Sum of Squares	df	Mean Square	F	Sig.
colour	Sphericity Assumed	.023	5	.005	1.003	.422
	Greenhouse-Geisser	.023	2.770	.008	1.003	.396
	Huynh-Feldt	.023	3.460	.007	1.003	.407
	Lower-bound	.023	1.000	.023	1.003	.332
Error(colour)	Sphericity Assumed	.342	75	.005		
	Greenhouse-Geisser	.342	41.543	.008		
	Huynh-Feldt	.342	51.894	.007		
	Lower-bound	.342	15.000	.023		

Tests of Within-Subjects Contrasts

Measure:MEASURE_1

Source	colour	Type III Sum of Squares	df	Mean Square	F	Sig.
colour	Linear	.000	1	.000	.016	.900
	Quadratic	.010	1	.010	2.783	.116
	Cubic	3.660E-7	1	3.660E-7	.000	.991
	Order 4	1.075E-6	1	1.075E-6	.000	.987
	Order 5	.013	1	.013	3.558	.079
Error(colour)	Linear	.140	15	.009		
	Quadratic	.053	15	.004		
	Cubic	.039	15	.003		
	Order 4	.055	15	.004		
	Order 5	.055	15	.004		

Tests of Between-Subjects Effects

Measure:MEASURE_1
Transformed Variable:Average

Source	Type III Sum of Squares	df	Mean Square	F	Sig.
Intercept	4.115	1	4.115	114.035	.000
Error	.541	15	.036		

Estimated Marginal Means

colour

Estimates

Measure:MEASURE_1

colour	Mean	Std. Error	95% Confidence Interval	
			Lower Bound	Upper Bound
1	.197	.022	.150	.244
2	.202	.023	.153	.251
3	.236	.027	.179	.293
4	.199	.025	.146	.253
5	.218	.026	.163	.272
6	.190	.026	.135	.245

Pairwise Comparisons

Measure:MEASURE_1

(I) colour	(J) colour	Mean Difference (I-J)	Std. Error	Sig.[a]	95% Confidence Interval for Difference[a]	
					Lower Bound	Upper Bound
1	2	-.005	.022	.830	-.051	.041
	3	-.039	.023	.119	-.089	.011
	4	-.002	.021	.918	-.048	.043
	5	-.021	.030	.509	-.085	.044
	6	.007	.033	.828	-.064	.079
2	1	.005	.022	.830	-.041	.051
	3	-.034	.021	.124	-.079	.011
	4	.002	.020	.900	-.039	.044
	5	-.016	.020	.450	-.060	.028
	6	.012	.018	.516	-.027	.051
3	1	.039	.023	.119	-.011	.089
	2	.034	.021	.124	-.011	.079
	4	.037	.020	.094	-.007	.080
	5	.018	.024	.468	-.034	.070
	6	.046	.030	.141	-.017	.109

Based on estimated marginal means

a. Adjustment for multiple comparisons: Least Significant Difference (equivalent to no adjustments).

Pairwise Comparisons

Measure:MEASURE_1

(I) colour	(J) colour	Mean Difference (I-J)	Std. Error	Sig.[a]	95% Confidence Interval for Difference[a]	
					Lower Bound	Upper Bound
4	1	.002	.021	.918	-.043	.048
	2	-.002	.020	.900	-.044	.039
	3	-.037	.020	.094	-.080	.007
	5	-.018	.026	.487	-.073	.037
	6	.010	.027	.726	-.048	.067
5	1	.021	.030	.509	-.044	.085
	2	.016	.020	.450	-.028	.060
	3	-.018	.024	.468	-.070	.034
	4	.018	.026	.487	-.037	.073
	6	.028	.014	.066	-.002	.058
6	1	-.007	.033	.828	-.079	.064
	2	-.012	.018	.516	-.051	.027
	3	-.046	.030	.141	-.109	.017
	4	-.010	.027	.726	-.067	.048
	5	-.028	.014	.066	-.058	.002

Based on estimated marginal means

a. Adjustment for multiple comparisons: Least Significant Difference (equivalent to no adjustments).

Multivariate Tests

	Value	F	Hypothesis df	Error df	Sig.
Pillai's trace	.307	.975[a]	5.000	11.000	.474
Wilks' lambda	.693	.975[a]	5.000	11.000	.474
Hotelling's trace	.443	.975[a]	5.000	11.000	.474
Roy's largest root	.443	.975[a]	5.000	11.000	.474

Each F tests the multivariate effect of colour. These tests are based on the linearly independent pairwise comparisons among the estimated marginal means.

a. Exact statistic

F.7 Target Concentration

The content of this appendices shows the SPSS output of the statistical analysis undertaken on the target concentration data set in the fixation studies. The output contains the raw data used for the calculations as well as the repeated measures ANOVA. The output also contains a list of the pairwise comparisons undertaken when searching for significant differences between targets.

```
GLM Blank BlurredBullseye Bullseye ConcentrationBullseye
  /WSFACTOR=TargetConcentration 4 Polynomial
  /METHOD=SSTYPE(3)
  /EMMEANS=TABLES(TargetConcentration) COMPARE ADJ(LSD)
  /PRINT=DESCRIPTIVE
  /CRITERIA=ALPHA(.05)
  /WSDESIGN=TargetConcentration.
```

General Linear Model

Notes

Output Created		2011-10-12T12:31:39.827
Comments		
Input	Active Dataset	DataSet5
	Filter	<none>
	Weight	<none>
	Split File	<none>
	N of Rows in Working Data File	16
Missing Value Handling	Definition of Missing	User-defined missing values are treated as missing.
	Cases Used	Statistics are based on all cases with valid data for all variables in the model.
Syntax		GLM Blank BlurredBullseye Bullseye ConcentrationBullseye /WSFACTOR=TargetConcentration 4 Polynomial /METHOD=SSTYPE(3) /EMMEANS=TABLES (TargetConcentration) COMPARE ADJ(LSD) /PRINT=DESCRIPTIVE /CRITERIA=ALPHA(.05) /WSDESIGN=TargetConcentration.
Resources	Processor Time	0:00:00.062
	Elapsed Time	0:00:00.017

[DataSet5]

Within-Subjects Factors

Measure:MEASURE_1

Target...	Dependent Variable
1	Blank
2	Blurred Bullseye

Within-Subjects Factors

Measure:MEASURE_1

Target...	Dependent Variable
3	Bullseye
4	Concentration Bullseye

Descriptive Statistics

	Mean	Std. Deviation	N
Blank	.3679	.14759	16
BlurredBullseye	.1807	.05801	16
Bullseye	.2389	.12777	16
ConcentrationBullseye	.1475	.05987	16

Multivariate Tests[b]

Effect		Value	F	Hypothesis df	Error df	Sig.
TargetConcentration	Pillai's Trace	.832	21.511[a]	3.000	13.000	.000
	Wilks' Lambda	.168	21.511[a]	3.000	13.000	.000
	Hotelling's Trace	4.964	21.511[a]	3.000	13.000	.000
	Roy's Largest Root	4.964	21.511[a]	3.000	13.000	.000

a. Exact statistic

b. Design: Intercept
Within Subjects Design: TargetConcentration

Mauchly's Test of Sphericity[b]

Measure:MEASURE_1

Within Subjects Effect	Mauchly's W	Approx. Chi-Square	df	Sig.	Epsilon[a]		
					Greenhouse-Geisser	Huynh-Feldt	Lower-bound
TargetConcentration	.182	23.351	5	.000	.626	.712	.333

Tests the null hypothesis that the error covariance matrix of the orthonormalized transformed dependent variables is proportional to

a. May be used to adjust the degrees of freedom for the averaged tests of significance. Corrected tests are displayed in the Tests of

b. Design: Intercept
Within Subjects Design: TargetConcentration

an identity matrix.

f Within-Subjects Effects table.

Tests of Within-Subjects Effects

Measure:MEASURE_1

Source		Type III Sum of Squares	df	Mean Square	F	Sig.
TargetConcentration	Sphericity Assumed	.452	3	.151	23.937	.000
	Greenhouse-Geisser	.452	1.878	.241	23.937	.000
	Huynh-Feldt	.452	2.137	.212	23.937	.000
	Lower-bound	.452	1.000	.452	23.937	.000
Error (TargetConcentration)	Sphericity Assumed	.283	45	.006		
	Greenhouse-Geisser	.283	28.163	.010		
	Huynh-Feldt	.283	32.053	.009		
	Lower-bound	.283	15.000	.019		

Tests of Within-Subjects Contrasts

Measure:MEASURE_1

Source	Target Conce…	Type III Sum of Squares	df	Mean Square	F	Sig.
TargetConcentration	Linear	.291	1	.291	40.431	.000
	Quadratic	.037	1	.037	7.060	.018
	Cubic	.125	1	.125	19.187	.001
Error (TargetConcentration)	Linear	.108	15	.007		
	Quadratic	.078	15	.005		
	Cubic	.098	15	.007		

Tests of Between-Subjects Effects

Measure:MEASURE_1
Transformed Variable:Average

Source	Type III Sum of Squares	df	Mean Square	F	Sig.
Intercept	3.496	1	3.496	133.651	.000
Error	.392	15	.026		

Estimated Marginal Means

TargetConcentration

Estimates

Measure:MEASURE_1

Target Co…	Mean	Std. Error	95% Confidence Interval	
			Lower Bound	Upper Bound
1	.368	.037	.289	.447
2	.181	.015	.150	.212

Estimates

Measure:MEASURE_1

Target Co…	Mean	Std. Error	95% Confidence Interval	
			Lower Bound	Upper Bound
3	.239	.032	.171	.307
4	.147	.015	.116	.179

Pairwise Comparisons

Measure:MEASURE_1

(I) Target Concentration	(J) Target Concentration	Mean Difference (I-J)	Std. Error	Sig.[a]	95% Confidence Interval for Difference[a]	
					Lower Bound	Upper Bound
1	2	.187*	.035	.000	.112	.262
	3	.129*	.035	.002	.055	.203
	4	.220*	.033	.000	.151	.290
2	1	-.187*	.035	.000	-.262	-.112
	3	-.058*	.025	.037	-.112	-.004
	4	.033*	.010	.004	.012	.054
3	1	-.129*	.035	.002	-.203	-.055
	2	.058*	.025	.037	.004	.112
	4	.091*	.022	.001	.045	.138
4	1	-.220*	.033	.000	-.290	-.151
	2	-.033*	.010	.004	-.054	-.012
	3	-.091*	.022	.001	-.138	-.045

Based on estimated marginal means

*. The mean difference is significant at the .05 level.

a. Adjustment for multiple comparisons: Least Significant Difference (equivalent to no adjustments).

Multivariate Tests

	Value	F	Hypothesis df	Error df	Sig.
Pillai's trace	.832	21.511[a]	3.000	13.000	.000
Wilks' lambda	.168	21.511[a]	3.000	13.000	.000
Hotelling's trace	4.964	21.511[a]	3.000	13.000	.000
Roy's largest root	4.964	21.511[a]	3.000	13.000	.000

Each F tests the multivariate effect of TargetConcentration. These tests are based on the linearly independent pairwise comparisons among the estimated marginal means.

a. Exact statistic

Appendix G

Graphical Data: Self Alignment

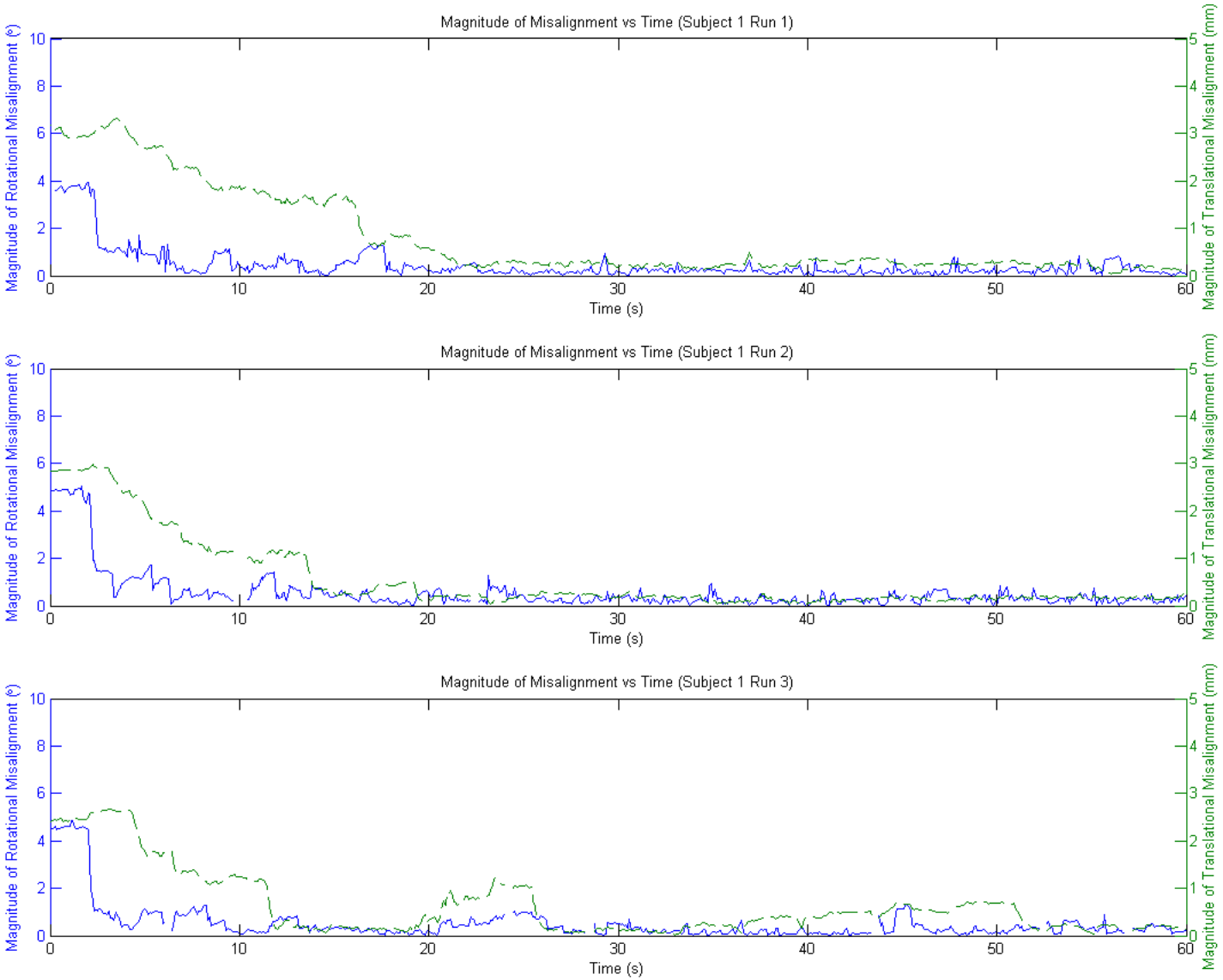

Figure G.1: Self alignment subject 1.

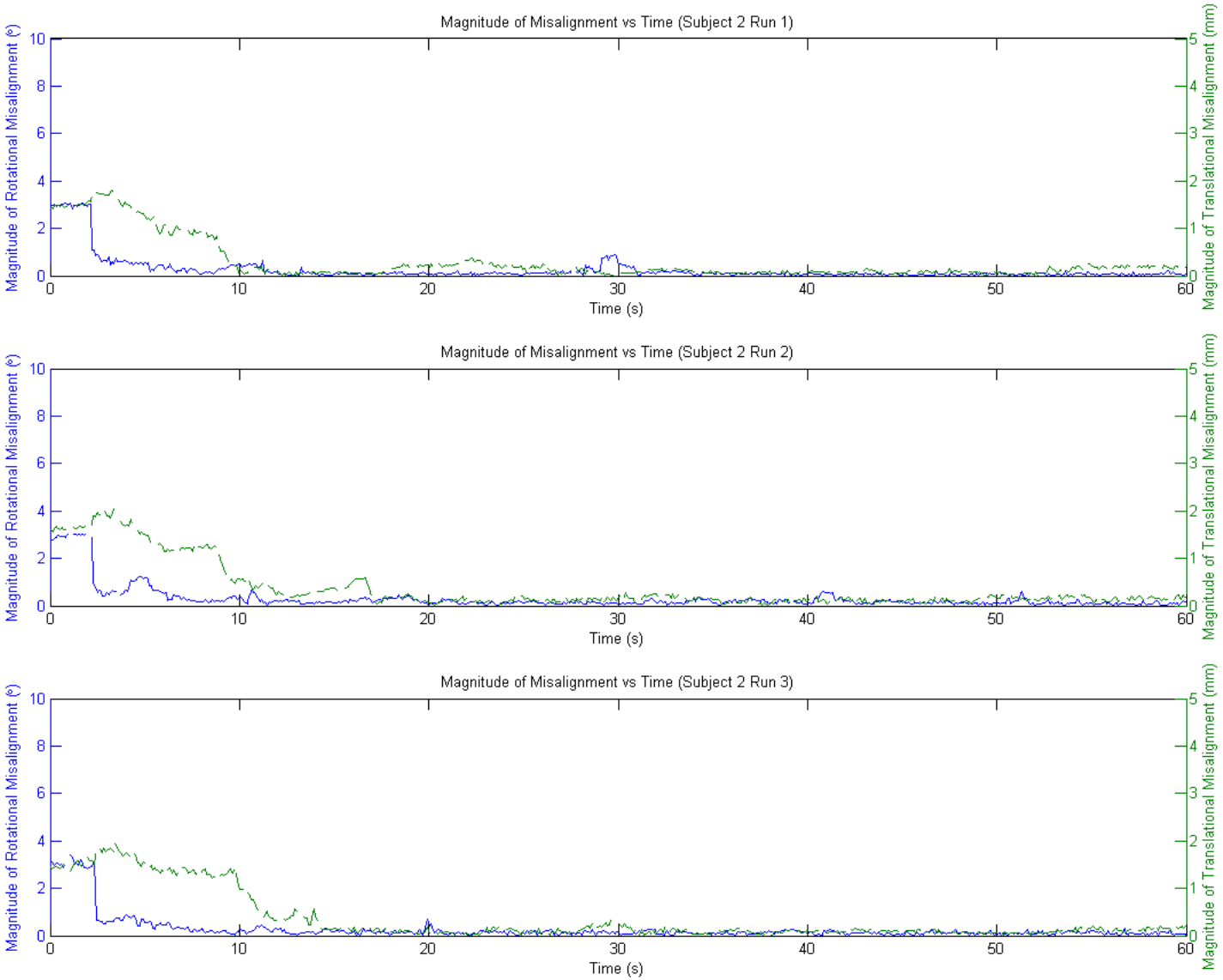

Figure G.2: Self alignment subject 2.

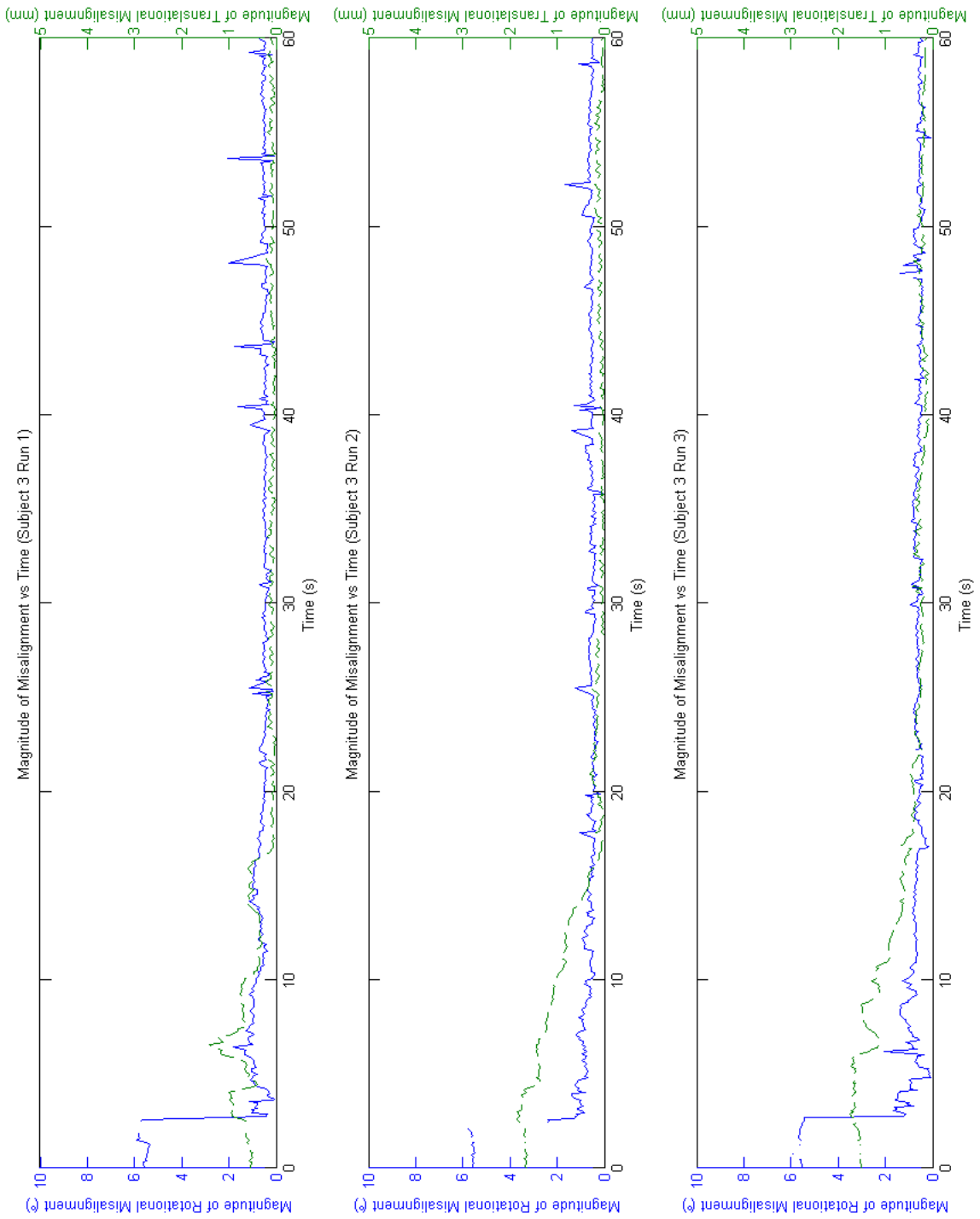

Figure G.3: Self alignment subject 3.

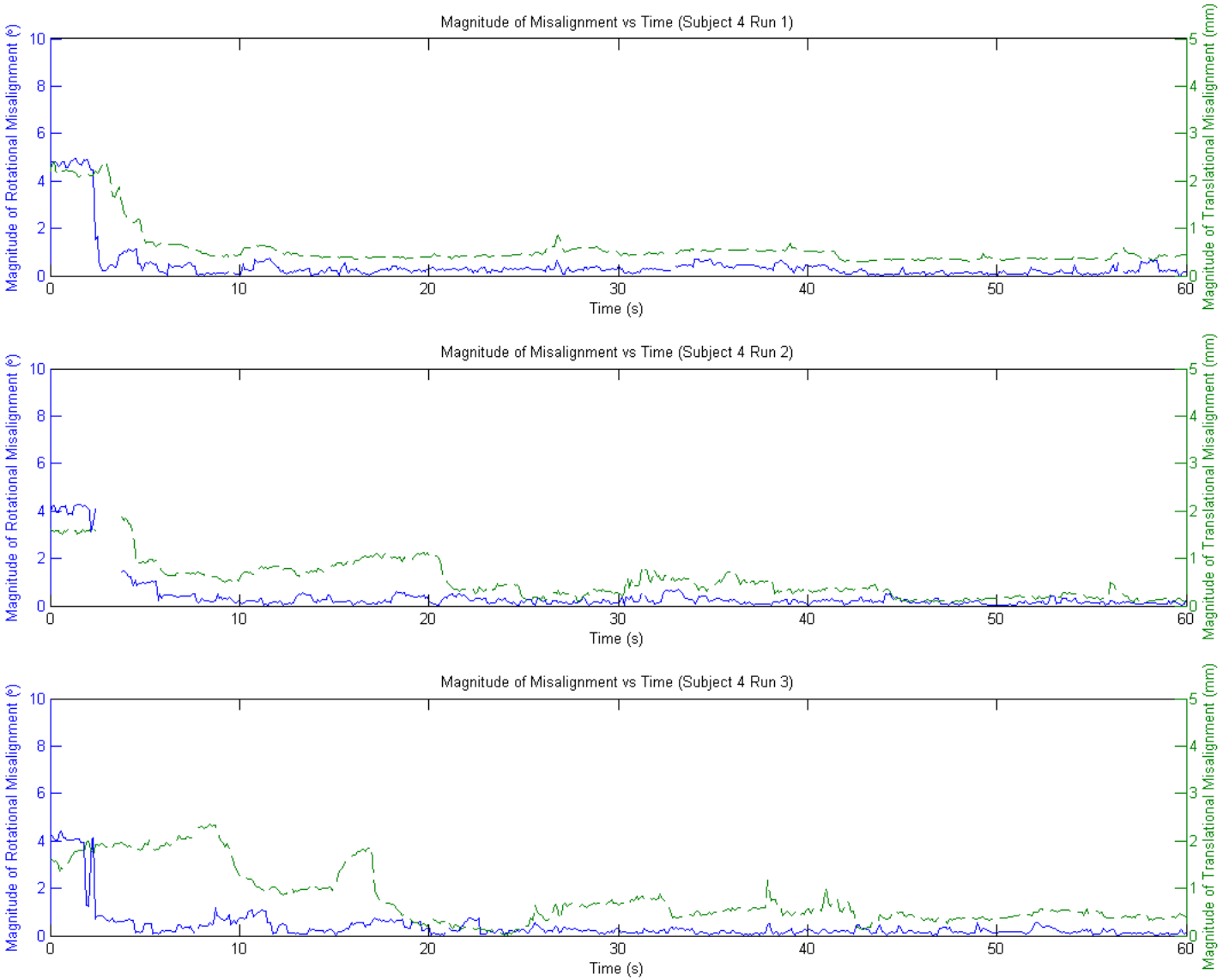

Figure G.4: Self alignment subject 4.

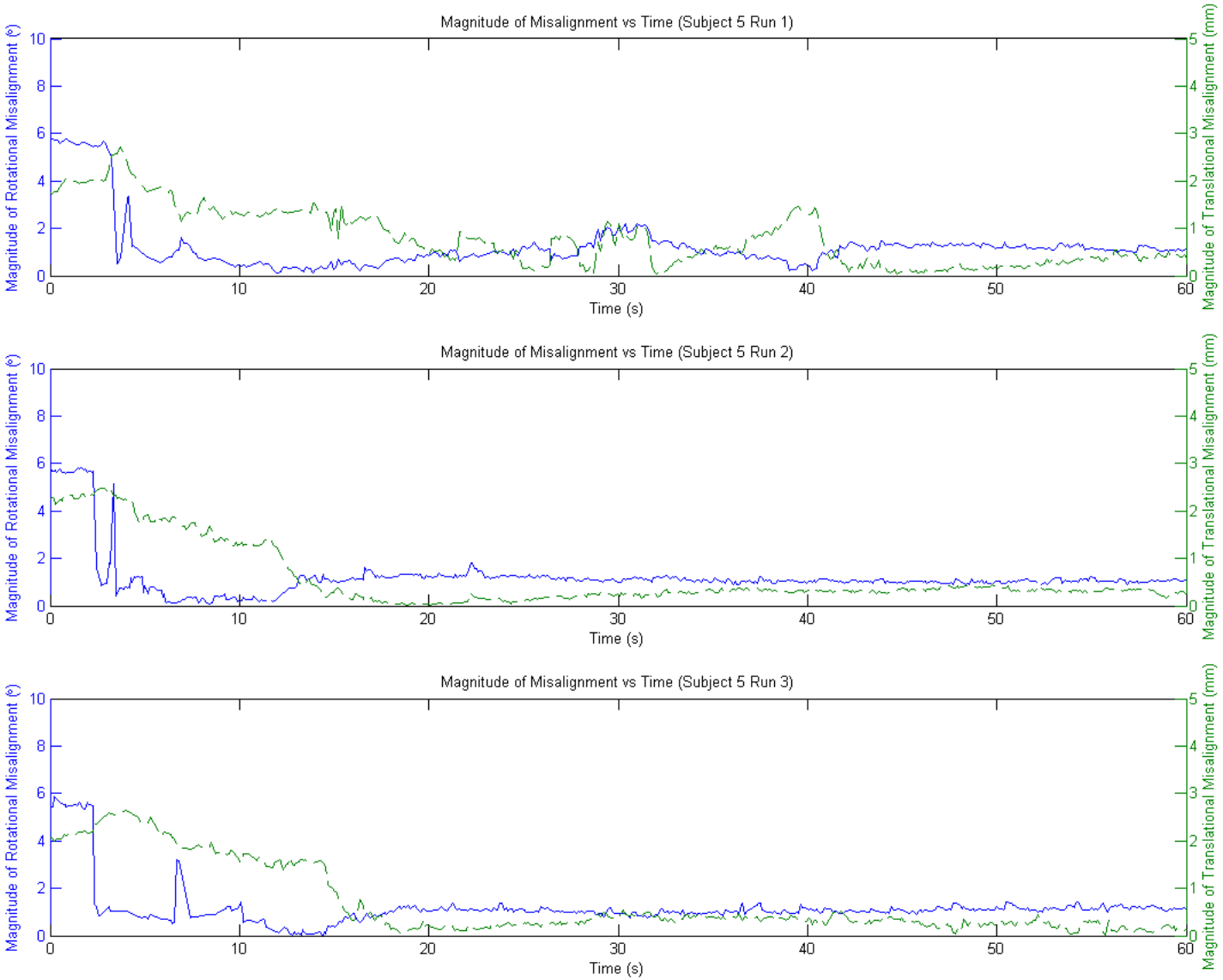

Figure G.5: Self alignment subject 5.

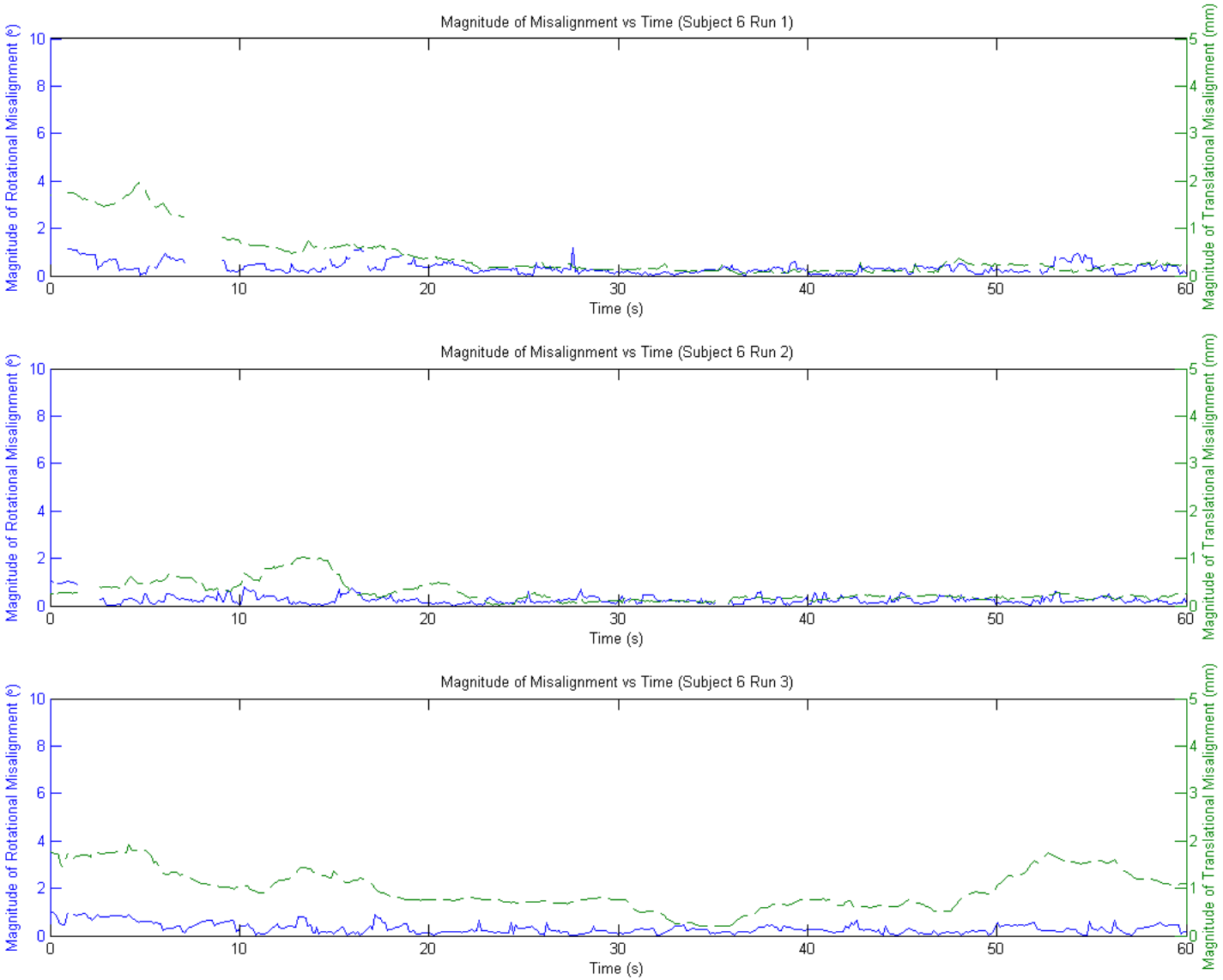

Figure G.6: Self alignment subject 6.

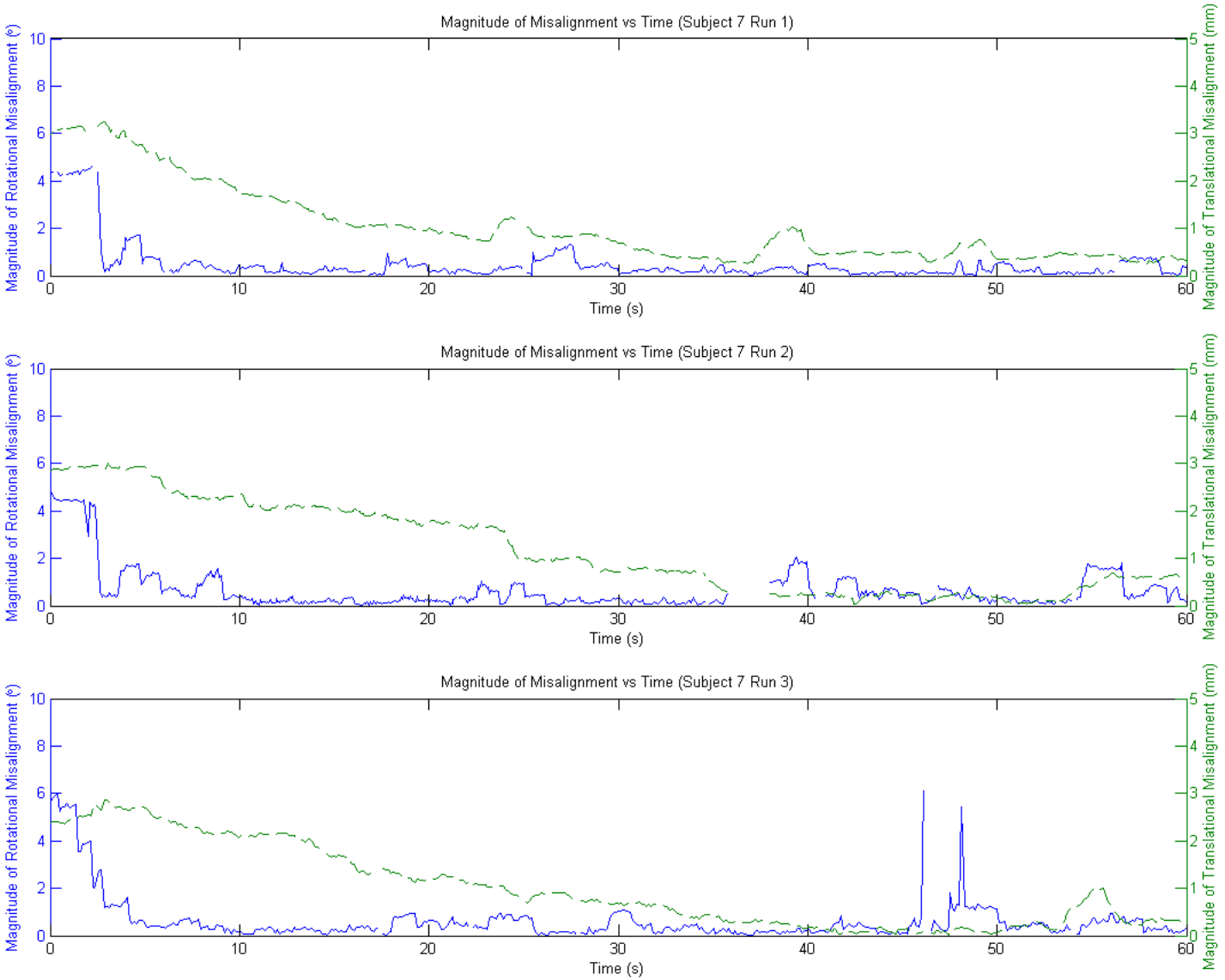

Figure G.7: Self alignment subject 7.

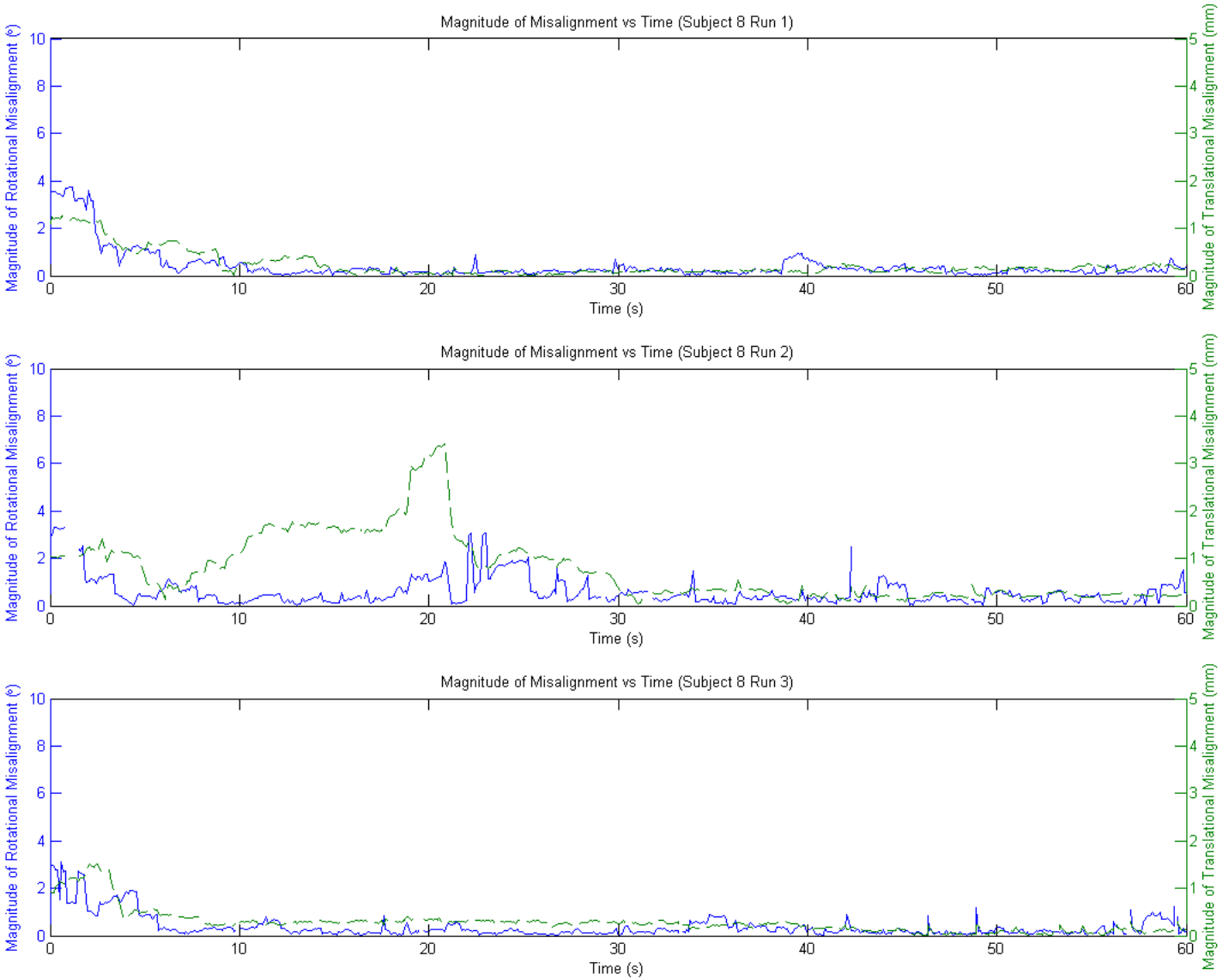

Figure G.8: Self alignment subject 8.

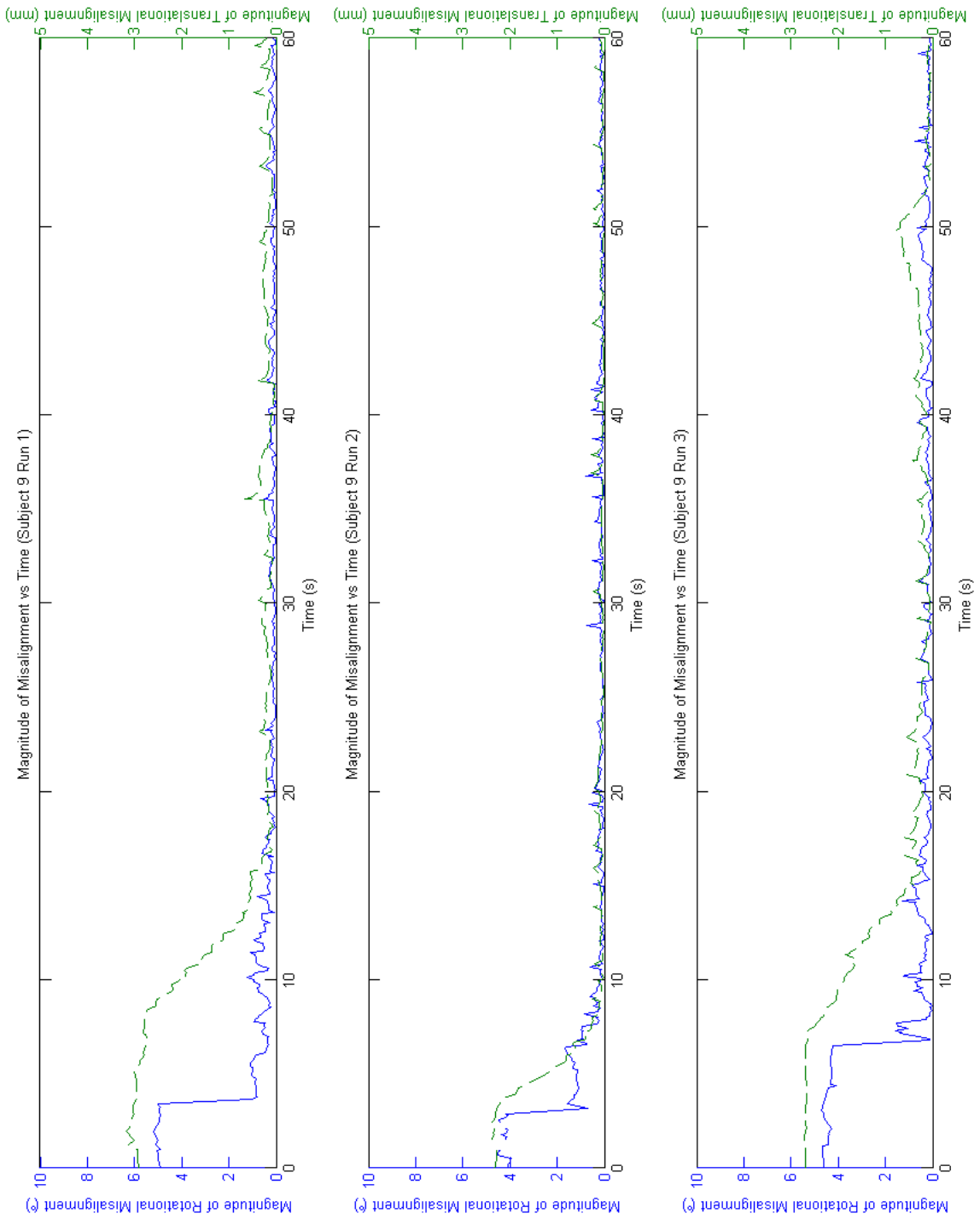

Figure G.9: Self alignment subject 9.

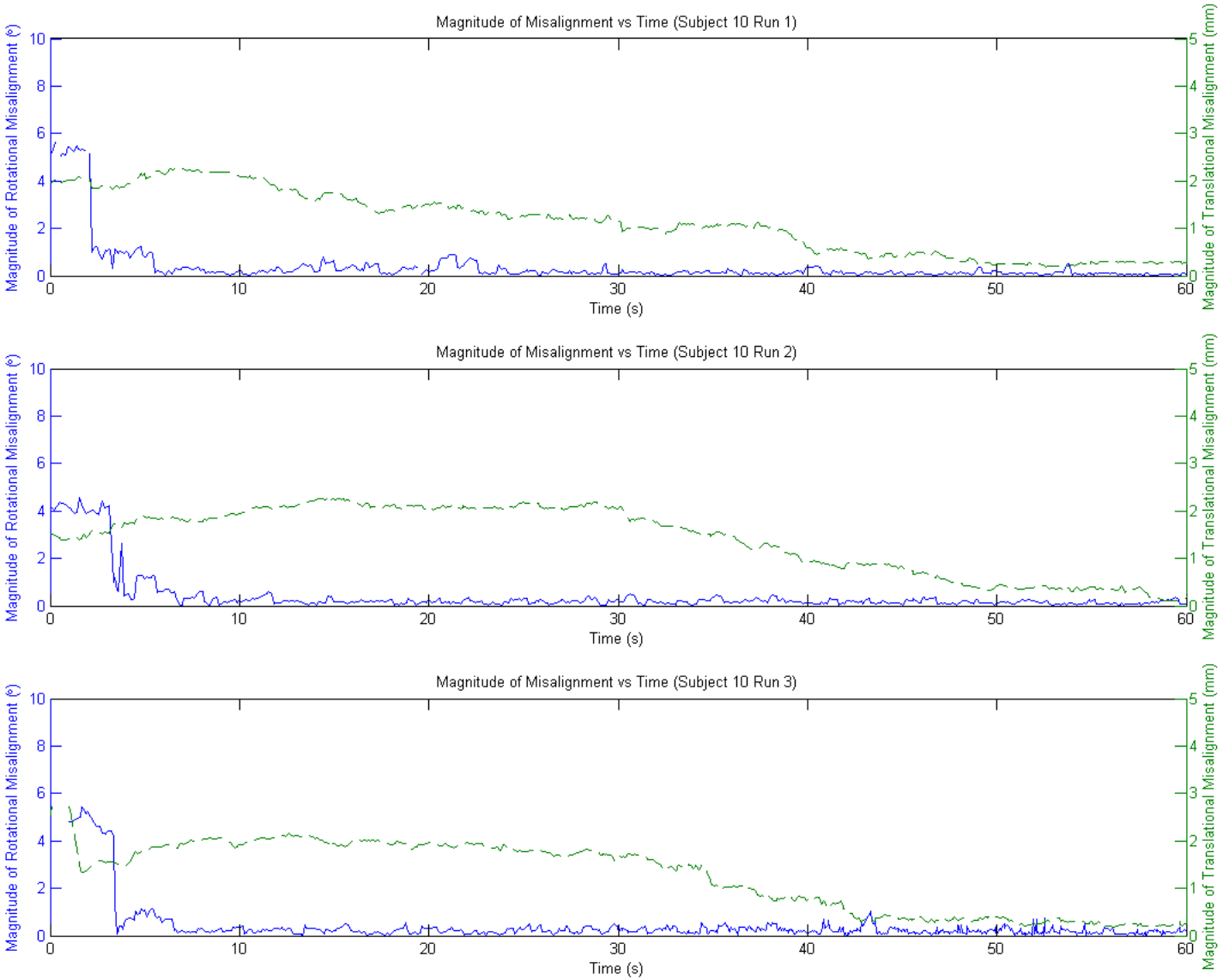

Figure G.10: Self alignment subject 10.

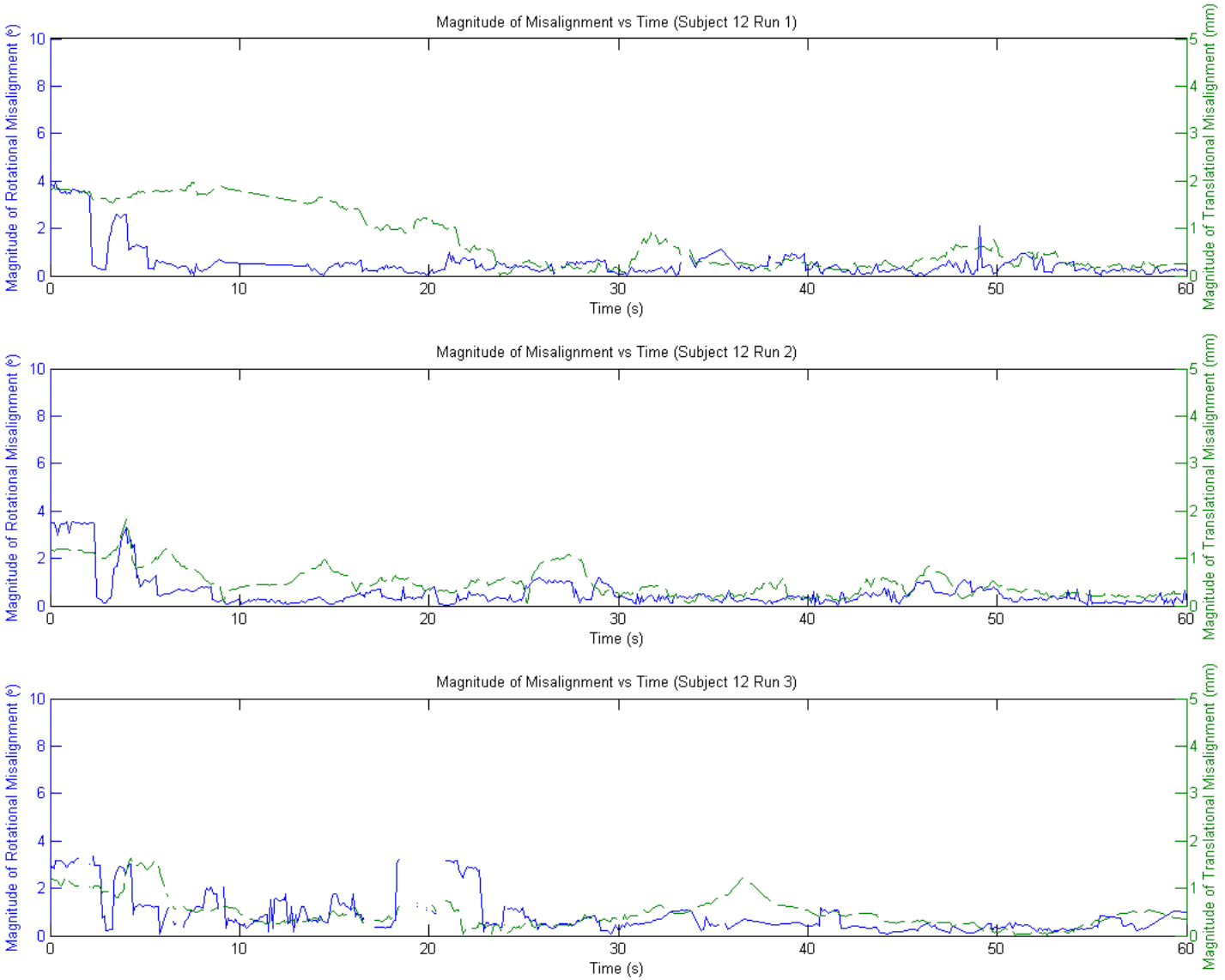

Figure G.11: Self alignment subject 12.

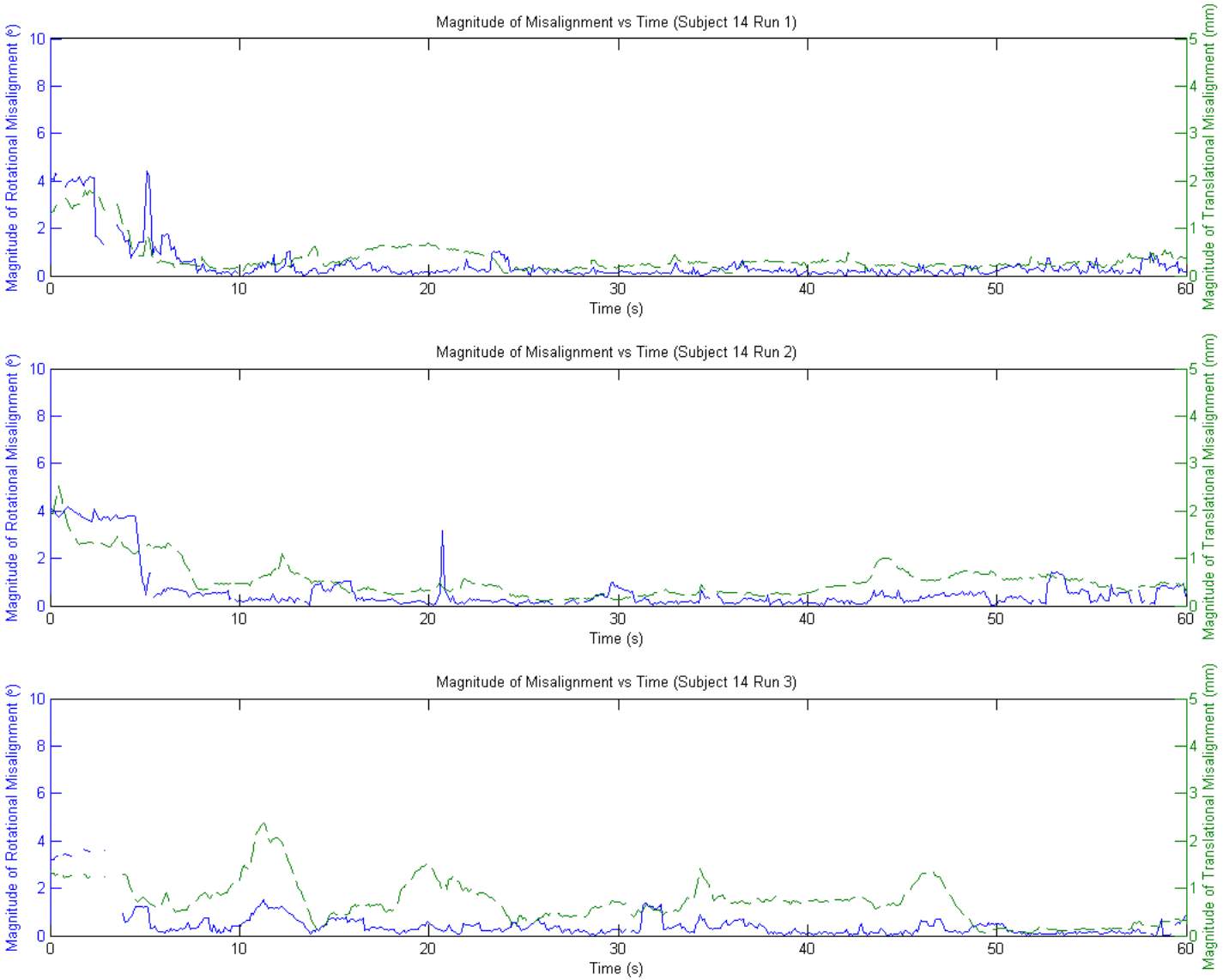

Figure G.12: Self alignment subject 14.

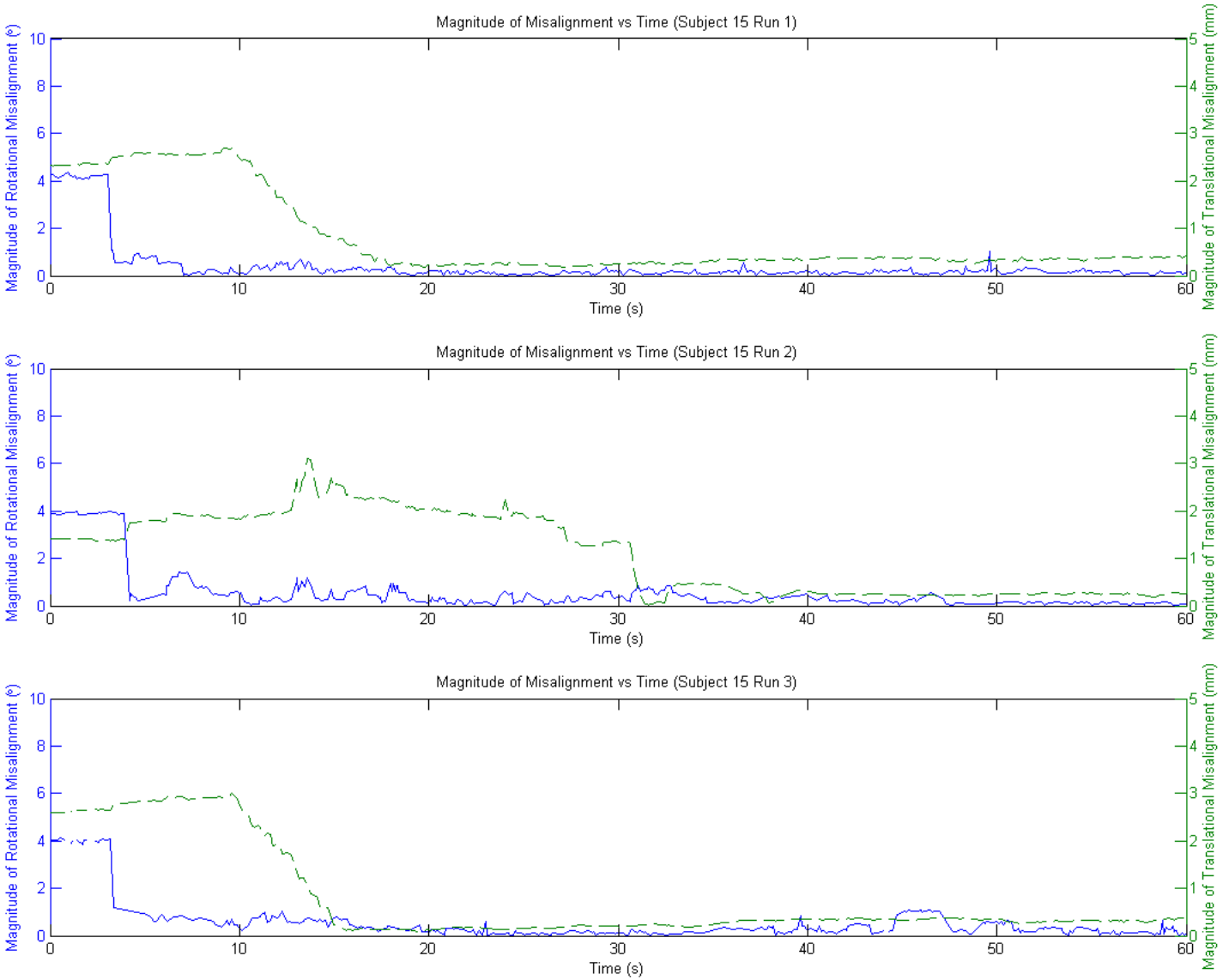

Figure G.13: Self alignment subject 15.

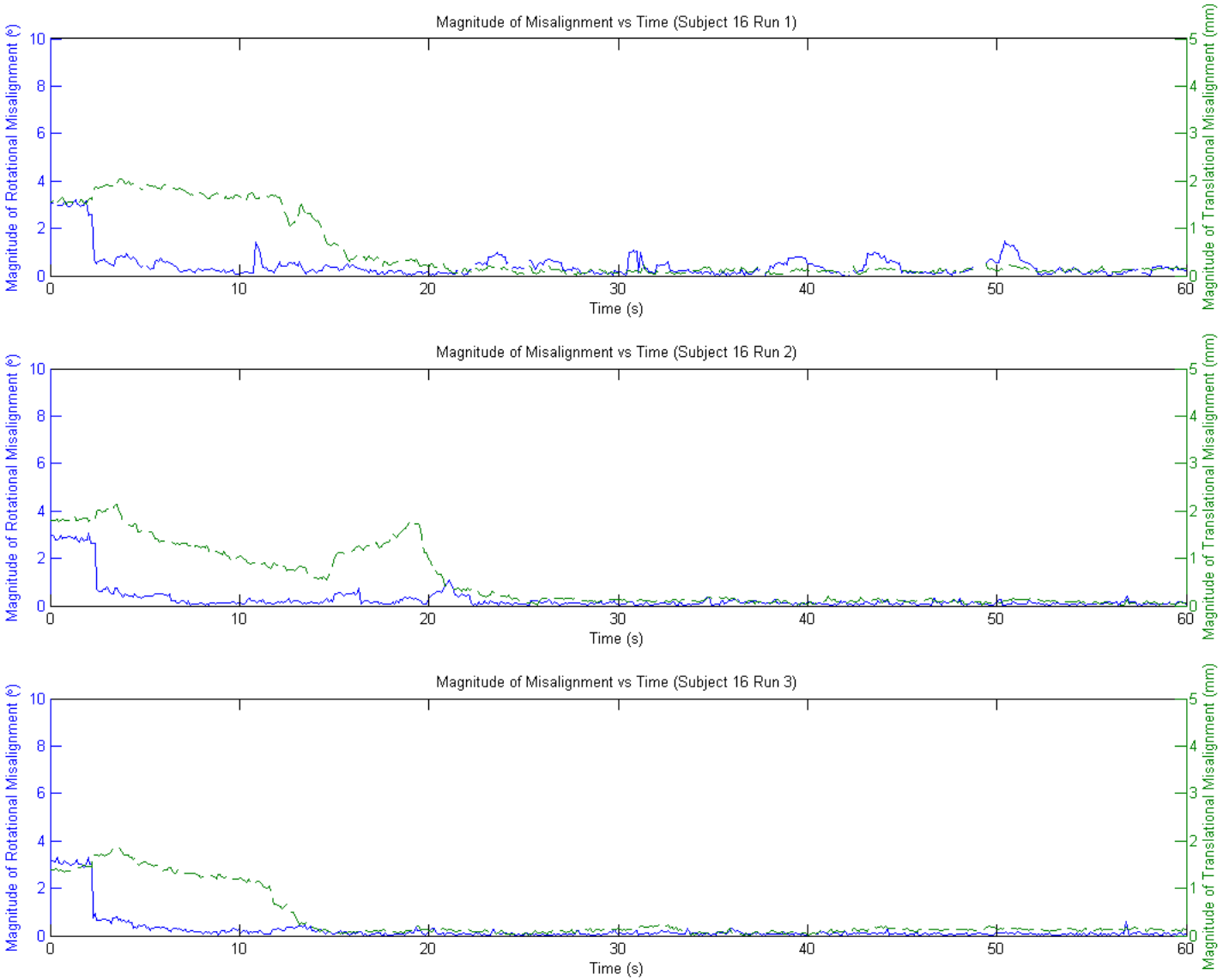

Figure G.14: Self alignment subject 16.

Appendix H

Manual JEDEye Alignment

H.1 Introduction

Prior to the development of a self alignment strategy the JEDEye alignment/tracking system was first developed to allow manual alignment, where manual alignment is defined by the ability of a clinician or operator to align the instrument to the optical axis of the eye. Thus manual alignment was considered an intermediate step; however, there are several advantages to manual alignment which warrants its development.

Firstly, manual alignment serves as a proof principle for the self alignment strategy, if the alignment can be performed by the operator then the process can be automated to allow it to be used by the patient.

In the initial development of the alignment algorithm, manual alignment serves a robust method to achieve alignment. Operator inspection of the tracking images allows quick determination of the validity of the tracking data. Automated self alignment would be nieve to errors in the tracking data which had not been eradicated in the algorithm.

The operator control of the JEDEye system also allows the speed in misalignment correction to be controlled. While the initial self alignment algorithms are oblivious to a subject struggling with the alignment process the operator would have a greater sensitivity. The operator would then have the ability to adjust the alignment process accordingly.

There is also an ascetic value to manual alignment. In using the standard chin-rest design, and mimicking interfaces used in other ophthalmic instruments the clinician will feel a certain amount of familiarity with the device, thus encouraging its use.

H.2 Manual Alignment Arrangement

The manual alignment version of the JEDEye alignment/tracking system was approached by controlling the patent's direction of gaze with a fixation target and maneuvering the instrument to the correct location using the standard chin-rest arrangement. Movement of the fixation target was facilitated by a wii nun chuck, in which the joy stick was responsible for the position of the target. Figure H.1 shows the instrument arrangement for manual alignment.

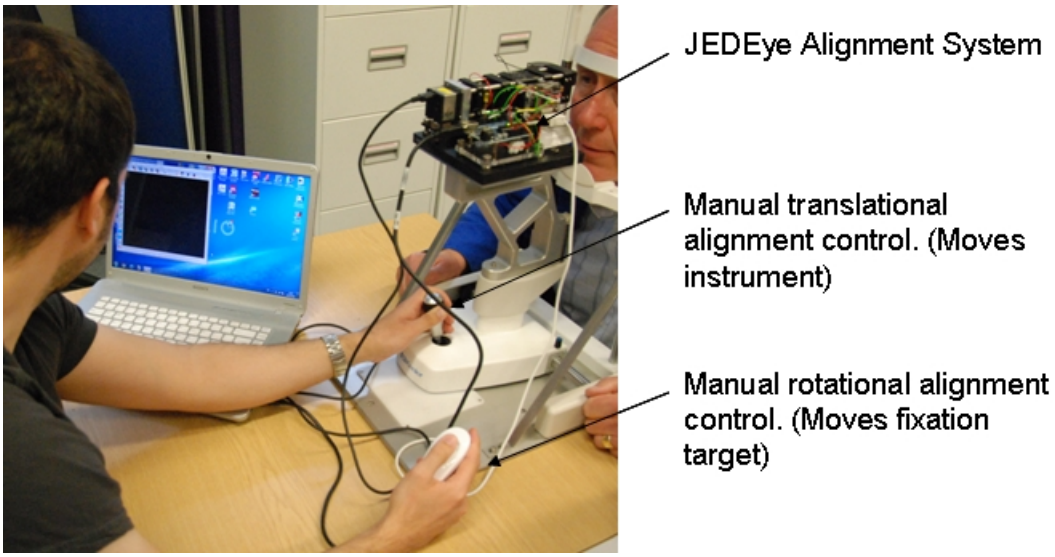

Figure H.1: JEDEye manual alignment set up.

H.3 Manual Alignment Results

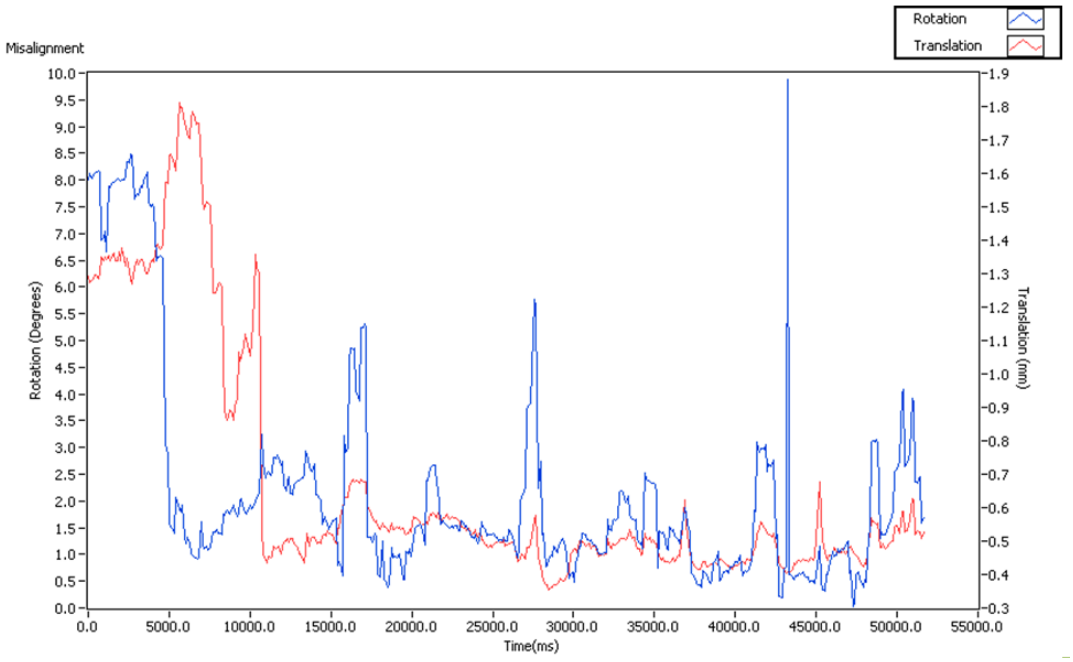

Figure H.2: Sample manual alignment data.

Figure H.2 describes alignment correction by manual methods. It can be seen that the operator is able to move the instrument from an initially unaligned position to an aligned position.

H.4 Conclusions

While the operator was able to achieve manual alignment there were some notable difficulties; however, these difficulties emanated from the method of manual alignment rather than the technique. The position of the fixation target was related to the orientation of the wii nun-chuck joystick, thus when the patient was in the correct location the operator had to physically hold the joystick in that specific location. There are a number of other methods in which the fixation target could be controlled resulting in a more comfortable alignment process, this may result in a more stable alignment. The experiment does prove that manual alignment can be achieved with the JEDEye alignment/tracking system.

Appendix I

BCU Eye Head Mounted Eye Tracker

I.1 BCU Head Mounted Eye Tracker

The BCU (Birmingham City University) head mounted eye tracking device is an eye tracking device which makes use of dark pupil tracking. The intended purpose for the instrument was to allow researchers at Birmingham City University to investigate a subjects emotional response to an image. Subjects would give verbal feed back on the image while the eye tracker allowed precise knowledge of the direction of gaze. Development of the instrument was performed from conception through to manufacture. This included custom tracking algorithms and software allowing the researchers to set up the device and record data. The majority of the parts were designed and built in Aston Universities facilities while the software was written in National Instrument's LabVIEW Environment. The final version of the software was constructed as a stand alone executable.

The head mounted eye tracker's design is based on the standard head mounted eye tracking arrangement consisting of an eye camera and a head camera. Both camera are standard web cams, the eye camera contains 2 small IR LEDs, powered by USB, which illuminate the eye. The eye camera also contains an IR filter to only allow the illumination from the IR LEDs to be imaging. Both the housings for the eye camera and head camera are custom made on a SLA machine, the head band itself is taken from an indirect ophthalmiscope.

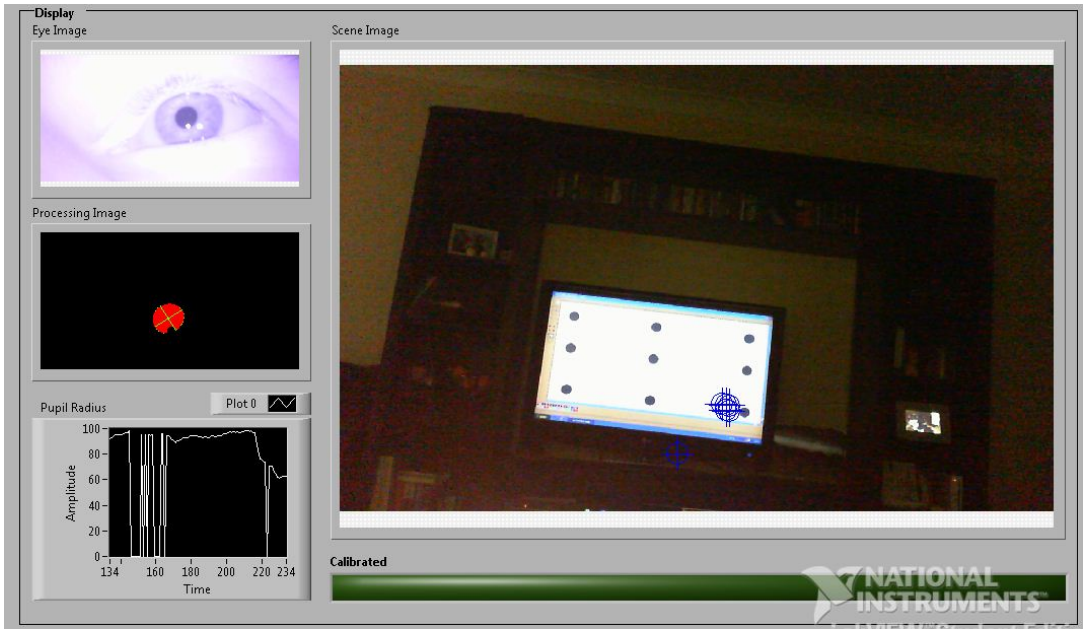

Figure I.1: BCU software.

Figure I.1 depicts the user interface for the BCU eye tracking device. Once calibrated the interface overlays the gaze point of the subject on the scene image acquired from the camera. This allows the observer to see exactly where the subject is looking in real time. The calibration method itself is achieved by correlating 9 image points with the central pupil position when the subject is regarding each point. The equation for a 3 dimensional plane is then fitted to the 9 points allowing the determination of gaze direction from the central pupil position.